

AD A995132

WT-1344 (EX)

EXTRACTED VERSION

OPERATION REDWING

Technical Summary of Military Effects, Programs 1-9

Pacific Proving Grounds
May – July 1956

Headquarters Field Command
Defense Atomic Support Agency
Sandia Base, Albuquerque, New Mexico

April 25, 1961

NOTICE

This is an extract of WT-1344, Operation REDWING, Technical Summary of Military Effects, Programs 1-9, which remains classified SECRET/RESTRICTED DATA as of this date.

Extract version prepared for:

Director
DEFENSE NUCLEAR AGENCY
Washington, D.C. 20305

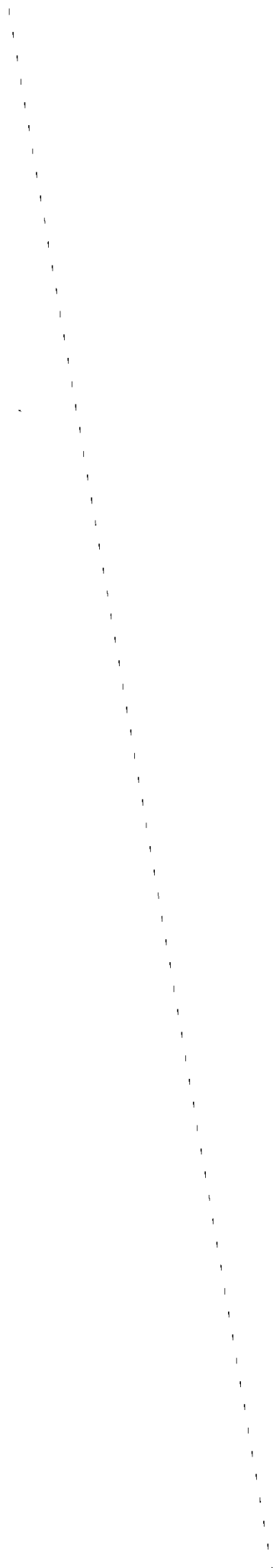
15 May 1981

100

100

100

100



REPORT DOCUMENTATION PAGE		READ INSTRUCTIONS BEFORE COMPLETING FORM
1. REPORT NUMBER WT-1344 (EX)	2. GOVT ACCESSION NO. A-7595132	3. RECIPIENT'S CATALOG NUMBER
4. TITLE (and Subtitle) Operation REDWING - Technical Summary of Military Effects, Programs 1-9		5. TYPE OF REPORT & PERIOD COVERED
		6. PERFORMING ORG. REPORT NUMBER WT-1344 (EX)
7. AUTHOR(s)		8. CONTRACT OR GRANT NUMBER(s)
9. PERFORMING ORGANIZATION NAME AND ADDRESS Office of the Deputy Chief of Staff for Weapons Effects Test HQ/FC, DASA, Sandia Base, Albuquerque, N.M.		10. PROGRAM ELEMENT, PROJECT, TASK AREA & WORK UNIT NUMBERS
11. CONTROLLING OFFICE NAME AND ADDRESS Headquarters Field Command Defense Atomic Support Agency Sandia Base, Albuquerque, New Mexico		12. REPORT DATE 25 April 1961
		13. NUMBER OF PAGES
14. MONITORING AGENCY NAME & ADDRESS (if different from Controlling Office)		15. SECURITY CLASS. (of this report) Unclassified
		15a. DECLASSIFICATION/DOWNGRADING SCHEDULE
16. DISTRIBUTION STATEMENT (of this Report) Approved for public release; unlimited distribution.		
17. DISTRIBUTION STATEMENT (of the abstract entered in Block 20, if different from Report)		
18. SUPPLEMENTARY NOTES This report has had the classified information removed and has been republished in unclassified form for public release. This work was performed by Kaman Tempo under contract DNA001-79-C-0455 with the close cooperation of the Classification Management Division of the Defense Nuclear Agency.		
19. KEY WORDS (Continue on reverse side if necessary and identify by block number) Operation REDWING Thermal Phenomenology Military Effects Nuclear Radiation Structures Biological-Effects		
20. ABSTRACT (Continue on reverse side if necessary and identify by block number) The blast program for this operation was designed to establish the basic blast phenomenology for specific shots. The nuclear-radiation program, larger than in any previous operation, has as its primary objective the determination of fallout contours and collection of data in connection with the mechanism of fallout for use in the development of a fallout model. This program also included projects to study decontamination and nuclear-radiation countermeasures and initial neutron and gamma radiations.		

FOREWORD

This report has had classified material removed in order to make the information available on an unclassified, open publication basis, to any interested parties. This effort to declassify this report has been accomplished specifically to support the Department of Defense Nuclear Test Personnel Review (NTPR) Program. The objective is to facilitate studies of the low levels of radiation received by some individuals during the atmospheric nuclear test program by making as much information as possible available to all interested parties.

The material which has been deleted is all currently classified as Restricted Data or Formerly Restricted Data under the provision of the Atomic Energy Act of 1954, (as amended) or is National Security Information.

This report has been reproduced directly from available copies of the original material. The locations from which material has been deleted is generally obvious by the spacings and "holes" in the text. Thus the context of the material deleted is identified to assist the reader in the determination of whether the deleted information is germane to his study.

It is the belief of the individuals who have participated in preparing this report by deleting the classified material and of the Defense Nuclear Agency that the report accurately portrays the contents of the original and that the deleted material is of little or no significance to studies into the amounts or types of radiation received by any individuals during the atmospheric nuclear test program.



Accession For	
NTIS GRA&I	<input checked="" type="checkbox"/>
DTIC TAB	<input type="checkbox"/>
Unannounced	<input type="checkbox"/>
Justification _____	
By _____	
Distribution/ _____	
Availability Codes	
Dist	Avail and/or Special
A	

UNANNOUNCED

ABSTRACT

All of the 17 devices detonated during Operation Redwing were basically developmental in character, { One of the significant design features of several of the large-yield devices }

The blast program for this operation was designed to establish the basic blast phenomenology for specific shots.

The nuclear-radiation program, larger than in any previous operation, had as its primary objective the determination of fallout contours and collection of data in connection with the mechanism of fallout for use in the development of a fallout model. This program also included projects to study decontamination and nuclear-radiation countermeasures and initial neutron and gamma radiations.

The structures program was chiefly concerned with checking the effect of the duration of the positive phase of blast { on structural response.

The biological-effect program consisted of a project to study chorioretinal burns.

The primary objective of the program on effects on aircraft structures was to ascertain the reliability of current weapons-delivery criteria. A secondary objective consisted of the collection of basic input and response data for use in analyses of delivery capability of other aircraft.

In the program of tests on service equipment and studies of electromagnetic effects, the emphasis was placed on studying long-range detection of nuclear explosions. An additional objective was the study of the effects of nuclear detonations on the ionosphere and microwave attenuation studies in the highly ionized regions near the burst point.

The primary objective of the thermal program was the complete documentation of thermal phenomenology, {

The support-photography program had the mission of documenting photographically the history of the nuclear cloud and supplying various technical and documentary photographic coverage to essentially every project in the military-effect programs.

The organization of Task Unit 3 within Joint Task Force 7 is discussed. A brief summary of the functions and operations of the various staffs of Task Unit 3 is also presented.

With the exception of the loss of data caused by the delivery error of Shot Cherokee, the objectives of the blast and shock experiments were attained. Some good data was obtained at the surface during that event. Although the free-air data was disappointing, the analysis suggested slight upward revision of the then currently accepted positive-phase duration standard curve.

Surface data was recorded on both Shots Lacrosse and Zuni, permitting a composite curve to be drawn representing the pressure-distance relation on the ground from surface bursts. The drag-force data compared with the field results of Operation Teapot and correlated reasonably well with data from identical scale models tested under laboratory conditions in the shock tube and wind tunnel. Precursor-type waveforms were recorded on both surface events, and the propagation of the precursor was documented over a vegetated area.

A good range of crater data was measured under a wide range of source conditions and environment. Water-wave measurements were obtained from the directly generated lagoon waves and from those generated indirectly by an air-water coupling mechanism and observed at distant islands. On all shots, a high percentage of instrumentation operated at, and through, shot time.

The documentation of the fallout distribution by various coordinated projects was successfully accomplished. Evaluation of laboratory data yielded the necessary conversion factors to correct any quantitative errors in the measured patterns. Final data analysis included corrections for background radiation. The combining of the corrected fallout distribution with data from incremental and total samplers and with reduced data from the rocket flights through the mushroom yielded sufficient information for the construction of a detailed model of the initial conditions for fallout-prediction methods.

The initial-radiation studies extended the previous data to different weapons and yields. The documentation of the radiation from a thermonuclear airburst was not accomplished because of the drop error of Shot Cherokee.

Valuable data on contamination was gathered on ships, although the results are not complete because of the lack of high contamination levels. Removal of contamination by weathering during the journey back to Site Elmer was instrumental in limiting many of the contamination-decontamination studies.

Because of the error in the delivery of Shot Cherokee, all six of the steel-frame industrial buildings (30 feet in height, 40 feet in span, 40 and 80 feet long), which comprised the relatively large structures program, were subject to higher pressures than expected. As a result, the planned gradation of damage to the various structures was not achieved, and all structures collapsed. However, a direct comparison of the results with those from four similar structures tested during Operation Teapot shows that, in the case of one drag-type structure, the damage suffered was much greater at a smaller overpressure during Operation Redwing (multimegaton device, long-duration-positive-phase blast) than during Operation Teapot (kiloton-range device, short-duration-positive-phase blast). Thus, a full-scale, qualitative demonstration and an agreement with theoretical studies were accomplished. The test results were analyzed to determine the quantitative magnitude of the bonus effect of the long duration of the positive phase.

Results from the biological-effect program showed that climatic conditions and the thermal-pulse characteristics at some exposure stations reduced the radiant exposure below the threshold necessary to produce chorioretinal burns. Both the first and second peak irradiances may produce chorioretinal burns. Blink reflex is not sufficiently fast to protect the eye.

The limitations of the capability of the aircraft tested to deliver nuclear weapons were determined. Basic thermal and blast data was obtained for aircraft-design research. Results showed that primary structural components are not always the factors limiting delivery capability; the secondary structural parts and miscellaneous non-load-carrying elements frequently establish the limits.

It was successfully demonstrated that: (1) operationally usable lines of position and fixes could be obtained from the bomb pulse at great distances when time of detonation and yield were known; (2) airborne flush-mounted antenna and photocell combinations would pick up electromagnetic and thermal pulses giving results that could meet the requirements for yield determination; (3) high-yield nuclear detonations produced effects upon the ionosphere that were more pronounced in the test site area to the south than to the east of ground zero; and (4) the microwave attenuation versus time in the ionization region resulting from atomic detonations makes it advisable to store telemetry information during the initial 10 to 20 μ sec, afterward utilizing UHF or SHF to telemeter technical information.

The thermal program was generally successful from an instrumental point of view but the interpretation of the results is uncertain because of the lack of sufficient atmospheric attenuation data, the excessive obscuration at several of the stations, and the large delivery error of Shot Cherokee.

On the basis of the limited results, the scaling of surface bursts appears to be different from the scaling for airbursts. The time to second maximum for surface bursts appears to scale about $W^{0.5}$ whereas the second maximum for airbursts appears to scale more to $W^{0.42}$. The scaling of thermal yields for surface bursts is not well established but appears to be different from the $W^{0.95}$ scaling that has been observed for airbursts at low altitudes.

The support photography program fulfilled its overall mission of providing technical photographic support to the various projects. A documentary motion picture of the Redwing weapon-effect programs was produced and distributed. Excellent navigation together with improved camera installations made it possible to obtain more complete cloud-survey data than on any previous operations.

PREFACE

With the firing of Shot Huron on 22 July 1956, Operation Redwing, the most extensive series of nuclear tests to that date, was brought to conclusion. On 10 August 1956, the Commander, Joint Task Force 7, terminated the Redwing Operational phase, during which 17 nuclear devices had been detonated.

This report is the final summary of the technical results from the eight programs implemented during Operation Redwing. It has been prepared by the Director, Test Division, and his staff of the Office of the Deputy Chief of Staff for Weapons Effects Tests, Field Command, Defense Atomic Support Agency (DASA). At the time of Operation Redwing, the Command was designated Field Command, Armed Forces Special Weapons Project (AFSWP).

Grateful acknowledgement is made of the invaluable assistance of J. R. Kelso, Blast Branch, Weapons Effects Division, Headquarters, DASA, in the preparation of Chapter 2 of both the preliminary report and this final report, and of P. R. Perkins, LCDR, USN, Fallout Branch, Radiation Division, Headquarters, DASA, in the preparation of Chapter 3.

The preliminary summary report, ITR-1344, prepared by the Commander, Task Unit 3, Operation Redwing, and his staff, has been used as a point of departure in preparing this final summary; thus, much of the material herein is based directly on the preliminary version.

Chapter 1 contains a summary of the functions and activities of the several operational and support staffs of Task Unit 3. Subsequent chapters contain general discussions of the findings of each test program. In many cases, these findings are consolidated for a number of coordinated projects designed to give an overall result; therefore, the results from individual projects are not always considered separately. The appendix contains brief abstracts and bibliographical information on the projects.

For more detailed technical information, the reader is referred to the final reports of the individual projects. The final reports (WT reports) are listed under the projects described in the appendix.

A preliminary summary report of the fallout studies of Program 2 was published as ITR-1354. No final report of that study will be published; therefore, the useful portions of the canceled WT-1354 have been incorporated into Chapter 3 of this report.

CONTENTS

ABSTRACT -----	5
PREFACE -----	8
CHAPTER 1 INTRODUCTION-----	19
1.1 Background-----	19
1.2 Objectives-----	19
1.3 Summary of Shot Data-----	20
1.4 Participation-----	21
1.5 Organization-----	21
1.6 Personnel-----	21
1.7 Administration-----	21
1.8 Security and Classification-----	22
1.9 Operations-----	22
1.10 Communications and Electronics-----	23
1.11 Timing Signals-----	23
1.12 Logistic Support-----	24
1.13 Construction-----	24
1.14 Fiscal-----	24
1.15 Reports-----	25
CHAPTER 2 BLAST MEASUREMENTS-----	34
2.1 Objectives-----	34
2.2 Background-----	35
2.2.1 High-Yield Airburst-----	35
2.2.2 Surface Bursts-----	36
2.2.3 Operation Ivy-----	36
2.2.4 Operation Castle-----	36
2.2.5 Precursors-----	37
2.2.6 Drag-Force Measurements-----	38
2.2.7 Crater Survey-----	39
2.2.8 Water Waves-----	40
2.2.9 -----	40
2.2.10 Scaling Factors-----	40
✓ 2.3 Results: Shot Cherokee-----	41
2.3.1 Free-Air Data-----	42
2.3.2 Surface Phenomena-----	43
✓ 2.4 Results: Shot Lacrosse-----	44
2.4.1 Free-Air Data-----	45
2.4.2 Surface Phenomena-----	45
✓ 2.5 Results: Shot Zuni-----	47
2.5.1 Shock Photography-----	47
2.5.2 Surface Instrumentation-----	49

✓ 2.6 Results: Shot Inca -----	50
2.7 Results: Direct-Shock Photography of Shots Inca, Mohawk, and Seminole -----	51
2.8 Results: Drag-Force Measurements -----	52
2.8.1 NOL Models -----	52
2.8.2 BRL Full-Scale Structural Members -----	58
2.8.3 BRL Spherical Drag Gages -----	59
2.8.4 Military Vehicles -----	59
2.8.5 Cubicle Target Structure -----	62
2.8.6 Electronic Instrumentation -----	63
2.9 Results: [] -----	63
2.10 Results: Crater Measurements -----	64
✓ 2.10.1 Shot Lacrosse -----	64
✓ 2.10.2 Shot Zuni -----	64
✓ 2.10.3 Shot Seminole -----	64
✓ 2.10.4 Shot Mohawk -----	65
✓ 2.10.5 Shot Tewa -----	65
2.10.6 Correlation of Crater Data -----	65
2.11 Results: Water-Wave Studies -----	66
2.11.1 Direct Waves -----	66
2.11.2 Indirect Waves -----	67
2.12 Discussion: Free-Air Data -----	68
✓ 2.12.1 Shot Cherokee -----	68
✓ 2.12.2 Shot Zuni -----	69
2.13 Discussion: Surface Data -----	69
✓ 2.13.1 Shot Cherokee -----	69
2.13.2 Shock Photography -----	70
2.13.3 Time of Arrival -----	70
✓✓ 2.13.4 Composite Lacrosse and Zuni Surface Data -----	71
2.14 Discussion: 2W Concept -----	71
2.15 Discussion: Precursor Phenomena -----	72
2.16 Review and Summary -----	74
 CHAPTER 3 NUCLEAR RADIATION -----	 126
3.1 Objectives -----	126
3.2 Background -----	126
3.2.1 Fallout Distribution -----	126
3.2.2 Distribution of Activity in Nuclear Mushroom -----	127
3.2.3 Initial Radiation -----	127
3.2.4 Contamination-Decontamination -----	128
3.2.5 Ship Shielding -----	128
3.2.6 Evaluation of Dosimeters -----	128
3.3 Instrumentation and Operations -----	128
3.3.1 Land Stations -----	128
3.3.2 Moored Stations -----	128
3.3.3 Fallout-Collection Ships -----	129
3.3.4 Survey Ships -----	129
3.3.5 Survey Aircraft -----	129
3.3.6 Cloud-Penetration Rockets -----	129

3.3.7	Cloud-Penetration Aircraft	129
3.3.8	Program 2 Control Center	129
3.3.9	Laboratory Facilities	130
3.4	Fallout Studies	130
3.4.1	Measurement of Radiation Contours	130
3.4.2	Characteristics of Fallout Contaminant	133
3.4.3	Characteristics of Arrival and Deposition of Fallout	136
3.4.4	Fallout Prediction Correlations	136
3.5	Distribution of Activity in the Mushroom	137
3.5.1	Rocket Data	137
3.5.2	Aircraft Data	138
3.6	Initial Radiation	139
3.6.1	Initial-Gamma Radiation	139
3.6.2	Neutrons	139
3.7	Contamination-Decontamination	140
3.7.1	Building Materials	140
3.7.2	Shipboard Materials	141
3.7.3	Washdown Effectiveness	141
3.7.4	Shipboard Decontamination Procedures	141
3.7.5	Aircraft Contamination	142
3.7.6	Skin Decontamination	143
3.8	Ship Shielding	143
3.9	Evaluation of Dosimeters	144
 CHAPTER 4 EFFECTS ON STRUCTURES		 177
4.1	Objectives	177
4.2	Background	177
4.3	Procedure	177
4.4	Site Construction	178
4.5	Instrumentation	179
4.6	Results	179
4.7	Conclusions	180
 CHAPTER 5 BIOMEDICAL EFFECTS		 184
5.1	Objectives	184
5.2	Background	184
5.3	Results	184
5.3.1	Chorioretinal Burns	184
5.3.2	Protective Devices	185
 CHAPTER 6 EFFECTS ON AIRCRAFT STRUCTURES		 188
6.1	Objectives	188
6.2	Background	188
6.3	Operations	188
6.3.1	Aircraft-Positioning Reports	188
6.3.2	Aircraft-Positioning Systems	189
6.3.3	Positioning Yields	189
6.4	Results	190

CHAPTER 7 ELECTROMAGNETIC EFFECTS -----	207
7.1 Objectives-----	207
7.2 Determination of Ground Zero Using Electromagnetic Pulse generated by Nuclear Detonation-----	207
7.2.1 Short-Baseline System -----	207
7.2.2 Long-Baseline System -----	208
7.2.3 Results -----	208
7.3 Ionospheric Effects of Nuclear Detonations-----	208
7.4 Airborne Antennas and Phototubes for Determination of Nuclear Weapon Yield -----	209
7.5 Measurement of Radiofrequency Electromagnetic Radiation from Nuclear Detonations-----	210
7.6 Electromagnetic Wave Attenuation at Super-High and Ultra-High Frequencies Resulting from Nuclear Explosions -----	211
 CHAPTER 8 THERMAL RADIATION -----	 217
8.1 Objectives-----	217
8.2 Basic Thermal Measurements -----	217
8.3 Critical Ignition Energies of Materials and Depth of Char in Wood-----	219
8.4 Test of New Types of Thermal Indicators -----	220
8.5 Test of Aircraft Structural Panels-----	220
8.6 Airborne Spectroscopy-----	221
 CHAPTER 9 SUPPORT PHOTOGRAPHY -----	 237
9.1 Objectives-----	237
9.2 Background-----	237
9.3 Instrumentation and Operations-----	237
9.4 Results-----	238
9.5 Conclusions -----	238
 APPENDIX PROJECT ABSTRACTS -----	 240
A.1 Program 1: Blast Measurements -----	240
A.1.1 Project 1.1-----	240
A.1.2 Project 1.2-----	240
A.1.3 Project 1.3-----	241
A.1.4 Project 1.4-----	241
A.1.5 Project 1.5-----	242
A.1.6 Project 1.6-----	242
A.1.7 Project 1.8-----	243
A.1.8 Project 1.9a-----	243
A.1.9 Project 1.9b-----	244
A.1.10 Project 1.10 -----	244
A.2 Program 2: Nuclear Radiation Studies -----	245
A.2.1 Project 2.1-----	245
A.2.2 Project 2.2-----	245
A.2.3 Project 2.4-----	245
A.2.4 Project 2.51-----	246

A.2.5	Project 2.52	-----	247
A.2.6	Project 2.61	-----	247
A.2.7	Project 2.62	-----	247
A.2.8	Project 2.63	-----	249
A.2.9	Project 2.64	-----	250
A.2.10	Project 2.65	-----	250
A.2.11	Project 2.66	-----	251
A.2.12	Project 2.71	-----	252
A.2.13	Project 2.72	-----	253
A.2.14	Project 2.8	-----	253
A.2.15	Project 2.9	-----	254
A.2.16	Project 2.10	-----	254
A.3	Program 3: Effects on Structures	-----	256
A.4	Program 4: Biomedical Effects	-----	257
A.5	Program 5: Effects on Aircraft Structures	-----	258
A.5.1	Project 5.1	-----	258
A.5.2	Project 5.2	-----	258
A.5.3	Project 5.3	-----	258
A.5.4	Project 5.4	-----	259
A.5.5	Project 5.5	-----	259
A.5.6	Project 5.6	-----	260
A.5.7	Project 5.7	-----	260
A.5.8	Project 5.8	-----	261
A.5.9	Project 5.9	-----	262
A.6	Program 6: Electromagnetic Effects	-----	264
A.6.1	Project 6.1a	-----	264
A.6.2	Project 6.1b	-----	264
A.6.3	Project 6.3	-----	264
A.6.4	Project 6.4	-----	265
A.6.5	Project 6.5	-----	265
A.6.6	Project 6.6	-----	266
A.7	Program 8: Thermal Radiation and Effects	-----	267
A.7.1	Project 8.1a	-----	267
A.7.2	Project 8.1b	-----	267
A.7.3	Project 8.1c	-----	267
A.7.4	Project 8.2	-----	267
A.7.5	Project 8.3	-----	268
A.7.6	Project 8.4	-----	268
A.7.7	Project 8.5	-----	269
A.8	Program 9: General Support	-----	270
A.8.1	Project 9.1a	-----	270
A.8.2	Project 9.1b	-----	270
REFERENCES		-----	271
TABLES			
1.1	Summary of Shot Data	-----	27
1.2	Project Participation	-----	29
1.3	Redwing Research and Development Budget	-----	29

2.1	Scaling Factors (Surface Ambient Conditions) -----	76
2.2	Scaling Factors (Ambient Conditions at Burst Height) -----	77
2.3	Comparison of Slant Ranges Computed by Different Methods -----	77
2.4	Observed Data for Shot Cherokee -----	78
2.5	Comparison Between Observed and Calculated Peak Overpressures-----	78
2.6	Shot Zuni, Approximation of Focusing Effect -----	79
2.7	Force-Gage Data, Shot Lacrosse -----	80
2.8	Final Drag Data -----	80
2.9	Comparison of Steady-State Drag and Lift Coefficients with those Obtained on Operation Redwing -----	81
2.10	Most Probable Peak Drag Coefficient Values -----	81
2.11	Dynamic Pressure Compared with Damage -----	81
2.12	Redwing Crater Data -----	82
2.13	First-Crest and First-Wave Data, Shots Zuni, Flathead, Dakota, Navajo, and Tewa -----	83
3.1	Projects and Objectives, Program 2 -----	145
3.2	Percent of Fission Fragments -----	147
3.3	Summary of Areal Extent of Fallout -----	147
3.4	Early-Gamma-Dose-Rate Decay Slopes -----	148
3.5	Comparison of Predicted and Observed Times of Arrival and Maximum Particle Size Variation with Time -----	148
3.6	Shot Zuni Cloud Penetration Data (P-meter) -----	149
3.7	Angular Variation of Neutron Flux for Shots Yuma and Kickapoo -----	149
3.8	Percent of Total Neutrons in Each Energy Interval-----	149
3.9	The e-Fold Distances from Shots Yuma, Kickapoo, Blackfoot, Erie, and Osage -----	149
4.1	Comparison of Results from Operations Teapot and Redwing -----	181
5.1	Summary of Data at Exposure Sites -----	187
6.1	Positioning Yield Information -----	193
6.2	Summary Data on Project 5.1 -----	193
6.3	Summary Data on Project 5.2 -----	193
6.4	Summary Data on Project 5.3 -----	194
6.5	Summary Data on Project 5.4 -----	194
6.6	Summary Data on Project 5.5 Capabilities Aircraft (F-84F) -----	194
6.7	Summary Data on Project 5.5 Research Aircraft (F-84F) -----	195
6.8	Summary Data on Project 5.6 -----	195
6.9	Summary Data on Project 5.8 -----	195
6.10	Effectiveness of Thermal Instrumentation -----	196
6.11	Thermal Exposure and Maximum Irradiance -----	197
6.12	Effectiveness of Photographic Instrumentation -----	204
6.13	Aircraft Positions at Time Zero -----	205
6.14	Summary of Test Specimen Exposure -----	206
7.1	Comparison of Long- and Short-Baseline Position Errors -----	213
7.2	Yields from Electromagnetic Signals -----	213
7.3	Photohead Yields -----	213
8.1	Station Locations -----	223
8.2	Comparison of Total Thermal Energy Received at Ground and Airborne Stations -----	224

8.3	Critical Ignition Energy Values Estimated for Various Materials Exposed to Shot Cherokee -----	224
8.4	Comparison of Radiant Exposure Values as Measured by the Three Types of Calorimeters -----	224
8.5	Aircraft Positions for Participating Events, Project 8.5 -----	225
8.6	Spectrometer Data, Shot Lacrosse, Project 8.5 -----	225
8.7	Spectrometer Data, Shot Zuni, Project 8.5 -----	225
8.8	Spectrometer Data, Shot Erie, Project 8.5 -----	226
8.9	Spectrometer Data, Shot Flathead, Project 8.5 -----	226

FIGURES

1.1	Organization of Office of Deputy Chief of Staff, Weapons Effects Tests -----	30
1.2	Organization of Joint Task Force 7 -----	31
1.3	Organization of Task Unit 3 -----	32
1.4	TU-3 Personnel Flow Chart -----	33
2.1	Surface overpressure versus range for Shot Cherokee (BRL) -----	84
2.2	Impulse, arrival time and duration versus range for Shot Cherokee (BRL) -----	84
2.3	Site Yvonne, looking toward ground zero of Shot Lacrosse -----	85
2.4	Overpressure versus range along water surface for Shot Lacrosse (NOL) -----	85
2.5	Overpressure versus range along ground surface for Shot Lacrosse (SC and BRL) -----	86
2.6	Dynamic pressure versus range for Shot Lacrosse -----	86
2.7	Overpressure versus time, showing shock-wave arrival time (seconds) and history after shock arrival (SC) -----	87
2.8	Horizontal and vertical overpressures for Shot Zuni -----	89
2.9	Comparison of peak-shock overpressure in vertical direction with 2.2W curve corrected for atmospheric inhomogeneity -----	89
2.10	Overpressure versus range for Shot Zuni (BRL) -----	90
2.11	Corrected peak dynamic pressure versus distance, Shot Zuni -----	90
2.12	Overpressure versus ground range for Shot Inca (SC) -----	91
2.13	Dynamic pressure versus ground range for Shot Inca (SC) -----	91
2.14	Layout of Shot Inca, Site Pearl -----	92
2.15	Peak-shock overpressure versus distance for Shot Inca, along surface -----	92
2.16	Peak shock overpressure versus distance along line up 10 degrees from horizontal through burst point for Shot Mohawk -----	93
2.17	Sketch of water tank, Shot Seminole -----	93
2.18	Views of development of luminous front, Shot Seminole -----	94
2.19	Typical station layout -----	95
2.20	Side-on pressure (P_g) and dynamic pressure (q) at A-station -----	96
2.21	Side-on pressure (P_g) and dynamic pressure (q) at B-station -----	96
2.22	Comparison of drag coefficients for spheres -----	97
2.23	Comparison of wind-tunnel drag coefficients of spheres -----	97
2.24	Field and shock-tube drag coefficients for spheres -----	98

2.25	Drag coefficients for cubes, cylinders, and parallelepipeds in 7- by 10-foot transonic wind tunnel -----	99
2.26	Comparison of wind tunnel drag coefficients for cylinders -----	100
2.27	Field and shock-tube drag coefficients for cubes -----	101
2.28	Typical structural member station-----	102
2.29	Drag force versus time for Sites Able, Manmade Island 2, and Dog, net drag force sensed by I beam -----	102
2.30	Vehicle damage obtained on Shot Lacrosse -----	103
2.31	Vehicle damage obtained on Shot Zuni-----	104
2.32	Vehicle damage obtained on Shot Yuma-----	106
2.33	Height-of-burst chart for damage to military vehicles-----	107
2.34	Ground range versus yield for various damage levels for EPG surface shots and NTS shots of low scaled HOB -----	108
2.35	Station 111 pressure gage positions -----	109
2.36	Predicted and actual pressure-time loading curves, Positions 24, 27, and 28 -----	110
2.37	Predicted and actual pressure-time loading curves, Positions 1, 9, and 15-----	111
2.38	Predicted and actual pressure-time loading curves, Positions 34, 44, and 50 -----	112
2.39	Dynamic and side-on record from Station 156.01 -----	113
2.40	Pressure versus range for Shot Yuma (BRL)-----	113
2.41	Overpressure versus range for Shot Yuma scaled to 1 kt and compared to Shot 4 of Operation Tumbler and Shot 3 of Operation Upshot-Knothole -----	114
2.42	Crater resulting from Shot Lacrosse -----	115
2.43	Crater radius versus burst position-----	116
2.44	Theoretical water-crater radius -----	117
2.45	First to second crest wave lengths versus range -----	118
2.46	Inundation effects on Site Nan following Shot Navajo -----	119
2.47	Predicted wave height versus range as a function of effective yield for surface shots over an atoll -----	120
2.48	Free-air overpressure versus slant range data, scaled to 1 kt at sea level -----	121
2.49	Surface peak overpressure versus range, scaled to 1 kt at sea level and compared with BRL ideal curve -----	121
2.50	Surface pressure-distance data scaled to 1 kt at sea level -----	122
2.51	Composite plot of time-of-arrival data from Operation Redwing scaled to 1 kt -----	123
2.52	Composite surface burst curve for Shots Lacrosse and Zuni-----	124
2.53	Comparison of composite surface burst curve for 1 kt with 1.6W free-air curve -----	125
3.1	Granville S. Hall (YAG-39) -----	150
3.2	Project 2.65 helicopter probe survey technique -----	151
3.3	Project 2.61 ASP rocket on launcher -----	152
3.4	Contours on D + 1 day at 3 feet above surface, Shot Flathead-----	152
3.5	Contours on D + 1 day at 3 feet above surface, Shot Navajo -----	153
3.6	Contours on D + 1 day at 3 feet above surface, Shot Tewa -----	153
3.7	Contours on D + 1 day at 3 feet above surface, Shot Zuni-----	154
3.8	Diagram of conversion factors -----	154

3.9	H + 1 hour contour locations decayed to D + 1 day at 3 feet above surface, Shot Zuni -----	155
3.10	H + 1 hour contour locations decayed to D + 1 day at 3 feet above surface, Shot Tewa-----	155
3.11	H + 1 hour contour locations decayed to D + 1 day at 3 feet above surface, Shot Navajo-----	156
3.12	H + 1 hour contour locations decayed to D + 1 day at 3 feet above surface, Shot Flathead -----	156
3.13	Accumulated dose (time of arrival to H + 50), Shot Zuni -----	157
3.14	Accumulated dose (time of arrival to H + 50), Shot Flathead -----	158
3.15	Accumulated dose (time of arrival to H + 50), Shot Navajo-----	159
3.16	Accumulated dose (time of arrival to H + 50), Shot Tewa -----	160
3.17	Areas of dose rate contours for Redwing shots normalized to 5-Mt 100-percent fission yield -----	161
3.18	Aerial survey readings at 3 feet, corrected to H + 1 hour in r/hr and dose rate contours, Shot Zuni -----	162
3.19	Aerial survey readings at 3 feet, corrected to H + 1 hour in r/hr and dose rate contours, Shot Tewa -----	162
3.20	Aerial survey readings at 3 feet, corrected to H + 1 hour in r/hr and dose rate contours, Shot Navajo-----	163
3.21	Aerial survey readings at 3 feet, corrected to H + 1 hour in r/hr and dose rate contours, Shot Flathead -----	163
3.22	Aerial survey reading at 3 feet on Site Yvonne after Shot Lacrosse, corrected to H + 1 hour in r/hr-----	164
3.23	Aerial survey readings at 3 feet in the vicinity of the Shot Mohawk crater, corrected to H + 1 hour in r/hr -----	164
3.24	Rates of arrival at major stations, Shot Flathead-----	165
3.25	Rates of arrival at major stations, Shot Tewa -----	165
3.26	Predicted and observed fallout pattern, Shot Zuni -----	167
3.27	Predicted and observed fallout pattern, Shot Tewa -----	168
3.28	Predicted and observed fallout pattern, Shot Navajo -----	169
3.29	Predicted and observed fallout pattern, Shot Flathead-----	170
3.30	Cloud model for fallout prediction -----	171
3.31	Trajectories of ASP rockets (mark on trajectories in 10-second intervals)-----	172
3.32	Activity distribution in the plane of rocket trajectories 7 minutes after Shot Zuni-----	173
3.33	Activity distribution in the plane of rocket trajectories 15 minutes after Shot Zuni-----	173
3.34	Shielded initial exposure rate within blast shield versus time for Shot Navajo-----	174
3.35	Initial gamma exposure versus distance for Shots Tewa, Navajo, Dakota, and Flathead-----	175
3.36	Dose per unit yield versus slant range for Operation Redwing shots with comparison to predicted values and previously detonated devices-----	176

4.1	Air view of structures on manmade Island 2, before Cherokee (looking toward Site Dog) -----	182
4.2	Air view of structures on manmade Island 2, after Cherokee (looking toward Site Dog) -----	182
4.3	Location of structures with reference to intended and actual ground zeros with orientation angles-----	183
7.1	Pulse-return phenomenon, Shot Zuni-----	214
7.2	Yield in kilotons versus first crossover point in micro- seconds -----	215
7.3	Shot Dakota waveforms -----	216
7.4	Typical attenuation (9,450 Mc) versus time, as determined from oscilloscope recording, Shot Blackfoot -----	216
8.1	Total thermal power versus time, Shot Lacrosse -----	227
8.2	Total thermal power versus time, Shot Cherokee-----	227
8.3	Total thermal power versus time, Shot Zuni-----	228
8.4	Temperature versus time, Shot Lacrosse, Site Wilma -----	228
8.5	Temperature versus time, Shot Cherokee, Site George -----	229
8.6	Temperature versus time, Shot Zuni, Site Nan, 42-foot tower -----	229
8.7	Irradiance versus time for total Zuni pulse, as recorded at Site Nan -----	230
8.8	Spectral distribution of the irradiance at the second maximum for Shot Zuni -----	230
8.9	Shot Lacrosse fireball radius versus time -----	231
8.10	Shot Cherokee fireball radius versus time -----	231
8.11	Shot Zuni fireball radius versus time -----	232
8.12	Shot Zuni from Site Nan at 1.95 seconds -----	232
8.13	Specimen array at Project 8.4 test site-----	233
8.14	Calculated irradiance at test site-----	233
8.15	Exposed facing temperature-time histories of GLM specimen with 0.016-inch white-painted skin -----	234
8.16	Exposed facing temperature-time histories of NAA specimen with $\frac{1}{8}$ -inch cell size and 0.016-inch white-painted skin -----	234
8.17	Relative spectral distribution of irradiance at t_{max_2} , Shot Zuni, Site Nan, composite, Project 8.1-----	235
8.18	Time to second maximum versus wavelength, Shot Lacrosse, P2V-2 airborne station, Project 8.5 -----	235
8.19	Time to second maximum versus wavelength, Shot Zuni, P2V-2 airborne station, Project 8.5 -----	236
8.20	Time to second maximum versus wavelength, Shot Erie, P2V-2 airborne station, Project 8.5 -----	236
9.1	Altitude above burst point of top and bottom of stabilized cloud versus weapon yield -----	239

Chapter 1

INTRODUCTION

1.1 BACKGROUND

In a letter dated 28 February 1955, Headquarters, Armed Forces Special Weapons Project (AFSWP), advised the services that Operation Redwing was scheduled to commence in the spring of 1956 and invited proposals for experiments, measurements, and tests.

After review and coordination of the proposals, an outline for the Redwing Weapons Effects Programs for 13 shots and an initial budget of \$15,385,350 were submitted to the Assistant Secretary of Defense for Research and Development on 29 June 1955 and were approved on 14 July 1955. The Joint Chiefs of Staff, on 18 July 1955, approved the incorporation of military-effect programs in Operation Redwing.

On 5 August 1955, the Chief, AFSWP, in a letter to the Commander, Field Command, AFSWP, directed the implementation of the military-effect programs of Operation Redwing. This was followed by a letter from the Chief, AFSWP, dated 18 August 1955, to the participating agencies, outlining certain policies and procedures essential to the successful execution of the Redwing military-effect programs.

As planning progressed, the number of shots in the series was increased from 13 to 17. Some new projects were added, and a few were deleted. The Redwing series was begun on 5 May 1956 when Shot Lacrosse was detonated on Site Yvonne, Eniwetok Atoll.

1.2 OBJECTIVES

All of the 17 devices detonated were basically developmental in character, Shot Cherokee was included in order to obtain basic military-effect and fallout data from a high-yield airburst over land. It also provided the first opportunity for the Air Force to study delivery technique of a multimegaton weapon.

There was one air drop in addition to Cherokee. Of the other devices, six were detonated on 200- or 300-foot towers, five on barges on the surface of the water, three on limited land surfaces, and one on a barge in shallow water over the reef. No underwater or underground bursts were planned for this operation. It was around the above family of devices and their detonation environments that the military-effect programs were formulated.

One of the significant design features of several of the large-yield devices This was in contrast to the multimegaton devices of Operation Castle,

One of the fundamental considerations in planning the technical programs for Redwing was the inclusion of projects to obtain data for which there was an urgent military need

and which could not be obtained with devices of smaller yields at the Nevada Test Site (NTS).

Program 1 (Blast Effects) was designed to establish the basic blast and shock phenomenology of specific shots in various environments. This was to be accomplished by measuring various blast-wave parameters in free air and along the surface.

Program 2 (Nuclear Radiation) represented the largest effort that had ever been expended for this program to date. The Redwing program was highlighted by a concerted effort to establish fallout contours and to obtain data on the mechanism of fallout. This increased effort evolved from the results of Shot 1 during Operation Castle, which clearly indicated the tremendous scope of the fallout hazard. The program in Redwing was designed to obtain complete data in the areas affected and to assist in the construction of a realistic fallout model that would permit extrapolation to different devices, burst heights, and surface conditions. In addition, a number of projects involving decontamination and nuclear-radiation countermeasures were included to close existing gaps in the knowledge of techniques to combat the fallout hazard. Finally, certain projects to study initial gamma and neutron radiations were included to obtain data in areas where existing knowledge was considered unreliable or incomplete.

Program 3 (Effects on Structures) was chiefly concerned with checking the effect of blast positive-phase duration of multimegaton devices on structural response. The response to blasts of short-duration positive phase had already been studied during Operation Teapot. There were a number of questions regarding the applicability of a simplified mathematical model to the load-duration problem where the particular model was considered a mass-spring system with one degree of freedom.

Program 4 (Biological Effects) consisted of one project that called for exposing animals to study chorioretinal burns.

Program 5 (Effects on Aircraft Structures) was primarily designed to make certain that the current weapon-delivery criteria were reliable and that the maximum delivery capability of the aircraft was correctly defined. Calculations indicated that, for large-yield devices, the delivery capability of aircraft was limited by thermal effects. A secondary objective consisted of the collection of basic input and response data for use in the theoretical analyses of the delivery capability of other aircraft types.

Program 6 (Studies of Electromagnetic Effects) placed emphasis on studying long-range detection of nuclear explosions, utilizing the electromagnetic signal. An additional objective was the study of the effects of nuclear explosions on the ionosphere and the attenuation of super-high-frequency (SHF) and ultra-high-frequency (UHF) radio waves in highly ionized regions.

Program 8 (Thermal Radiation and Effects) had a primary objective of documenting, as completely as possible, the thermal phenomenology associated with a multimegaton airburst. The secondary objective covered the collection of data on thermal phenomenology and thermal effects on materials on several of the other shots.

Program 9 (Supporting Photography) had the mission of documenting photographically the history of the nuclear cloud and supplying technical and documentary photographic coverage to essentially every project in the military-effect programs.

1.3 SUMMARY OF SHOT DATA

Table 1.1 gives yields and certain environmental data at the time of firing. The yields given in the table are the latest available at the time of publication of this report.

1.4 PARTICIPATION

Table 1.2 indicates the shots on which each project actually participated. In some cases this varied from planned participation, because of such factors as instrumentation difficulties at the time of a particular shot and changes in yield or firing schedule that would make participation on a different shot more desirable.

1.5 ORGANIZATION

A memorandum from the Joint Chiefs of Staff, dated 24 April 1953, directed the Chief, AFSWP, to exercise (within any task force organization) technical direction of weapon-effect tests of primary concern to the Armed Forces. Based on a directive to implement the military-effect programs from the Chief, AFSWP, to the Commander, Field Command, AFSWP, on 5 August 1955, the preoperational phase of Operation Redwing was executed by the Commander, Field Command, through the staff office of the Deputy Chief of Staff for Weapons Effects Tests (FCWT). Figure 1.1 shows the organization of this office.

In early January 1956, personnel began to arrive in the forward area to make preparations for the military-effect programs.

On 12 March, the Deputy Chief of Staff for Weapons Effects Tests and his Technical Director and Test Division Director, departed for the Pacific Proving Grounds (PPG). It was at this time that the military-effect programs entered the operational phase and were integrated into the organization of Joint Task Force 7 (Figure 1.2). The military-effect programs were organized as Task Unit 3 (TU-3) under Task Group 7.1 (TG-7.1). While at the PPG, the Commander JTF-7, through CTU-3, exercised operational control over all personnel associated with the Department of Defense (DOD) weapon-effect programs and the equipment and material in their possession. The Chief, AFSWP, retained technical direction of these programs during the operational phase. The dotted lines on the chart indicate the channels for this direction.

The organization of TU-3 is shown in Figure 1.3; it was activated on 16 March and deactivated on 10 August when the operational phase of Redwing ended.

1.6 PERSONNEL

It was considered advisable for the Personnel Officer from the Support Division, FCWT, to augment the TG-7.1 Staff as an Assistant Adjutant General at an appropriate time, primarily for the issuance of overseas travel orders, inasmuch as the plans and problems of TU-3 personnel (approximately half of TG-7.1) were more familiar to FCWT. All administrative procedures relative to requests for orders from DOD agencies were processed through FCWT and coordinated with Program Directors and the FCWT Security Officer prior to forwarding to TG-7.1 for issuance of orders. Requests for travel orders for TU-3 personnel continued to be processed through FCWT at Sandia Base, New Mexico, even after TU-3 was activated at the PPG. Figure 1.4 shows the TU-3 personnel strength as a function of time during the Redwing operational phase.

1.7 ADMINISTRATION

The Administrative Section of TU-3 maintained offices at Eniwetok and Bikini. Each office provided the following services for those TU-3 personnel on its respective atoll: (1) distribution of official and personal mail with related systems for suspense files,

locator files, and correspondence logs; (2) maintenance of TU-3 central files; (3) maintenance and supervision of the control and receipt system for classified documents; (4) processing of outgoing correspondence; (5) mustering of personnel; (6) assistance in the preparation and dissemination of administrative practices directed by higher headquarters; and (7) assistance in correspondence of service members with their parent organizations on military matters.

Headquarters TG-7.1, assisted by TU-3 personnel, prepared per diem vouchers for TG-7.1 as a whole.

The volume of the above activities was consistently large; in most instances, personnel, time, and working facilities were limited.

1.8 SECURITY AND CLASSIFICATION

During Operation Redwing, the TU-3 Security and Classification Officer assumed only certain aspects of the overall security function. These were mainly security liaison, the operation of the personnel security-clearance system for TU-3 personnel, the operation of the badge-request system for TU-3 personnel, and miscellaneous functions such as control of contraband. The remainder of the security function was retained by FCWT in the CONUS or assumed by other Task Groups. All physical security functions were the responsibility of TG-7.3 and TG-7.5, while CTG-7.1 exercised command security responsibility for TU-3.

A TG-7.1 and TU-3 Joint Classification Office was established. Upon the departure of JTF-7 and TG-7.1 classification personnel, the TU-3 Classification Officer assumed all classification functions at the PPG.

The organizational and operational arrangements of both the Security and Classification Offices were satisfactory and proved to be a decided advantage in accomplishing the overall mission of TU-3.

1.9 OPERATIONS

During the planning stage, the Operations Branch, FCWT, was primarily involved in coordinating and publishing general planning information for the projects and in coordinating operational requirements. Monthly consolidations of requirements were prepared for forwarding to Chief, AFSWP, CJTF-7, and CTG-7.1. Included were summaries of requirements involving ships, aircraft, sample-return flights, timing signals, navigational aids, and the like. Information on requirements was extracted from project status reports and this, with Castle experience, formed the basis of Redwing operational planning.

A Concept of Operations was published by CTG-7.1 on 12 April 1955, and it appeared that a TG-7.1 Operation Plan would not be available until shortly before some TU-3 projects were due to move to the PPG. In order to give projects some guidance on operational matters, a FCWT Planning Directive was published 26 September 1955. Although a number of changes were necessary, it served its purpose as a planning aid and was canceled upon publication of the TG-7.1 Operation Plan on 20 February 1956 and the TU-3 Administrative Plan on 15 February 1956.

In the field, the program officers did a large part of the operations work. The Operations Section within TU-3 assisted as requested, published information as necessary, and coordinated matters affecting more than one program. At Eniwetok, the project and program personnel usually placed their requirements for transportation and similar support directly with the J-3 section of TG-7.1. The Operations Officer with the TU-3

element on Bikini received all requests and relayed them to the J-3 office at Bikini.

1.10 COMMUNICATIONS AND ELECTRONICS

Coordination of communications and electronics matters pertaining to participation by the military-effect programs in the operation was a function of the TU-3 Operations Section, and one officer was assigned for this purpose.

Radio-frequency requirements, changes, and operational use were coordinated with JTF-7 through TG-7.1. TG-7.5 (AEC) provided and maintained basic interatoll and intra-atoll communication systems through its contractor organization.

At Eniwetok Atoll, the interisland telephone system was extensive enough so that only one base radio station and two portable units were maintained for TU-3 emergency communication. A separate net was provided for Program 2, because many surface vessels were involved and buoy cable facilities in the lagoon were limited and normally used only by major surface vessels.

At Bikini Atoll, a limited interisland telephone system necessitated the establishment of three separate radio nets. The TU-3 organization at Bikini utilized 9 base radio stations and 12 portable radio units. The Raydist positioning and tracking system utilized 5 base stations. Program 2 utilized 3 base stations, in addition to units installed aboard vessels operating in the program. The 12 portable radio units were controlled by TU-3 and assigned generally on a daily basis as required. The equipment used in these nets could be manually tuned and proved extremely flexible in operation.

Primary positioning and tracking of effects aircraft was accomplished by the use of Raydist navigation systems at Bikini and AN/MSQ-1A radar systems at Eniwetok.

The Air Task Group (TG-7.4) provided an air traffic control system consisting of radar and communications facilities at Eniwetok Island. The Air Operations Center (AOC) provided a secondary positioning system for effects aircraft and, in event of emergency, could take control of any aircraft participating in a particular event. This task group also provided all navigational aids required for the operation.

The JTF-7 Message Center facilities were utilized for traffic to Wotho, Kusaie, and Rongerik Atolls, when project stations had to be informed of shot alerts, delays, and cancellations.

1.11 TIMING SIGNALS

The TU-3 Electronics Staff Officer was responsible for the implementation of all timing signal requirements of the DOD projects. During the Redwing planning phase, the consolidated requirements for timing signals, after being reviewed, were forwarded through Requirements to the J-6 Section at Los Alamos. Holmes and Narver (H&N), an AEC civilian contractor, was charged by J-6 with laying the necessary wire. Another civilian contractor, Edgerton, Germeshausen, and Grier (EG&G), provided timing relays, made the required connections, and operated the timing system.

At the peak period of the operation (during Shot Cherokee), 26 hardwire timing signals and 10 radio timing signals were supplied to DOD stations. In addition, EG&G supplied the DOD projects with 44 blueboxes (timing relays) for activating the instrumentation.

Timing-signal dry runs were normally held twice daily. The last scheduled dry run usually occurred at 1500 hours on D-2 days for Bikini Atoll and 1000 hours on D-1 day for Eniwetok Atoll. However, for successive days that were designated either as D-2 or D-1, it became the practice to hold timing-signal dry runs at 1000 hours every other day.

The installation of the required wire and the checkout of the timing signal system proved to be one of the critical factors in the overall readiness for Shot Cherokee.

Although the use of radio timing signals in certain areas was less costly and more easily installed, the hardwire timing signals were more reliable.

1.12 LOGISTIC SUPPORT

The preparatory phase of logistic planning and support for the military-effect programs was accomplished by the Support Division, FCWT, and began in the spring of 1955. All participating agencies were advised of the supply and transportation limitations of a PPG operation. The preparatory phase required a monthly compilation of the support requirements, which the projects submitted in periodic status reports. Requirements for items such as vehicles, furniture, surface and air transportation, and special items were coordinated with TG-7.1. The requirements were screened, and consolidations were forwarded to CTG-7.1.

During the latter part of the preparatory phase and during the entire operational phase at the PPG, a Logistic Officer from the Support Division, FCWT, was assigned to the J-4 section of TG-7.1 as Military Property Officer. The Support Division maintained liaison in the ZI for TU-3 on property, fiscal, personnel, and related matters.

1.13 CONSTRUCTION

Early in April 1955, Headquarters AFSWP requested all approved Redwing projects to submit field construction requirements as soon as possible. The deadline for submission of the requirements was 1 May. Because many of the agencies approved for participation in Redwing were then engaged in Operation Teapot, very few construction requirements were submitted prior to 1 July. The bulk of the requirements were received and passed to the Architect-Engineer (H&N) during the period July through October 1955. These late submissions of construction requirements, coupled with the Architect-Engineer's subsequent delays in turning out preliminary and final design drawings, gave rise to many of the later difficulties in meeting test schedules.

During May 1955, a liaison officer from FCWT was assigned to the J-6 office of TG-7.1 at Los Alamos to expedite the handling of the DOD construction and other requirements. This arrangement continued until the departure of the TG-7.1 staff to the PPG.

Upon arrival of the FCWT (TU-3) personnel at the PPG, it was found that generally the test and support construction was from 4 to 6 weeks behind the desired progress schedule. Although the construction was eventually completed in time for scheduled shots, the deviations from the desired schedules did not permit early occupancy of test stations, for dry runs and testing of signal, recording, and operational procedures.

The construction costs of test structures and facilities, cumulative to 31 August 1956, totaled approximately \$1,139,000. Costs of support-type work orders issued in the PPG totaled approximately \$547,000. Costs of photography and timing signals was approximately \$458,000.

1.14 FISCAL

The original Redwing research and development (R&D) budget totaled \$15,385,350 when presented to the Assistant Secretary of Defense (R&D) by the Chief, AFSWP. It was computed from budgets submitted by the projects within the DOD in the early spring of

1955. The Chief proposed that funds in the amount of \$10,400,000 be furnished by AFSWP and \$4,985,350 be furnished by the three services. This budget was approved, and the control of funds was transferred to FCWT on 31 August 1955.

On 5 September 1955, all approved projects were requested to submit current budgets in order that a realistic total budget could be computed. These revised budgets requested additional funds amounting to \$3,040,000. Meetings between representatives of Headquarters AFSWP, the project agencies, and Field Command AFSWP, resulted in the reduction of this figure to \$1,800,000. A revised budget incorporating these increases was approved by the Chief, AFSWP and Secretary of Defense (R&D) in the spring of 1956, and the actual funds were received in May 1956. In general, the revised budget took into account the increased estimates of construction costs at the PPG, increased shipyard costs, increased costs of contracts with Scripps Institution of Oceanography and Horning-Copper, Inc., and participation by some projects on additional shots.

Table 1.3 shows the 5 October 1955 budget compared with the 5 September 1956 budget and in the last column, the AFSWP total costs as of 1 July 1959. The actual charges to AFSWP funds were well within the approved budget.

1.15 REPORTS

The TU-3 reports staff was responsible for reviewing certain aspects of the overall technical content of each Redwing preliminary report (ITR) and for detailed editing for organization, printing style, spelling, and grammar. Ordinarily, no attempt was made to rewrite reports or influence the overall literary style of the author. The illustrations were reviewed and, in certain cases, redone in the field.

Each edited draft was returned to the appropriate program and project for approval and then transmitted to CTU-3 and to the DOD Deputy Commander, TG-7.1. Upon the latter's approval, the manuscript was prepared by the reports staff for transmission to FCWT, where the actual camera copy was typed and finished artwork was prepared or completed.

The work included the processing of 41 ITR reports, some initial administration and consultation with authors on 13 additional ITR's (which were scheduled for submission to FCWT after rollup at the PPG), preparation and editorial processing of some DOD sections of the Summary Report of the Commander, Task Group 7.1, and collection and processing of individual DOD research project reports for each shot summary (published in each case by the laboratory responsible for the shot).

The final (WT) reports of the TU-3 projects were prepared by project personnel at the home agencies and sent to FCWT for processing, which included technical and editorial review. Manuscript copies of each final report were also sent to the Chief, AFSWP, for technical comments, which were consolidated with the Program Director's and editor's comments at FCWT and sent to the project agencies for revision of the report. The processing of the revised draft for printing was performed in FCWT. Actual presswork, binding, and distribution of the printed reports, both preliminary and final, was performed by the Technical Information Service Extension, AEC, Oak Ridge, Tennessee—the official printer of all reports in the weapon test series.

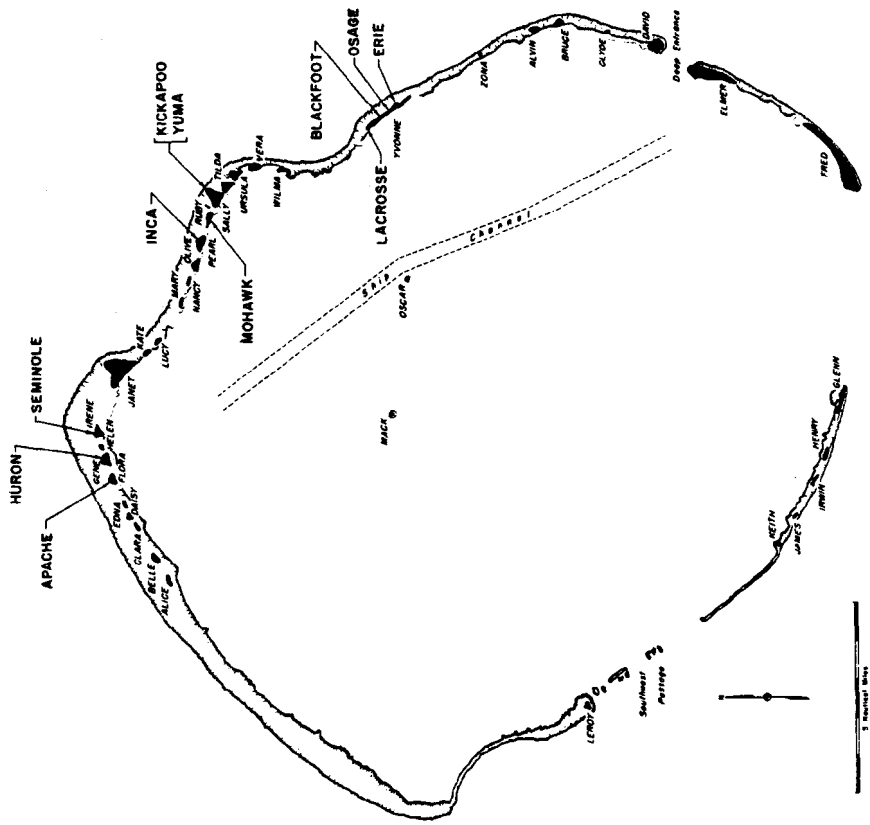
TABLE 1.1 SUMMARY OF SHOT DATA

Code Name	Lacrosse	Cherokee	Zuni	Yuma	Eric	Seminole	Flathead	Blackfoot	Kickapoo	Osgar	Inca	Dakota	Mohawk	Apache	Navajo	Tewa	Huron	
Sponsor	LASL	LASL-DOD	UCRL	UCRL	LASL	LASL	LASL	LASL	UCRL	LASL	UCRL	LASL	UCRL	UCRL	LASL	UCRL	LASL	
Date (P/O) 1948	5 May	21 May	28 May	28 May	31 May	6 June	12 June	12 June	14 June	15 June	22 June	26 June	3 July	9 July	11 July	21 July	22 July	
World Time*	0550:38:487	0550:38:487	0556:00:392	0754:00:486	0815:39:304	1253:30:292	0624:00:131	0626:00:256	1135:00:352	1313:53:049	0504:00:238	0604:00:246	0606:00:357	0606:00:232	0556:00:037	0545:00:015	0616:00:081	
Total Yield (Hydrodynamic)	39.5 ± 3 M		3.38 ± 0.17 Ml													4.6 ± 0.2 Ml		
Range-Zone (Radar/Watch)																		
Total Recommended Yield																		
Zero-Bolt Location																		
Atcl	Eniwetok	Bikini	Bikini	Eniwetok	Eniwetok	Eniwetok	Eniwetok	Eniwetok	Eniwetok	Eniwetok	Eniwetok	Eniwetok	Eniwetok	Eniwetok	Eniwetok	Bikini	Eniwetok	
Site	Yome	Off Charlie	Taro	Yome	Off Dog	Yome	Yome	Yome	Sally	Yome	Pearl	Off Dog	Ruby	Eniwetok	Off Dog	Charlie-Dog Reef	Eniwetok	
Station Number	144814 E	88200 ± 100 E	110295 E	110152 E	116708 E	116708 E	116708 E	116708 E	116708 E	116708 E	116708 E	116708 E	116708 E	116708 E	116708 E	116708 E	116708 E	116708 E
HN	106885 N	195100 ± 500 N	100154 N	132494 N	164044 N	164044 N	164044 N	164044 N	132228 N	132228 N	132494 N	132228 N	132494 N	132494 N	132494 N	132494 N	132494 N	132494 N
Geographic Coordinates	11°33'59"N	11°33'59"N	11°29'45"N	11°37'47"N	11°37'47"N	11°37'47"N	11°37'47"N	11°37'47"N	11°37'47"N	11°37'47"N	11°37'47"N	11°37'47"N	11°37'47"N	11°37'47"N	11°37'47"N	11°37'47"N	11°37'47"N	11°37'47"N
Coordinates	162°21'18"E	169°34'46"E	165°22'09"E	162°14'37"E	162°14'37"E	162°14'37"E	162°14'37"E	162°14'37"E	162°14'37"E	162°14'37"E	162°14'37"E	162°14'37"E	162°14'37"E	162°14'37"E	162°14'37"E	162°14'37"E	162°14'37"E	162°14'37"E
Height of Burst, feet	17	4,326 ± 150	9	200	200	200	200	200	300	200	200	200	300	200	200	200	200	200
Tide at Zero Time †	2.2	2.3	5.9	2.7	3.6	3.4	4.6	4.6	2.5	2.6	1.1	5.5	2.0	4.6	6.0	2.7	3.4	3.4
Dew Point, °F	77.0	75.0	75.0	75.0	75.0	75.0	75.0	75.0	75.0	75.0	75.0	75.0	75.0	75.0	75.0	75.0	75.0	75.0
Sea-Level Pressure at Ground Zero, mb	1,008.5	1,009.0	1,010.5	1,010.2	1,009.1	1,010.5	1,012.9	1,012.5	1,009.8	1,006.5	1,009.8	1,009.1	1,010.2	1,010.5	1,010.2	1,009.3	1,007.8	1,007.8
Surface-Air Temperature, °F	81	81	81	81.7	82.0	81.1	81.1	81.1	85.6	85.9	83.3	82	79.6	80.3	81.2	82.0	81.4	81.4
Surface Relative Humidity, pct	84	76	80	80	84.0	84.0	84.0	84.0	71	74	81	80	81	84	80	85	84	84
Surface Wind Direction, deg	080	140	090	080	050	075	075	075	090	140	130	070	100	030	090	110	090	090
Surface Wind Velocity, knots	19	10	12	18	12	11	10 to 14	10 to 14	6	11	11	14	16	15	8	8	17	17
Visibility, miles	>10	>10	8	10	>10	>10	10	10	10	10	>10	>10	10	>10	10	>10	10	10

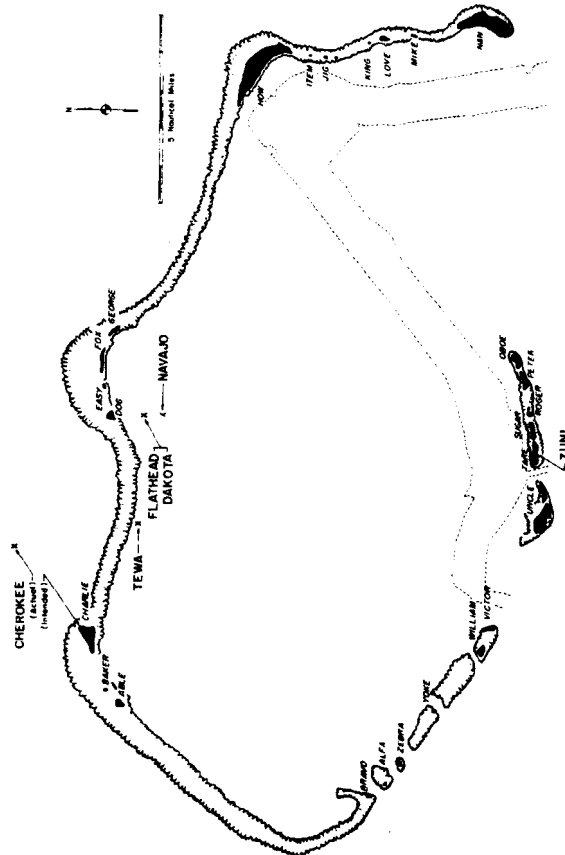
* Station WWVH, not corrected for delay in transmission. † World time clock not operative. ‡ Water-tank zero point caused large uncertainty in hydrodynamic yield determination. § Enclosed ground zero. ¶ Datum, 6 inches below mean low-water spring tides.

2

TABLE 1.1 CONTINUED



Araaburu	Vera	Chintero	Alvin	Igrin	Olema	James
Alisu	Otte	Chintini	Clyde	Japian	David	Leroy
Aniyaniil	Bruce	Cochita	Daisy	Arimlan	Lacy	Urella
Amon	Sally	Coral Heads	Macl, Oscar	"M"	Zona	Clara
Biljiri	Thida	Eberiah	Ruby	Mal	Henry	Pearl
Bogairik	Helen	Eugeiab	Flora	Maun	Kate	Fyome
Bogallua	Alice	Zugel	Janet	Perry	Eimer	Zona
Bogombogo	Belle	Eniwetok	Fred	Pirral	Wilma	Gane
Bogom	Irene	Grimlin	Keith	Potom	Irwin	Nancy
Bokomasarapu	Mary					



Airauji	Oboe	Bokasetohoku	Uncle	Enirikku	Enirikku	Alia
Airakiraru	Peter	Bokoyasada	Tare	Ezinman	Ezinman	Able
Aomon	George	Bokowejim	Nan	Ezyu	Nan	Baker
Arriban	Yoko	Bokontanaku	Mike	Ionchebi	Ionchebi	Bern
Bigiren	Roger	Bokoroyuru	Charley	Namu	Namu	Bravo
Bikini	How	Chieesete	Zebra	Ouruken	Ouruken	William
		Eniairo	Sugar	Reere	Reere	King

BIKINI ATOLL

ENIWETOK ATOLL

Locations of test detonations during Operation REDWING are indicated by large lettering and arrows. Native island names and corresponding military identifiers are given in the tabulations.

TABLE 1.2 PROJECT PARTICIPATION

Project	Bikini Events					Eniwetok Events							Project	Bikini Events					Eniwetok Events																
	Cherokee	Zuni	Flathead	Dakota	Apache	Navajo	Tewa	Lacrosse	Yuma	Eric	Seminole	Blackfoot		Kickapoo	Inca	Ojaga	Mohawk	Huron	Cherokee	Zuni	Flathead	Dakota	Apache	Navajo	Tewa	Lacrosse	Yuma	Eric	Seminole	Blackfoot	Kickapoo	Inca	Ojaga	Mohawk	Huron
1.1																																			
1.2																																			
1.3																																			
1.4																																			
1.5																																			
1.6																																			
1.8																																			
1.9																																			
1.10																																			
2.1																																			
2.2																																			
2.4																																			
2.51																																			
2.52																																			
2.61																																			
2.62																																			
2.63																																			
2.64																																			
2.65																																			
2.66																																			
2.71																																			
2.72																																			
2.8																																			
2.9																																			
2.10																																			
3.1																																			
4.1																																			
5.1																																			
5.2																																			
5.3																																			
5.4																																			
5.5																																			
5.6																																			
5.7																																			
5.8																																			
5.9																																			
6.1a																																			
6.1b																																			
6.3																																			
6.4																																			
6.5																																			
6.6																																			
8.1a																																			
8.1b																																			
8.1c																																			
8.2																																			
8.3																																			
8.4																																			
8.5																																			
9.1a, b																																			

☒ Indicates participation

TABLE 1.3 REDWING RESEARCH AND DEVELOPMENT BUDGET

Program	AFSWP Funds		Agency Funds		Total		Total AFSWP Costs
	Oct 55	Sep 56	Oct 55	Sep 56	Oct 55	Sep 56	1 Jul 59
1	\$ 1,079,400	\$ 1,030,135	None	None	\$ 1,079,400	\$ 1,030,135	\$ 902,126
2	2,760,950	4,152,381	None	\$ 502,859	2,760,950	4,655,240	3,624,654
3	876,000	967,471	None	None	876,000	967,471	700,070
4	24,000	24,000	\$ 30,000	30,000	54,000	54,000	23,923
5	2,896,550	3,455,415	3,161,500	3,781,750	6,058,050	7,237,165	2,338,384
6	200,000	210,000	1,735,700*	73,000	1,935,700	283,000	184,743
8	584,100	697,200	58,150	75,060	642,250	772,260	716,134
9	650,000	895,070	None	None	650,000	895,070	543,870
Total Program	\$ 9,071,000	\$11,431,672	\$4,935,350	\$4,462,669	\$14,056,350	\$15,894,341	\$9,033,904
F. O. Costs†	929,000	315,710	None	None	929,000	315,710	143,158
Delay Costs	355,000	396,795	None	None	355,000	396,795	—
Reports	45,000	85,000	None	None	45,000	85,000	9,487
Total Operation	\$10,400,000	\$12,229,177	\$4,985,350	\$4,462,669	\$15,385,350	\$16,691,846	\$9,186,549

* Not R&D funds. Later deleted and not reflected as FCWT-controlled funds in the 5 Sep 56 budget.

† Field Operation.

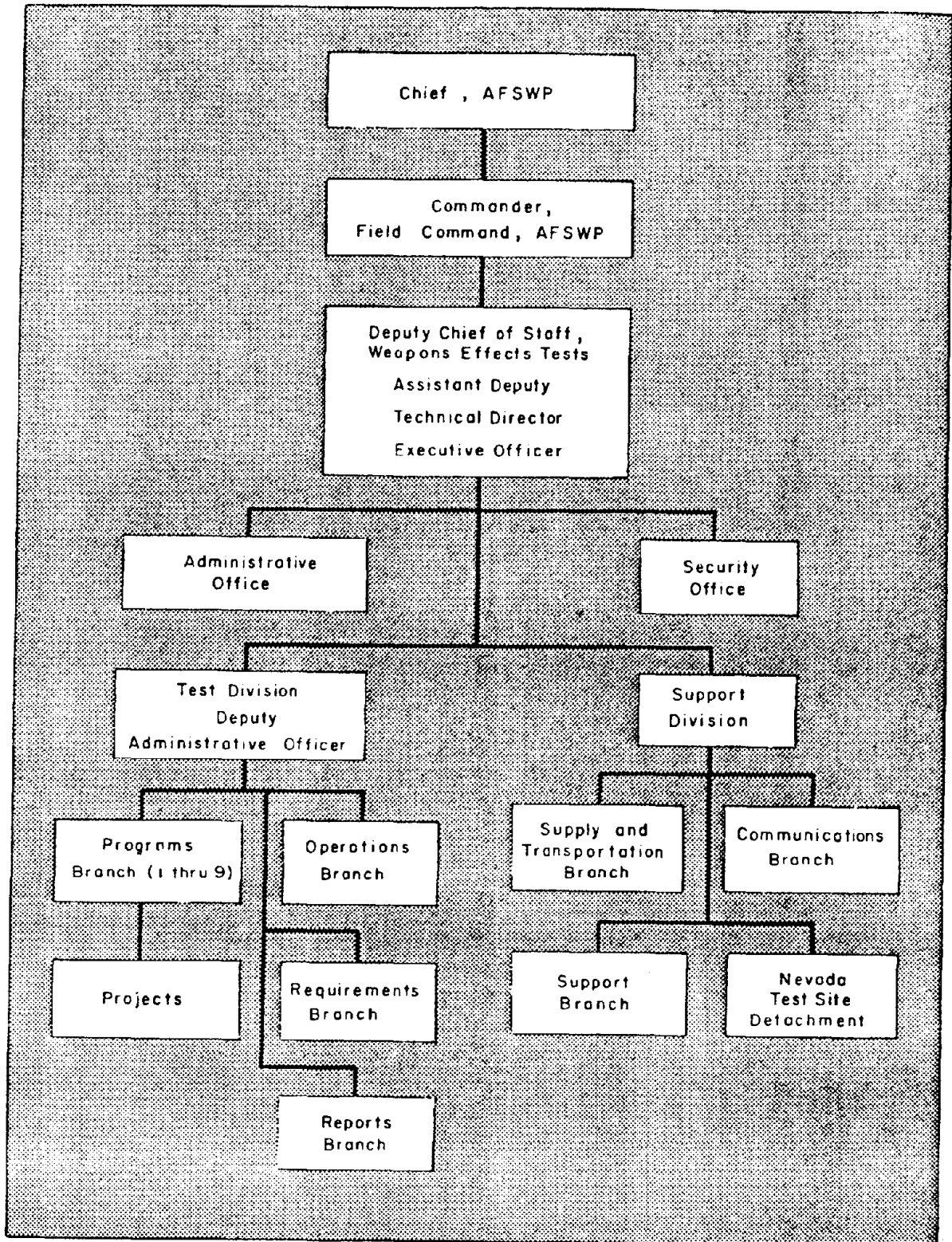


Figure 1.1 Organization of Office of Deputy Chief of Staff, Weapons Effects Tests.

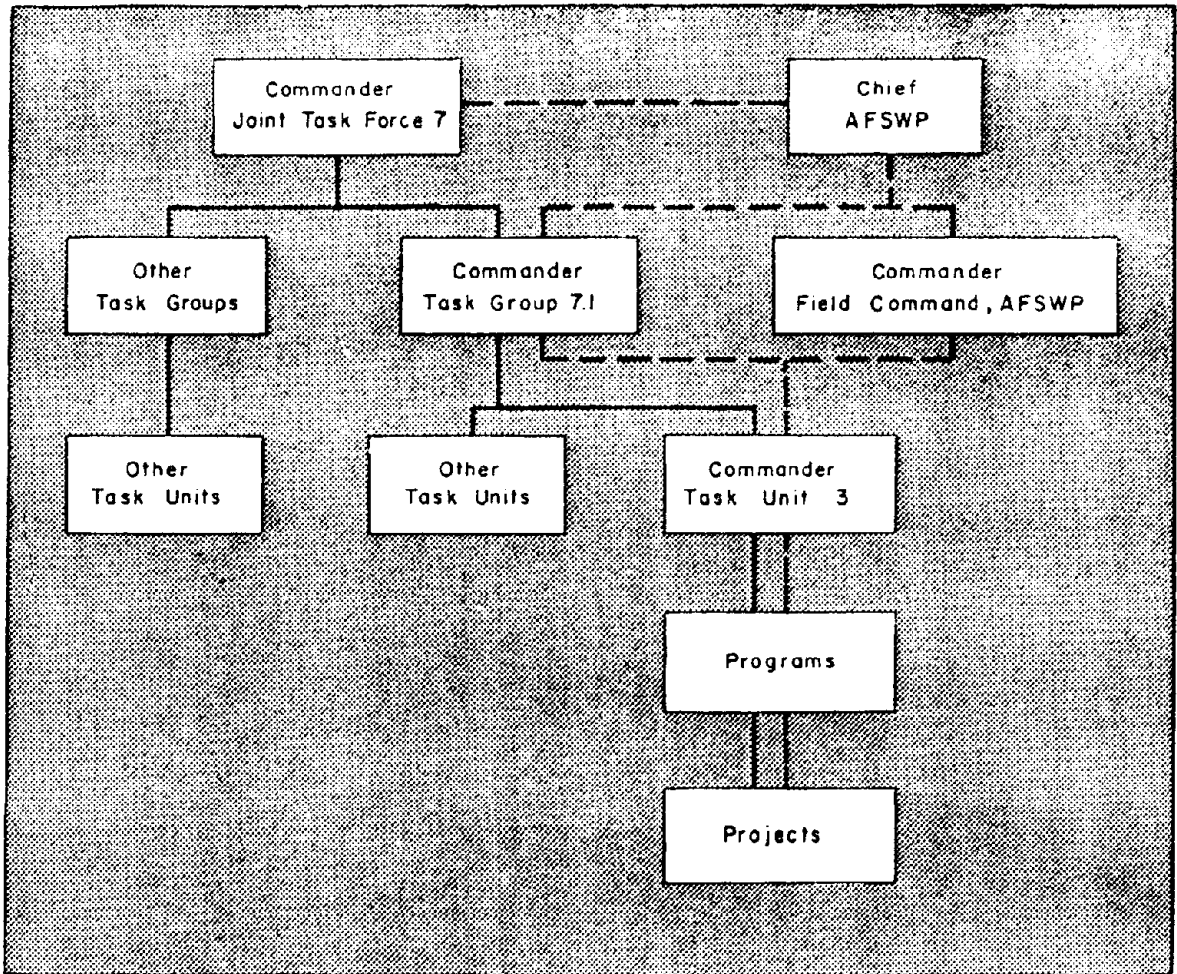


Figure 1.2 Organization of Joint Task Force 7.

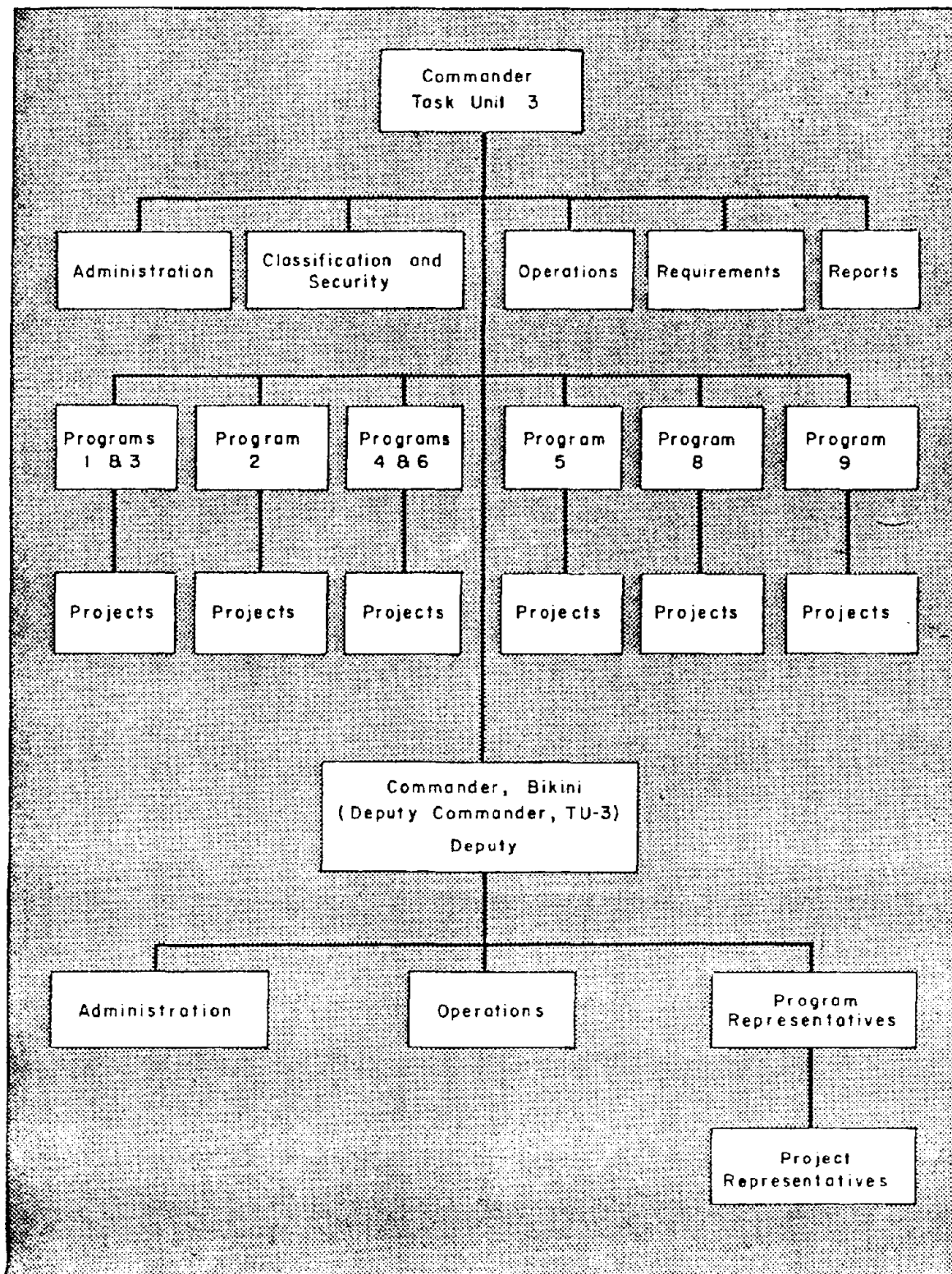


Figure 1.3 Organization of Task Unit 3.

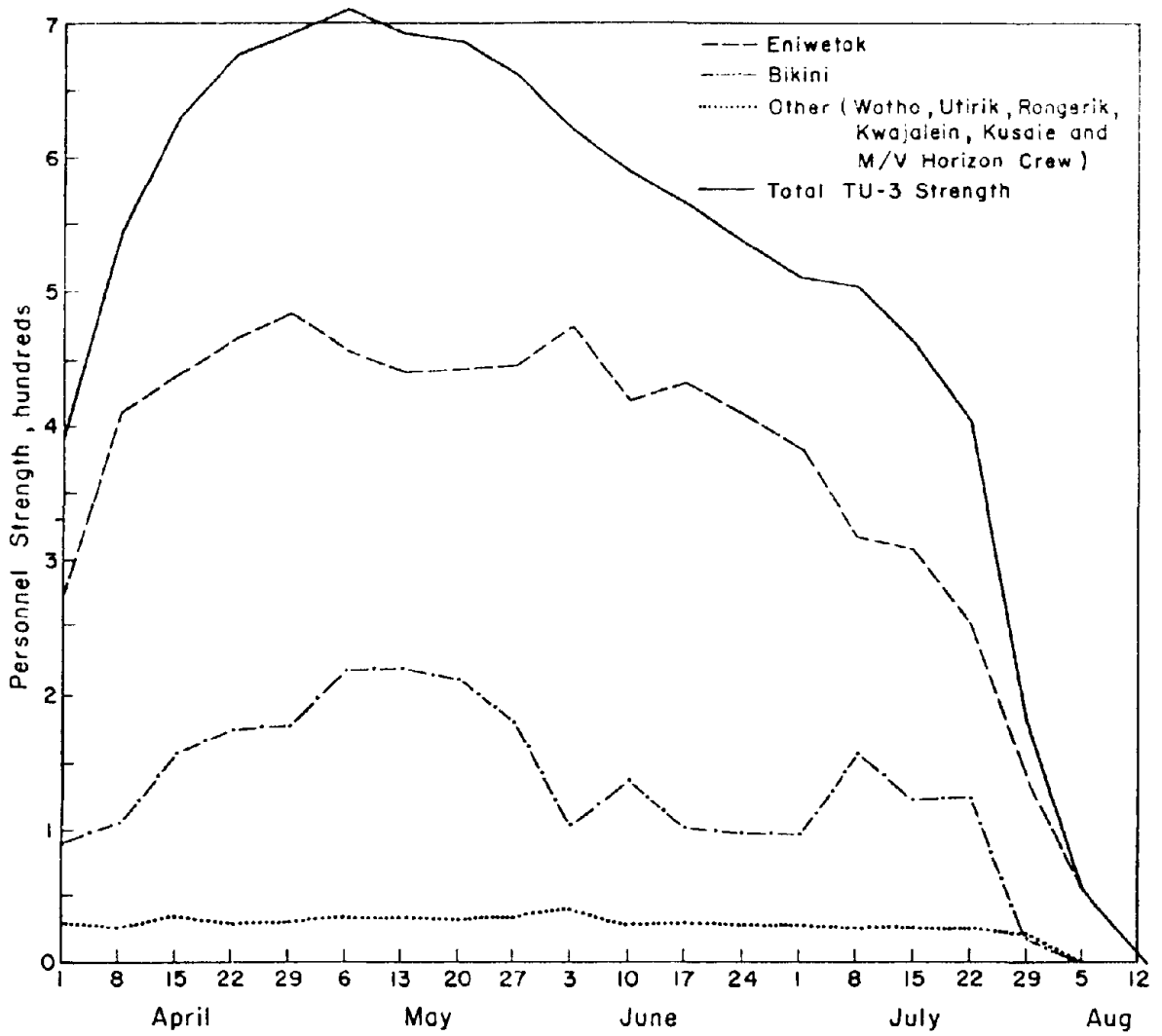


Figure 1.4 TU-3 Personnel Flow Chart.

Chapter 2

BLAST MEASUREMENTS

2.1 OBJECTIVES

The blast and shock projects conducted during Operation Redwing were designed to obtain data for which there was an urgent need and which for the most part could not be obtained at the Nevada Test Site (NTS). The greatest effort was planned toward establishing the basic blast phenomenology of a high-yield airburst by measuring various blast wave parameters in free air and along the surface, as well as determining the loading and response of various targets from a long-duration blast wave. The next most important task was to establish the basic blast phenomenology of a medium-yield land surface burst by similar means although in a less extensive manner.

It was recognized that neither of these tests were to be conducted under conditions representative of many target areas that would generally require a semi-infinite land mass. However, the safety requirements were such as to preclude such tests within the continental United States. Therefore, every effort was made to obtain representative effects data that could be applied to areas of more significant military interest.

It was realized that environmental conditions in the Pacific were such as to give rise to many difficult problems in making blast and shock measurements, such as the availability of suitable land areas, yield variation for developmental shots, weather delay, and wave action, as well as construction costs that made it necessary to use self-recording gages or existing shelters wherever possible, with a minimum of new construction. In general this philosophy governed the establishment of the overall objectives for the blast and shock projects of Operation Redwing, which are listed below. Justification of these major objectives was documented in Reference 7. These major objectives are related to specific shots in Section 2.2.

The principal objectives of the blast and shock measurements made by projects in Program 1 were as follows, listed in order of priority:

- a. Establish the basic phenomenology of a high-yield true airburst including blast wave propagation along the surface and in free air through a nonhomogeneous atmosphere.
- b. Establish the general phenomenology of a medium-yield land surface burst, including blast wave propagation along the surface and in free air, as well as damage to drag-sensitive targets.
- c. Continuation of the drag force gage development program and application to structural shapes over a wide yield range.
- d. Obtain data on blast wave parameters over a vegetated area for a precursor-forming tower shot.
- e. Measure apparent craters resulting from land surface bursts over a wide yield range.
- f. Determine basic blast phenomena from detonation of a fractional-kiloton device.
- g. Investigate water-wave generation and propagation from high-yield bursts.

In order to obtain data to satisfy these principal objectives, participation by various projects in Program 1 was therefore scheduled on one or more events on a priority basis.

A number of the events on which such participation was originally planned are discussed in the next section. As the operation developed, however, a number of changes were necessarily made in the field, because of changes in weapon design and configuration that would affect yields (usually based on information from earlier shots in the series), also the substitution, addition, or elimination of developmental shots for the same reason, as well as delays due to weather. Other delays resulted when devices were not ready on time. For some projects, then, additional participation was authorized on other events, depending on the availability of personnel and equipment as well as requirements for operational support. Participation over and above that required to insure maximum success in achieving the major objective of the project was approved only on a noninterference basis and at no additional cost, contingent upon the availability of suitable land areas and recording shelters if required.

The project abstracts are given in Section A.1 of the appendix.

2.2 BACKGROUND

2.2.1 High-Yield Airburst. Basic measurements were needed to determine the pressure-distance relationship vertically above burst zero through a nonhomogeneous atmosphere. It would then be possible to evaluate the significance of the differences between observed values and those that might be predicted by various methods currently used to account for the effect of altitude on blast wave propagation. These differences could be most easily analyzed in a vertical direction above the burst. For small devices the effect of nonhomogeneity was not considered significant. However, for weapons in the megaton range the influence of the variation of ambient pressure and temperature, with altitude, on the propagation of the blast wave could not be neglected. Data obtained on the effects of inhomogeneity from Operations Ivy and Castle was inconclusive.

This operation also presented the first opportunity since Shot King of Operation Ivy to obtain pressure-distance data along the surface from a high-yield airburst. The data was necessary to confirm the height of burst curves for large weapons. Shot Cherokee was planned as an air drop [redacted] to detonate at a height of 5,000 feet above Charlie Island in the Bikini Atoll. This altitude was selected as being almost equivalent [redacted] thus insuring a true airburst where the reflected wave would not pass through the fireball and catch up with the incident wave. Such coalescence had been observed on two shots during Operation Teapot at lower scaled heights of burst and had affected pressures in the incident wave. [redacted]

Consequently, it would be possible to examine various scaling methods used to reduce pressure-distance data measured along the surface to 1 kt under sea level ambient conditions. Heretofore Sachs scaling factors based on burst-height conditions had been used to correct such data for plotting on the height of burst curves. On the other hand, it was proposed to use modified Sachs scaling factors based on target ambient conditions. Under this concept, data measured at the surface would be corrected to standard conditions using meteorological data at the surface and not at burst altitude. As a burst height of a large-yield device increased, there would be a greater difference between the correction factors obtained by both methods. The surface data obtained during Cherokee would provide a check as to which method of scaling is more appropriate.

2.2.2 Surface Bursts. Somewhat meager data was available on true land surface bursts where the blast wave propagated over a continuous land surface. Data from previous events was largely obtained in the low-pressure range and under conditions where blast wave propagation occurred over water. Confirmation of the limited data obtained along a land surface was therefore needed. Further supporting data was needed to determine the free-air equivalence factor which might be applied to surface bursts. The 2W theory considered the surface as a perfect reflector and stated that the blast wave should propagate with a pressure-distance relation of twice the yield of the device detonated in free air. Previous measurements indicated that the free-air equivalence factor for shots in the megaton range on Eniwetok and Bikini Atolls, might be closer to 1.6W. This value could not be independently confirmed, however, because the yields were determined by the hydrodynamic method that is based on a 2W concept for fireball growth for surface bursts. An independently obtained yield, such as that derived by the radiochemical method; _____ was required before a true value of the free-air equivalence could be determined. Consequently, participation was planned during Shot Lacrosse where the yield could be determined essentially independent of the 2W concept as well as during Shot Zuni where it could not. However, because blast measurements could be made essentially over land for both shots, it would be possible to determine the applicability of cube root scaling for yield under such conditions.

2.2.3 Operation Ivy. Shot Mike was the first thermonuclear detonation in the megaton range. It was fired as a surface burst on Flora Island in the Eniwetok Atoll. Measurements of peak pressure were made on other islands in the atoll at fairly long ranges consequently, measured values were below 20 psi and essentially represented data for a surface burst over water, because a considerable portion of the blast wave travel took place over the surface of the lagoon.

Shot King was the first air drop of a large-yield weapon although its yield was only about half a megaton. Good data was obtained on the propagation of the shock wave in free air horizontally from the burst, i.e., in a homogeneous atmosphere. Little information on the effects of inhomogeneity were obtained, because data obtained from the analysis of the particle motion of smoke puffs did not agree with pressure-time measurements made with parachuteborne canisters. Surface data consisted of measurements made on parallel blast lines over water and land. Essentially ideal waveforms were observed over water; however, degraded waveforms characteristic of the precursor were observed over land. Measured values of overpressure on Yvonne, a narrow island, were less than measured values of overpressure on the water line at the same ranges.

2.2.4 Operation Castle. It was planned to document the behavior of the blast wave over land from a land surface burst by establishing a blast line down the Tare complex. Unfortunately, the yield of this device went low, so that the range of overpressure data obtained was not as extensive as originally intended. Measurements made on Uncle Island over a second blast line which was approximately 180' from the first were consistently higher than those measured on the Tare complex. Consequently, there appeared to be measurable attenuation of the blast wave as it traveled down the Tare complex, due to the presence of a rainstorm over this area at the time of detonation.

It was also planned to make measurements of the blast wave behavior over a cleared and vegetated area on Pearl Island from the detonation of the _____ device or Ruby. Other elaborate instrumentation was planned for this shot, including a study of damage to crops which were considered representative of drag-sensitive targets such as military field

equipment. This shot was subsequently canceled.

On the other shots in the Castle series, namely, 1, 2, 4, 5, and 6, airblast phenomena was documented at various pressure levels by means of electronic and mechanical gages as well as by analysis of rocket trail photography. Most of the data involved blast wave travel over water and minor anomalies with respect to waveform perturbation were observed. In addition, measurements of dynamic pressure indicated the presence of water loading in the blast wave. Consequently, the Castle data indicated that water did not constitute as good a reflecting surface as had previously been assumed.

12.5 Precursors Two problems relative to precursor formation and propagation were to be studied during this operation: (1) The formation of a precursor from a surface burst, and (2) the effect of vegetation on the propagation of the precursor.

Up to this time, there was not sufficient data to allow a positive conclusion to be drawn as to precursor formation from a surface burst. An examination of the rocket trail photography and electronic gage records for the surface shot during Operation Jangle did not show a precursor. However, this event was a low yield device (~1 kt), which may not have produced a strong enough thermal layer, and in addition, the pressure-time measurements were all below 20 psi. Data obtained from Operations Ivy and Castle represented the other extreme in yield, but involved extensive blast wave travel over a water surface. As mentioned previously, Castle Shot 3 was a land surface burst with a blast line down the Tare complex. However, there was considerable rain over the shot point and the Tare complex so that, although no precursor tendencies could either be detected in the pressure distance curve or observed in the shape of the recorded pressure-time waveform data, its formation may have been suppressed by the moisture in the air and on the ground.

After Castle and early in the planning stages of Teapot, a requirement for a surface burst of greater than 10-kt yield was recognized, to provide basic information on blast, thermal, and nuclear radiation. However, AEC safety criteria established for NTS operations precluded the possibility of such a shot being included in the Teapot schedule. A medium-yield surface burst, Shot Lacrosse (~40 kt), planned for Redwing was expected to satisfy this requirement and, in particular, to answer the question of precursor formation from such a burst. In addition, blast measurements would also be made on Shot Zuni, a large-yield surface burst (3 to 4 Mt), which would be positioned near the [] crater with a blast line down the Tare complex. This would permit an evaluation of the effect of yield scaling over a wide range on precursor formation.

Shot 12 (MET) of Operation Teapot gave considerable insight into the effects of different surfaces on the formation and propagation of the precursor. However, the two artificial surfaces represented extremes as compared to the dusty desert surface, i.e., the asphalt being essentially an organic or thermally absorbing dust-free surface, while the water supposedly was an ideal, thermally reflecting surface. How well these test surfaces achieved their purpose is discussed in WT-1153, Summary Report for Operation Teapot. From a more practical consideration, however, there still remained unanswered the question of the effect of real vegetation on the precursor. Small plots of ivy leaves and fir boughs had been set out for Shot MET over which direct temperature and acoustic velocity measurements were made for the comparison with similar measurements over the three test surfaces. It was desired to ascertain if the air medium over the vegetated plots was changed to a state that might itself support a high sonic velocity. Most of the data obtained over the various surfaces was difficult to reconcile with other supporting measurements and was incompatible with previous data obtained by the same method on

other operations as well as being internally inconsistent. It was, therefore, necessary to plan an experiment to observe the effect of a full-scale vegetated surface on the precursor characteristics.

For Operation Castle, a blast line had been prepared on Pearl Island for Shot [redacted]. This shot was canceled, but meanwhile half of the island had been cleared, leaving the other half with a vegetation stand of grass and 10-foot shrubs. When it was found that a precursor-forming tower shot, [redacted] was planned for the same island during Operation Redwing, the Castle project was reinstated in order to measure blast wave parameters over a vegetated surface and over a cleared area.

2.2.6 Drag-Force Measurements From nuclear test series prior to Operation Teapot, it was recognized that the drag forces and damage to drag-sensitive targets in the precursor region did not correlate with the results anticipated from utilization of measured overpressures. Limited dynamic pressure measurements indicated nonideal blast phenomena in the precursor region, because values recorded under dusty flow conditions were substantially higher than those calculated from measured overpressures by classical shock relations. During Operation Upshot-Knothole, reinforced concrete structures previously subjected to 12-psi overpressure in a clean shock region from a high airburst without damage were translated 25 feet by 9-psi overpressure in the dusty precursor region from a low airburst. Tests were incorporated into Operation Teapot to study and measure the quantitative relationships between the various airblast parameters experienced in the precursor region in order to determine their influence on the loading of targets. These tests included extensive measurements of dynamic pressure on Shot 12 with the pitot static gage, for direct correlation with drag force measurements on various nearby targets.

These targets consisted of ideal simple shapes such as 3- and 10-inch diameter spherical models, rectangular boxes and cylinders, which were placed at various ranges so as to evaluate the total effect of the precursor from a nominal yield tower shot (MET) over three different test surfaces. It was found that the drag forces were much higher over the dusty desert line that had a precursor than in either the nondusty precursor region over asphalt or over a water line where no substantial precursor was observed.

Attempts to relate the field test drag data to that obtained in the laboratory from wind tunnels and shock tubes on the same models met with limited success, although the drag coefficients from the laboratory tests were fairly consistent with similar data available in the literature. However, laboratory experimentation was difficult, because of the size of these models, which resulted in blockage in available wind tunnels, as well as the extremely short shock durations in relation to transit times in shock tubes. In order to eliminate thermal gradients and dust effects from the loading problem, it appeared desirable to obtain additional full-scale data with improved versions of these drag force gages in a region where clean shocks were expected.

Because precursor effects from surface bursts were expected to be less severe than for low airbursts, these models would be positioned at higher overpressure levels on the Pacific shots to get the same dynamic pressure levels as were obtained during Shot MET. Therefore, drag measurements were planned for Shot Lacrosse using various types of gages, the majority of which were to be used in stingless-type configurations. These included midsections of long cylinders and parallelepipeds, as well as cubes on ground planes. Because it was also considered desirable to make such measurements on idealized shapes under long-duration loading for a better understanding of the problem, spherical models on strings were also to be exposed during Shot Cherokee.

At the same time, there were other problems that required consideration in a field

test program to facilitate theoretical analysis of damage predictions. Drag characteristics of structural members appeared to be of great importance in the analysis of structures with complex configurations of trusses and lattice-type networks, particularly for long-duration loading. Although these characteristics are somewhat altered when individual members are combined into a network, a great deal of basic information could be gained by studying single elements of various simple shapes. Consequently, for Shot Cherokee drag force measurements were to be made on full-scale structural members such as 8-inch wide flange beams and 8- by 8-inch angle irons. These drag force measurements would be compared with free-field dynamic pressure measurements at the same location to obtain more reliable transient drag coefficients. These, in turn, could be correlated with laboratory experiments as well as with field tests of high explosives.

As part of the drag force program, it was planned to position jeeps for Shots Lacrosse, Zuni, and Yuma. Such exposure would provide data for a continuation of the statistical damage evaluation studies of the jeep under environmental conditions different from those previously considered. These studies had shown that the response of all types of drag-sensitive military field equipment could be predicted on the basis of damage to jeeps. In previous operations dating back to Buster-Jangle, it had also been found that vehicles of different sizes placed at the same distance from ground zero experienced approximately the same degree of damage; therefore only one type needed to be tested. Response data to be obtained from Shot Lacrosse would allow vehicle damage for a classical waveform to be compared with that for nonclassical waveforms obtained from a precursor-forming tower shot at NTS (Shot 4 [Turk], Operation Teapot) of approximately the same yield. Data from Zuni and Yuma would extend the Lacrosse data over a wide yield range to check scaling [] to 3,500 kt.

Another phase of the drag force program concerned the use of an existing structure from Operation Castle, Station 310. Measurements of airblast loading on full-scale structures such as concrete cubicles had been made on a number of previous field tests, primarily in the low-pressure clean Mach region (below 6 psi). Perhaps the largest effort on nonresponsive targets of this type was undertaken during Operation Upshot-Knothole. Scaled models of cubicles had been tested in various shock tubes, but the emphasis had been directed toward the initial or diffraction loading. For large megaton-yield weapons with long positive-phase durations, drag loading had become more important as a damage criterion for many typical structures. Shot Zuni afforded an excellent opportunity to instrument a 6- by 6- by 12-foot concrete structure in a higher pressure region and a longer positive-phase duration than had previously been recorded. It was hoped that the loading data to be obtained would validate model scaling in the moderate pressure range (15 to 20 psi) and would correlate with predictions based on semiempirical methods developed on previous full-scale operations.

2.2.7 Crater Survey. Previous crater studies utilizing full-scale high-explosive and theoretical data had reached a point where additional full-scale data was desirable for surface and underground shots, to supplement that obtained from three low-yield shots at NTS under controlled conditions. Available data from the Pacific consisted of that obtained from larger yield surface bursts during Operations Ivy and Castle but fixed under uncontrolled conditions involving a water-soil interface. Because of the radiological fallout hazard limitations imposed, there was no prospect of gathering data for yields larger than 1 kt from continental tests. The Pacific Proving Grounds (PPG), later called Eniwetok Proving Ground (EPG), offered the only immediate opportunity to obtain additional crater data.

A further compromise was conceded in that the measurements were of the apparent crater rather than of the more desirable true crater. This was necessary because of the lack of detailed information on the geologic structure at each of the detonation sites. Previous deep drilling and core borings at Eniwetok and Bikini indicated the presence of extensive sand lenses and other geologic nonhomogeneities in the coral atolls which made it uncertain that the demarcation line between true and apparent craters could be readily ascertained by any means. Therefore, the expense of any extensive effort to measure true craters by drilling or core boring would hardly be warranted.

There were to be four shots in Operation Redwing that were to be fired at or relatively near the surface so as to produce craters. These were Lacrosse, Zuni and Seminole, all essentially surface bursts of varying yields, and Mohawk, a large yield tower shot. It was determined that measurements of the apparent physical characteristics of these craters should be obtained using aerial photography and lead-line sounding techniques. Project participation during Shot Tewa was added in the field after a change in the operational plan placed the site location in a shallow water area.

2.2.8 Water Waves Results of the water-wave studies during Operations Ivy and Castle indicated that megaton-yield devices could generate surface water waves by two related but distinctive processes. Energy transfer in the form of initial impulse and displacement produced significant waves in the central region, while at more distant ranges different waves were apparently generated by a coupling phenomenon not completely understood. These two wave systems resulting from the same source, seemed subject to different laws of generation, propagation and termination. Participation during Redwing was designed to obtain data on both systems. Originally measurements of both direct and indirect water waves were planned at various locations on only four shots: Zuni, Cherokee, Navajo, and Apache. However, participation on Flathead, Dakota, Tewa, and Mohawk was subsequently authorized using available instrumentation already installed and in operation for previous events.

2.2.10 Scaling Factors. In order to compare the airblast data from certain shots of the Redwing series with other nuclear detonations, it is necessary to normalize such data to 1 kt of radiochemical yield at a sea level ambient pressure of 14.7 psi and an ambient temperature of 15°C. However, the only possible way to determine the fission yield for a given shot is by radiochemistry.

Table 1.1 in Chapter 1 gives the fission yield and the total energy release for each shot as calculated by hydrodynamic methods that involve photographic analysis of fireball growth before breakaway. Wherever appropriate, the fission yield values for certain shots also include consideration of radiochemical analysis. Further, when radiochemical analysis of different isotopes gave yield values for the same shot that did not exactly agree, an average yield was used. Consequently, the recommended yield in Table 1.1 represents the best value that can be determined for each shot based on the judgment of experienced AEC laboratory personnel who have available all the many variables of the device and its environment as well as the quality of the data obtained that would affect the relative reliability of each method of yield computation.

The scaling factors presented in Table 2.1 were determined by use of the Sachs's correction factors for atmospheric temperature and pressure at the surface. This procedure of scaling to ambient conditions at the target or gage height is known as modified Sachs scaling. The reasons for adopting this method of scaling for the Redwing shots that were not detonated at the surface will be discussed in more detail in Section 2.12.1. Scaling to ambient conditions at burst height is known as straight Sachs scaling or A-scaling and has been used for reduction of surface data on previous operations. Scaling factors computed on this basis for the tower shots and the Cherokee airburst are listed in Table 2.2.

$$\begin{aligned} \text{Pressure:} \quad S_p &= \left(\frac{14.7}{P_0} \right) \\ \text{Distance:} \quad S_d &= \left(\frac{P_0}{14.7} \right)^{1/3} \left(\frac{1}{W} \right)^{1/3} \\ \text{Time:} \quad S_t &= \left(\frac{T_0 + 273}{293} \right)^{1/2} \left(\frac{P_0}{14.7} \right)^{1/3} \left(\frac{1}{W} \right)^{1/3} \\ \text{Impulse:} \quad S_z &= \left(\frac{T_0 + 273}{293} \right)^{1/2} \left(\frac{14.7}{P_0} \right)^{2/3} \left(\frac{1}{W} \right)^{1/3} \end{aligned}$$

Where: W = yield of the device in kilotons

P_0 = ambient pressure in psi at burst height or measurement height

T_0 = ambient temperature in °C at burst height or measurement height

Tables 2.1 and 2.2 present the pertinent scaling factors used in converting the observed data to standard conditions for both methods of scaling.

2.3 RESULTS: SHOT CHEROKEE

This event was the first airburst of a device in the megaton-yield range. The drop was planned so that the burst position would be at an altitude \square the maximum fireball radius by cube-root scaling. This would be a true free-air burst, from a blast point of view, making it one of considerable interest for documentation of basic blast phenomenology in the free-air region and on the ground. Inasmuch as this type of event had to be restricted to the PPG it could not be considered as taking place over a homogeneous surface of infinite extent. Nevertheless, by planning the air zero position over an island, and by placing much of the surface instrumentation on islands, both

artificial and natural, it was felt that the data to be obtained would approach that for a semi-infinite land surface particularly at the longer ranges. However, the positioning error in air zero almost nullified project participation in Program I because of the extreme range of the burst and its azimuth relative to the blast line. The results obtained are presented in the following paragraphs.

2.3.1 Free-Air Data. The shock photography technique, which included the use of smoke rockets, was employed on this event in a manner similar to that during previous operations. The rocket array was arranged so that a fan of trails would pass in a vertical plane behind the burst (relative to the camera). By observing the passage of the shock front against this background, it would be possible to measure the time of arrival in the horizontal and vertical direction. From this data, peak overpressure can be calculated as a function of distance by use of the Rankine-Hugoniot relations at the shock front. Camera locations and rocket stations were so placed that it would be possible to determine the pressures vertically above the burst out to a range of about 10 psi. The offset in air zero was such that the device light was too weak and the shock strength too low by the time that both entered the field of view of the cameras, to enable an analysis of the film to follow blast wave propagation.

In order to extend the Naval Ordnance Laboratory (NOL) vertical pressure distance data into the low-pressure region, it was planned to position canisters directly over air zero covering a range in altitude between 14,000 and 39,500 feet. Measurements to be made by instrumentation contained in the parachuteborne canisters would overlap the NOL data, thus providing an independent check on pressures computed by the shock velocity technique. In addition it would be possible to document the time history of the blast wave passing through a nonhomogeneous atmosphere in the 1- to 20-psi region. Location of the canisters at shock arrival would be determined by a method of photographic triangulation previously used during Operation Teapot, aided by the installation of flares in the individual canisters to assist in their identification. Measured blast data would be telemetered to surface stations.

On D-Day for Shot Cherokee, all 12 canisters were dropped from a B-36 at 44,000 feet within 1 second of the planned release time and an essentially vertical array of canisters was positioned above intended ground zero (IGZ). In fact, during a postshot survey of the target island, Charlie, two of the canisters were observed lying offshore in the shallow water over the reef. However, because the detonation occurred at a point some 19,500 feet from the IGZ, the array of canisters was not above the burst as originally planned. In addition, because of a delay in timer initiation caused by a minor operational difficulty, the large 28-foot parachutes on five of the canisters opened later than planned. Consequently, these canisters remained on their small drag chutes for a longer time than was planned and were therefore at much lower altitudes at shock arrival than desired. In fact, the records on the two lower canisters indicate that they were in the Mach region below the triple point. The other seven canisters were all within 3,000 feet of their intended altitudes at shock arrival. This was due to the fact that the time required for the shock wave to travel the extra distance involved was partially compensated for inasmuch as the detonation occurred approximately 21 seconds early.

Because of partial cloud cover, only the five highest canisters could be identified on the films from one camera station; therefore, it was not possible to obtain accurate positioning data by photographic triangulation. Consequently, slant ranges from bomb zero were determined by three different methods. One method used the photographic line-of-sight data with the canister altitudes determined from the telemetered ambient pressure measurements to find canister coordinates. Another method used the canister

ballistic trajectory data, the wind structure at the time of the shot, and telemetered information on release time and altimeter altitudes to find canister locations. In the third method, slant ranges were computed from the observed shock-arrival time, measured peak overpressure, and ambient pressure data.

The slant ranges computed by these various methods are compared in Table 2.3. On the whole, the agreement is surprisingly good, although those calculated from the shock travel times and peak overpressures are believed to be the most accurate. No correction for wind drift was made, because the displacement of shock front by the wind was not considered to cause a corresponding change in peak overpressure.

Table 2.4 lists the observed data. The pressure reference chambers for the five highest canisters were not sealed prior to shock arrival; therefore, the recorded pressure time waveforms were distorted. Consequently measurements of positive-phase duration for these canisters were considered inaccurate and are not listed in this table. The average pressure reading represents the average of both a high- and low-range gage on each canister. The values given for the corrected peak overpressure were obtained by applying a gage correction based on the measured shock strength and an assumed probe orientation.

For comparison with the observed data, values of peak overpressure were calculated at canister locations by various methods currently employed to correct for the effects of atmospheric inhomogeneity. These calculations involved the use of new AFCRC (Air Force Cambridge Research Center) experimental free-air curve that was based on empirical data from previous nuclear tests weighted according to the type and locations of measurement. The three methods examined were modified Sachs, Ledsham-Pike, and Theilheimer-Rudlin; α is also dependent upon various assumed initial conditions. A number of computations were made, allowing α to go to zero at various shock strengths. The trend of these figures indicated that optimum agreement with the observed values is obtained somewhere between the $\alpha(5) = 0$ and $\alpha(10) = 0$. Assuming that $\alpha = 0$ for $Q_H = 10$ in the Theilheimer-Rudlin method, a comparison of pressures predicted by these three methods is shown in Table 2.5. The percentage duration for each method is also shown together with the algebraic mean and the root mean square for the eight highest canisters. In general, the difference between all three methods appears to be small, and no systematic trend appears evident. Although modified Sachs scaling is a simple and practical method for predicting free-air overpressures, it is essentially empirical in nature and lacks a firm theoretical background. For extrapolation to situations that lie far outside the range of yields and altitudes for which experimental data exists, the Theilheimer-Rudlin method is preferable over the Ledsham-Pike method. However, it should be remembered that integration of the differential equation of the Theilheimer-Rudlin theory requires an initial condition that is not provided by the theory itself. Consequently, for very large yields, additional numerical integrations of the exact equations of motion may be required, taking gravity and atmospheric structure into account.

2.3.2 Surface Phenomena. Because of the bombing error, no shock photography data was obtained for Shot Cherokee. Furthermore, this error affected the ground surface instrumentation in three ways.

First, the offset position was such that the gage locations did not constitute a blast line spanning a pressure range from 200 to 1 psi, as intended. Rather, the effect was to essentially shorten the length of the blast line, eliminating the high- and low-pressure ends. The result was data that spanned an overpressure spectrum from 4.1 to 12.9 psi. Second, the pitot-static gage, which is unidirectional when oriented to intended ground zero, received the blast onset at excessive angles to the axis of the tube. It was found

that a lowering of recorded pressures of both the total and static pressures occurred. Therefore, the dynamic pressure records from these gages were essentially a complete loss. As a result, those gages that were essentially omnidirectional and could record the blast from any direction did not effectively cover a long enough blast line, and the data from those gages recording dynamic pressure was not interpretable because of the orientation of the pitot tube away from actual burst zero. A third effect of the offset was manifested by the recording of unexpected pressures. The range setting of the gage capsule is adjusted to a certain span of pressure based on the predicted input. The actual air zero position caused higher pressures to be recorded at some stations and lower pressures at others, to the effect that records were overranged in the one case and gave deflections too small to read in the other.

Figure 2.1 shows the plot of measured peak overpressure against ground range. Distinction is made between the various types of stations, i. e., reef stations, those on artificial islands, and those on the natural islands. It will be noted that a marked deviation occurs in some of the data recorded by the reef stations. These stations consisted of a pitot-static gage and three ground baffles. The latter were mounted on pipes of sufficient height to keep the baffle above high tide stages. At shot time, the baffle was some 3 feet above the tide level. Essentially, this arrangement amounted to a gage on the end of a 3-foot sting whose diameter was about equal to that of the baffle plate. Subsequent tests by the Ballistic Research Laboratories (BRL) in the shock tube indicated that the recorded values of overpressure could be attenuated because of this mount configuration. It was found that, under the same input conditions, the gages mounted on a pipe recorded overpressures 25 percent lower than the same gage mounted on a flat surface. On the other hand the value of 10.9 psi at 19,143 feet was recorded on Site Charlie where the capsule had been set to record near 200 psi. The very small deflection was difficult to read accurately, and the reading is undoubtedly too high. Figure 2.2 plots recorded values of arrival time and duration.

Following Shot Cherokee and the realization that the extreme angular offset of the pitot tube to the onset of the blast wave would probably negate usefulness of the field data obtained by that type "q" gage, plans were made for field tests during the remainder of the series to obtain some correlative data. The basic idea was to place some of these gages for one or more subsequent events, in a comparable pressure field, oriented at 0, 32, 42 and 50 degrees to the line of sight from gage to ground zero. Ideally, it would have been desirable to place the gages back on one of the artificial islands, using one of the barge shots. This plan was infeasible however for a number of reasons, mainly that the exact diffraction and orientation conditions could not be duplicated, and the area was already well contaminated by one or two following events before the plan could be put into effect. It was thought that a more practical approach, and one that would result in useful data, could be accomplished by placing the four gages on one of the kiloton-yield range tower shots. This was done for Shot Inca. Analysis of the data obtained shows that the effect of a large-angle offset to the shock front is to reduce the overall recorded pressure, total and static, below the true pressure effective at that range. A similar test was hurriedly adopted for Shot Zuni where two gages, one electronic and one self-recording, were oriented at an angle of 45 degrees to the shock wave. Only one gage survived the blast, but the results confirmed the Inca findings.

2.4 RESULTS: SHOT LACROSSE

This shot was detonated on an artificial island at the end of a causeway about 450 feet off the north end of Site Yvonne. The device was placed on a support so that its height

was 17 feet above the datum plane (datum taken as $\frac{1}{2}$ foot below mean low water springs). Tide conditions at shot time have been estimated at 2.2 feet (above datum). It is, therefore, considered that the shot was detonated 14.8 feet above a water surface. For diagnostic measurements, extensive pipe arrays were laid out on the island (Figure 2.3). Two of these consisted of 16-inch pipe suspended at a height of 4 to 6 feet above the ground, running down one side of the island. Parallel to these and in the middle of the island, an earth berm (10 to 12 feet above grade) covered a coaxial cable line. In order to preclude any possibility that the gages would record perturbations in the blast wave caused by these obstructions, it was necessary to locate instrument stations well clear of the berm line. In some cases this moved the gages close to the shoreline of the lagoon. There was some concern felt that the pipe might part at one or more places down its length and whip across the gage stations. Closer study of this problem relieved the concern somewhat, and as it turned out, although the pipe did break in several places, sections of it were not thrown for any great distance to either side.

2.4.1 Free-Air Data. By use of the smoke rocket technique, it was hoped that pressure-distance data could be obtained vertically above this surface shot. These data could then be compared to the composite free-air curve and to other data available or to be obtained from the large yield (Zuni) surface burst, for example. A similar comparison to the surface data would disclose possible asymmetry in the vertical propagation of the blast wave. The rate of growth of the fireball in the vertical direction was greater than the growth along the surface. However, there was not sufficient arrival time data measured above ground zero to warrant fitting.

2.4.2 Surface Phenomena. Direct-shock photography of the blast wave was taken from the Mack photo tower situated in the lagoon. The objective was to observe blast wave propagation over a water surface to the north and over the island to the south. The question of water pickup by the blast wave was of considerable interest, involving the effect of suspended water droplets which would be carried along with the shock. The results from this station were negative, because the cameras on the tower did not operate at shot time. However, supplementary film, from fireball photography taken from Wilma (to the north of Yvonne), were made available to the project. Analysis of the film produced good pressure-distance data over the water surface from 600 to 3,250 feet in range as shown by Figure 2.4. In conjunction with the blast line records of Sandia Corporation (SC) and BRL, it is possible to compare data collected over a land surface and over water, to note qualitatively the effect of these surfaces on the shock wave.

The objective of the surface blast lines for Lacrosse was to document basic blast data from a medium kiloton-yield surface burst. The length of the line was designed to include possible precursor formation, propagation, and decay, and to extend to low pressures in the clean shock region. The primary line was instrumented with electronic blast gages, backed up and extended by a secondary line of self-recording gages. At two ranges, 2,500 and 2,900 feet, the electronic instrumentation was located in support of a project taking drag force measurements.

In addition to backup, the self-recording gage was added to continue a study of comparison of these two types of blast gages. Figure 2.5 shows the mechanically recorded (BRL) peak overpressures to be consistently higher than the electronic. At the one station, at 2,500-foot ground range where both projects had gages side by side the self-recorded values are 2 to 3 psi higher in about a 19-psi region—greater than 10 percent deviation. At the BRL 1,180-foot station where the waveform shows good evidence of precursor formation, the pressures recorded by two ground baffles are as much as 15

to 25 percent higher than ideal, where less than ideal precursor overpressure would be expected. The recordings are consistently high, but the deviation appears to become less approaching the low-pressure end of the curve. This would seem to be a mechanical effect inherent in the gage and not a statistical variation. It should also be pointed out that the comparison here is made on peak overpressures only. Complete waveforms of both sets of records show general similarity. This confirms the results of previous laboratory work where comparison of records obtained from both types of gages, mechanical and electronic, have shown correlation in waveforms.

Both (SC and BRL) sets of gages gave definite evidence of precursor formation along a portion of the blast line. The significant characteristic that should be noted, however, is that the shock existed over a limited radial extent, having formed around 900 feet from ground zero but clearing up by 1,800 feet. The BRL station at 1,180 feet and the SC gages at 1,400 feet recorded typical precursor-type waveforms. The SC station at 920 feet gave a small indication of a precursor at one of the ground baffles, not at the other, whereas the station at 1,800 feet recorded a clean wave. The records of the BRL gages at 1,590 feet are inconclusive regarding a precursor; however, the station at 1,950 feet shows a typical ideal waveform.

Arrival-time data seems to show that the shock propagated asymmetrically, the wave having arrived simultaneously at gages at different ground ranges. The pressure-time records at ground baffles at the same range show differences indicative of an asymmetrical wave. The SC and BRL overpressure data differ in values in the precursor region, as shown by Figure 2.5—the BRL station at 1,180 feet giving a somewhat high value. However, the record at this station certainly shows a precursor, as has been pointed out.

A comprehensive study in WT-1302 indicated that under certain conditions a precursor could form from a surface burst. These conditions specify a lower limit of total yield at about 10 kt and include two concepts: (1) the larger the product of the total thermal input, incident normal to the ground before shock arrival, and the sine of the angle the shock front makes with the ground, the more probable a precursor and (2) the larger the ratio of shock arrival time to time of thermal maximum, the less likely is precursor formation. Tentatively, taking the SC station at 1,400 feet as an example, the ratio of time of arrival versus time to thermal maximum is about 1.3, which is between 1.0 and 2.4, the limits for this ratio during which, according to the National Bureau of Standards, the surface reaches its maximum temperature.

The fact that the precursor cleaned up before the 1,800-foot range (at pressures greater than 35 psi) indicates lack of an intense thermal layer, or that the layer has cooled prior to shock arrival. This also implies that the thermal radiant energy was received at a small angle with the ground, and so gave a small thermal input normal to the surface. Overpressures appear slightly reduced at the SC 920- and 1,400-foot stations; whereas the dynamic pressure values for SC at 1,400 feet and BRL at 1,590 feet are both higher than values calculated from measured overpressures. All of this is indicative of nonideal conditions, i.e., a precursor, but of suppressed intensity. The measured values of dynamic pressure versus range are shown in Figure 2.6.

The significant fact to be noted from the records of overpressure versus time (Figure 2.7) is that a precursor of limited radial extent was formed that had typical distorted waveforms and for which the dynamic pressure was somewhat high. This precursor appeared to have been limited also in directional extent, in that some stations at the same ground range recorded significantly different waveforms. This can be seen from inspection of the 1,400-foot stations of Figure 2.7, which were separated laterally by 138 feet.

Another factor of interest to the blast program on this event was further study of the

2W concept. This concept states that, since for a surface burst the growth and development of the shock front is confined to a hemispherical space above the ground plane, its propagation acts like one of twice the burst yield in an unbounded atmosphere. The pressure-distance relation for a device of yield W burst on the ground is then obtained by determining the free-air pressure-distance curve for one of yield $2W$. Data from previous operations has shown that, because of a number of factors that affect the phenomena, $2W$ represents ideal theory, and that actually the relation may be closer to $1.6W$. However, most of the data available prior to Redwing was obtained from measurements made on high-yield two-stage devices where the hydrodynamic methods used to calculate yield were themselves based on $2W$ theory. Lacrosse gave an opportunity to obtain data from a surface burst whose yield could be obtained by radiochemistry— independently of any reflection theory. Results and discussion of the Lacrosse and Zuni data as related to this problem are presented in Section 2.13.

2.5 RESULTS: SHOT ZUNI

This shot was detonated on the island land mass of Tare, close to the east edge of the old Morgenstern crater. The device was placed some 11 feet above grade in close proximity to two collimating shields. These were of concrete, approximately 30 feet high and 3 feet thick, placed at right angles to the centerline through ground zero. One of these collimators, placed some 30 feet east of the ground zero working point, had wing walls angling back toward ground zero for about 20 feet. Another, without wing walls, was located about 50 feet from the first shield. Other shields were at varying greater distances from ground zero down the Tare complex. It is felt that for a device of this yield size even the close-in shield did not affect the generation of the shock wave nor propagation of its energy down the east blast line.

There were two blast lines established for Zuni. One, to the east, had stations located on the islands of the complex, out to Site Oboe, the last island. This constituted, essentially, a ground surface blast line. The other line, to the west, began at the eastern tip of Site Uncle and extended west and west-northwest, terminating at the Castle target cubicle, which was being instrumented again for this shot. This line was therefore preceded by the deep water channel between Tare and Uncle, representing a water path over which the blast wave traveled before reaching the first gage. Because of the configuration of Site Uncle, the cubicle and its associated free-field gages were exposed to a line of sight to ground zero almost completely over a water surface.

2.5.1 Shock Photography. The propagation of the blast wave in air from Shot Zuni was observed by means of high-speed photography. High-altitude Deacon rockets were employed as well as the more conventional 5-inch smoke rockets to lay a background grid of smoke trails in a manner similar to that described for Shot Cherokee. The experimental plan for Zuni was similar to that for Cherokee and included direct shock photography along the surface. This latter technique involves observation of the shock front as a result of light refracted by the change in density at the front. Peak overpressures as a function of distance can be determined from the time of arrival data along the surface, provided the local velocity of sound is known. Ambient conditions are usually known along the water surface; however, sound velocity may not be the same over a land surface. A comparison of land and water surface data observed during Shot 2 of Operation Castle indicates that this difference may exist.

Participation in Shot Zuni was considered extremely successful in that all rockets fired, and excellent photographic coverage was obtained. Analysis of the films by the

Naval Ordnance Laboratory (NOL) indicates that it was possible to observe the shock front out to a range of 14,750 feet and to a height of 13,680 feet, from the Nan camera station.

It should be noted that at a given distance from ground zero, the shock arrives earlier in the vertical direction than along the surface. This means that both the absolute velocity U and the Mach number U/C_0 of the shock is larger at a given height than at the same horizontal range, because the ambient sonic velocity C_0 usually decreases with altitude. The measured time of arrival data has been used to determine the pressure distance data presented in Figure 2.8. Also shown in this figure for comparison are the measurements at the surface with mechanical gages by another project.

In Figure 2.8 it may be seen that the peak pressures obtained aloft are greater than the peak pressures obtained along the surface at the same distances to a range of about 11,000 feet, beyond which point the pressures obtained aloft become less. The difference between the data obtained aloft and along the surface is believed to be real and not attributable to the experimental or analytical difficulties encountered.

Two basic physical phenomena can be used to explain, qualitatively, the variation in the measured pressures with distance: focusing and atmospheric inhomogeneity. Focusing is a term used to describe the phenomena observed on high-explosive tests when the explosive is detonated on a surface. At reduced distances, (range in feet)/(charge weight in pounds)^{1/3}, between 6 and 25 the ratio of the pressure in the vertical to that along the horizontal is equal to or greater than 1.5. This corresponds to a region between 750 and 3,150 feet for a 1-kt nuclear surface burst. Atmospheric inhomogeneity is a term used to describe the effect of the variation of ambient pressure and temperature with altitude on the pressure-distance curve of a given explosive in any direction except the horizontal.

The extent of the applicability of either phenomenon to nuclear shots is not known as yet. In the case of Zuni, the vertical pressures at close distances are greater than the corresponding horizontal pressures, which is a characteristic associated with the focusing observed with high explosives, even though the ratio of the two pressures is only 1.42. Further, the peak pressures measured above ground zero decrease faster with distance than in the horizontal direction, a characteristic predicted by all theories dealing with atmospheric inhomogeneities. Hence, at the greater distances the vertical pressures go below the horizontal pressures, and the ratio of the two pressures becomes less than unity.

An attempt to separate these effects in order to study each separately was made using the computing facilities at NOL. The data in the horizontal direction was approximated by the modified Ledsham-Pike free-air pressure-distance curve. The pressure-distance variation predicted by NOL theory in the vertical direction was computed for this same arbitrary yield, using an atmosphere based on the NACA model atmosphere. The ratio of the vertical to the horizontal computed pressures was assumed to be representative of the effects of atmospheric inhomogeneity in the case of Zuni. By dividing the above ratio into the vertical pressure-distance points obtained by shock photography, a new set of vertical pressure-distance values was obtained. This new set of vertical data is now representative of the data that might be obtained from a 3.53-Mt burst on a surface in a uniform atmosphere. Only the focusing effect remains. The results of these computations for several points are shown in Table 2.6. The average value of the pressure ratio is seen to be 1.42.

The combined effect of both focusing and atmospheric inhomogeneity can be expressed in terms of a new equivalent yield in the vertical direction, in the same manner as has been suggested for pressure-distance data along the surface from a surface burst. If W is the yield, it has been proposed for surface bursts that the free-air equivalent be taken as $1.6 W$ in determining the pressure at a given distance along the surface from

the blast. In the same manner, but without the same amount of confirmatory evidence, an equivalent yield in the vertical direction would be 2.2 W. This would mean that a free-air nuclear pressure distance curve, scaled to 2.2W and corrected for atmospheric inhomogeneity, would give a rough approximation to the data obtained vertically above a surface burst. A plot of the vertical shock photography data on Zuni, and on Romeo (11 + 0.5 Mt, Shot 2, Operation Castle) is presented in Figure 2.9. The 2.2 W curves, corrected for atmospheric inhomogeneity, are seen to approximate the original data. The verification of this interpretation, in general, will require further testing and evaluation.

2.5.2 Surface Instrumentation. Measurements were made with the BRL self-recording gages, both pt and q. There was some damage to the close-in q gages (pitot-static tube 3 feet above ground) and mounts, as well as the pressure-time ground baffles. Record disks were broken and unreadable, and 4 of the 21 pt records gave a peak pressure value only.

Figure 2.10 shows the measured overpressures versus ground range for both blast lines, to the east and to the west. At the further ranges, beyond 8,000 feet, a smooth curve fits both sets of data within normal scatter. However, at the intermediate ranges between 5,000 and 8,000 feet, there appears to be a deviation between the two sets, with those gages at 5,000 feet exhibiting the most deviation. This deviation may be attributable to a deformed gage mount on Uncle. Around 7,000 feet, two gages at the Uncle station support a higher pressure value than that recorded on the Tare line. This apparent discrepancy is believed to be real, not instrumental or statistical variation, and is believed to be caused by different waveform development within the precursor. Arrival time as read at the stations on the two lines seem to be consistent, with only normal scatter. No clue to the answer can be found in this data. The dynamic pressures (corrected for Mach flow and compressibility) are not conclusive (Figure 2.11). The few records obtained on the Tare blast line give values that agree closely with a calculated ideal curve of dynamic pressure using measured overpressures and the relation:

$$q = \frac{2.5 (\Delta p)^2}{7 p_0 + \Delta p}$$

p_0 = ambient pressure.

Two values of dynamic pressure obtained on Uncle are not consistent in themselves, a higher value being recorded at a farther range, and both being almost twice as high as recorded at the same range on the other blast line. These two stations (115.12 and 156.02), however, represent different conditions of environment. The one on the south end of Uncle (115.12) was located in such a manner that the blast wave traveled some 5,000 feet along the island complex before reaching the station, whereas the station on the north side of Uncle (156.02) faced an almost continuous water path to ground zero. The high q at the south station may be due to a thermally induced precursor shock. The waveform is nonideal in shape. The q recorded at the north station may be caused by mechanical pickup and water loading of the blast wave.

The gage records for Zuni show definite evidence of nonideal or precursor wave generation. Stations 115.11 and 115.12 were on Uncle at distances of 7,020 and 9,880 feet, respectively. Station 115.06 at 5,800 feet on the Tare complex shows the slow rise and suppressed peak of the precursor, cleaning up at Station 115.08 at 10,400-foot range. The Uncle records show the stronger precursor, supported by further evidence from those gages on the cubicle target (Project 1.5) at 10,000-foot ground range. However, overpressures along the Tare complex, and the shape of the pressure-time histories, are

indicative of precursor formation. This is not, however, supported by the dynamic pressure readings, which agree with a curve calculated from measured overpressures, where precursor dynamic pressures would ordinarily be two to three times the calculated value. The evidence seems to indicate precursor formation on both lines, stronger over Uncle but relatively weak on both lines.

The Zuni surface results are not consistent when analyzed as a group. There are probably one or more factors influencing these results that are not being considered. Almost identical blast lines, east and west, were instrumented during Castle for the Morgenstern event. Results from that experiment also gave attenuated pressures along the Tare line as compared to those recorded on Uncle. This situation for Zuni does not seem comparable however. As shown by the pressure-distance curves for the Castle Shot, there was an increasing spread in the pressures with increasing range. The evidence is fairly conclusive that this effect was due to a rainstorm over the Tare complex at shot time. No such consistent deviation appears in the Zuni data; and it appears certain that there was no shower activity in the area at the time.

2.6 RESULTS: SHOT INCA

Participation on this event was designed to obtain information on the propagation of a precursor shock wave over a vegetated surface. Inca was detonated on a 200-foot tower.

This scaled height of burst is somewhat below the range where strong precursors have been found during previous shots.

Although the fundamental causes of precursor formation are not clearly understood, it is generally accepted that the immediate causes are related to a surface layer with a sonic velocity well above ambient, and that this layer is caused by thermal radiation from the explosion. One method whereby the ambient sound speed could be increased is by the release of a high sonic velocity gas such as hydrogen from the heated surface. During Operation Teapot, small plots, including ivy and fir boughs, were laid out and instrumented with sound speed and direct temperature gages. The results were inconclusive, and in some cases showed actual disagreement. This experiment, as designed for Inca, was originally conceived for Castle. It was dropped when Shot Echo of Operation Castle was canceled. Inca allowed for the reinstatement of the test at the same location.

Blast lines were laid out along both the vegetated area and the cleared, sandy section. Stations were located at equal ranges, i. e., a station at a particular range in the vegetation was duplicated at the same distance along the cleared line. Both SC electronic instrumentation and the BRL self-recording gages were used. At two ranges, both types were located side by side. Surface results from Shot MET of Operation Teapot were used for predicted pressures. The MET desert line results could be scaled to predict Inca's cleared area, and the results of the asphalt surface might approximate those to be expected over the vegetation of this test. It was thought that the vegetation might resemble the asphalt surface qualitatively in the production of smoke and gases.

Figure 2.12 shows the data from the MET desert and asphalt curves, scaled to Inca yield. These are included for comparison. The results used here are from the electronic gages only. In general, the peak overpressure values from self-recording gages seem to follow the same relationship, ground surface to that obtained at 3 feet, vegetation to cleared, as did the electronic records. However, as a group, the peak overpressure values were consistently higher than the electronic gage data. Because of the unexpected

high yield of the shot (more than double the predicted yield), these gages were subjected to pressures well above their rated value.

From the data obtained, it was concluded that a vegetated surface such as that found on Pacific atoll islands does not support as strong a precursor as that formed over the cleared, sandy surface. In fact, it appears that the thick stand of brush mechanically reduces the severity of the precursor. Overpressures are more degraded over the cleared area than over the vegetation, with earlier arrival times being recorded. Both of these parameters are indicative of precursor formation. Their magnitude may thus be used as a measure of the severity of the precursor, and in this case for comparison over the two surfaces. The relative strength of the precursor over each area is also obvious from examination of the pressure-time trace, or waveform. Those stations in the vegetation did not record the front porch during the rise to peak, which is typical of precursor formation. Rather, the recorded wave shows merely a slow rising pressure pulse.

Another point of interest shown by the data lies with a comparison between the ground surface overpressure records and those obtained at the 3-foot level of the pitot tube. The ground level pressures in the cleared area are less than those at the 3-foot level, while in the vegetation they are about the same. This difference in pressure with height over a sandy or desert surface has been noted before at NTS. The small spread in pressure value with height in the vegetation indicates a mechanical interaction of the shock with the vegetation.

Dynamic pressures corroborated the overpressure findings by indicating the relative strength of the precursor over the two surfaces as shown in Figure 2.13. Pressures were higher in the cleared area, particularly at the closest station. At the farthest station, pressures were below the curves for Shot MET, indicating an early cleanup of the precursor.

Therefore, it appears that vegetation consisting of grass, vines, and tall (10 to 15 foot) shrubs reduces the severity of a precursor compared to a cleared sandy surface. The spatial extent of the vegetation apparently changes the distribution of the thermal energy in the air and provides a mechanical diffuser to slow down the wave and make the pressure uniform.

2.7 RESULTS: DIRECT-SHOCK PHOTOGRAPHY OF SHOTS INCA, MOHAWK, AND SEMINOLE

Project 1.3 participated during Shot Inca (Table 1.1) to study the effect of vegetated and nonvegetated surfaces on precursor phenomena. A disturbance along the ground over the vegetated area was visible in two of the shock photography films. This disturbance appeared to be a precursor. The phenomenon was obscure, and hence it was impossible to make reliable measurements. The layout of the blast line relative to the photo station is shown on Figure 2.14. The peak shock overpressure data obtained along the surface is presented in Figure 2.15. For comparison, some points from mechanical (Wiancko) gages used by Project 1.10 are included on Figure 2.15. The gage values are generally higher than the optically determined values at distances greater than 1,100 feet.

The data obtained during Shot Mohawk was of doubtful value. The fireball was anamorphic, and no attempt to fit a curve to the radius-time envelope was made. The peak-shock overpressures were found in the same manner described previously. They are presented in Figure 2.16.

Shot Seminole was fired in a large tank of water on the ground. The tank dimensions and orientation are shown in Figure 2.17. No shock fronts were detected in the detailed examination of all available Seminole films. The development of the luminous front of expanding matter is indicated by the contours presented in Figure 2.18, which shows three views of this shot. Velocities in excess of 24,000 ft/sec occurred as can be seen from the rough distances and times indicated in each view. The effect of design of the nuclear device and associated diagnostic equipment on the contour shape is not known. No true fireball was observed in any of the films examined. The presence of the water around the chamber containing the device can be reasonably considered the chief reason for the lack of fireball characteristics.

2.8 RESULTS: DRAG-FORCE MEASUREMENTS

2.8.1 NOL Models. Shot Lacrosse offered a good opportunity to obtain the desired correlation between field and laboratory tests discussed in Section 2.2.6, by providing the necessary experimental requirements. Essentially clean shocks were expected from the device at the two gage stations in the area of interest, that is, at relatively high and low levels of dynamic pressure. These stations were 2,500 and 5,200 feet, respectively, from ground zero, at expected side-on overpressure levels of about 22 and 5 psi and corresponding dynamic pressure of about 10 and 0.5 psi. Some thermal and dust disturbance could be anticipated at the close-in station, but their gross effect was expected to be small.

These particular distances and pressure levels were selected in order to best tie in with the Operation Teapot experiments. On that test, gages were located at a 10-psi dynamic pressure (q) level in a dusty precursor region. Consequently, comparison of data for similar model targets from these two operations would give some clue as to the importance of dust and thermal influences on q and drag force. At the 0.5-psi q level during Shot Lacrosse, where nearly ideal shock waves were expected, additional data would be obtained to supplement the limited results from Operation Teapot in this region.

It was therefore planned that a similar configuration or set of models would be located at each of these stations. Model shapes, sizes, and aspects to blast were selected so that drag data from these models could best be integrated with the existing body of drag information. For instance, cylinders and parallelepipeds in two-dimensional configurations had been the object of considerable wind-tunnel and shock-tube experimentation in the past. Also, rectangular and square concrete block houses had been used as full-scale targets on nuclear weapon effect tests in the past; hence, models of these structures were included. The drag coefficients of spheres had been extensively investigated in wind tunnels and shock tube and also during Operation Teapot; hence, spherical targets were once again included. Also, all force gages were designed as multicomponent gages so that any force as a vectoral quantity could be measured regardless of the angle of approach of the loading function. In addition, all models tested for Operation Redwing were of such sizes and geometric configurations that the same models could be used in shock-tube and wind-tunnel tests in subsequent laboratory study. In this way, variations in data due to sting effects, model surface roughness, edge sharpness, and other such variables would be reduced or eliminated, thus enhancing the ease of correlation between laboratory and field data. The layout of the models, which was similar for both stations, is shown by Figure 2.19, which represents the B station at 5,200 feet.

The various model targets withstood the blast wave in good condition. Although the gages at the close-in station were subjected to uniform sandblasting on the sides facing ground zero, no denting or scoring were observed on the gages at the more distant station. The force gage and other instrumentation operated satisfactorily and gave electronic

records fairly good in quality except for the dynamic pressure gage. Some of the model-string-mount combinations were acceleration sensitive so that oscillations resulting from both air and ground shock appeared on the records. However, it was possible to fair an average curve through each record from which the data points were obtained.

The experimental free-field airblast phenomena measured at these two stations came close to that desired. No precursor was evident; also, thermal and dust effects appeared to be minor, although not negligible. Hence the clean, Mach-shock conditions were obtained to the degree anticipated at both gage stations. The actual overpressures and dynamic pressures measured by NOL above the ground plane mount were 18.4 and 5.7 psi, respectively, at a range of 2,500 feet (Station A) and 4.52 and 0.46 psi, respectively, at a range of 5,200 feet. In general, the data corresponds to that measured in the force field by SC and BRL. Some discrepancies were noted in the dynamic pressure measurements, and the quality of the records was questionable. Such behavior has previously been observed for the pitot-static gage in both field and laboratory tests. Also this gage is dust sensitive to some extent, but its actual registry coefficient is unknown. For these reasons and in order to be consistent with previous laboratory work, the dynamic pressure used in reducing the force-time records to drag coefficient-time records was computed from the overpressure-time records according to the following equation:

$$q = \frac{2.5 P_0 (P_S/P_0)^2}{7 + (P_S/P_0)}$$

Where P_0 = ambient pressure and P_S = side-on overpressure. The actual measured data and that derived by the above relation are compared in Figures 2.20 and 2.21.

The drag coefficients for the various models as a function of time were obtained from the force-time record by means of the following equation:

$$F = C_D qA$$

Where: F = drag force of the model

C_D = drag coefficient of the model

A = cross sectional area of model

q = dynamic pressure

As noted above the dynamic pressure used in data reduction was that computed from the peak overpressure time record. Some of the results obtained are shown in Table 2.7, which presents data corresponding to the peak overpressure measured at each station. Excessive emphasis should not be placed on this table, because it gives only a single comparison of values. However, in most cases, the values at the shock front are fairly representative of the overall curve. For a closer examination of the data for a specific model, reference should be made to the detailed C_D versus time plots for each gage in WT-1306.

Subsequent to the field test, the same models as those used for Shot Lacrosse, similarly mounted, were tested in the wind tunnel at Mach numbers of 0.2 to 0.5 and in the shock tube at shock overpressures from 3 to 30 psi. In order to correlate the data obtained in the wind tunnel and shock tube with that obtained from the field tests, several mechanical and aerodynamic problems had to be considered.

The major mechanical difficulties include sealing of the force gages against external pressure, or applying the proper correction factors when inadequate sealing causes internal pressures on the model or model-sting combination, resulting in extraneous net

forces. Furthermore, gage mounts must be rugged enough to withstand the blast during field tests but not so large as to influence the aerodynamics of the flow near the gage or to be unusable in identical form for the laboratory tests.

Aerodynamic problems involve the difficulty of determining the dynamic pressure or forcing function in both the field and laboratory; the lack of sufficient data on boundary layer development under transient conditions (particularly for the laboratory tests); the choking or blockage of the airflow when actual size models are used for the laboratory tests; and finally, the transient drag or the varying nature of the drag coefficient in steady flow until equilibrium is reached. The latter is particularly troublesome for low shock strengths in the laboratory. The change in C_D as a function of Reynolds and Mach number due to turbulence, surface roughness, and corner sharpness must also be considered in evaluating the results of laboratory and field tests.

Spheres. The laboratory sphere data from Operation Teapot was used for most of the correlation of the Redwing field data on spheres, because all pertinent aerodynamic properties were similar. The variation of the drag coefficient when the model is below the critical Reynolds number is very large. For 3- and 10-inch spheres in the wind tunnel, this number is about 3.5×10^5 as may be seen from Figure 2.22. All sphere data was taken above this value, so that no large variation of C_D with Reynolds number was observed. Consequently, for supercritical Reynolds number, the drag coefficient becomes fundamentally dependent on Mach number and was found to be fairly constant for these models, for Mach numbers up to $M = 0.2$ where the critical Mach number effects are strongly evidenced with the drag coefficient increasing sharply. This is clearly shown in Figure 2.22 and also in 2.23 where a comparison is made with previous data.

The shock tube data required a correction for gage leakage as previously discussed. However neither the uncorrected nor corrected data appeared to give realistic values of C_D at the lower pressures; however, at the higher pressures, where the correction was less important, the results appeared to be more satisfactory. This trend is evident for the corrected shock tube data in Figure 2.22, where good correlations with the wind tunnel data is obtained for Mach 0.5 to 0.6, while at lower Mach numbers, the shock tube data is low. However, no strong effects of critical Mach or Reynolds number are evident, inasmuch as the range of measurements for the shock tube data did not include either critical region. Because a large and uncertain correction for leakage was required for the field test data, it is believed that the corrected data is erroneous at the lower pressure levels and within an accuracy of ± 20 percent for the higher pressures. The shock-tube data is compared to the field data in Figure 2.24 at essentially two starting pressure levels under clean shock conditions. Although fair agreement is shown for gages loaded under similar field conditions—either high or low initial overpressures—the data does not compare well at the same pressure level for different starting conditions. This discrepancy is probably a result of the fact that the percentage error in this analysis increases as the shock wave decays. Further, although the field data was fairly consistent, it differed from the shock tube data. The reason for this difference has not been determined. The same pattern is evident in Figure 2.22, where there are three distinct groupings, according to the type of test, on the C_D or Mach number plot. The field results fall above both the wind-tunnel and shock-tube results. Apparently, there is a distinct difference for each of the testing conditions, which would bear further investigation. There is no explanation for the excessively high drag coefficient values obtained at these low Mach numbers during the field tests, except that dust loading may have had a significant effect at the close-in station on Redwing even though a precursor was not observed. It is concluded that spheres as force-measuring models are replete with interrelated difficult-to-establish parameters, which require extensive and detailed investigation.

before completely meaningful and correlative information is obtainable.

Cylinders. Although considerable information is available in the literature on drag coefficients for infinite cylinders in wind tunnel and shock tube tests, correlation with the Redwing laboratory and field data is subject to the differences in test conditions and the problems and errors previously enumerated. In wind-tunnel tests conducted for this program, the drag coefficients were found to be relatively constant over the range of Mach numbers from 0.2 to 0.5 and, accordingly, Reynolds numbers from 7.7×10^5 to 1.7×10^6 . The total variation in C_D was from 1.02, at Mach number of 0.2, to 0.93 at a Mach number of 0.5 and showed no indication of effects of the critical Mach or Reynolds number regions (Figure 2.25). The data correlated reasonably well with previous data when surface roughness was considered (Figure 2.26). The surface condition of the NOL test cylinder was considered unsmooth because of machining, countersunk holes, and unsealed gaps between the test section and sting—all of which produced a condition that was conducive to early turbulence and a drag coefficient independent of Reynolds number over the range of measurements.

Essentially flat-topped forcing functions were used in the shock-tube tests on the cylindrical models. The drag coefficients were found to be time-dependent, particularly at the lower pressures. Such fluctuation in C_D at early times is an indication of the diffraction-transition phase of the aerodynamic forces. It appeared that the steady drag phase of force was not reached in the 25 Msec or 50 transit times used in the measurements. Further investigation is necessary to establish the actual drag coefficients under steady-state conditions in the shock tube.

The drag coefficients obtained in the field test show good agreement between gages at Station B; however, the differences in force and C_D at Station A appear excessive after 50 msec. Inasmuch as C_D was essentially constant over a long time at Station B (during the decay phase), it can be assumed that the long-duration transient blast wave was approaching the characteristics of a steady-state function for the models tested. The field results gave an average C_D of 0.82, which was intermediate between the values derived from wind tunnels (steady state) where an average C_D of 0.97 was obtained and shock tube (short duration) where a C_D of 0.65 was reached for the later-time higher pressure situation. Consequently, for the model size used, wind-tunnel data could be used to predict field results with an accuracy of about 20 to 25 percent.

Parallelepiped. The drag coefficient for parallelepipeds is reported in the literature as 2.0 ± 10 percent for steady-state conditions in the wind tunnel and after 150 transit times in the shock tube. This drag coefficient is essentially independent of Reynolds number, because a turbulent boundary flow condition is established at a very low value of Re , which is maintained as the flow velocity and Re increase. The drag coefficients obtained in the wind tunnel varied from a C_D of 1.46 for $M = 0.2$, increasing to a C_D of 1.83 for $M = 20.4$ as shown by Figure 2.25. These results are lower than previously reported values. This was believed to be due to loss of seals between the test section and the supporting numbers, which resulted in a reduction of the translational force and a decreased C_D . The shock-tube parallelepiped data reflects the same varying characteristics as did the cylinders. Steady-state conditions may not be reached in the shock tube until after more than 100 transit times. Consequently, a comparison of the results of this program with other investigations was not justified, because C_D was obtained only up through about 50 transit times in the shock tube tests and represents conditions existing in the transition phase of the loading function.

The drag coefficients computed from the force measurements of the field data were internally consistent between gages and fairly constant with pressure at both stations. Average values were $C_D = 1.5$ for $M = 0.5$ at Station A and $C_D = 1.2$ for $M = 0.2$ at

Station B. These values are lower than those obtained in the wind tunnel for similar flow conditions, but in both cases, higher drag coefficients were found at the higher Mach numbers. This indicates that for these models the long-duration nuclear blast was approaching steady-state wind tunnel conditions. Therefore, it appears that wind-tunnel data can be used to predict field results for specific models with accuracies up to about ± 25 percent.

Cubes. Only limited data on cubes and rectangular shapes was available from previous laboratory work. A drag coefficient of 1.35 had been obtained for a 4-inch cube tested in a wind tunnel at extremely low flow velocities, i. e., natural winds on an elemental building form.

Tests were conducted in a wind tunnel using 4- and 10-inch cubes. Drag coefficients were found to be fairly constant for cubes of the same size but differed greatly between sizes as shown by Figure 2.25. However, all appeared to be independent of Mach number within the measured range. An average value of $C_D = 0.75$ was found for the 4-inch cube, and an average value of $C_D = 1.4$ was found for the 10-inch cube. This difference in the drag coefficient for the two sizes can probably be attributed to the boundary layer on the ground plane, which would have a larger effect on the smaller model.

Shock-tube data was obtained only on the 4-inch cube. The 10-inch cube could not be mounted so as to be independent of the motion of the walls of the shock tube in the expanded test section. The drag coefficients obtained in the shock tube for 4-inch models (Figure 2.27) agree closely with those obtained in the wind tunnel with 10-inch cubes (Figure 2.25) but not those of the 4-inch cubes. The differences in the 4-inch cube data are probably due to differences in testing conditions between the shock tube and wind tunnel, which reduced boundary layer effects in the shock tube. Readings were taken in the shock tube for durations of 150 transit times, and it appears that pseudo-steady-state conditions prevailed.

The drag coefficients obtained for the 4- and 10-inch cubes at Station B on the field test correlate fairly well with wind-tunnel data. However, the 4-inch gage at Station A agrees better with the shock-tube data and shows a strong time dependence (Figure 2.27). A strong sandblasting effect was noted on the front face of the 4-inch gage at Station A although no evidence of a precursor appeared on the pressure records. Under these conditions, some influence must have been exerted on the overall loading by the sand, which would not be reflected in laboratory or theoretical investigations. Difficulty was also experienced in attempting to correlate the field data to that obtained for a cubical structure on Operation Upshot-Knothole (Figure 2.27). Further study is necessary before laboratory data can be applied to field structures.

Comparison of the Effects of Nonideal Blast. The essentially ideal shock-wave conditions of Operation Redwing can be compared to those existing on the precursor regions of Operation Teapot, because the force gages were similar. In addition, the dynamic pressure levels were approximately the same, as measured by the pitot-static gage, which is sensitive to dust in an unknown manner.

For this comparison it is necessary to review the Teapot data. The photographic coverage of the 2,500-foot station on the desert line indicated the dust arrival lagged the shock arrival and coincided with a sharp increase in the force reading for an initial peak force around 70 msec later, as well as a gradual increase in the side-on pressure and a q maximum of 10 psi at this time. However, a second major maximum of force was reached after about 600 msec. At the 2,500-foot station on the asphalt line, the dust front arrived about 20 msec after shock arrival while the force and q reached a sharp maximum about 250 msec after shock arrival. However, at the 3,000-foot stations on both lines, where the dust arrived considerably behind the shock front, there were no strong

and distinct evidences of dust loading. It is believed that the initial dust resulted from particles picked up from nearby locations, whereas the second peak reflects the arrival of heavier, slower moving particles and inhomogeneities drawn into the airstream at locations considerably closer to ground zero.

In Operation Redwing, the contribution of dust can be evaluated by examining the cube data at two stations. Although the records indicated a clean shock condition at Station A, the gage faces suffered severe, uniform sandblasting on the ground zero side only. This indicates an impact of particles transported radially and horizontally from ground zero. It is likely that the sand was picked up well ahead of the gage station, possibly in the observed precursor region, and thus arrived behind the shock front to load the gage. The drag coefficients computed for these gages (as well as others) at Station A are higher (and increased with time) than those for Station B, which was not subject to this sandblasting.

Comparing the 10-inch spheres of Operations Teapot and Redwing, it is significant that the Teapot sphere on the desert line at 2,500 feet was subjected to a force of approximately 600 pounds, which is appreciably greater than that measured by similar gages at the same q level on the asphalt line (about 60 pounds), or at the relatively clean 2,500-foot station of Redwing (about 300 pounds).

It is evident that dust makes an important contribution to the total drag force measured by target models. It is also obvious that the dust registry coefficient is higher for these gages than for the pitot-static gage. Consequently, the response of these idealized shapes can be related more closely to the actual damage to drag-sensitive targets than phenomena measurements. However, more and better data are needed before quantitative values can be established.

Conclusions. The general test objectives were realized; satisfactory drag force time records were obtained for all target models under nuclear-blast, shock-tube, and wind-tunnel conditions. The data obtained appears accurate within ± 15 percent but is complicated by extraneous signals. Although the findings of this investigation compare favorably to the data previously available, much depends on the validity of certain assumptions in the interpretation of aerodynamic phenomena. The shock-tube wave durations were too short to establish steady flow for the two-dimensional models, and the drag coefficients for the cylinder and parallelepiped are time-dependent, indicating data within the transitory phase. The drag coefficients for the cubes require consideration of the boundary layer existing on an artificial ground plane. Also, particulate matter in the airstream was found to contribute significantly to the measured drag force for the same model in different environments but at the same dynamic pressure level.

The following specific conclusions reflect the above considerations:

(1) For the model sizes used and shock-wave characteristics obtained, the nuclear-blast wave approached the steady-state conditions of the wind tunnel. In the shock-tube tests, shock conditions did not approach steady state conditions except for small three-dimensional models because of size limitations and short wave durations.

(2) Although the drag coefficients of round-edged models (spheres and cylinders) are somewhat unpredictable in the present test range, equivalent tests on identical models, in the wind tunnel and in the field, gave consistent results.

(3) Although drag coefficients for cubes mounted on planes depend on size relative to boundary layer effects, wind-tunnel tests can be used for predicting force on cubes in the field if similar mounting surfaces are used.

(4) For two-dimensional models under shock-wave conditions, 75 or more transit times are necessary to establish steady-state conditions. Three-dimensional models require less time.

(5) Force-gage models are more sensitive to dust and sand loading than are gages which measure free-field phenomena, primarily because of differences in size of sensing area. The dust loading may be several times greater than that of a clean or pure aerodynamic airblast loading, particularly in the precursor region. However, dust loading can occur in what may normally be considered clean ideal regions. This additional loading may have a damaging effect on a target, even though not completely evident in measurements of overpressure and dynamic pressure.

2.8.2 BRL Full-Scale Structural Members. Shot Cherokee presented an opportunity to obtain the drag loading on full-scale structural members in an essentially clean shock region of a long-duration blast wave. Consequently, measurements of net force versus time on wide-flange steel beams and angles were planned at four stations located at ranges of 12,000, 20,500, 24,000, and 35,600 feet from intended ground zero. As seen in Figure 2.28, these structural members were simply supported between two much heavier elements used as posts. The total lift and drag forces exerted upon the beams were transferred to the instrument mount by the sensors, which provided a ball-and-socket joint at each end to approximate an ideal pinned connection. Response of these sensors was measured by SR-4 strain gages.

Despite the error in the drop of the device, the gages and recording apparatus operated successfully with the loss of only a few records. The measured peak values of the drag and lift forces acting on the angles and beams are given in Table 2.8. However, the deviation between actual and intended ground zero resulted in an unexpected flow direction and higher overpressures than anticipated. In one case (the angle member on Site Dog) the instrumentation failed to function properly, because it was not shielded from thermal radiation for this angle of yaw. The records of drag force versus time for the wide flange beams are shown in Figure 2.29. However, only the peak forces were read from the angle-iron recordings, because they experienced signal shifts when loaded.

The accuracy of the drag and lift coefficients obtained depended mainly on the correct determination of the dynamic pressure experienced by the test members. Because there was a deviation of flow from that expected at each station, the test members did not receive the full impact of the free-stream dynamic pressure. Consequently, only that part of the flow normal to the beams was considered, because the test members can only sense forces in the same direction as the sensors. Further, dynamic pressure is a scalar and cannot be resolved into components. However $q = \frac{1}{2} \rho v^2$ where particle velocity v is a vector, and ρ is the density. The particle velocity normal to the beam is then $v \cos \theta$ where θ is the angle of yaw. Then the corrected dynamic pressure q' can be found by substitution in the following manner:

$$\begin{aligned} q' &= \frac{1}{2} \rho (v \cos \theta)^2 \\ q' &= (\frac{1}{2} \rho v^2) \cos^2 \theta \\ q' &= q \cos^2 \theta \end{aligned}$$

This procedure was used to determine the lift and drag coefficients in Table 2.8. These are compared to steady state values in Table 2.9. In general, the agreement is good, although all of the coefficients derived from field data are larger than steady-state values. The BRL results from Shot Cherokee are in contradiction to the NOL results on cylinders and parallelepipeds from Shot Lacrosse where the wind tunnel drag coefficients were generally larger than the field results. However, such a comparison should not be taken as being proof of a yield dependence because of the yaw correction required by the Cherokee data.

2.8.3 BRL Spherical Drag Gages. Shot Cherokee also provided an opportunity to study the nature of the drag exerted on spheres in the transient-flow field following a long-duration classical blast wave. The results obtained could be compared with previous measurements during Operation Teapot with the same gages as well as with results obtained by NOL with similar gages during Shot Lacrosse. In this manner, the effects of blast wave duration and dust loading could be determined as well as Reynolds number scaling between two sizes of spheres.

The gage was essentially a spherical shell coupled to a rigid support sting by a 3-dimensional sensing element consisting of a precompressed aluminum linkage. The design of the gage resulted in a high natural frequency, a slippage-free action, and an inherent ease of being damped. Two drag stations were constructed prior to Shot Cherokee, one on Site Able and the other on Site Dog. One 10-inch diameter gage and two 3-inch diameter gages were mounted 3 feet above the ground at each station on a 6-inch double extra-heavy pipe. All gages were statically calibrated in the field after installation along the three sensitive axes, because measurements of net force versus time were desired in three mutually perpendicular directions.

Unfortunately, the field results were seriously affected by the drop error, which caused great differences between the pressures predicted and those obtained. Site Able had a signal recorded which was about one-thirtieth of that expected—barely exceeding the noise level of the instrumentation. Site Dog, on the other hand, received about twice the pressure expected, giving peak values sufficient to overstress the sensing element in some cases. The dynamic pressures measured were also considered unreliable, because of angle effects and small signal amplitudes.

Corrections were applied to the data to account for such factors as sting size, gage leakage, and nonaxial flow. Dynamic pressures were computed from side-on pressure values with the aid of the Rankine-Hugoniot relationship. The most probable peak drag coefficient values are given in Table 2.10. These values should not be considered as authoritative, but rather an attempt to determine trends and general behavior from that information gleaned out of the test data on the basis of past experience in related studies. Little similarity was found to exist in a comparison of Teapot and Redwing data. Consequently, the objective set down for the spherical drag gage investigations on Shot Cherokee were not achieved.

2.8.4 Military Vehicles. This phase of the drag force program was designed to obtain information on the response of drag-sensitive targets to a classical blast wave, for comparison with that observed for a nonclassical wave. More specifically, the variation of vehicle damage with range for a medium-yield surface burst at the PPG (Shot Lacrosse, 39.5 kt) was to be investigated and compared with similar data for a medium-yield tower shot during Operation Teapot at the NTS—Shot 4 (Turk), 43.2 kt. Although both shots were approximately the same yield, a strong precursor was observed during Shot Turk, whereas a precursor was not expected for Shot Lacrosse. As previously noted, however, a limited precursor was observed at close-in stations during Lacrosse, but it cleaned up rather quickly, and its effects did not extend to the vehicle stations.

It was also planned to expose military vehicles on a [redacted] tower shot (Yuma, [redacted]) and a [redacted] surface burst (Zuni, 3.53 Mt) in order to obtain additional data on jeep damage over a wide yield range. Such empirical information would be evaluated in terms of the environmental conditions at the PPG and consolidated into statistical damage evaluation studies, which are used as a basis for prediction of damage to all types of military field equipment. In addition, the data from all three shots would be compared with isodamage curves from Reference 4 in order to verify scaling and confirm or extend

current prediction methods.

A preshot vehicle-condition inspection was performed, during which all major components were numbered for later identification. Only the windshields, bows, and canvases were removed.

The postshot evaluation consisted of inspecting each vehicle and measuring displacements. An attempt was made to start and operate each vehicle where practicable. Vehicles that could be operated within one man-hour of maintenance time were considered to be immediately combat usable. Damage levels (light, moderate, and severe) as well as type of maintenance were selected on a basis of man-hours required for repair:

Damage Level	Man-hours	Type of Maintenance	Man-hours
Light	0 - 1	Organizational	0 - 6
Moderate	1 - 32	Field	6 - 32
Severe	> 32	Depot or Salvage	> 32

Ten vehicles were exposed during Shot Lacrosse. The vehicles were placed in pairs at five stations ranging from 2,500 to 4,378 feet from ground zero, with one vehicle facing into the blast and the other broadside to the blast. Ten vehicles, including two recovered from Shot Lacrosse, were exposed during Shot Zuni. Eight vehicles were placed in pairs (one face-on and one side-on) at four locations ranging from 8,300 to 13,800 feet. One side-on vehicle was placed at 7,000 feet, and one side-on vehicle was placed at 16,500 feet.

Eight vehicles were exposed during Shot Yuma;

The
vehicles were placed in pairs at four stations ranging from 150 to 400 feet from ground zero.

All of the test stations were selected on the basis of predictions from the 1955 edition of Reference 4, which would provide levels of damage ranging from light to severe. The height of burst was scaled as $W^{0.33}$ while the ground range was scaled as $W^{0.4}$. Following each shot, vehicle damage at all stations was evaluated in terms of man-hours required for repair. Damage at typical stations for each shot is shown in Figures 2.30 through 2.32.

The damage resulting from Shot Lacrosse was slightly less than expected, at overpressure levels ranging from 19.5 to 7 psi. Only the side-on vehicles at the two closest stations suffered moderate damage. The other eight were only lightly damaged, and six of these were considered immediately combat usable.

Severe and moderate damage resulted from Shot Zuni, at overpressure levels ranging from 35 to 8.3 psi. All vehicles at stations closer than 13,800 feet suffered severe damage. No vehicles were considered immediately combat usable.

A gradation of damage from severe to light was obtained on Shot Yuma, at overpressure levels ranging from 107 to 20 psi. Only the two vehicles at 400 feet were considered immediately combat usable.

Following Operation Redwing, the isodamage curves for military vehicles in Reference 4 were revised, because the preliminary data for the two surface bursts indicated a significant decrease in damage radii. The final Redwing data has been scaled to 1 kt by $W^{0.4}$ and compared to the current isodamage curves in the 1957 edition of Reference 4. This comparison is shown in Figure 2.33.

Because the bulk of available nuclear data on blast damage to military vehicles was obtained at the NTS, it is not surprising that the data from Shot Turk shows the best agreement. However, it should be remembered that most of the NTS damage information was taken under strong precursor conditions for low heights of burst, involving nonideal

dynamic pressures, irregular waveforms and dust-laden airflow. In contrast, all of the vehicle damage data from the PPG involved essentially ideal dynamic pressures, classical waveforms, and a minimum of dust. The effect of orientation is also visible in Figure 2.33.

Another comparison of the PPG data with the NTS data is made in Figure 2.34, which shows ground range and yield for various damage levels.

A line showing the variation of damage radius with yield raised to the 0.4 power was drawn through the NTS data points. The line fits the data points well and substantiates the use of this scaling factor for the range of yield measured. The damage radius for Shot Lacrosse was significantly less than that of the corresponding NTS shots. When a line corresponding to scaling damage radius of $W^{0.4}$ was drawn through the point for Shot Lacrosse, it intersected the data points for the other PPG surface shots. Hence, the NTS shots and the PPG shots formed two groups with different damage radii but with similar scaling properties.

The NTS shots were detonated primarily at a scaled height of burst (HOB) between 100 and 300 feet, while the PPG shots considered were surface shots. However, under ideal conditions, the data of the two groups should overlap, because the ideal dynamic pressure and dynamic impulse contours are essentially vertical for a range of HOB from 0 to 300 feet. Consequently it would appear that the difference in damage radii observed is due primarily to the nonclassical disturbed wave shapes that occurred at the ranges of significant vehicle damage on the NTS shots and the essentially classical wave shapes that occurred on the PPG shots. This conclusion is supported by the fact that peak dynamic pressure data obtained at the NTS showed considerable variation from the ideal values in the range of interest for damage to vehicles. However, the peak dynamic pressure data recorded at the PPG corresponds to a classical wave.

Figure 2.34 also shows the empirical data from Shot Yuma, which corresponds to a scaled height of burst of feet for 1 kt. Although this scaled HOB is in the region where the bulk of the NTS data was taken, the data falls below the $W^{0.4}$ scaling line. This lack of agreement may be due to the fact that relatively clean waveforms were observed all along the Yuma blast line.

On the other hand, it is also possible that scaling by $W^{0.4}$ does not apply!

It is interesting to compare the actual damage or target response to classical waveforms over a wide yield range at the PPG. Table 2.11 gives vehicle orientation and damage with corresponding values of peak dynamic pressure for the three Redwing shots. The significance of this increase in peak dynamic pressure required for a given level of damage on a low-yield shot compared to a high-yield shot becomes evident when the corresponding durations are compared. On Shot Yuma, severe damage to a side-on vehicle was achieved at 24.8 psi with a duration of 45 msec whereas the same damage was observed for Shot Zuni at 6.4 psi with a duration of 3,500 msec.

Some reduction in the observed damage radii compared to the NTS may have been due to the soft sandy surface at the PPG. This would have had the effect of reducing the displacement and decreasing the force of impact of the vehicles with the surface while they were tumbled by the blast wave. This effect is believed to have been small, and compensated for by the differences in atmospheric conditions under which the two sets of data were taken.

It is therefore concluded that the large differences in damage radii observed as a result of the Redwing tests when compared to the previous NTS data are due to differences in wave shape and dust loading, so that damage did not extend as far for Lacrosse and Zuni at the PPG on the basis of $W^{0.4}$ scaling. The same conclusion may apply to the Yuma data, but it is not certain whether this method of scaling will extend to this

2.8.5 Cubicle Target Structure. A structure previously used during Operation Castle was renovated for use during Operation Redwing. It was desired to obtain diffraction and drag data on a nonresponsive target at a higher pressure and a longer positive-phase duration than had previously been recorded in the field as well as to validate model-scaling methods for classical waveforms in the moderate pressure region (15 to 20 psi). These methods had been verified for clean blast waves in the low-pressure region (3 to 6 psi) by successful correlation of target loading measurements on a number of full-scale test operations with shock-tube tests on scaled models. Consequently a 6- by 6- by 12-foot concrete cubicle located 9,700 feet from ground zero was subjected to the blast effects of Shot Zuni (3.53 Mt). Free-field measurements of overpressure and dynamic pressure were made near the structure with electronic gages, supplemented by self-recording gages.

Prior to Operation Redwing a $\frac{1}{36}$ scale model was tested in the BRL shock tube at the predicted overpressure level of 17.5 psi for a 2.5 Mt yield so that correlation between field and laboratory data could be attempted. An idealized free-stream overpressure versus time curve was determined from the nearby free-field measurement of 23 psi with a positive-phase duration of 2,500 msec, using an empirical decay constant. This curve was then used to scale the shock-tube data obtained with flat-topped waves. Readings were taken at identical gage positions on the model and full-scale cubicle as shown in Figure 2.35. Although 29 gage positions were planned for the full-scale cubicle, the time available between Shot Cherokee and Shot Zuni was not sufficient to calibrate more than nine channels. These were chosen as the most representative over the four surfaces but were not necessarily adequate to determine the average pressure over a surface, or a drag coefficient.

The pressure versus time records from the shock tube are compared to the full-scale data in Figures 2.36 through 2.38. The front face records depart from the trend expected for classical waveforms in that the reflected pressure should have decayed to a stagnation pressure in about 25 msec; however, there was very little decay within the first 100 msec at Positions 24 and 27. The decay shown at Position 28 was still less than expected.

Good pressure measurements were obtained on the top face. The effects of vortex action on attenuation of the initial pressure rise can be seen from Position 15. This effect becomes weaker as the shock front moves across Positions 9 and 1. There exists some evidence of a rarefaction wave moving from the rear edge back over the top face. Only the diffraction phase of the record for Position 9 was considered valid, because there appeared to be a gage malfunction after about 200 msec.

The records for the two positions on the back face appear valid. There was a slow buildup of pressure to a value slightly less than the incident side-on or free-stream

pressure. However, some differences in impulse and duration between the two records were noted. The side face record at Position 44 also appears valid.

In general, the field data compares very favorably to the shock tube results when input conditions are considered, although some minor inconsistencies were observed. A classical waveform was not obtained in the field. The slow rise and irregular shape is evident on the dynamic and side-on free-stream pressure records shown in Figure 2.39 for Station 156.01 located 100 feet to the side of the structure. Further, during the first 100 msec the dynamic pressure exceeds that calculated from the measured overpressure with the Rankine-Hugoniot relationship.

The primary objective for this part of Project 1.5 was achieved. However, it is evident that adequate coverage with field instrumentation is required if correlation and interpretation of laboratory data is to be undertaken. The diffraction-phase loading on the top, back, and side was similar to what might be expected from shock-tube tests, but the loading on the front face was quite different. Indications are that the drag-phase loading was much higher on all faces than would have been predicted from laboratory data.

2.8.6 Electronic Instrumentation. A separate project was formed to provide support with electronic instrumentation for drag studies involving structural members, spherical drag gages, damage to military vehicles, the cubicle target structure, and effect of length of the blast wave positive phase on drag and semi-drag industrial buildings. Measurements of side-on and dynamic pressures, column deflections, column strain, accelerations of columns and footings, all as a function of time, were required as well as time of break of frangible siding. These measurements were taken during Shots Cherokee and Zuni. The multichannel, phase-modulated magnetic tape recording equipment used during Operation Teapot was modified and used in Operation Redwing.

The overpressure measurements were made with Wiancko type 3PAD-R pressure gages. The Sandia Corporation pitot static gages were utilized for dynamic pressure measurements. Wiancko Type 3AA-T accelerometers were used for acceleration measurements. Column strain measurements were obtained with SR-4 strain gages. The time-of-break gage was developed by BRL, using a resistance bridge arrangement. Prior to each shot, all gages were calibrated statically in conjunction with the entire recording system in its field setup.

The probable accuracy of the full scale data is ± 12 percent, based upon the observed accuracy of ± 6 percent for dynamic measurements in the laboratory with this recording equipment.

A summary of instrumentation results is contained in WT-1305. Considering environmental factors and other factors at the PPG, the percentage of good records is fairly high. However, the drop error on Shot Cherokee caused the loss of some records, because the thermal radiation arrived from an unexpected direction, and the shock wave came in at a different angle and with a different magnitude than predicted. Also a number of deflection gage records were lost because of corrosive effects of the salt water atmosphere on the gage wire.

2.9 RESULTS:

2.10 RESULTS: CRATER MEASUREMENTS.

Crater measurements were made on five shots: three fired on or near the surface of the ground (Lacrosse, Zuni, and Seminole); one tower shot (Mohawk); and one shot over shallow water (Tewa).

The physical characteristics, i. e., apparent diameter and depth and approximate profile, were measured for all of the five craters. Aerial mapping photographs were taken of the craters after the shots, and these were used to plot ground elevations and give initial crater diameters. At a later time, lead-line soundings were made along at least three diameters of each crater to determine depth and average profile.

The results of the crater surveys are given in Table 2.12.

2.10.1 Shot Lacrosse. This shot was fired over a reef off Charlie, with about 2 feet of water over the reef at shot time. The crater lip did not breach, which effectively prevented rapid flow of water into the crater. This was the first incidence of such an unbreached lip at the PPG. Scalewise, the crater was smaller in radius and greater in depth than PPG washed craters and falls between the scaled results expected for NTS soil and that for PPG soil. Figure 2.42 is a photograph of the Lacrosse crater indicating the crater lip formation. It is believed that the soil (or coral rock) at this particular location is considerably stronger than the average soil conditions of the atoll.

2.10.2 Shot Zuni. This shot was fired approximately 9 feet over Site Tare at a location adjacent to the east of the crater left from Shot 3 of Operation Castle. The Zuni crater engulfed the old crater, which was on the lagoon side of the island, but did not breach on the southern, ocean side of the island. It remained sufficiently intact on the western and southern sides of the island to prevent any extreme waves on nearby islands. Except for its eastern and southern sides, the crater was completely submerged.

The Zuni crater results must be looked at rather critically before being included in the weapons effects literature because of the above-mentioned conditions. The size of the crater is smaller than expected, both in radius and depth, and because of the many difficulties in explaining the conditions surrounding the burst, it is not felt that this departure from average PPG results should be considered serious.

2.10.3 Shot Seminole. This shot was fired 4 feet above ground level in a tank of water on Site Irene. The tank was 50 feet in diameter and 25 feet deep. The device was surrounded by an air chamber and was slightly offset from the center of the tank. The

western side of the crater was breached to the water over the reef and destroyed a small portion of the causeway joining the adjacent island. Because of the 20 feet of water above the center of gravity of the device, it is felt that the shot tended to behave as an underground shot fired about 12 feet below the surface of a knoll at ground zero. A more detailed discussion of the reasoning behind this assumption can be found in WT-1307. However, there appears to be little doubt that firing in a water tank can have an appreciable effect of increasing the crater dimensions, even if the shortest distance to the outside air is as little as 10 feet, as was the case for Seminole. In fact, the radius of the water was somewhat longer in the direction of greatest thickness of water in the tank.

2.10.4 Shot Mohawk. This shot was fired on a 300-foot tower on Site Ruby. The crater diameter compares favorably with predictions, although the existence of a lip may indicate that full washing did not occur.

2.10.5 Shot Tewa. This shot was fired on a barge in approximately 20 feet of water adjacent to the Charlie-Dog reef. Although the bottom slopes from north to south through ground zero, this variation is small compared to the crater size. Because of the air-water and water-ground interfaces, however, it is believed that less than the expected energy was channeled into cratering. It is also difficult to assume a height of burst, but it is believed that it should be between 0 and 20 feet.

2.10.6 Correlation of Crater Data. All previous PPG results on crater radius as a function of burst position are presented with the reducing data in Figure 2.43, scaled to 1 kt by cube-root scaling. In this figure the lower line is the dry-soil curve from Reference 4 representing NTS conditions; the upper line is a curve drawn through data available from PPG. The actual measurements at PPG are scaled to 1 kt with the exception of those for Seminole whose burst position has been adjusted for the location of the device in the water tank as given in Table 2.12. Also shown is a saturated washed curve as defined from Reference 4.

The cases in which the crater radii do not fit the adjusted curve from Reference 4 may be explained by the extreme difficulty in obtaining crater dimensions at PPG—especially for tower bursts or for large craters; an unwashed crater such as Lacrosse; different degrees of washing in the cases of Seminole, Mohawk, and Shot 3 of Operation Castle (the radius of these shots should be adjusted upward by at least 10 percent); or unusual environmental conditions, as for Seminole, Zuni, or Shot 3. The Seminole device was placed in a tank of water, part of the energy from Zuni vented into the lagoon, and Shot 3 had different radii listed at 380, 400, and in excess of 600 feet (the true radius is probably closer to 500 feet rather than the 400 feet commonly listed). For near-surface bursts, a soil factor of 2.0 can be derived for comparing the radius of the PPG washed craters in saturated coral to the Nevada cratering curve given in Reference 4. This factor is substantiated by a series of HE surface charges fired in Eniwetok during Operation Ivy and compared to similar data gathered at NTS during the Mole experiment and Operation Jangle.

As more Pacific operations were conducted and additional cratering data was obtained, a trend became apparent in the data from surface explosions. This trend shows the increase in the ratio of the crater radius to crater depth as the yields increased into the multimegaton range. It would be expected that as the yield and, correspondingly, the duration of the positive phase of the airblast gets very large, a lower pressure would be required to produce measurable displacement at ground surface. In other words, if it is assumed that a certain value of impulse is required to produce ground displacement

sufficient to be measured as part of the crater, this value of impulse can be obtained from lower pressures as the yield and duration increase.

The crater depth data is not as consistent as the radius data and does not readily lend itself to soil factors. As mentioned above, as the yield increases so does the ratio of radius to depth, because the depth does not increase at the same rate as the radius. It is believed that this is caused by the increasing lack of similitude of the soil with increasing real depth as the yield increases. Simply stated, the hydrostatic forces at a point in soil 300 feet below the surface are much greater and different from those at a point 30 feet below the surface. Scalewise, these are the same cube-root scaled depths for a 1-Mt and a 1-kt device.

Consequently, the larger the yield, the greater the deviation in depth from cube-root scaling. This lack of scaling should apply to all soils and indicates the danger of extrapolating the present data on crater depth to extremely high yields.

2.11 RESULTS: WATER-WAVE STUDIES

2.11.1 Direct Waves. The waves generated in the lagoon were recorded at various stations in midlagoon, around the inner periphery, and on the islands. These records were analyzed in order to separate and study the effects of shot yield, bottom topography at shot site, topography over the propagation paths, depth of water at measuring site, and reflections from neighboring reefs. Records from Operations Crossroads and Castle were also used in the analysis.

For the Redwing tests, the waves had the following general characteristics. The first wave was always a crest followed by a trough. Following this trough was a series of waves occurring as a discreet group, or groups, of waves. For near ranges, the first wave was the highest, but as range increased the first wave progressively diminished in amplitude relative to the amplitude of the following waves.

It was found that the characteristics of generated waves, i.e., the arrangement and energy distribution of waves within a group, change over a wide spectrum as the relative magnitude of the parameters of generation change, and therefore it is not sufficient to group waves into shallow water and deep water types for purposes of scaling. In particular, the product of height and range (HR) cannot be indiscriminately scaled. The change in spectrum as the depth of water is changed was examined, but no complete model is available by which the types of waves produced by a given set of conditions can be predicted.

This analysis of wave generation in shallow water was based on an assumed initial condition of a water crater where the lip represents the initial wave and the collapse of the crater generates the succeeding wave train. The crater dimensions were calculated by equating the wave train energy, as deduced from the records, to the potential energy of a cylindrical crater of height equal to the depth of water at the shot site. These dimensions were used to obtain theoretical wave trains, using the theory in Reference 8, which were compared with the actual records. The agreement was poor. Calculations were also made using an energy equivalent to the cylindrical depression but with this energy in the form of an initial impulse with parabolic distribution and also using exponential distribution. Essential differences between these theoretical wave envelopes and the actual waves were found. Figure 2.44 shows the calculated crater radii plotted against yield. The plot indicates a variation of crater radius with the fourth root of the yield.

The basic data for the first-crest height and the first wave (first crest plus following trough) are shown in Table 2.13. The data contain the effects of reflection from near

shorelines. A scaling equation for the first crest height was derived:

$$H_C R^{0.95} = 0.0234 h_g^{1.38} W^{0.34}$$

Where: H_C = first crest height in 60 feet of water, feet

R = refracted range from zero point, feet

h_g = average water depth over area of generation

W = TNT equivalent yield, pounds.

Basic data on wavelengths for three of the shots is plotted in Figure 2.45 as a function of range. The first-crest to second-crest distance was chosen as the most representative wavelength. A plot of wave length versus yield shows that, at a fixed range, the wavelength increases with the fifth root of the yield. This is in fair agreement with the previous finding that crater dimension varies with the fourth root of the yield. Wave speeds and arrival times for the first crests of the wave system can be calculated by standard methods for refracted wave paths over shoaling water.

No quantitative analysis of the effects of shoaling at the beaches on the wave heights was made. However, it can be concluded that the large waves are altered to a greater extent than small waves.

A crude correlation of inundation with the recorded waves was made, taking into account only the first crests. The extent of inundation, however, is affected by the number of waves—succeeding waves pump more water into already flooded areas. It is also, of course, dependent on tide stage and wave size. Consequently, it was not possible to develop methods for prediction of inundation.

The question of inundation of various scientific and support installations from the large-yield lagoon shots of Operation Redwing was of particular concern to the Task Force Commander and his staff. Various precautions were taken to minimize these effects, such as securing all buildings, placing all vehicles in the center of the island, and surrounding the motor pool with earth berms. Surveys of areas certain to be affected by inundation were made before and after each event. Figure 2.46 shows the condition of Nan Island following Shot Navajo. The large refrigerator shown was half full, yet was moved approximately 90 yards inland.

Considerable interest had been aroused in speculation as to possible inundation of Site Nan from Shot Zuni. It appeared possible that, if the crater breached through the reef to the open ocean side, sufficient energy would be released to flood at least the south end of Nan. This inundation would be caused by refraction along the Tare-Oboe complex so as to produce convergence of energy into the first wave as it traveled across the Nan channel. As it turned out, wave action at Nan was negligible. The crater did not breach into the open ocean, and energy absorption was almost complete along the Tare complex. However, Uncle Island was swept clean of vegetation by wave action, as was expected.

2.11.2 Indirect Waves. Long-period waves produced by megaton-yield explosions had been detected during Operations Ivy and Castle. These waves have the characteristics of tsunamis, or earthquake-produced waves, which can create extensive damage at long distances from their source. Generally speaking, it appears that the amount of energy going into wavemaking increases as the square of the shot yield.

Waves were measured at Ailinginae Atoll, Eniwetok Atoll, Wake Island, and Johnston Island, which ranged from 59 to 1,500 miles from the shot points. A special long-period-wave recorder was used, which is capable of resolving waves less than 1 mm high.

Microbarograph stations were also operated at Wake and Johnston Islands, and supplemented by similar observations made by Project 30.1. The data from Operation Castle was also utilized in the analysis of wave generation contained in Reference 9.

This analysis of the wave generation uses a theoretical model of air overpressure versus time and range, which is integrated to obtain the impulse. This model, applied to geometry of the shot location within the atoll, can explain the observed variation of wave energy with the square of the yield as being due to the effect of atoll shadowing.

The waves observed had deep-water heights of from $\frac{1}{2}$ to 10 inches. The wave heights varied inversely with range out to about 200 miles, as predicted for dispersive waves. Beyond this distance there is an apparent change, and they vary inversely with the square root of the distance, which is not in accordance with the theory in Reference 8. In view of the fact that the data supporting this anomalous decay is meager and not entirely consistent, predictions of waves based on this reported behavior should be used with caution.

The wave periods observed varied from 200 to 600 seconds. A comparison with the theory in Reference 8 again shows discrepancies that are not accounted for. However, in view of the odd geometry of the shots, where the wave generation begins at the edges of the atoll and the edges are at varying radial distances from the shot location, it would have been surprising indeed to find agreement between the observed results and any theory.

On the basis of the impulse model used, curves of wave heights versus range were constructed and extrapolated down to yields of 1 pound and up to 500 Mt. These curves are shown on Figure 2.47. The wave heights predicted by this figure for surface shots over deep water are smaller than those predicted on the basis of small HE shots by a factor of eight. Because there are also many uncertainties connected with extrapolation of HE results to the nuclear range, the discrepancies between the two results cannot be resolved. The true answer can lie anywhere between these two. The curves give accurate predictions for the types of atoll shots fired during Operations Castle and Redwing. In this case the curves are entered with an effective yield, which is determined by multiplying the actual yield by that fraction of the total impulse that falls over the sea. The procedure for computing the effective yield is also given in Reference 9.

2.12 DISCUSSION: FREE-AIR DATA

2.12.1 Shot Cherokee. The only free-air results obtained from Shot Cherokee were the Pressure-time measurements made by Project 1.4 (AFCRC) with parachute-borne canisters. Because of the offset of the actual detonation from intended air zero, all canisters were at slant ranges greater than 17,000 feet from the burst point, and the highest measured free-air pressure was 5 psi. Furthermore, although these measurements covered an altitude range from 5,600 to 33,800 feet over the shot island, the horizontal displacements were considerably longer than expected. Consequently, it was not possible to isolate the effects of the inhomogeneous atmosphere from refractive effects or spherical divergence in the way originally intended, i. e., by positioning the canisters directly over the burst point. In addition it was not possible to position the canisters independently by photography, or to correlate the data obtained from measurements of peak pressure in the horizontal and vertical directions that were expected to result from analysis of rocket-trail photography. As noted in Section 2.3.1, it was not possible to follow shock propagation across the rocket-trail grid background, because the shock strength was too low and the device light too weak when the blast wave entered the field of view of the cameras.

In view of these considerations, it is felt that documentation of the free-air blast wave from a multimegaton airburst has met with only limited success. It should be noted that

the measured data is considered valid to within instrumental error; however, the uncertainty lies in the fact that the precise locations of the canisters in space at shock arrival is not independently known, nor was it possible to correlate the data with other measurements.

For purposes of comparison with various free-air curves, the AFCRC canister data has been reduced to 1 kt at sea level by use of the Theilheimer-Rudlin equation with $\alpha = 0$ when the function $Q_h = 10$. The scaled data is shown in Figure 2.48, together with the AFCRC mean curve derived from small-yield tests at the NTS by the same procedures. Figure 2.48 also presents the AFSWP composite curve for airborne targets from Reference 4. However, the AFSWP curve is based on modified Sachs scaling of all available aircraft and canister data for a wide range of yields. In deriving the AFSWP curve in this manner, most of the canister data tended to fall below the aircraft data, of which there was a considerably larger amount. This tendency also appears in the Redwing canister data shown in Figure 2.48. The scaled data appears to fit the AFCRC curve somewhat better than the AFSWP curve, which would give somewhat higher pressures at the same ranges. Use of modified Sachs scaling to reduce the duration data from Shot Cherokee to 1 kt at sea level gives good agreement with the curve in Reference 4 for positive-phase duration in free air, with an average deviation less than 4 percent. For time of arrival, either modified or straight Sachs scaling gives comparable results with Reference 4.

2.12.2 Shot Zuni. Excellent data on shock wave propagation vertically above a large-yield surface burst was obtained on Shot Zuni. The time of arrival was earlier at all ranges in the vertical direction as compared to the horizontal. Consequently the isotime contours apparently retained the semielliptical shape of the fireball past shock wave breakaway, out to the limit of photographic observation. On the other hand, the vertical pressures exceeded the horizontal pressures for all ranges out to about 18 psi, beyond which the reverse is true. Consequently, the isopressure contours appear to have been initially elliptical, then to have flattened out as the shock wave progressed upward and outward, eventually becoming parabolic. This behavior is essentially the same as that which would result if an altitude correction were applied along various ray paths from a large-yield surface burst. Indeed, these conformations are similar to those prepared for Zuni in order to determine the optimum positioning of the aircraft which participated in this event. However such predictions assumed an equivalent free-air yield of 2W for all angles above the surface for a large-yield surface burst. Based on the Zuni data, it appears that the equivalence in the vertical direction is 2.2W before the altitude correction is made, in contrast to 1.6W along the surface.

2.13 DISCUSSION: SURFACE DATA

2.13.1 Shot Cherokee. Surface measurements of blast phenomena for the multimegaton airburst were limited to the region below 11 psi. It was hoped to obtain overpressure data all the way to ground zero, but this was not achieved because of the error in delivery of the device. Furthermore, because of the orientation of the blast wave, it was not possible to make any reliable measurements as a function of range. The overpressure data has been reduced to 1 kt at sea level and plotted in Figure 2.49 for comparison with an ideal pressure-distance curve for this burst height. It may be seen that the agreement is quite good, except for the original data from some of the reef stations. However, when 25-percent correction for the gage mount (as determined from shock-tube tests discussed in Section 2.3.2) is applied to the data, better agreement is obtained. It should

be noted that the data was reduced to a standard sea level atmosphere by modified Sachs scaling to target ambient conditions instead of burst height as has previously been done. Because the data was recorded at sea level, the blast wave had already traversed the non homogeneous atmosphere before impinging upon the gages. For this reason, only a slight correction to standard conditions should be considered necessary.

In view of the results of this experiment as applied to more realistic situations, involving large-yield airbursts over long ranges, it would appear that scaling overpressure data in terms of the local ambient conditions at the surface is more appropriate than scaling to burst height or some intermediate altitude. Consequently, the HOB curves in Reference 4 have been prepared on the basis of this concept, in order to facilitate scaling and make them more reliable for large yield airbursts.

2.13.2 Shock Photography. The rocket trail data obtained over a water surface for Shots Zuni and Lacrosse was found to be compatible with similar data for previous events when scaled to 1 kt in a standard sea level atmosphere with ambient conditions of 20° C and 14.7 psi. A comparison of peak overpressure as a function of distance for these two shots with NOL results from Operation Castle is shown in Figure 2.50 together with the composite free-air curves for 1 and 2 kt. The 2-kt curve represents the values of peak overpressure to be expected at various ranges based on the theoretical 2W concept for a surface burst as previously discussed in Section 2.4.2. However, the scaled data over a water surface corresponds to a free-air equivalent yield of 1.6W and is in general agreement with corresponding data obtained over a land surface for Lacrosse and Zuni by other projects with electronic and mechanical instrumentation. It should be noted that independent yields from radiochemistry are available for only two low-yield surface shots—Shot S (surface) of Operation Jangle and Shot Lacrosse—while the 2W assumption has been used in determining the hydrodynamic yields for the multimegaton detonations. Figure 2.50 also presents data for Shot S and for Shot Mike of Operation Ivy obtained by other projects over a land surface.

The direct-shock photography for Shots Inca, Mohawk, and Seminole did not produce results as good as the rocket-trail techniques. Measurements of overpressure versus distance for Inca are also shown in Figure 2.50. Shot Inca produced surface data compatible with previous scaled data for a short distance (up to 430 feet, scaled), but then the scaled data deviated markedly from previous data out to 900 feet, scaled, where the detectable shock disappeared. The reason for the deviation can only be conjectured as due to detection of the shock front along the land-water interface, rather than in the proper plane of measurement or surface heating resulting in a change of ambient conditions, and the like.

Shot Mohawk shock data was very fragmentary, with only a short section of shock visible, and this occurred only radially outward from a protrusion on the fireball. This short piece of data was not compatible with any previous data when reduced to 1 kt.

Shot Seminole had no visible shock fronts on the available films, and no data was obtained on this shot. Some explosion growth profiles were taken from three views of the shot, which present a qualitative picture of its anomalous behavior at early times after detonation.

2.13.3 Time of Arrival. The plot of time-of-arrival data from Operation Redwing in Figure 2.51 shows regular behavior for Shots Lacrosse and Zuni along the surface. The Inca data is seen to follow the other surface data for a distance and then to deviate to later arrival times (and hence to lower pressures) at larger distances. The reason for the deviation is not known, although several mechanisms might be postulated. Should

the disturbance read on the original films be shock interactions along the water edge, or the line which separated the vegetated and cleared areas, then some explanation for the deviation might be made. An optical correction, however, when applied to the arrival-time data does give a correction in the proper direction but not large enough. The data is presented uncorrected for such possible effects.

2.13.4 Composite Lacrosse and Zuni Surface Data. The surface blast-line data of Shots Lacrosse and Zuni has been reduced to 1 kt at sea level and plotted together in Figure 2.52. A smooth curve was then drawn representing a composite pressure-distance relation along the ground from a 1-kt surface burst. The data was recorded by both mechanical and electronic gages, at the ground surface and at a height of 3 feet. Two blast lines were instrumented for Zuni, one over an island complex and the other on an island separated from ground zero by 4,000 feet of water. The Lacrosse line was confined to the shot island. Lacrosse fireball formation and initial growth took place over a water surface; however, breakaway occurred over the island. Despite these differences, which may account for the scatter in the data to some extent, the agreement between these two shots on a scaled basis is generally quite good. The data appears internally consistent for a range in overpressures from 400 to 4 psi. Such correlation over a yield range of almost 100 or 200 orders of magnitude indicates the validity of cube-root scaling for airblast phenomena.

Consequently, it is believed that the composite overpressure-distance curve for a 1-kt surface burst in a standard sea level atmosphere as derived from pressure-time measurements for these two shots is fairly representative of a 1-kt surface burst over a semi-infinite land area and can be scaled up to any reasonable yield.

2.14 DISCUSSION: 2W CONCEPT

As a result of Operation Redwing, it would appear that some fairly definite conclusions can be drawn regarding the theoretical 2W concept for airblast phenomena from a surface burst. The important difference between the Redwing and Castle data is the fact that it was possible to make an independent yield determination for Lacrosse by radiochemical analysis, whereas the yield determination for all multimegaton surface bursts involves hydrodynamic scaling of fireball growth, which incorporates the 2W concept prior to breakaway. Another important difference is that, for Redwing, it was possible to document the blast wave passing over essentially a continuous land surface for two surface bursts, from the high- to the low-pressure region, whereas this was true only for the low-pressure regions for Shot 3 of Operation Castle and Shot S of Operation Jangle. All other measurements for multimegaton surface bursts involved varying amounts of travel over a water surface.

Following Operation Castle, it was found that the measured overpressure versus distance data for the various surface bursts tended consistently to fall between curves drawn for the 1W and 2W free-air values. However, it appeared that the equivalent free-air yield value could be different for each of the various shots, ranging from 1.6 to 2.0W and could vary as a function of pressure level or type of surface for data measured over water as well as land, based on fireball yields. For Shot 2 of Operation Castle, for example, data measured by the shock velocity technique over land was consistently higher than data for the same shot measured by the same method over water, thus indicating the possible existence of a region of higher sound velocity over land than water, i.e., a heated layer. Consequently, in view of the limitations attached to the Castle data, it was hoped that a more complete understanding of the airblast phenomena for a surface burst could be obtained for Shots Zuni and Lacrosse.

The results obtained support the Castle, Ivy, and Jangle data and indicate that the deviation from the ideal 2W concept is real. The 1.6W figure, proposed after Operation Castle as an overall grand average of free-air equivalence for surface bursts, appears to hold reasonably well for a fairly wide range of overpressures and yields based on Redwing data. However, this value of 1.6W is not without limitation. It does not apply to shock front pressures before breakaway; the radius-time plot actually fits the 2W concept. Consequently, there must be a transition zone outside the fireball. Nor does it appear uniformly well over the entire pressure-distance curve. Data points at specific pressure levels may have an equivalent free-air value somewhat higher or lower than this average value. Also it does not apply very well to other blast wave parameters, such as dynamic pressure values that are higher than 1.6W in the limited precursor zone. Moreover, measured impulses and durations from both the Castle and Redwing data tend to be larger than the corresponding theoretical 2W values.

Consequently, the 1.6W value appears most useful as a quick convenient reference to estimate the overpressure versus distance curve for a surface burst. In view of these considerations, it appears more fundamentally correct to use empirical curves such as the composite overpressure distance curve that was derived from the Redwing data. A comparison between this curve and the 1.6W free-air curve is shown in Figure 2.53. Although the agreement is good, the empirical curve is to be preferred, because it represents the actual experimental measurements in the field.

2.15 DISCUSSION: PRECURSOR PHENOMENA

Important contributions toward a better understanding of precursor phenomena were made as a result of the blast and shock experiments conducted during Operation Redwing. The most significant of these was the verification of precursor formation for surface bursts. This had been predicted by F. H. Shelton (Reference 10) for yields greater than about 80 kt, but not by the AFSWP-NOL criteria, which required a scaled height greater than 50 feet. This requirement was not consistent with photographic data from Shot Trinity and from Shot George of Operation Greenhouse, both at a scaled height of 35 feet, which showed some sort of disturbance running ahead of the main shock and Mach stem. During Operation Teapot, however, the existence of precursors on certain low-yield tower shots, where Shelton had predicted none, favored the AFSWP-NOL method.

Consequently, in Redwing Project 1.2 (WT-1302), C. D. Broyles proposed several modifications to Shelton's theory to make thermal radiation more effective in precursor formation by lowering the threshold for propagation velocity in the thermal layer and introducing a height of burst and yield dependence. These modifications were such as to account for the existence of precursors on the Teapot shots (where Shelton had predicted none); confirm Shelton's predictions of precursors for Shots Trinity and George; and predict a precursor for Shot Lacrosse. This latter prediction was based on an assumed thermal yield of 10 kt derived from Greenhouse data although later Tumbler data would indicate the thermal yield should be about 15 kt.

It is difficult to interpret the thermal measurements from Lacrosse because of partial shielding by diagnostic equipment. A thermal yield ranging from 3 to 6 kt was measured at distant stations along two directions. Pressure stations were at an angle in between these two measurements and at much closer distances. Measurements indicated that the thermal energies at close distances would be greater than those predicted from the measurements at large distances, with an assumption that the thermal energy was inversely proportional to the distance squared; however, no close measurements were available for this shot.

Despite this apparent inconsistency, precursors were documented in the higher pressure region on both Lacrosse and Zuni. The experimental data was marked by such typical characteristics as early arrival times, disturbed pressure waveforms, and higher than ideal dynamic pressures. However, thermal effects did not appear to depress peak pressures to any appreciable extent. Also the precursor appeared to die out sooner than might be expected; a classical waveform was realized at about 35 psi on Lacrosse and 20 psi on Zuni. This difference in pressure level for precursor cleanup might possibly indicate a yield dependence. Consequently, it appears that the strength of the precursor for surface bursts at the PPG is considerably less than that observed for low airbursts at NTS where clean or classical wave shapes are not realized until the 6- or 8-psi region is reached. However, it should be noted that a precursor has not been documented from a surface burst at the NTS, and therefore, no direct comparison can be made.

The extent of the precursor cycle is a function of both the yield and HOB. As the HOB is lowered, the angle of incidence of the thermal radiation is increased, and there is less heating of the surface at the greater distances. Therefore, for surface and near-surface bursts, the precursor will complete its cycle sooner, and a classical wave shape will appear at shorter ground distances and higher pressures than would be expected for the same yield at higher HOB's.

It should be noted that the angle of incidence used for computing preshock thermal radiation at various distances in order to predict precursor formation for various yields assumes a stationary source and not a rising fireball. The effect of geometry in reducing thermal yield for a surface burst was considered by Broyles in improving Shelton's theory. He concluded that there was no appreciable reduction in thermal yield for surface bursts above 10 kt compared to airbursts, because the former have the same hemispherical shape during the radiation of almost all the thermal energy.

There are also environmental conditions which may help to explain differences in precursor characteristics noted between PPG and NTS. These include such factors as atmospheric attenuation of thermal radiation as well as surface conditions. The transmission of thermal energy is less effective at PPG, and more scattering occurs because of higher humidity and background albedo than in the clear dry air of the Nevada desert. Also laboratory tests have shown that Eniwetok coral is less susceptible to thermal explosion, i. e., popcorning than NTS desert sand and therefore requires a higher energy value in cal/cm² before the critical threshold is exceeded.

Of course, the surface material on the various islands of Eniwetok Atoll is not uniform; it consists of inhomogeneous patches of sand over coral of various densities. In addition, the surface tends to be damp more often in the Pacific because of intermittent rains and, in certain areas, wave action on tidal changes. These conditions would generally tend to inhibit formation of a strong thermal layer, and local differences might result, such as was observed during Shot Lacrosse. It is believed to have rained on the night prior to this shot. However, this may not have been significant, because the island is covered mostly by sand underlaid by hard coral. Conceivably, the surface may have been dry at shock time, inasmuch as sand drains easily, and runoff could have been fairly rapid.

Neither of the precursor prediction methods described previously allows for differences in surface conditions. However, it is known from Shot MET during Operation Teapot that distinct differences in precursor formation and propagation may occur, depending on type of surface. Further evidence of the importance of this parameter was shown by the data from Shot Inca, where the precursor was definitely weaker in the vegetated area than in the cleared area. It appears that density, height, and strength of the vegetation were such as to reduce thermal effects on the blast wave by shielding the

surface and changing the nature of the thermal layer. Because the vegetation provided an almost continuous cover to a height of 10 feet, mechanical effects on the blast wave due to interaction and turbulence were probably more important than usual. In any event, it would appear that further consideration of the thermal characteristics over which the blast wave passes is necessary in prediction of precursor formation.

In fact, surface conditions may be more important than yield in determining whether or not a precursor forms for a surface burst. Precursor characteristics for surface bursts or near-surface bursts up to a scaled height of 100 feet in all test areas (PPG, NTS, and Alamogordo) have been markedly different from the characteristics for shots at higher scaled heights at NTS. This may be due to a fundamental change in the mechanism of precursor formation and propagation. However, all available evidence leads to the belief that, as the burst height is lowered to a near-surface or surface burst, the existence of a precursor becomes marginal. Consequently, small differences in environmental factors from those under which Lacrosse and Zuni were detonated may prevent precursor formation.

2.16 REVIEW AND SUMMARY

The principal objective of Program 1 during Operation Redwing as outlined in Section 2.1 were generally accomplished, with one major exception; that of documenting the basic blast phenomenology of a high-yield true airburst. Reliable data was obtained in more than sufficient quantity to meet minimum requirements for successful participation by each project on all events of interest except Shot Cherokee.

The delivery error for Shot Cherokee was of such magnitude that there was a serious loss of data due to the increased range and orientation. Overpressure data for Shot Cherokee was recorded along the surface over a limited region, but no reliable dynamic pressure measurements were made. The free-air data was equally disappointing. The rocket trail photography was unsuccessful, and the canister results do not permit unambiguous conclusions to be drawn on blast wave propagation directly above a high-yield airblast.

The general phenomenology of a medium-yield land surface burst along the surface was established by the Lacrosse data and, with scaling to a larger yield, confirmed by the Zuni data. Blast wave propagation in free air above a large-yield surface burst was successfully documented by rocket-trail photography for Shot Zuni. Damage data for drag-sensitive targets was obtained on both events; as a result, scaling of damage radii for PPG surface bursts has been established over a wide yield range.

The drag force experiments were only partially successful. Whereas satisfactory data was obtained on model targets for Shot Lacrosse, similar measurements on spherical gages and full-scale structural elements could not be reliably interpreted because of low input values of free-field blast parameters and a large deviation in direction of flow from that originally intended.

Blast wave parameters from a precursor-forming tower shot were successfully measured over a cleared and vegetated surface. The comparison of data obtained provided a better understanding of the effects of natural vegetation on precursor propagation.

Measurements of apparent crater radii, depth, and profile were obtained under a wide range of source conditions and environment.

Satisfactory measurements of both overpressure and dynamic pressure were obtained for correlation with observed damage to drag-sensitive targets on this event.

Water-wave measurements were successfully made on both lagoon-generated waves and those propagating across the ocean to distant islands. Sufficient information was obtained to provide a basis for adequately predicting the deep-water height of waves produced by nuclear tests set off over atolls within the range of yields covered during Operations Castle and Redwing

TABLE 2.1 SCALING FACTORS (SURFACE AMBIENT CONDITIONS)

Shot Yield* Method	Lacrosse 39.5 kt Radiochemical	Cherokee	Zuni 3.5 Mt Hydrodynamic	Yuma	Seminole	Inca	Mohawk	Tewa 5.0 Mt Hydrodynamic
Actual Height of Burst (ft)	17	4,320	9	200	4	200	300	0
P ₀ (psi)	14.62	14.62	14.64	14.64	14.64	14.63	14.64	14.64
T ₀ (°C)	27.2	27.2	27.2	27.5	30.5	28.6	26.5	27.8
S _p	1.005	1.005	1.004	1.004	1.004	1.0048	1.0041	1.0041
S _d	0.2931	0.0645	0.0658	1.7526	0.4194	0.4066	0.1404	0.0584
S _t	0.2993	0.0658	0.0672	1.7894	0.4306	0.4160	0.1432	0.0596
S ₁	0.2979	0.0649	0.0659	1.7644	0.4356	0.4125	0.1437	0.0588
Height of Burst Scaled to 1 kt at Sea Level	4.98		0.59					0

* These yields are those used for data reduction and preparation of curves in this chapter.
The latest and most accepted yields are those given in Table 1.1.

TABLE 2.2 SCALING FACTORS (AMBIENT CONDITIONS AT BURST HEIGHT)

Shot Yield*	Cherokee	Yuma	Inca	Mohawk
P_0 (psi)	12.60	14.53	14.53	14.50
T_0 (°C)	16.3	25.2	24.3	26.0
Height of Burst	4.320	200	200	300
S_p	1.167	1.012	1.012	1.014
S_d	0.0635	1.7482	0.4056	0.1398
S_t	0.0610	1.7779	0.4123	0.1424
S_i	0.0701	1.7694	0.4122	0.1449
Height of Burst Scaled to 1 kt at Sea Level				

* These yields are those used for data reduction and preparation of curves in this chapter. The latest and most accepted yields are those given in Table 1.1.

TABLE 2.3 COMPARISON OF SLANT RANGES COMPUTED BY DIFFERENT METHODS

All ranges are in feet.

Canister Number	Slant Range		
	Photo and Altimeter	Canister Ballistics and Wind Drift	Travel Time and Overpressure
Free-Air Region:			
2	—	18,580	16,830
3	—	18,730	17,300 to 17,700
1	—	22,370	21,890
12	—	22,480	22,370
4	—	25,640	26,730
5	29,110	28,770	28,410
6	30,270	29,870	29,740
8	31,010	30,710	30,490
9	33,050	32,250	32,580
11	34,760	33,690	34,640
Mach Region:			
7	—	19,770	17,640 to 19,410
10	—	21,340	21,860

TABLE 2.4 OBSERVED DATA FOR SHOT CHEROKEE

Canister Number	Shock Arrival Time	Ambient Pressure	Altitude	Peak Overpressure		Apparent Positive-Phase Duration	Reflected Shock	
				Average	Corrected Average		Arrival Time	Overpressure Increment
	sec	psi	ft	psi	psi	sec	sec	psi
7	8.207 to 9.489	14.24	850	6.75	7.70	*	In Mach region	
10	11.437	13.70	1,900	6.65	7.65	*	In Mach region	
2	8.131	12.03	5,600	4.50	4.95	*	9.117	1.90
3	8.632 ± 0.176	11.15	7,700	2.75	2.86	*	10.321	1.20
12	12.531	9.14	13,100	2.55	2.70	*	15.262	0.95
1	12.139	7.56	18,100	2.55	2.68	5.90	18.130	0.95
4	16.146	6.24	23,100	1.85†	1.91	—	23.465 ± 0.015	0.65
5	17.571	5.40	26,600	1.52	1.55	6.20	26.044	0.30
6	18.724	5.11	28,000	1.35	1.37	6.20	27.231	0.27
8	19.373	4.91	28,800	1.27	1.29	6.41	28.324	0.27
9	21.222	4.57	30,500	1.125	1.14	6.60	29.543	0.23
11	23.065	3.93	33,800	0.98	0.99	6.80	33.143	0.27

* Reference Chamber did not seal; pressure-versus-time waveform is not a true representation.

† Extremely noisy trace due to low radiofrequency carrier signal strength.

TABLE 2.5 COMPARISON BETWEEN OBSERVED AND CALCULATED PEAK OVERPRESSURES

Canister Number	Observed	Calculated Peak Overpressure			Percentage Deviation*		
		Theilheimer-	Ledsham-	Modified	Theilheimer-	Ledsham-	Modified
		Rudlin	Pike	Sachs	Rudlin	Pike	Sachs
	psi	psi	psi	psi	pct	pct	pct
2	4.95	5.73	5.71	5.77	-13.6	-13.3	-14.2
12	2.70	2.99	2.95	3.05	-9.7	-8.5	-11.5
1	2.68	2.84	2.75	2.95	-5.6	-2.5	-9.2
4	1.91	1.81	1.73	1.90	+5.5	+10.4	+0.5
5	1.55	1.51	1.44	1.61	+2.6	+7.6	-3.7
6	1.37	1.38	1.30	1.45	-0.7	+5.4	-5.5
8	1.29	1.29	1.22	1.37	0.0	+5.7	-5.8
9	1.14	1.11	1.05	1.18	+2.7	+8.6	-3.4
11	0.99	0.93	0.87	1.00	+6.5	+13.8	-1.0
Algebraic mean (for eight highest canisters)					+0.2	+5.1	-5.0
Root mean square (for eight highest canisters)					5.2	8.4	6.2

* Percentage deviation = 100 [(observed-computed)/computed].

TABLE 2.6 SHOT ZUNI, APPROXIMATION OF FOCUSING EFFECT

Horizontal and Vertical Distance	NOL Computation		Shock Photography Results				Focusing Effect
	(1)	(2)	(3)	(4)	(5)	(6)	(7)
	1.6 W =	5.648 Mt	2.2 W =	Overpressure	Overpressure	Overpressure	Pressure Ratio
	5.648 Mt	5.648 Mt	7.766 Mt	in Horizontal	in Vertical	in Vertical	
	Overpressure	Overpressure	Overpressure	Direction	Direction	Direction	
	in Horizontal	in Vertical	in Vertical	Corrected for	Corrected for	Corrected for	
	Direction	Direction	Direction	Inhomogeneity	Inhomogeneity	Inhomogeneity	
ft	psi	psi	psi	psi	psi	psi	
3,086	360.0	310	405	303	400	464	1.53
3,885	195.0	173	226	170	230	260.0	1.53
5,487	85.0	74.2	94	78	94	108	1.38
6,900	51.2	45.0	53.5	47	53	60.4	1.29
8,696	31.2	24.3	30.1	27.8	31	39.7	1.43
10,950	19.2	14.2	17.5	18.1	18.5	25.0	1.38
13,000	13.45	9.0	12.1	13.1	12.3	18.3	1.40
						AVERAGE	1.42

Column (1) No atmospheric correction.

(5) Compares with column (3).

(6) Ratio of column (1) to column (2) multiplied by column (5).

It is assumed that the ratio of column (1) to column (2) changes only very slightly with yield.

(7) Column (6) divided by column (4).

TABLE 2.7 FORCE-GAGE DATA, SHOT LACROSSE

Peak Aerodynamic Conditions	NOL Gage Desig- nation	Type of Gage	Nominal	Peak Force	C_D at Peak †	Average C_D
			Gage Range *	(Drag Component)		
			lb	lb		
Station 160.01, 2,500 feet from ground zero, A-station						
$P_s = 18.4$ psi $q = 7.0$ psi ‡ $M = 0.55$ $R = 6.2 \times 10^6$ /ft	A ₁ 10	10-in sphere	1,000	330	0.37	0.30
	A ₂ 10	10-in sphere	1,000	250	0.22	
	A ₁ 4	4-in sphere	125	54	0.38	0.38
	A ₂ 4	4-in sphere	125	54	0.38	
	A ₁ C	6 ⁵ / ₈ -in cylinder	1,000	245	0.88	0.87
	A ₂ C	6 ⁵ / ₈ -in cylinder	1,000	240	0.86	
	A ₁ P	6 ⁵ / ₈ -in parallelepiped	1,500	370	1.33	1.36
	A ₂ P	6 ⁵ / ₈ -in parallelepiped	1,500	390	1.40	
	A ₁ 4 ³	4-in cube	600	106	0.95	0.95
	A ₂ 4 ³	4-in cube	300	106	0.95	
Station 161.01, 5,200 feet from ground zero, B-station						
$P_s = 4.5$ psi $q = 0.48$ psi ‡ $M = 0.19$ $R = 1.5 \times 10^6$ /ft	B ₁ 10	10-in sphere	50	57.7	0.68	0.59
	B ₂ 10	10-in sphere	50	50.9	0.50	
	B ₁ 4	4-in sphere	10	6.85	0.31	0.34
	B ₂ 4	4-in sphere	10	7.20	0.37	
	B ₁ C	6 ⁵ / ₈ -in cylinder	75	16.0	0.84	0.84
	B ₂ C	6 ⁵ / ₈ -in cylinder	75	16.0	0.84	
	B ₁ P	6 ⁵ / ₈ -in parallelepiped	100	25.5	1.34	1.34
	B ₁ 10 ³	10-in cube	200	74	1.55	1.55
	B ₁ 4 ³	4-in cube	20	5.6	0.76	0.90
	B ₂ 4 ³	4-in cube	40	8.0	1.05	

* Maximum gage range 30 to 50 percent above nominal range.

† Sphere data corrected for pressure sensitivity.

‡ Based on Equation 1.2.

TABLE 2.8 FINAL DRAG DATA

Location	Angle of Yaw	Measured Over- pressure	Computed* Dynamic Pressure	Peak Drag Forces			Coefficients		
				Angle Iron		WF-Beam	Drag		Lift Angle Iron
				Vertical	Horizontal		WF-Beam	Angle Iron	
	degrees	psi	psi	lb	lb				
Able	12	4.1	0.40	540	500	1,100	2.52	2.11	2.28
Manmade 1	58	8.7	1.71	840	740	—	—	2.40	2.73
Manmade 2	50	7.2	1.19	—	800	1,600	2.82	2.61	—
Dog	32	4.5	0.47	—	—	950	2.44	—	—

* Dynamic pressure computed using Rankine-Hugoniot relations.

TABLE 2.9 COMPARISON OF STEADY-STATE DRAG AND LIFT COEFFICIENTS WITH THOSE OBTAINED ON OPERATION REDWING

Structural Members	Steady-State	Dynamic Operation Redwing
WF-Beam (drag)	2.03	2.52, Able 2.82, Manmade Island 2 2.44, Dog
Angle iron (drag)	1.83	2.11, Able 2.40, Manmade Island 1 2.61, Manmade Island 2
Angle iron (lift)	2.07	2.28, Able 2.73, Manmade Island 1

TABLE 2.10 MOST PROBABLE PEAK DRAG COEFFICIENT VALUES

Site	Gage*	Predicted Values		Actual Values†		
		Over-pressure psi	Dynamic Pressure psi	Over-pressure psi	Dynamic Pressure psi	Drag Coefficient
Able	10-1	23	10.8	4.1	0.395	0.53
Able	3-1	23	10.8	4.1	0.395	0.61
Able	3-2	23	10.8	4.1	0.395	0.55
Dog	10-2	3.2	0.26	4.5	0.475	0.91
Dog	3-3	3.2	0.26	4.5	0.475	0.47
Dog	3-4	3.2	0.26	4.5	0.475	0.38

* First number is gage diameter in inches; second number is serial number.

† Dynamic pressure computed using Rankine-Hugoniot relations.

TABLE 2.11 DYNAMIC PRESSURE COMPARED WITH DAMAGE

Shot	Orientation	Dynamic Pressure (psi) for Damage which is:		
		Light	Moderate	Severe
Yuma	FO	9.2, 9.6	24.8	136.8*
	SO	9.2, 9.6	—	24.8, 136.8*
Zuni	FO	— —	3.3	6.4, 7.5, 16.9
	SO	— —	1.6, 3.3	6.4, 7.5, 16.9, 24.6
Lacrosse	FO	0.8, 1.0, 2.2, 5.3, 7.4	—	—
	SO	0.8, 1.0, 2.2	5.3, 7.4	—

* Computed.

TABLE 2.12 REDWING CRATER DATA

Shot	Location	Yield	Height of Center of Gravity of Device Above Ground	Preshot Water Depth at Site Zero	Crater Diameter	Apparent Crater Depth at Time of Survey	Lip Formation
			ft	ft	ft	ft	
Lacrosse	Coral reef	39.5 kt	17	2	404	44	15 feet high
Zuni	Island	3.38 Mt	9.3	0	2,310	103	None apparent
Seminole	Island		4.5 (-12)	0	660	47	15 feet high
Mohawk	Island		300	0	1,340	8	and irregular
Tewa	Water (barge)	4.6 Mt	15 (above water)	20	4,000	129	None apparent

TABLE 2.13 FIRST-CREST AND FIRST-WAVE DATA, SHOTS ZUNI, FLATHEAD, DAKOTA, NAVAJO, AND TEWA

Station	Refracted Path Range	First-Crest Height in 60 Feet of Water	First-Wave Height in 60 Feet of Water	Water Depth of Generation	First-Crest Height in Water Depth of Generation
	10 ³ ft	ft	ft	ft	ft
Shot Zuni					
191.01	18.0	2.6	5.1	—	—
192.01	33.0	1.5	3.4	—	—
196.02	52.8	1.1	1.9	—	—
190.01	69.0	0.5	1.2	—	—
193.01	73.8	0.2	1.0	—	—
Shot Flathead					
197.04	7.5	6.4	17.9	120	5.4
196.03	35.5	0.9	2.4	120	0.76
191.01	60.6	0.8	2.1	120	0.67
193.01	64.6	0.4	0.9	120	0.34
192.01	64.2	0.6	1.2	120	0.5
190.01	79.8	0.4	1.3	120	0.42
Shot Dakota					
197.04	7.5	14.8	26.0	140	12.0
197.06	7.5	6.7	23.8	140	5.4
196.02	53.8	1.5	3.5	140	1.2
191.01	60.6	2.3	5.3	140	1.8
193.01	64.6	0.8	1.8	140	0.6
192.01	64.2	1.0	2.1	140	0.8
196.01	64.8	0.9	2.2	140	0.7
190.01	79.8	1.1	2.7	140	0.9
Shot Navajo					
197.06	6.5	28.8	68.0	230	20.6
197.04	8.5	20.6	38.6	230	14.7
197.05	14.4	—	34.5*	230	—
196.02	50.1	4.4	8.8	230	3.14
191.01	57.3	6.9	14.7	230	4.93
193.01	58.5	2.9	4.9	230	1.86
196.01	63.3	3.4	5.9	230	2.43
192.01	62.1	4.8	10.8	230	3.43
190.01	77.7	4.5	8.3	230	3.21
Shot Tewa					
192.01	57.0	3.7	7.6	20	4.9
191.01	66.0	3.4	7.7	20	4.5
190.01	93.9	1.5	2.9	20	2.0

* Total wave height estimated as twice the first-trough depth.

Pg. 84 Deleted.

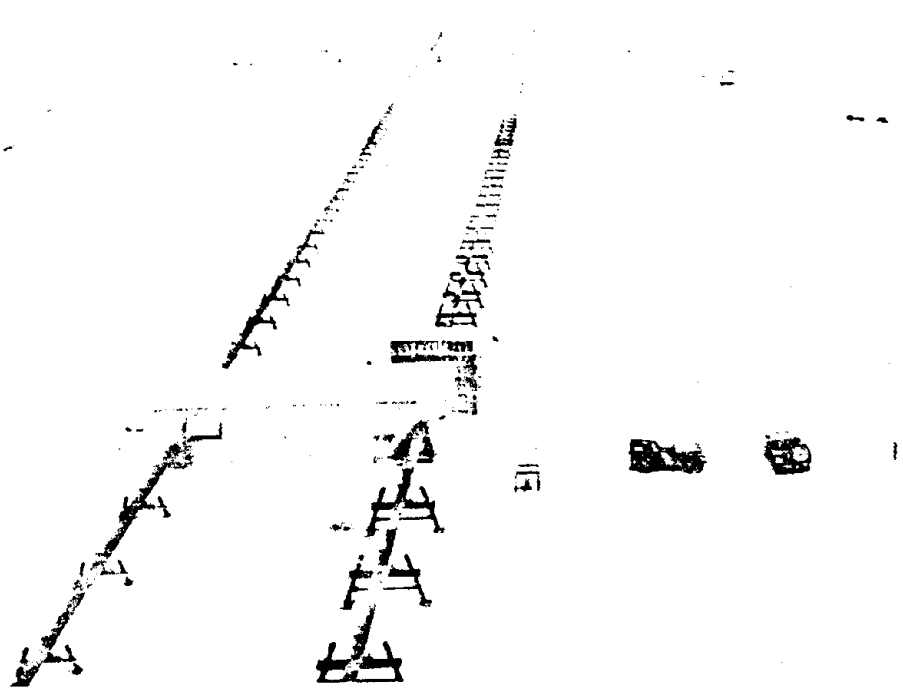


Figure 2.3 Site Yvonne, looking toward ground zero of Shot Lacrosse.

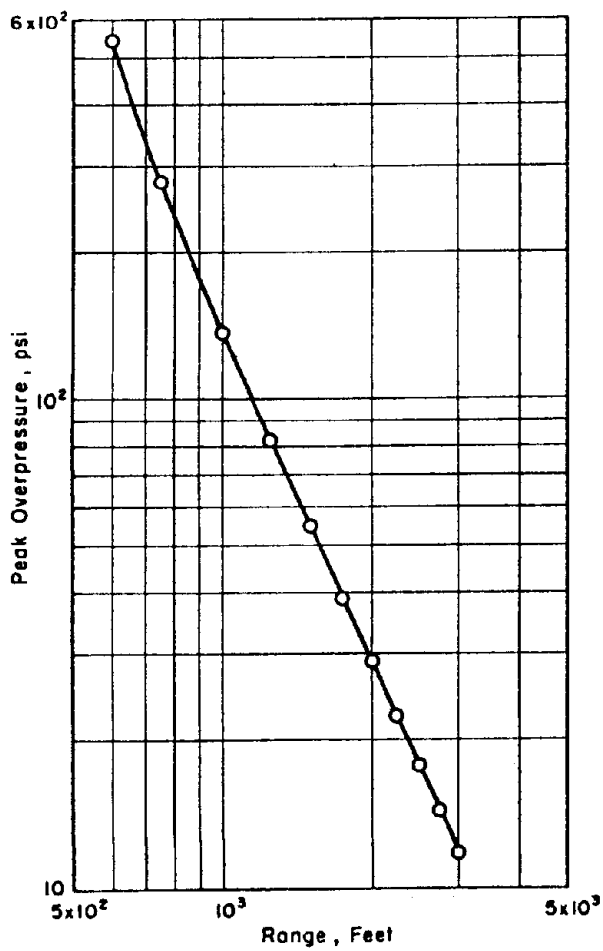


Figure 2.4 Overpressure versus range along water surface for Shot Lacrosse (NOL).

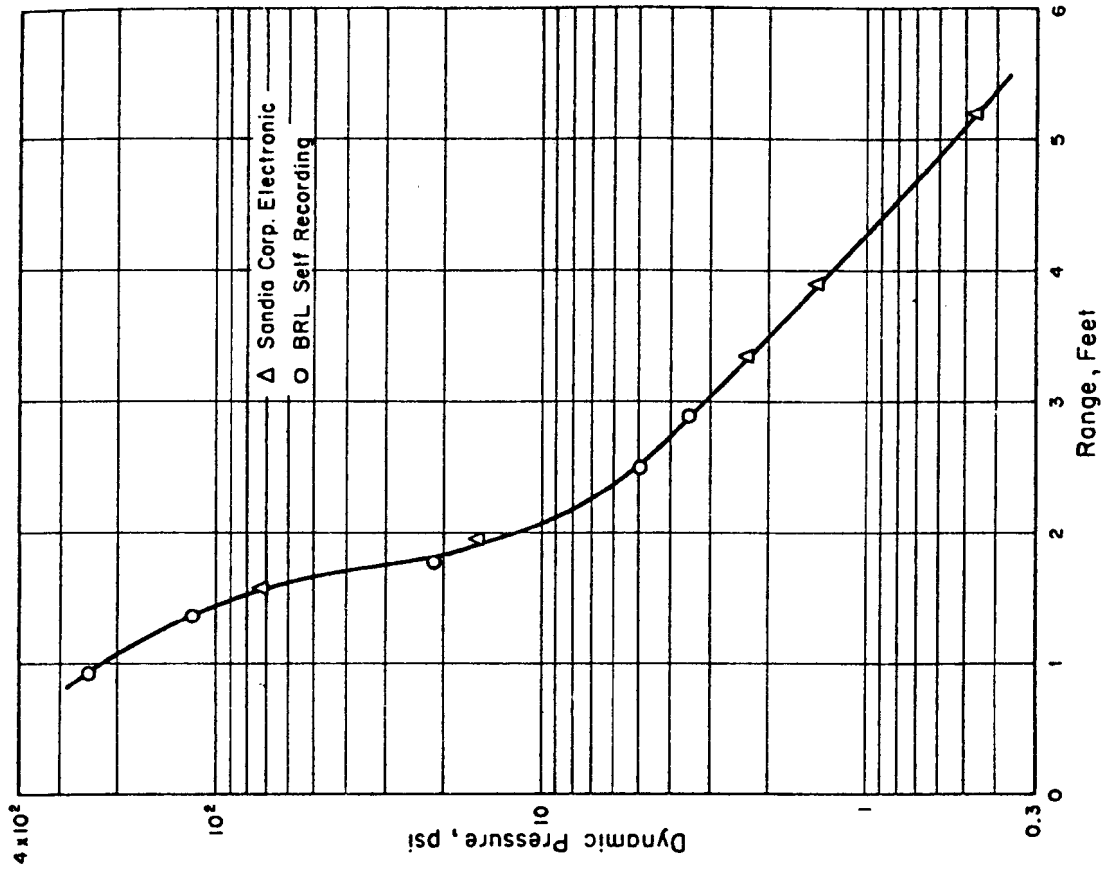


Figure 2.6 Dynamic pressure versus range for Shot Lacrosse.

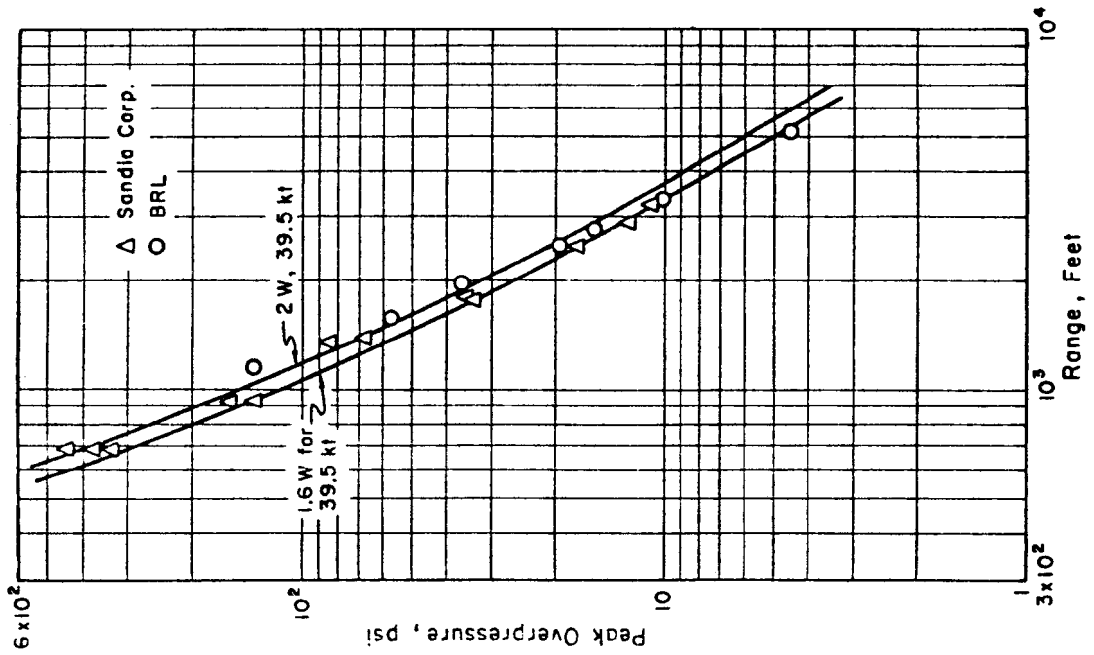


Figure 2.5 Overpressure versus range along ground surface for Shot Lacrosse (SC and BRL).

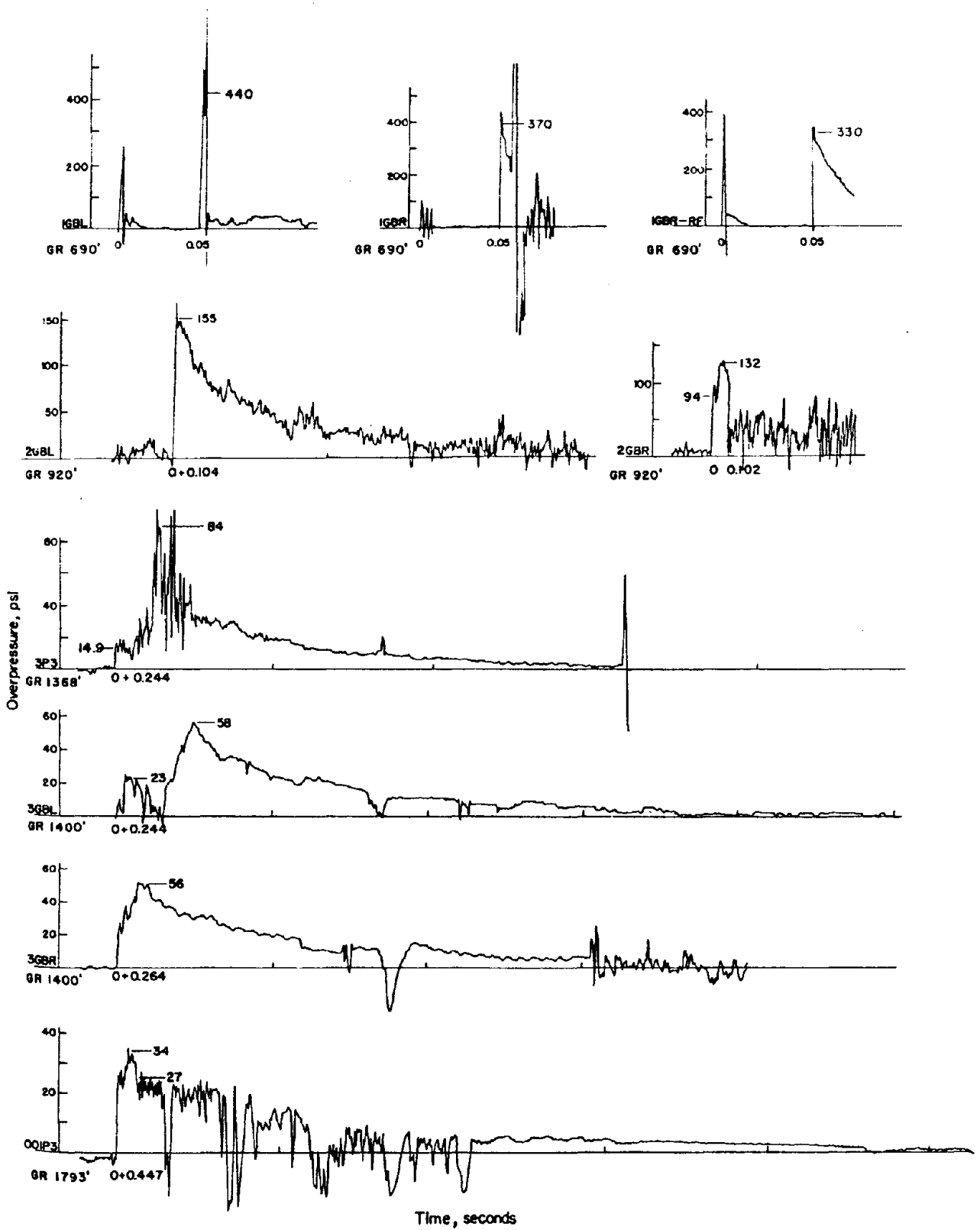


Figure 2.7 Overpressure versus time, showing shock-wave arrival time (seconds) and history after shock arrival (SC).

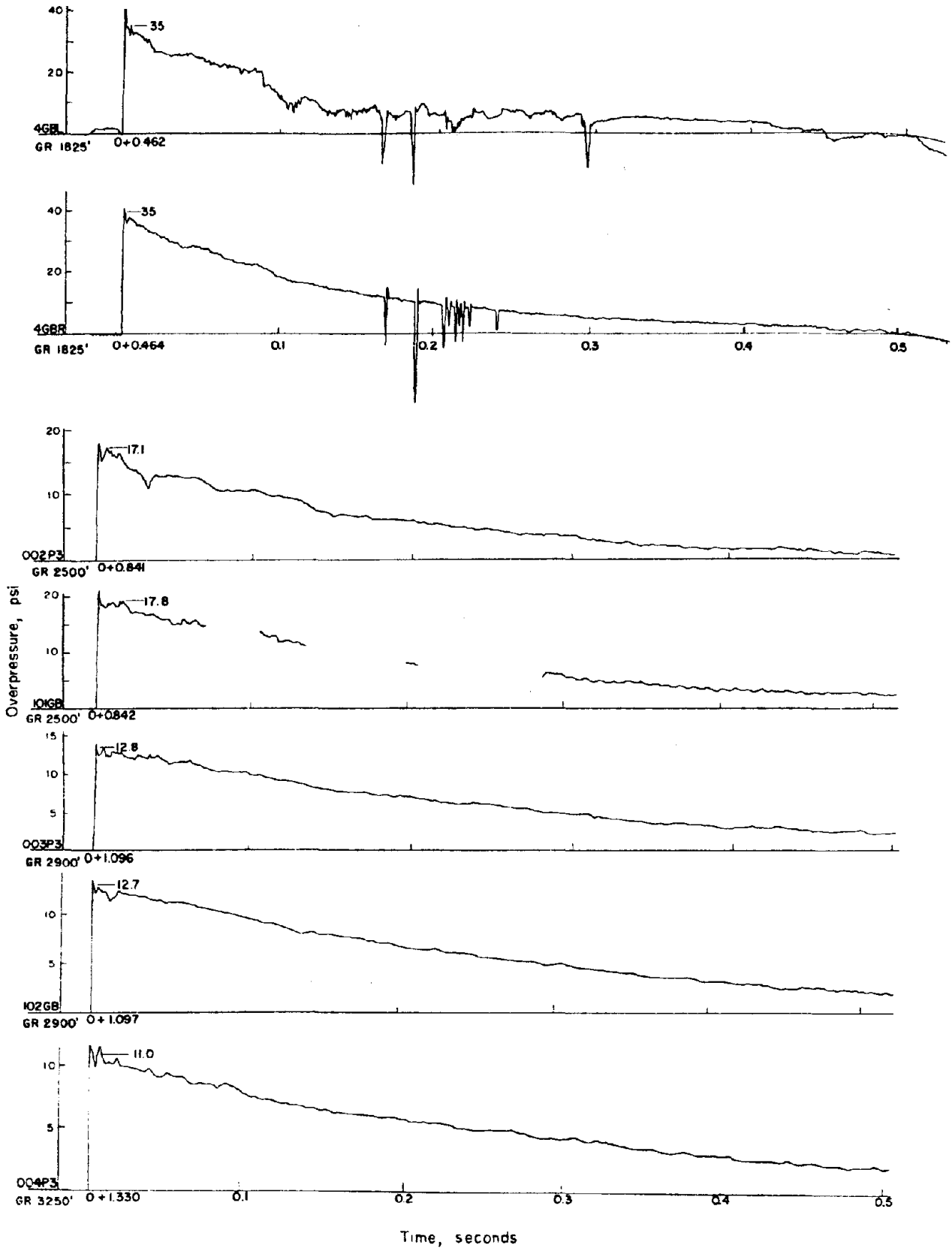


Figure 2.7 Continued.

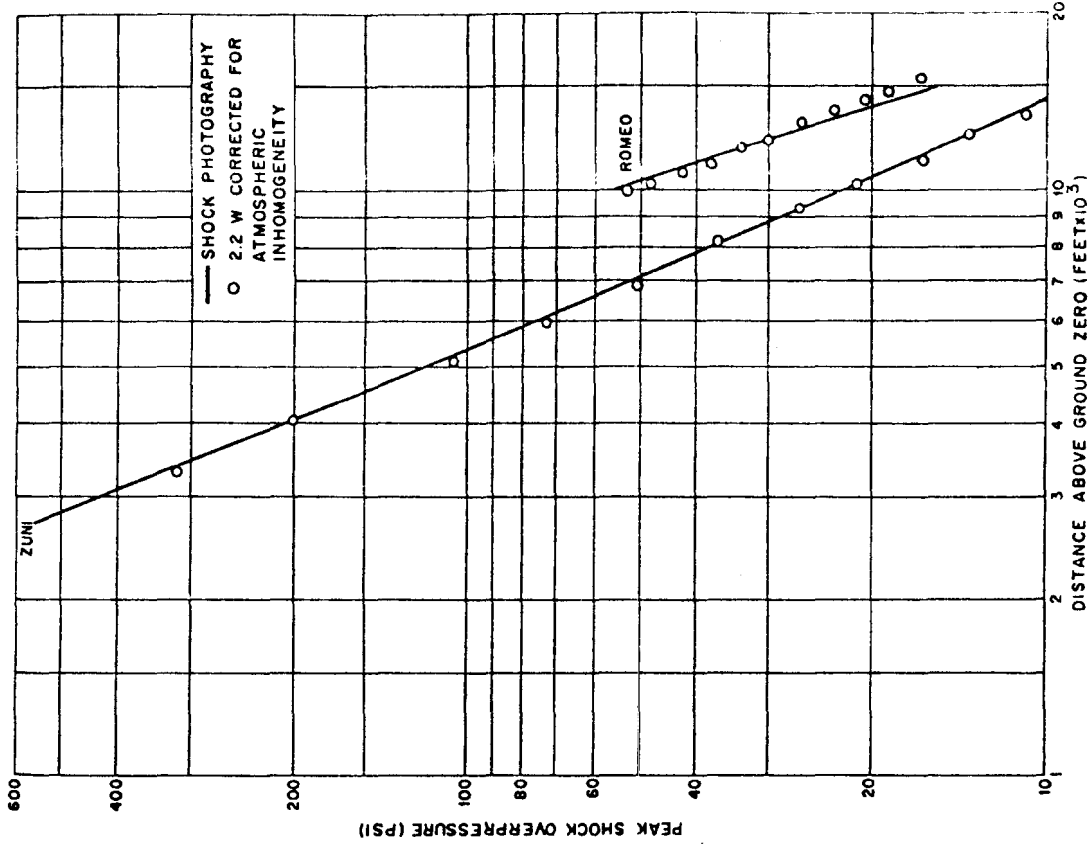


Figure 2.9 Comparison of peak-shock overpressure in vertical direction with 2.2W curve corrected for atmospheric inhomogeneity.

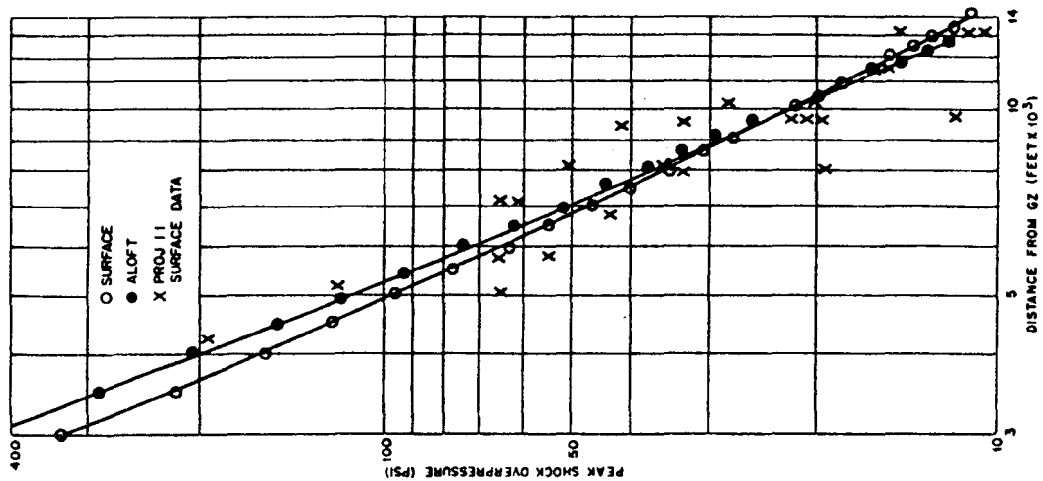


Figure 2.8 Horizontal and vertical overpressures for Shot Zuni.

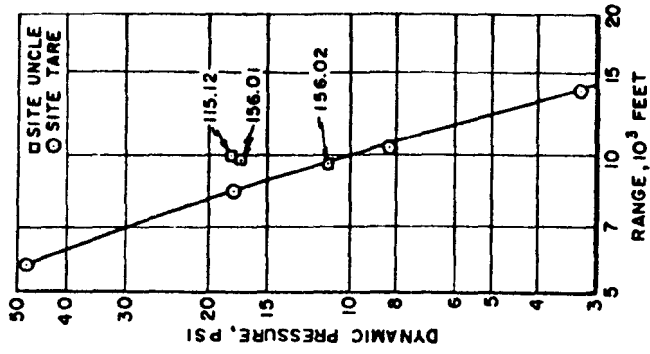


Figure 2.11 Corrected peak dynamic pressure versus distance, Shot Zuni.

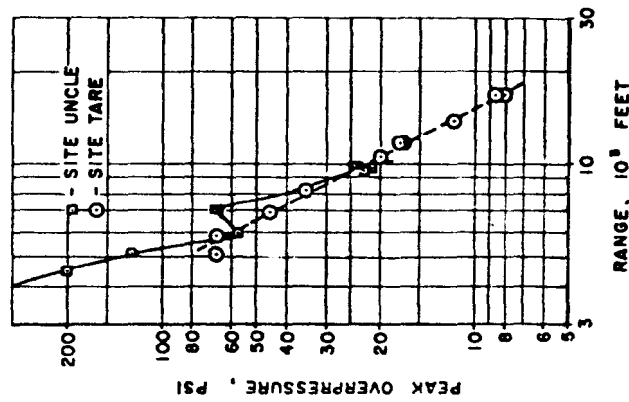


Figure 2.10 Overpressure versus range for Shot Zuni (BRL).

Pg. 91 Deleted.

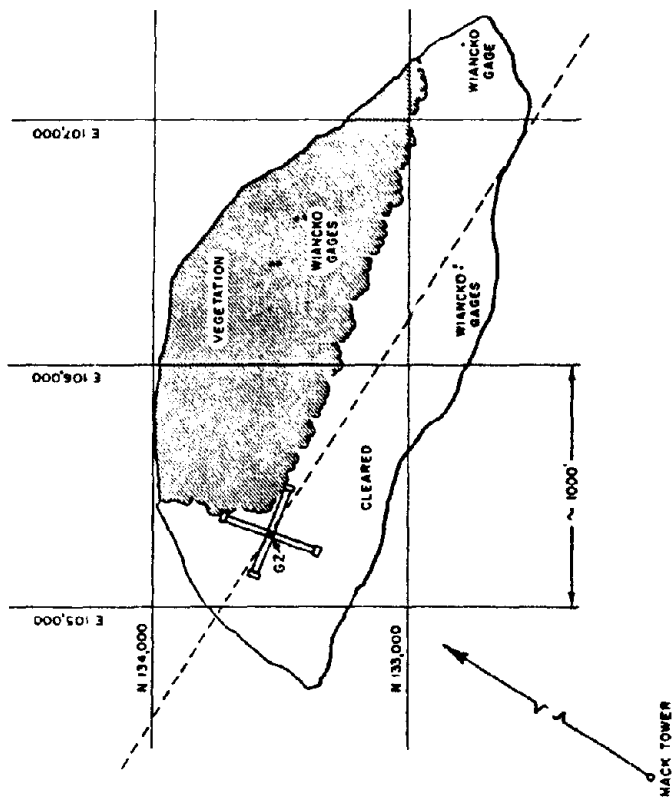


Figure 2.14 Layout of Shot Inca, Site Pearl.

Pgs. 93 & 94 Deleted.

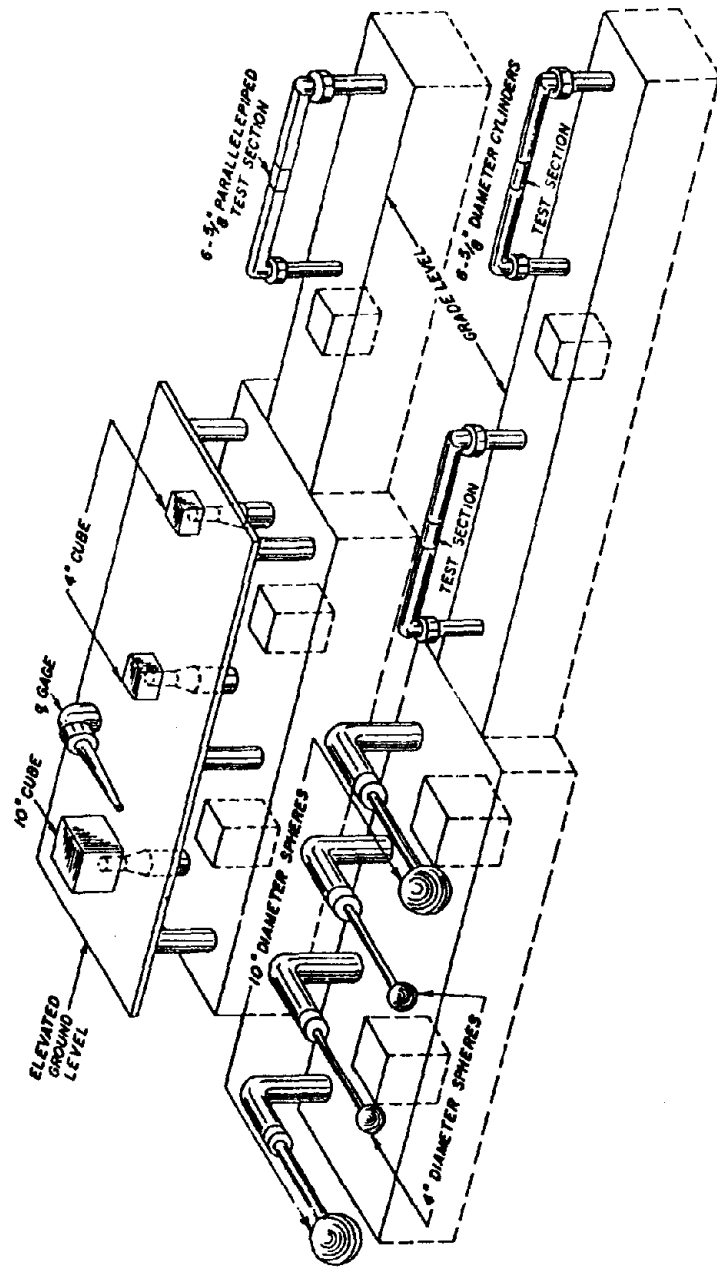


Figure 2.19 Typical station layout.

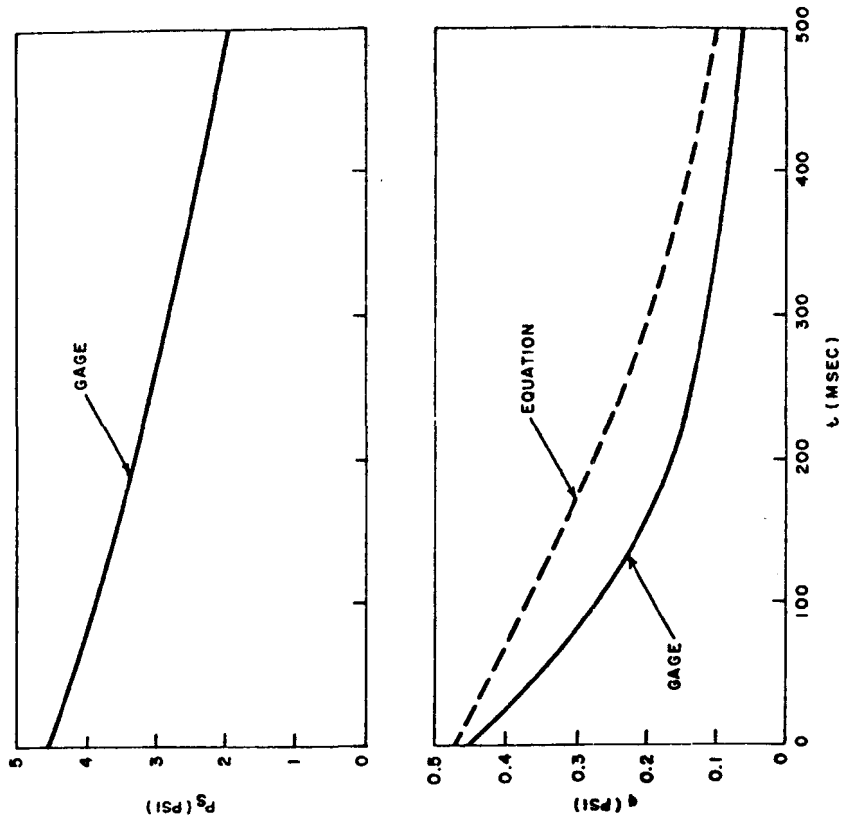


Figure 2.21 Side-on pressure (P_s) and dynamic pressure (q) at B-station.

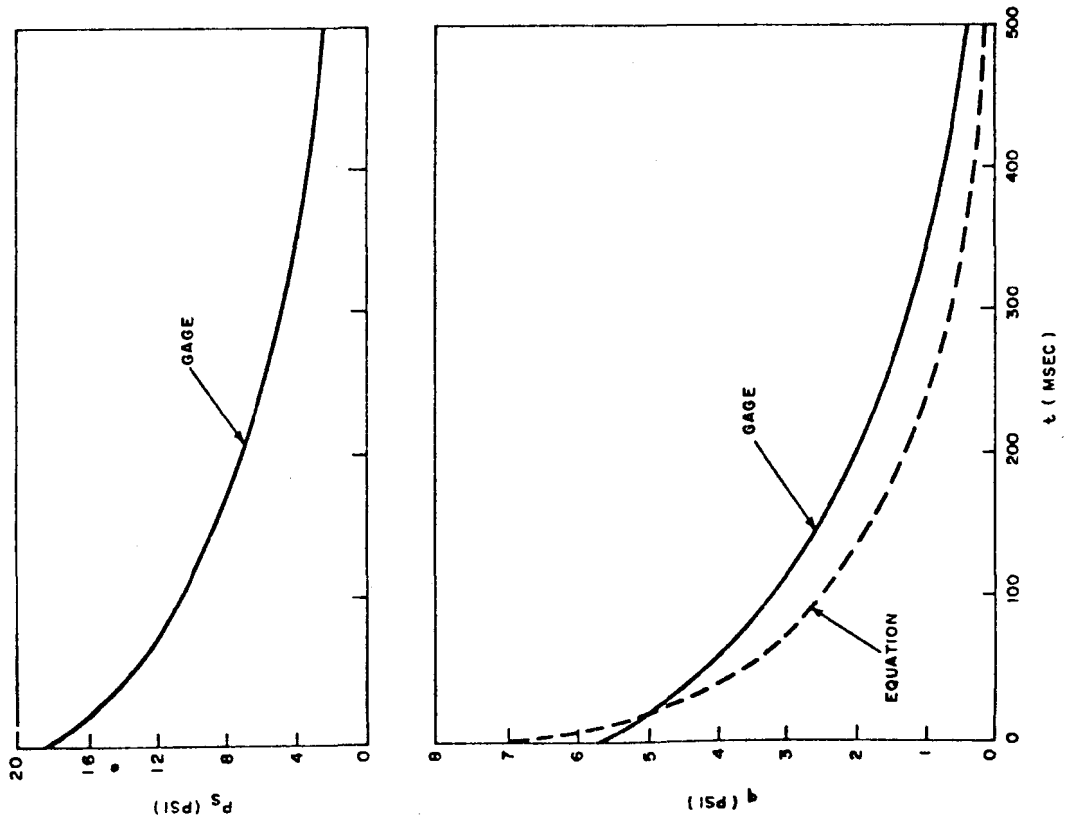


Figure 2.20 Side-on pressure (P_s) and dynamic pressure (q) at A-station.

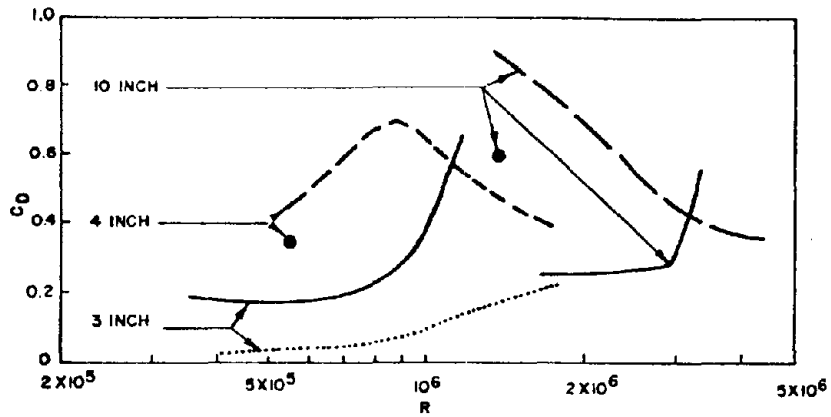
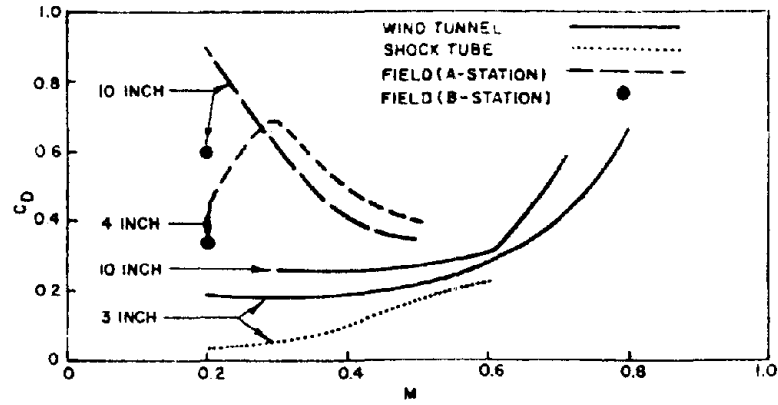


Figure 2.22 Comparison of drag coefficients for spheres.

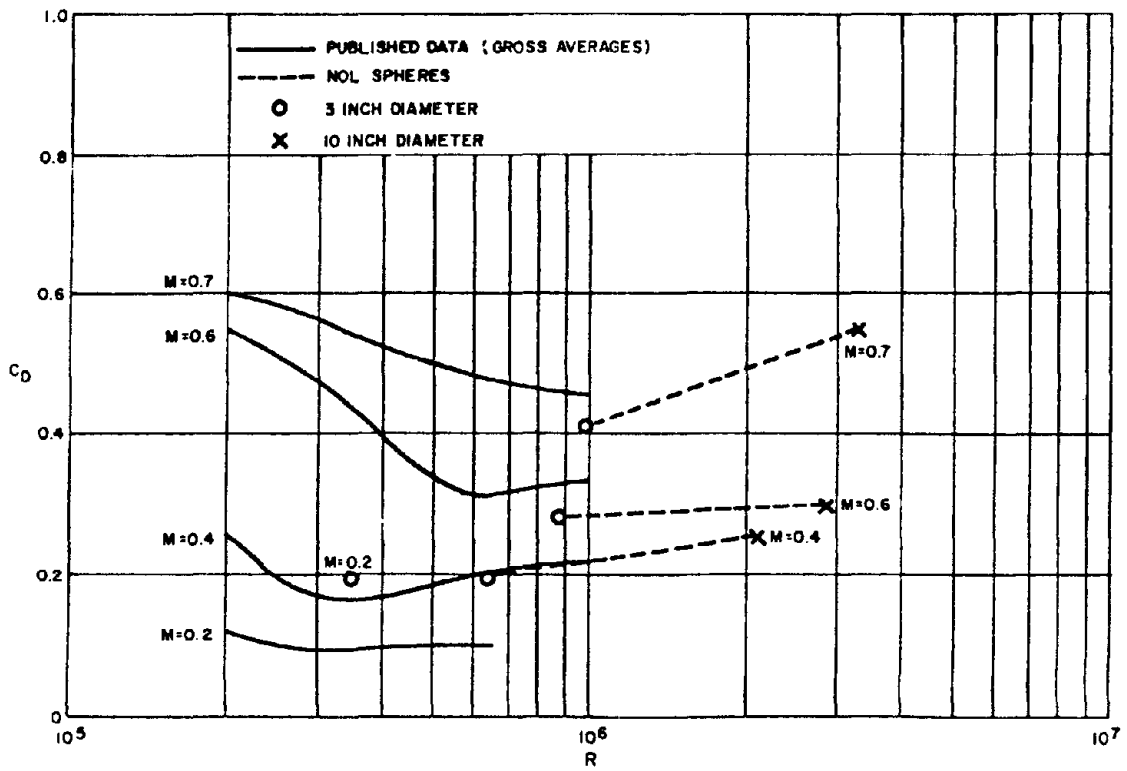


Figure 2.23 Comparison of wind-tunnel drag coefficients of spheres.

3 INCH (SHOCK TUBE)
 3 INCH - - - - (TEAPOT)
 4 INCH - - - - (REDWING)
 10 INCH - - - - (TEAPOT AND REDWING)

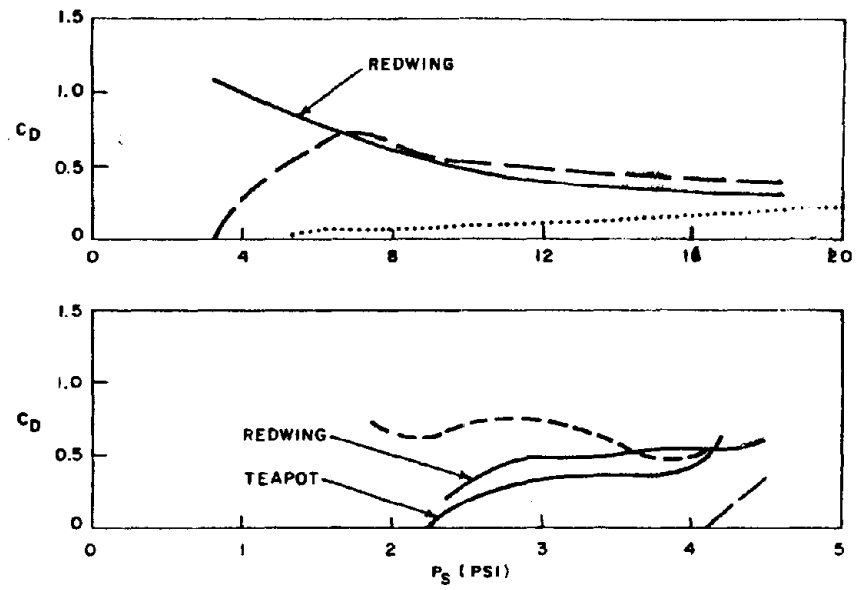


Figure 2.24 Field and shock-tube drag coefficients for spheres.

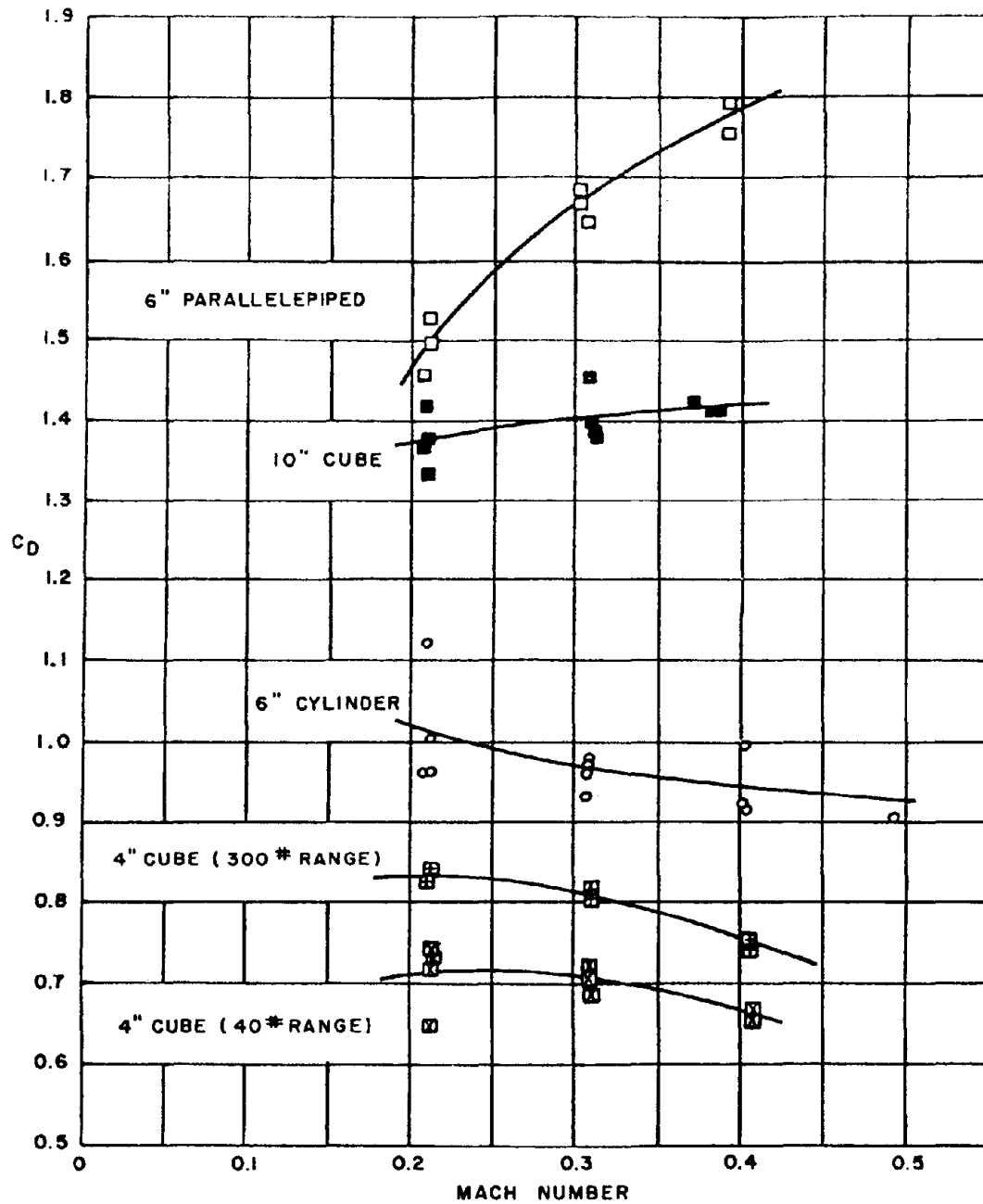


Figure 2.25 Drag coefficients for cubes, cylinders, and parallelepipeds in 7- by 10-foot transonic wind tunnel.

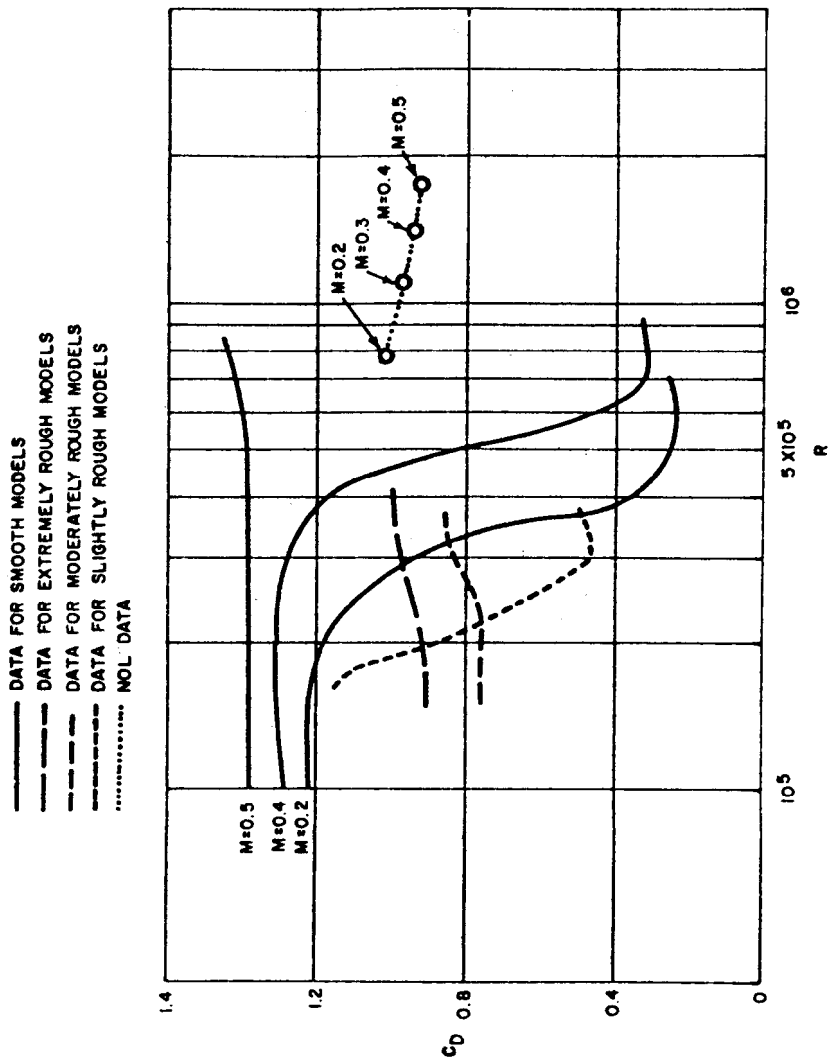


Figure 2.26 Comparison of wind tunnel drag coefficients for cylinders.

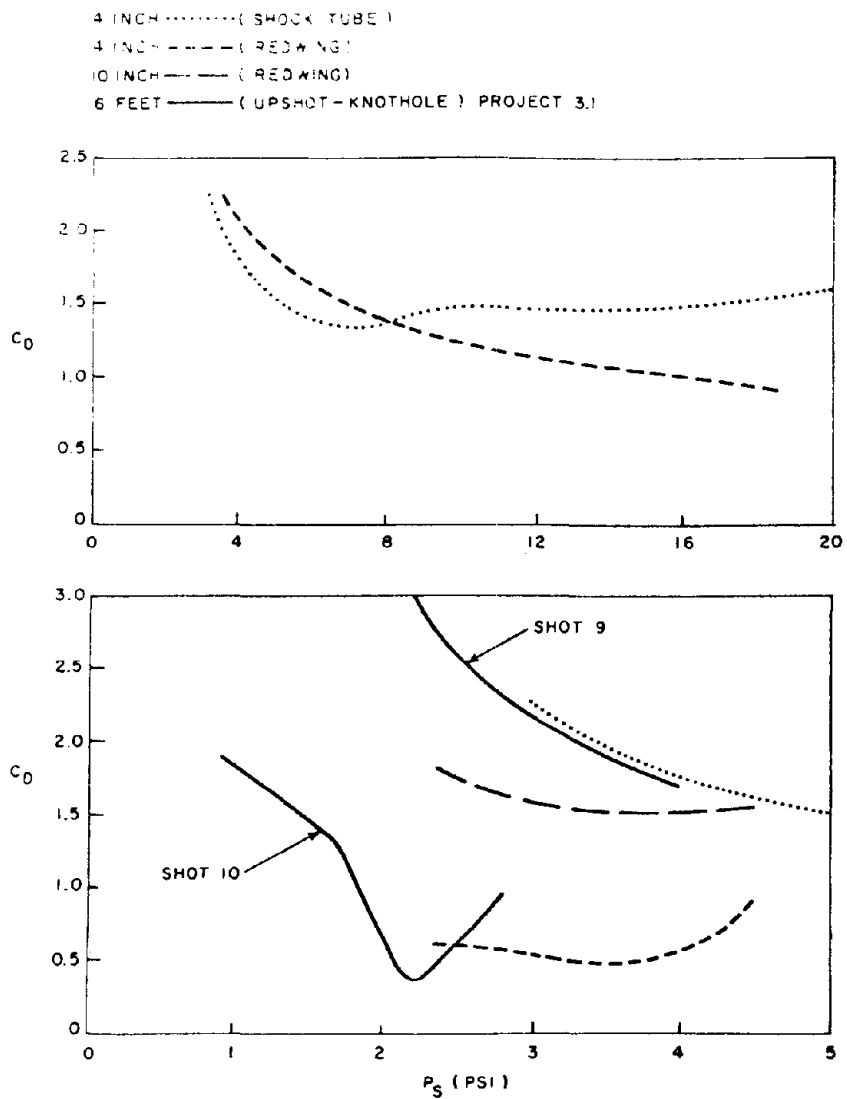


Figure 2.27 Field and shock-tube drag coefficients for cubes.

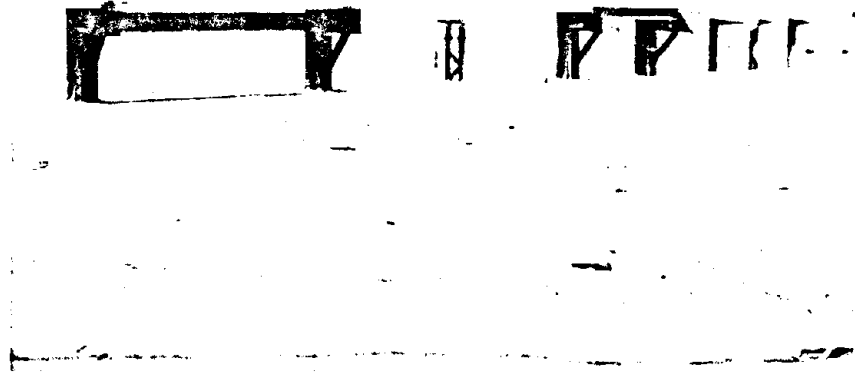


Figure 2.28 Typical structural member station.

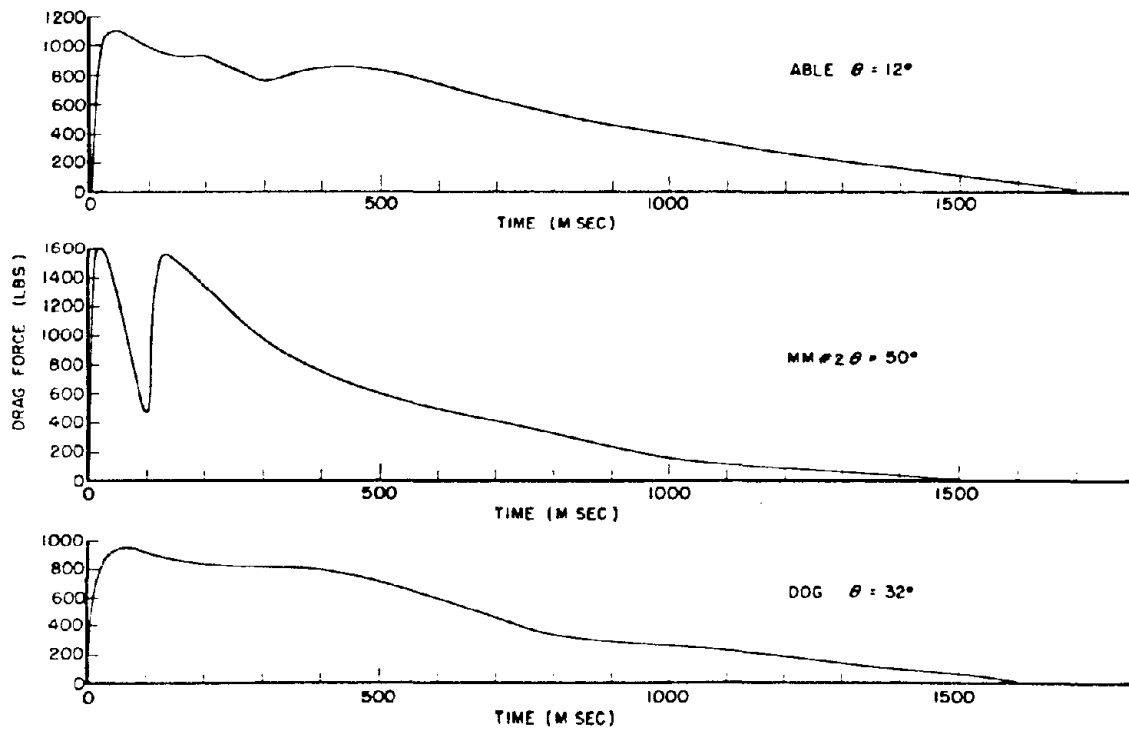
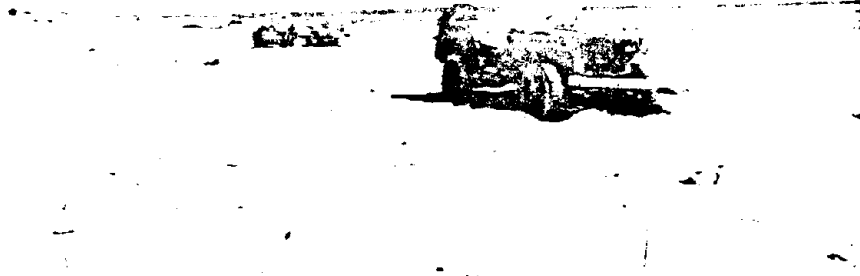


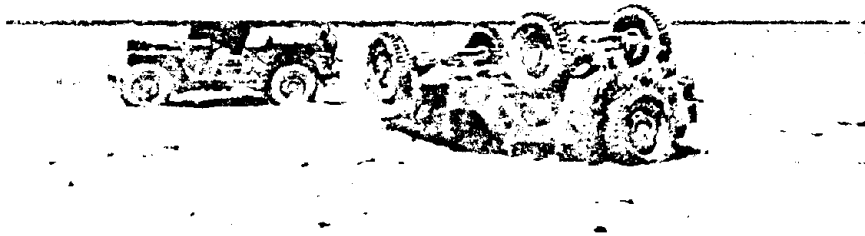
Figure 2.29 Drag force versus time for Sites Able, Manmade Island 2, and Dog, net drag force sensed by I beam.



(a) Station 154.09, 2,500 feet

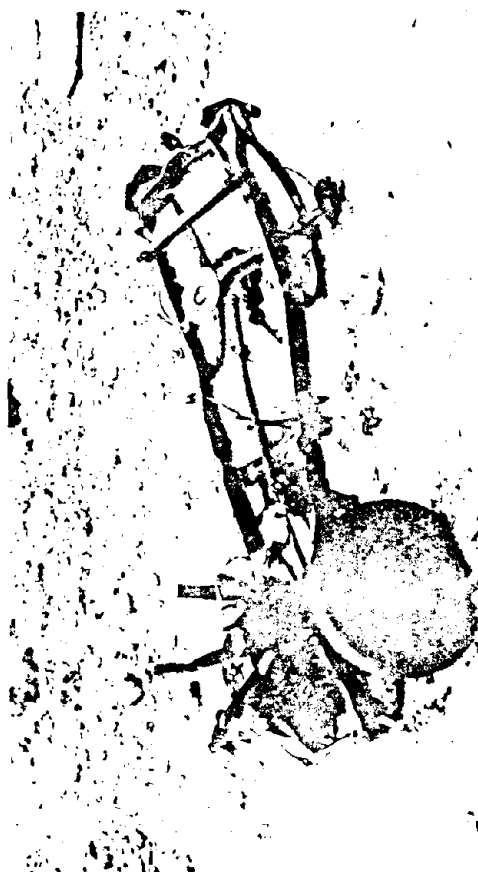


(b) Station 154.11, 3,350 feet



(c) Station 154.13, 4,378 feet

Figure 2.30 Vehicle damage obtained on Shot Lacrosse.



(a) Station 154.01, 8,300 feet, FO vehicle



(d) Station 154.03, 11,700 feet, SO vehicle



(b) Station 154.01, 8,300 feet, SO vehicle

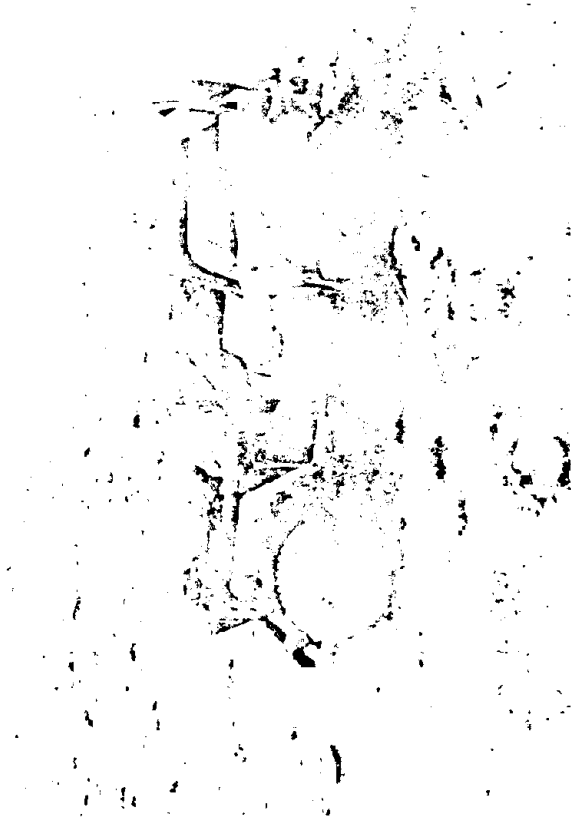


(c) Station 154.03, 11,700 feet, FO vehicle

Figure 2.31 Vehicle damage obtained on Shot Zuni.

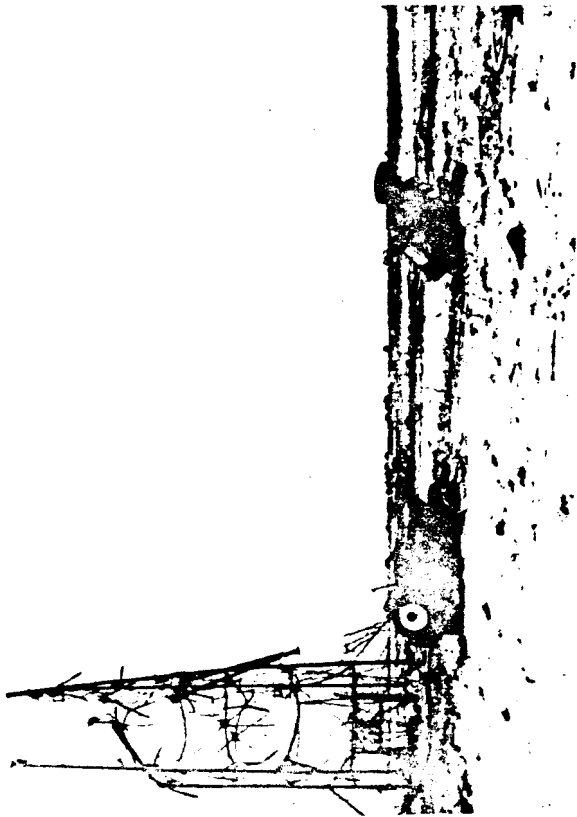


(e) Station 154.04, 13,800 feet, SO vehicle.



(f) Station 154.04, 13,800 feet, FO vehicle.

Figure 2.31 Continued.



(a) Station 154.05, 150 feet



(c) Station 154.07, 350 feet



(b) Station 154.06, 250 feet



(d) Station 154.08, 400 feet

Figure 2.32 Vehicle damage obtained on Shot Yuma.

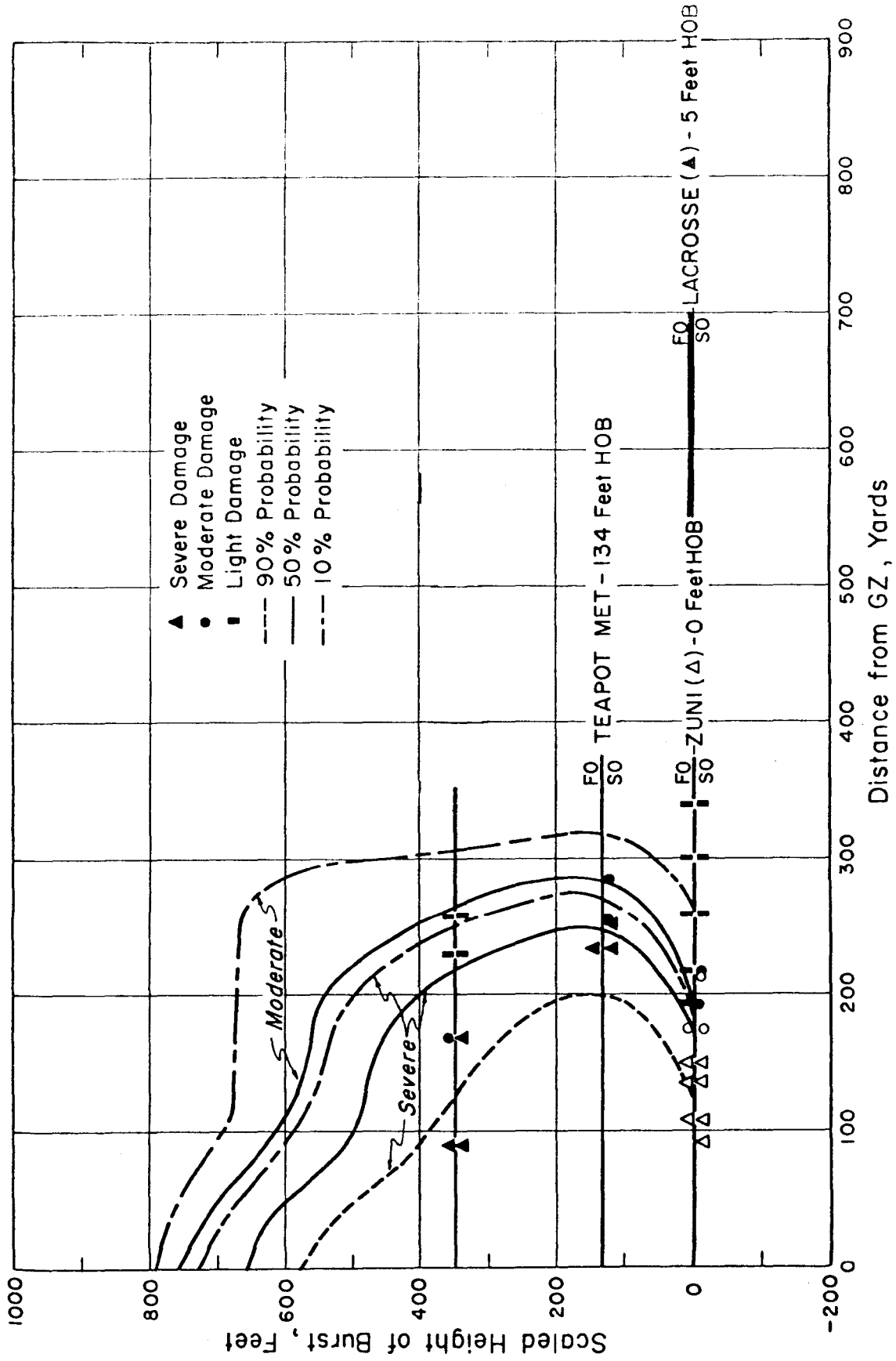


Figure 2.33 Height-of-burst chart for damage to military vehicles (Reference 4).

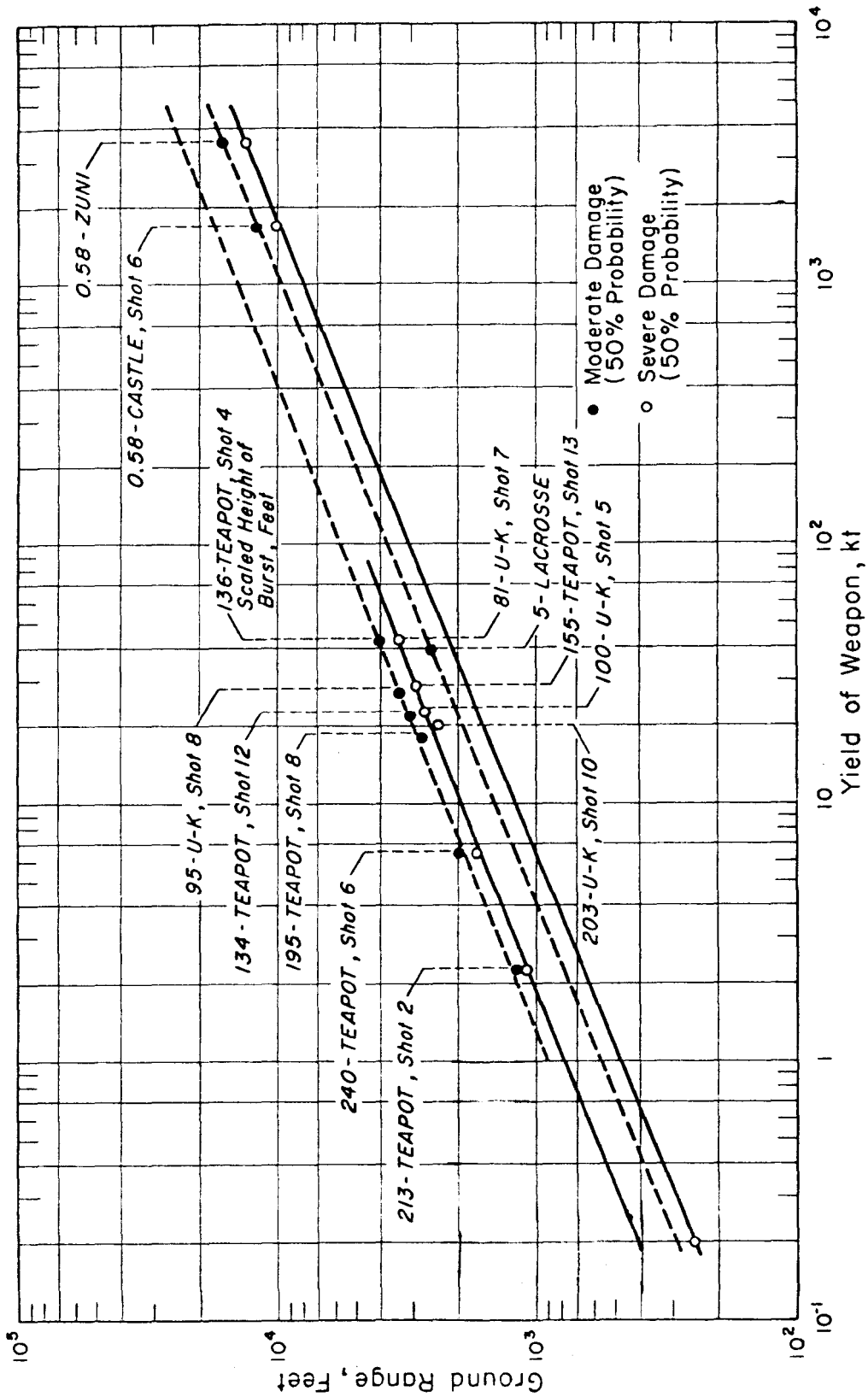


Figure 2.34 Ground range versus yield for various damage levels for EPG surface shots and NTS shots of low scaled HOB.

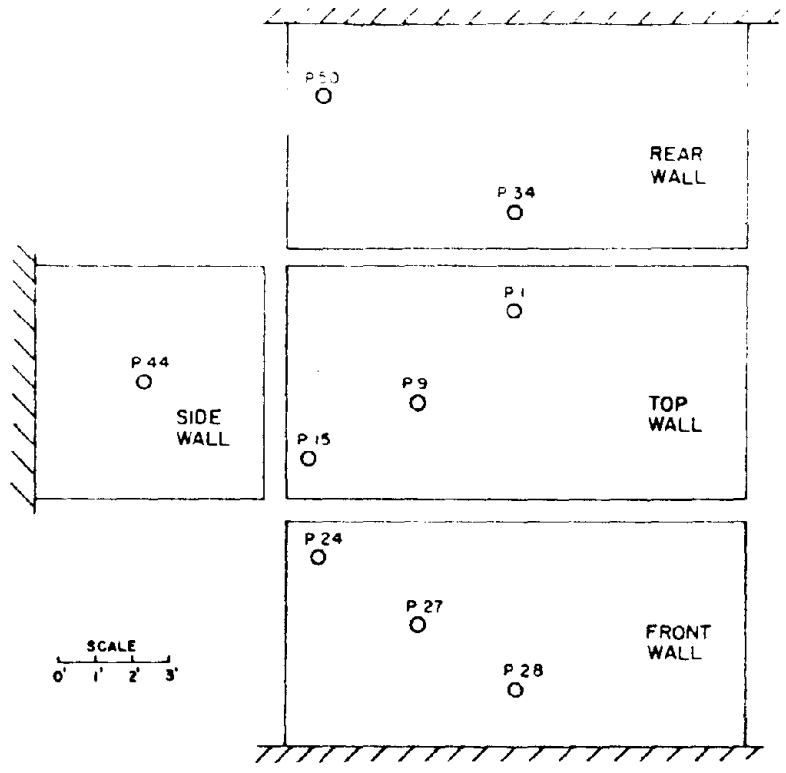


Figure 2.35 Station 111 pressure gage positions.

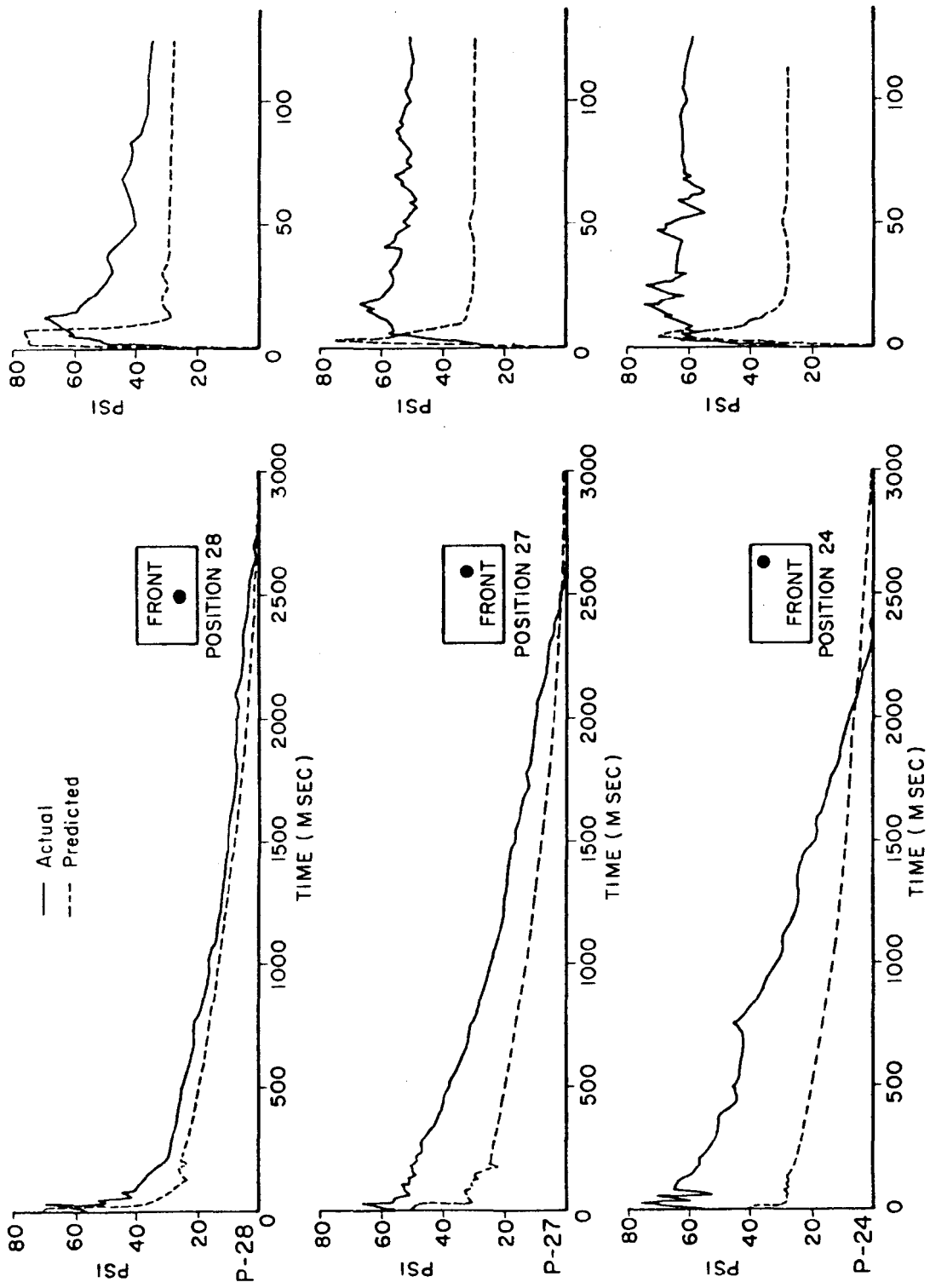


Figure 2.36 Predicted and actual pressure-time loading curves, Positions 24, 27, and 28.

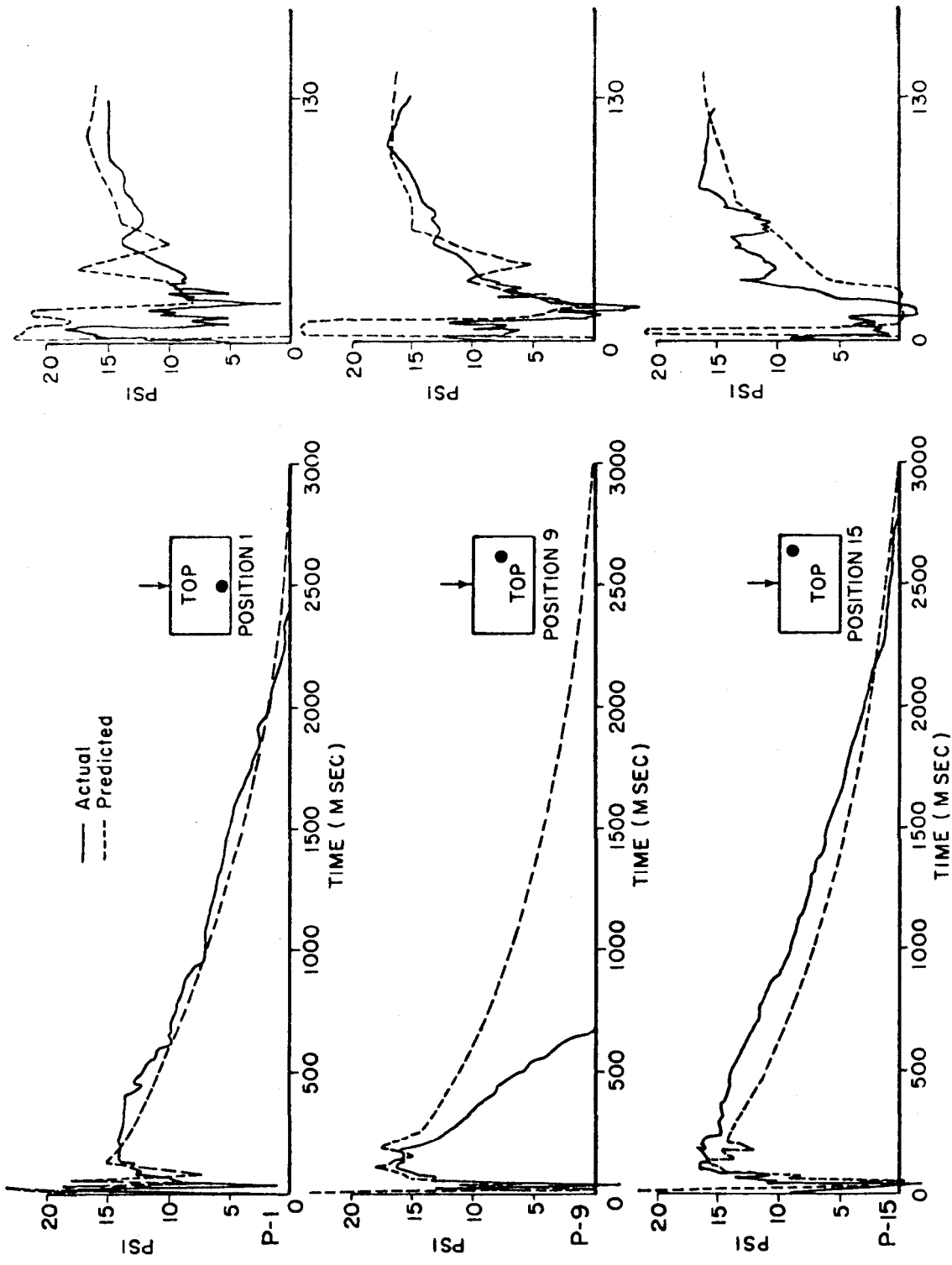


Figure 2.37 Predicted and actual pressure-time loading curves, Positions 1, 9, and 15.

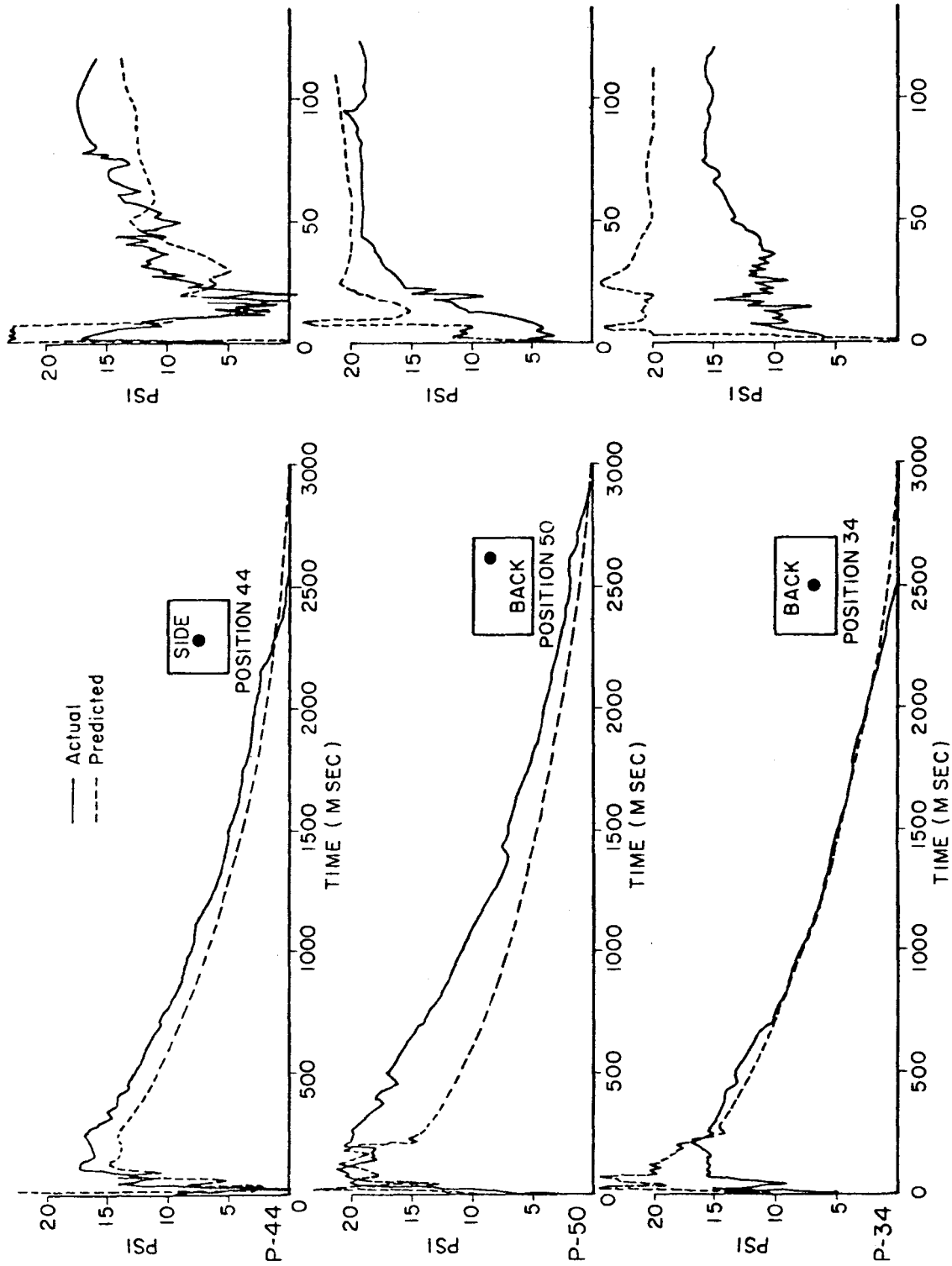


Figure 2.38 Predicted and actual pressure-time loading curves, Positions 34, 44, and 50.

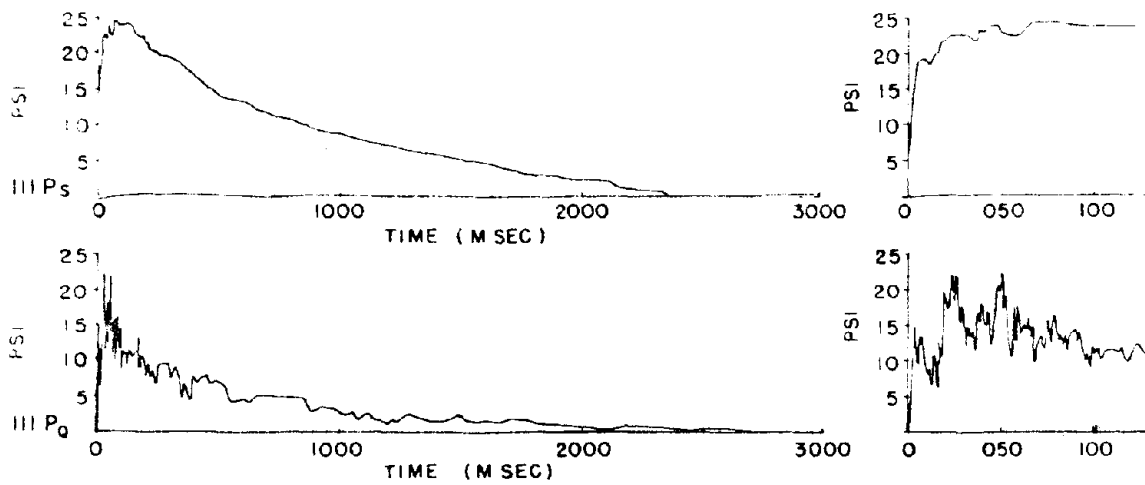


Figure 2.39 Dynamic and side-on record from Station 156.01.

Pg. 114 Deleted.



Figure 2.42 Crater resulting from Shot Lacrosse.



Figure 2.46 Inundation effects on Site Nan following Shot Navajo.

Pg. 120 Deleted.

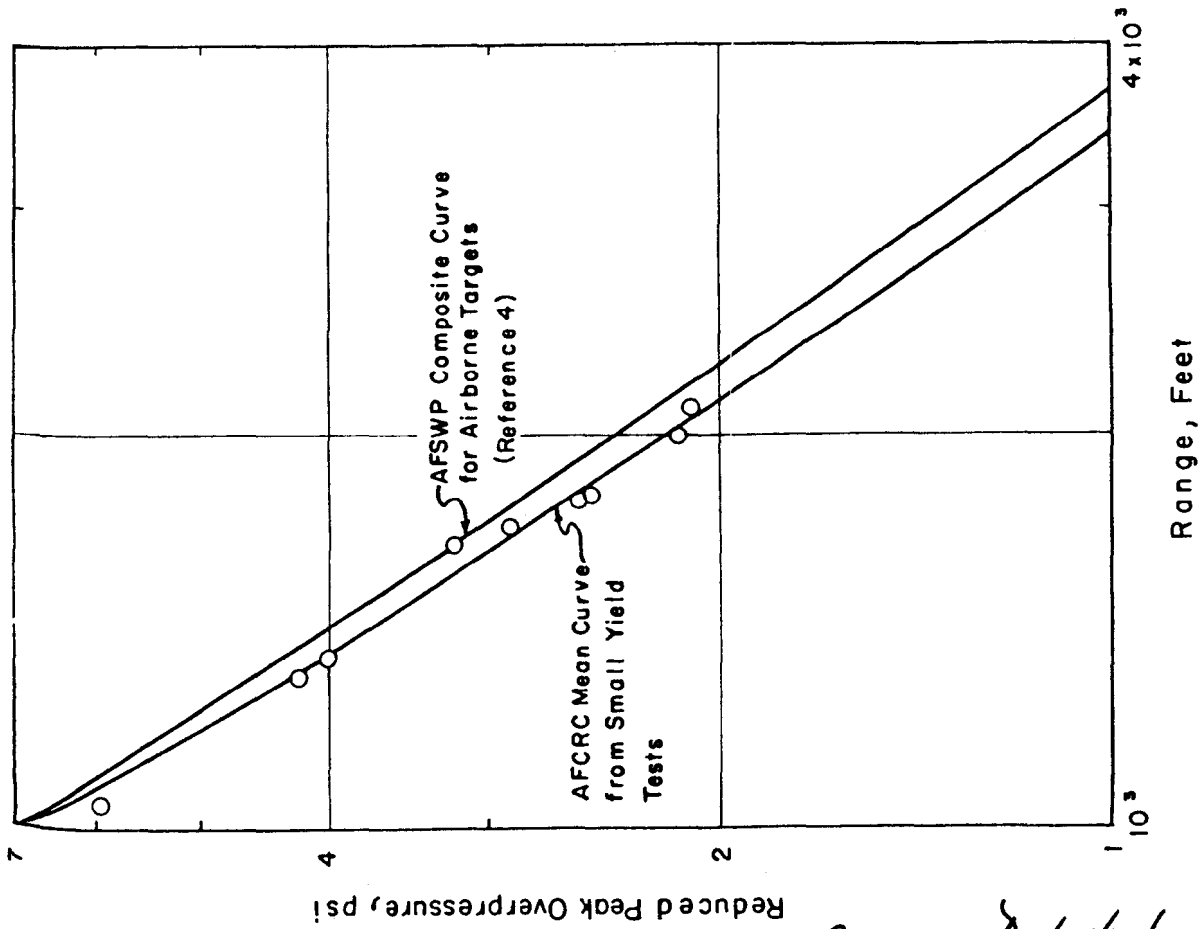


Figure 2.48 Free-air overpressure versus slant range data, scaled to 1 kt at sea level.

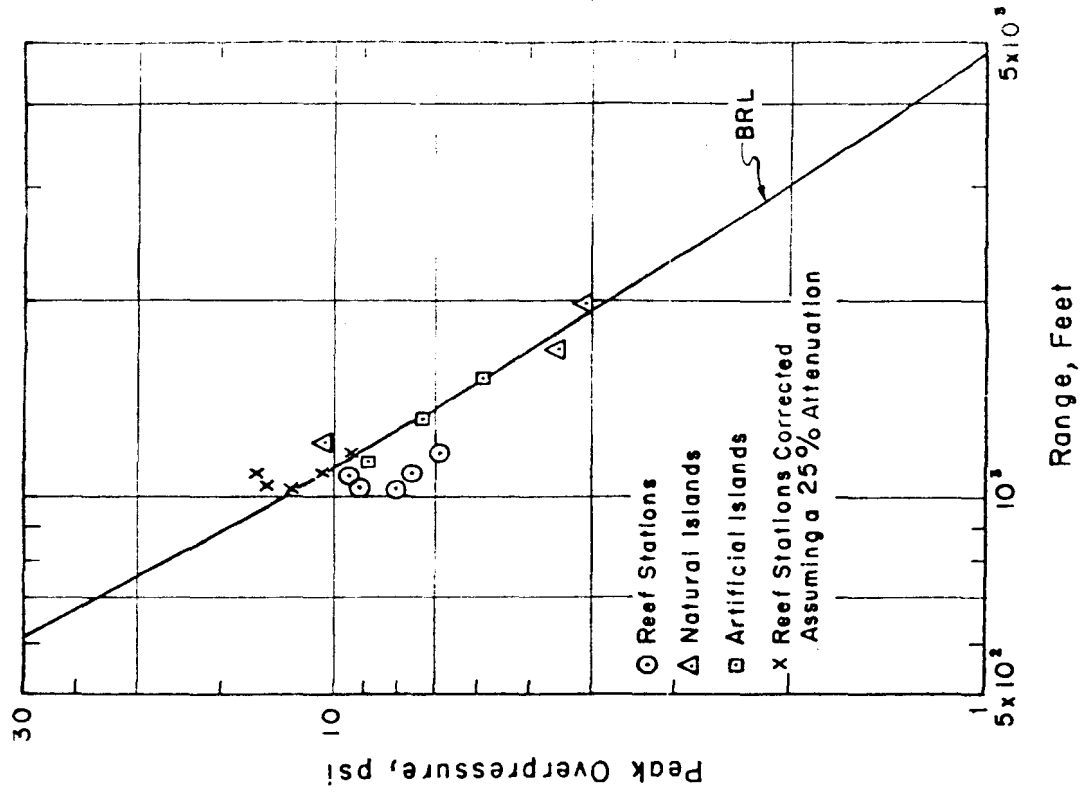


Figure 2.49 Surface peak overpressure versus range, scaled to 1 kt at sea level and compared with BRL ideal curve.

Pg. 122 Deleted.

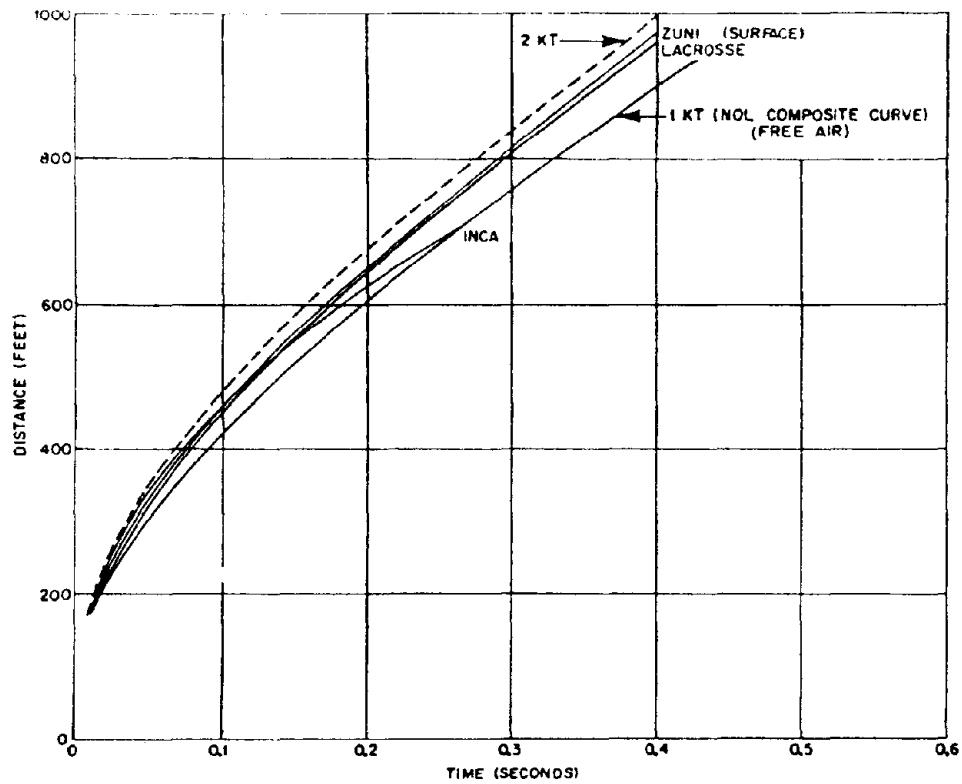


Figure 2.51 Composite plot of time-of-arrival data from Operation Redwing scaled to 1 kt.

Pg. 104 Deleted.

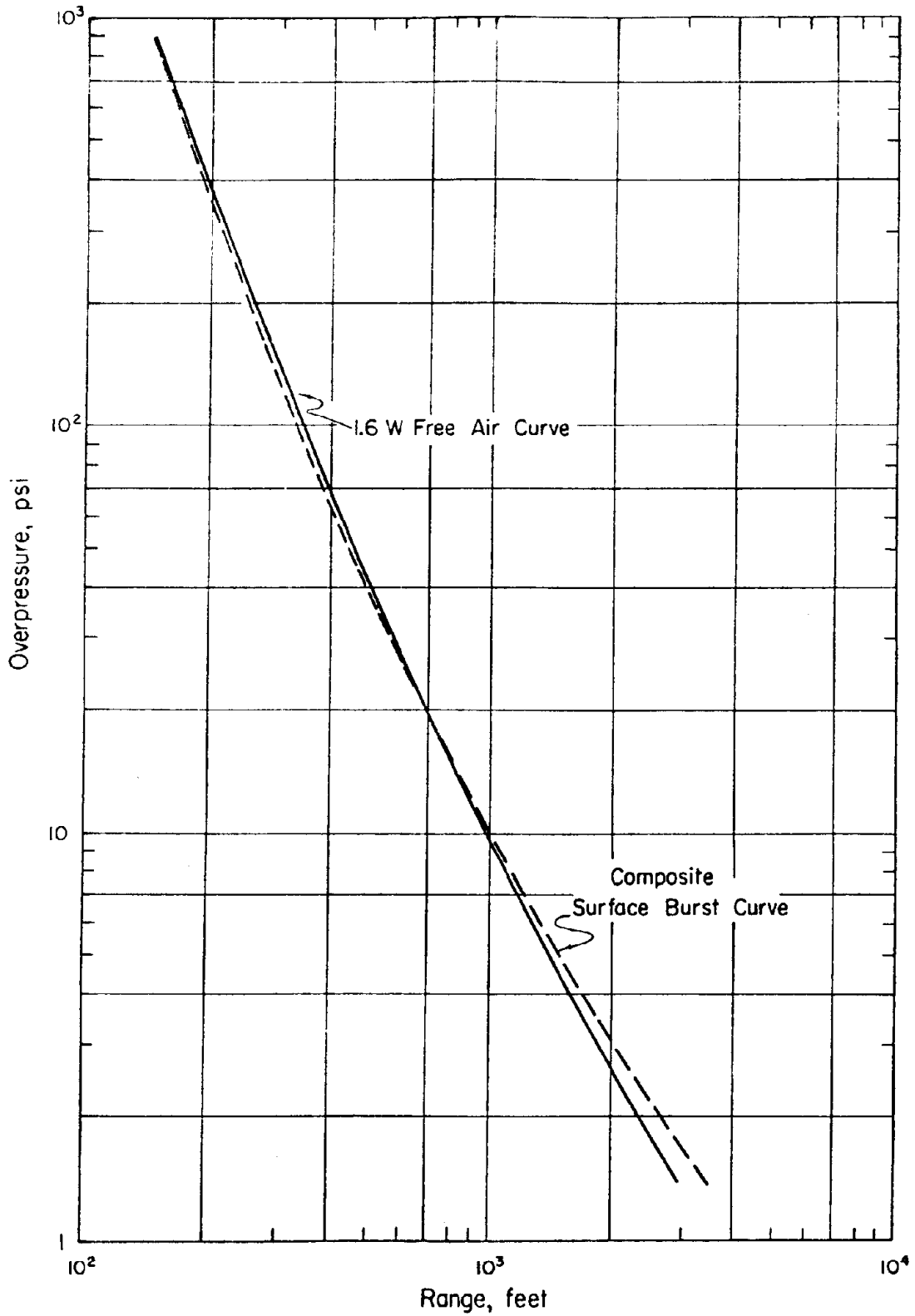


Figure 2.53 Comparison of composite surface burst curve for 1 kt with 1.6W free-air curve.

Chapter 3

NUCLEAR RADIATION

The major effort of Program 2 during Operation Redwing was directed toward gathering data on the nature and distribution of radioactive products from high-yield thermonuclear devices detonated on or near the earth surface. Such data could eventually be applied to a method of predicting fallout from any specified burst. In particular, this goal involved the measurement of radiation fields inside the mushroom cloud, above land surfaces, and above and in the sea water, as well as the collection of fallout material. Other experiments dealt with the initial radiation from the nuclear detonations; still others made use of the fallout contamination to perform tests of shielding, decontamination, and instrumentation.

3.1 OBJECTIVES

A list of the projects and objectives of Program 2 is given in Table 3.1. More detailed information is contained in Section A.2 of the Appendix.

3.2 BACKGROUND

3.2.1 Fallout Distribution. The status of fallout-prediction models and methods before Operation Redwing is best summarized in the report of the AFSWP (DASA) Fallout Symposium (Reference 1). Briefly, there are two stages: (1) the construction of a model for the initial distribution of radioactive material, involving the assumption of the distribution of activity as a function of position and particle size in the nuclear mushroom, and (2) the projection, by graphical or computational means, of the activity onto its final position on the surface through the influence of the wind structure and gravity. During the Fallout Symposium, it became clear that insufficient information was available on the initial distribution in the nuclear mushroom, and radically different models were assumed by different agencies. The second stage, the projection calculation, differed among the various methods chiefly in the amount of simplifying assumptions and, hence, in the time needed to perform the computation. The applicability of the different methods depends mostly on the desired accuracy of the result and the time available to achieve it.

Until Operation Redwing, no concerted effort had been made to document the complete fallout pattern from high-yield thermonuclear surface bursts. The previously available information consisted principally of radiation and fallout collection data on the nearby atoll islands for Shot Mike of Operation Ivy and Shots 1 and 3 of Operation Castle, together with some ocean survey data from Shots 5 and 6 of Castle. Therefore, it was considered necessary to document, as completely as possible, the fallout, both near the detonation and throughout the extensive ocean area, from several large-yield surface bursts.

Participation of the fallout program during Shot Cherokee seemed to verify the hypothesis that megaton-range airbursts produced negligible local fallout contamination, such a hypothesis being an extrapolation from kiloton-range airbursts.

3.2.2 Distribution of Activity in Nuclear Mushroom. Knowledge of the distribution of activity in the nuclear mushroom was needed: (1) as a part of the model of the initial conditions for fallout prediction, and (2) for evaluation of the radiation hazard to crews of aircraft, which might be forced to fly through a nuclear mushroom during atomic warfare. Previous measurements, which had consisted principally of drone-aircraft flights through the mushroom of kiloton-range detonations, indicated that the exposure rate in the cloud was not a function of the yield and decayed with time as $t^{-2.0}$. The Redwing experiment was intended to extend these measurements to megaton-range detonations, by measuring the distribution in detail and checking the effect of varying the weapon's fission yield with the same total yield.

3.2.3 Initial Radiation. The scaling of initial gamma radiation from kiloton-range detonations to high-yield thermonuclear detonations is affected by the following factors: (1) the number of gamma rays, as well as the portion of fission neutrons that produce gamma rays through the $N^{14}(n, \gamma)$ reaction, depends on the fission yield of the device; (2) the fusion reaction produces large numbers of high-energy neutrons that can react with nitrogen to form gamma rays; and (3) the gamma flux emitted by the fireball of a megaton-range thermonuclear detonation is intense for a number of seconds after the detonation, thereby allowing time for the blast wave to carry much of the absorbing material toward and past the observing station. This hydrodynamic effect produces an enhancement of the total initial exposure beyond that to be expected from linear scaling with yield.

The theory and experimental measurements through Operation Ivy on initial gamma rays have been summarized in Reference 2. Limited measurements performed during Operation Castle indicated that the initial gamma exposure was not of military significance to exposed personnel, because of overriding blast and thermal effects. The measurements performed during Operation Redwing were designed to establish valid scaling laws for initial gamma exposure and to extend the data to devices in which the fission yield comprised a small fraction of the total yield.

Neutron-flux measurements have been performed at many previous test operations, principally with gold detectors for thermal neutrons. During Operation Teapot, these measurements were extended through the use of fission detectors, in addition to gold and sulfur activation detectors, so that the thresholds covered the energy range from thermal energies to 3 Mev. In general, the neutron flux and energy spectrum are functions of the nature of the nuclear reaction and the nature and geometry of the absorbing material in the device. Therefore, during Redwing it was necessary to make a set of neutron-flux measurements for new types of devices, as well as to make correlated energy-spectrum and air-absorption studies to evaluate the effective neutron dose. Only a small amount of data was available from Operation Castle on neutrons from thermonuclear detonations; therefore, it was proposed to document the neutron flux and energy spectrum from Shot Cherokee.

The gamma activity induced in soil has been studied for Nevada Test Site (NTS) soil irradiated by neutrons from kiloton-range weapons. Limited measurements were also made during Operation Teapot on other types of soils. The Cherokee airburst of Redwing was intended to furnish further data on samples of different soils, for correlation of effects of thermonuclear airbursts with the lower yield NTS shots.

3.2.4 Contamination-Decontamination. Contamination-decontamination experiments have been performed since Operations Greenhouse and Jangle. The results, as amplified particularly by data from Operation Castle, indicated that a land-surface burst produced a dry particulate that was easily removable, whereas the wet contaminant from a water burst had greater penetrability and was more difficult to remove.

Operation Castle also furnished some data on ship protection by a washdown system and subsequent decontamination by scrubbing and paint-removal techniques. Comparison of exposure readings on adjacent washdown and nonwashdown ships indicated a reduction of approximately 90 percent by the washdown system. The most practical decontamination procedures consisted of firehosing, handscrubbing with detergent, and a second firehosing; but a procedure of hot-liquid-jet cleaning with detergent seemed to be a promising procedure as well.

3.2.5 Ship Shielding. Calculations have been performed to evaluate the effect of intervening ship's structures on the gamma exposure to personnel located inside the weather envelope. These calculations needed verified input data on two points: (1) the relative contributions of airborne, waterborne, and shipboard contamination to the exposure at various locations aboard ship, and (2) the effective absorption coefficient of steel for the time-varying complex gamma-spectrum characteristic of fission product and induced gamma activity. Previous limited measurements during Operations Crossroads and Castle provided only a few points for the calculations and pointed out the problems. Therefore, fairly extensive shipboard instrumentation was provided for Operation Redwing to determine the needed answers.

3.2.6 Evaluation of Dosimeters. An experiment had been performed during Operation Teapot to establish the relation between the exposure measured at the surface of a tissue-equivalent masonite phantom and the biologically significant depth dose measured at 3- to 5-cm depth in the tissue-equivalent material. Because the dosimeters used primarily by the U. S. Navy are now the DT-60/PD (phosphate glass) and the IM-107/PD (quartz fiber), it was desirable to test these instruments in the presence of fallout radiation, using the depth-dose measurements as standards.

3.3 INSTRUMENTATION AND OPERATIONS

3.3.1 Land Stations. The islands of Bikini Atoll were utilized extensively as bases for fallout-collection and radiation-measuring devices. In general, fallout-collection and residual-radiation measurements were performed throughout the atoll, whereas the station locations for gamma and neutron initial-radiation measurements were chosen on the islands near the surface zero. The fallout collection included both total collection and time-increment collection; the radiation measurements included fallout time of arrival, exposure rate versus time, and total exposure.

3.3.2 Moored Stations. Because the available land areas covered only a small fraction of the fallout pattern, an array of floating instrument stations was moored within Bikini Lagoon and to the north of the atoll. Three pontoon rafts, instrumented to measure time of arrival and total exposure and to collect total-fallout samples, were located along an east-west line approximately bisecting the lagoon. Two YFNB barges with complete total and time-incremental samplers and radiation detectors were moored at various locations in the lagoon for the different shots, as determined by expected fallout

zones and peak overpressures. Approximately 16 skiffs were moored in the deep ocean, northerly from the atoll, by a special technique devised by the Scripps Institution of Oceanography (SIO). These were instrumented to collect total-fallout samples and to measure integrated exposure, time of arrival, and, in some cases, penetration of activity to various depths in the ocean.

3.3.3 Fallout-Collection Ships. Three ships (YAG-39, YAG-40, and LST-611), which had been modified to permit operation from a shielded control room, were moved to positions in the expected fallout zone prior to the arrival of fallout. These then served to collect fallout on the ship surfaces and in incremental and total collectors. The LST and the aft sections of the YAG's were washed down during fallout. Panels of various building materials, samples of common shipboard items, and the masonite phantoms were exposed on the nonwashdown deck of the YAG's.

Instruments aboard some, or all, of the ships performed the following functions: (1) exposure-rate measurements versus time at many locations above and below decks, (2) incremental air filtering, (3) gamma spectroscopy of individual particles and samples, (4) early-time decay studies on particles and samples, (5) exposure-rate measurements versus depth in the water, (6) exposure-rate measurements versus time above water, and (7) incremental and total fallout collection. The instrumentation located aboard the YAG's is illustrated in Figure 3.1.

3.3.4 Survey Ships. Two Navy destroyer escorts (DE's) and the SIO research vessel, M/V Horizon, proceeded into the ocean fallout area after the radioactive material had been deposited and performed the following functions: (1) exposure-rate measurements just below the ocean surface along the ship's tracks, (2) occasional measurement of exposure rate versus depth, and (3) water sampling.

3.3.5 Survey Aircraft. Two P2V5 aircraft, instrumented to measure exposure rate versus time, were flown at constant altitude over the ocean fallout area. The records then provided the data for construction of contours of constant exposure rate above the ocean surface.

A radiation-sensitive probe was suspended on a long cable below a helicopter and was lowered to positions 3 feet above the surface of contaminated islands. The detector readings were noted inside the helicopter. The technique employed in making these measurements is shown in Figure 3.2.

3.3.6 Cloud-Penetration Rockets. A salvo of six rockets was fired at H + 7 minutes and another at H + 15 minutes into the mushrooms of Shots Cherokee, Zuni, and Navajo. Four rockets were fired at H + 7 minutes into the Tewa Cloud. Data from ion-chamber radiation detectors in the rockets was telemetered to receiver-recorder stations at Site Nan and aboard the USS Knudson (APD-101). The rocket employed by Project 2.61 is illustrated in Figure 3.3.

3.3.7 Cloud-Penetration Aircraft. Several B-57B aircraft, instrumented to measure exposure rate and total exposure, were flown through the nuclear clouds and stems from Shots Cherokee, Zuni, Flathead, Dakota, Apache, and Navajo as early as 20 minutes and as late as 78 minutes after detonation. In addition, upon return to base on Site Fred, the aircraft were subjected to contamination-decontamination studies, and the contact hazard, which personnel experience when working on such aircraft, was investigated.

3.3.8 Program 2 Control Center. During Shots Cherokee, Zuni, Flathead, Navajo,

and Tewa, in which the fallout surveys were performed, a control center aboard the USS Estes (AGC-12) was manned by representatives of Program 2 and the projects performing the surveys. This center served to send out instructions to the survey vehicles and to coordinate and compare the data.

3.3.9 Laboratory Facilities. The principal laboratory facilities available to the fallout-documentation projects included equipment to perform chemical analysis, particle-size analysis, radioautography, gamma and beta counting, gamma spectroscopy, and photographic development and densitometry. These facilities were located, in part, aboard the YAG-40, on Site Elmer, at the Naval Radiological Defense Laboratory (NRDL), and at the Chemical Warfare Laboratories (CWL).

3.4 FALLOUT STUDIES

The experiments relating to documentation and characterization of fallout were conducted on Shots Cherokee, Zuni, Flathead, Navajo, and Tewa (Table 1.1). Cherokee produced no fallout. Flathead and Navajo produced slurry. Zuni and Tewa produced dry fallout. Supplementary individual measurements were made on a number of other shots.

As previously described, the fallout location, delineation, and sample-collection efforts were carried out by a number of individual projects, with the overall effort being coordinated through a program control center. The control center served to provide predicted fallout patterns, based on the latest weather forecast prior to the events, for location of the mobile elements of the fallout documentation array.

Following the detonations, revised predictions, based on shot-time weather and subsequent time and space variations, were prepared to maneuver these elements to desired locations. During the actual survey operations, the control center coordinated the movements of the survey units so as to resolve any apparent discrepancies in measured values, insured that all areas of the fallout pattern were surveyed in sufficient detail to yield a complete picture, and directed the various survey units to rendezvous points for inter-calibration checks. The control center performed these functions with exceptional success, and comprehensive and satisfactory documentation of the fallout fields resulted.

3.4.1 Measurement of Radiation Contours. Aerial Surveys. The aerial surveys conducted over the fallout-contaminated ocean areas resulted in relative radiation intensity mappings. Flights were flown on D Day, D+1, D+2, and D+3 days; however, the D+1 day readings were the basis for the reported contours. By application of air absorption and decay factors of questionable validity, these mappings were converted to isodose-rate contour charts of the radiation field 3 feet above the ocean surface at a reference time of H+24 hours.

The D+1 day contour plots were converted to a land-equivalent fallout field by multiplication of the 3-foot contour intensities by a factor of approximately 1,000—this factor having been determined from calculations involving: (1) the depth of mixing, which was assumed to have an average value of 60 meters; (2) the average gamma emission energy, which determines the thickness of the surface layer contributing to the ocean surface gamma field; and (3) the air absorption, which determines the surface area that constitutes the field observed by the airborne detector. In addition to the uncertainties inherent in relating the altitude measurements to 3-foot values and in converting these 3-foot values to equivalent land values, there was the further effect of distortion of the initial fallout pattern by influence of the ocean currents. For these reasons the accuracy

of the land-equivalent fallout contours produced by the aerial survey method are subject to severe limitations. However, these surveys were not intended to give exact, quantitative data, but rather to provide an early definition of the overall fallout pattern, which could be subsequently investigated by the surface survey elements; in this sense the aerial surveys were successful.

Figures 3.4 through 3.7 show the contours on D+1 day for Shots Flathead, Navajo, Tewa, and Zuni, as determined by aerial surveys. No detectable ocean area contamination was found after the airburst of Cherokee, although the area in which fallout would have been deposited, should it have occurred, was searched thoroughly. Similar surveys after Shot Osage, an airburst, confirmed the Cherokee finding that significant fallout does not occur after airbursts.

The many conversions necessary to construct a 3-foot equivalent contour from readings taken in an airplane at 300-foot altitude above the ocean surface of necessity contain many assumptions, uncertainties, and instrumentation limitations. Figure 3.8 presents a diagram of the conversion factors selected for this report.

The assumption that the detectors used in the aircraft were uncollimated is subject to serious doubt in the light of the strong collimation effects previously reported. This alone would cause a variation in the final answer by a factor of four.

The depth of mixing used—60 meters—is confirmed for Shot Navajo by NRDL; however, it is generally agreed that there was considerable fall through and a deeper depth of mixing for Zuni. Thus, the resultant calculated land-equivalent dose contours should be increased by a significant portion, at least a quarter. SIO reports average depth of penetration from 52 to 80 meters, depending on the shot. This could cause a variation in the final answer by 25 percent.

Altitude absorption factors were confirmed for the four shots by simultaneous measurements at the 3-foot level over water and at the 300-foot altitude. Measurements were taken at different places for various shots, and theoretical curves were used to normalize the air measurements with the 3-foot dose expected over water. The top hat instruments used were not calibrated to energy levels high enough to show the variation in dose computations that could result from the 1.38 and 2.75 Mev gammas from Na^{24} , which created a large portion of the resultant dose rates of [redacted] Navajo and Zuni. The altitude absorption was calculated for an average energy of fission product gamma of 0.5 Mev, which is not considered representative for this fallout from [redacted] Navajo and Zuni.

A large portion of the resulting dose rates for [redacted] Navajo and Zuni, may have come from the induced radioactivity in the sodium of the sea water. At H+24 hours the estimates range as high as 65 percent (Reference 3) and as low as 33 percent (WT-1317). No attempt was made to subtract this portion of the dose rate from the dose rate contours reported by Project 2.64, or by Project 2.62. The presence of such a high fraction of Na^{24} gamma will significantly affect the decay rates necessary to resolve all readings to a common time base. The aircraft project used the contour measurements taken on D+2, D+3, and D+4 days to refine the D+1 contours. The contours in Figures 3.9 through 3.12 are presented as D+1 day contours, because the differences in decay exponents used by various agencies for different shots would result in a further divergence of dose rates when converted to H+1 hour readiness.

The percent of the fission products that fell inside the measured contours was estimated in the basic report. These estimates did not take into consideration the Na^{24} contribution. The interpretation of the measurements is so dependent on energy spectrum and instrument response that the percentages have little more than academic meaning.

Possible corrections to reported percentages have been tabulated in Table 3.2.

Surface Ship Surveys. The ship surveys recorded measurements of gamma dose rate 3 feet below the water surface as they traversed the contaminated ocean areas. They made frequent stops to measure gamma dose rate as a function of water depth at selected geographic locations within these areas. During these surveys, water samples were collected at the surface and at various depths. Because the final desired product of these surveys was a plot of the isodose-rate contours that would exist at an altitude of 3 feet, had the fallout been deposited on an infinite hypothetical land plane, a number of corrections and conversions of the measured data were necessary. Because the contaminated water mass would be distorted through the influence of ocean currents, the initial correction involved restitution of the observed water masses to their positions at the time fallout was deposited. An oceanographic survey of the currents in the ocean area of expected fallout was conducted early in the operation, before any actual shot participation, and the data obtained provided the information necessary for accomplishing these drift corrections.

Numerous observations of depth of contamination mixing and depth of thermocline were made throughout the fallout survey operations. It was found that, except for close-in areas of the land surface shots, the fallout contamination deposited on the ocean waters remained in solution or suspension in the mixed ocean layer above the thermocline for periods exceeding the duration of the ship surveys. Thus, from a knowledge of the activity concentration and depth of mixing, an estimate of the total deposited activity was possible. To improve the accuracy of this estimate, the survey instruments used were frequently calibrated before and during all operations, and a thorough post-operational evaluation of the energy and angular response of the instruments in measuring activity in a contaminated water medium was accomplished.

The D + 1 day isodose-rate contours determined for the four shots are shown in Figures 3.9 through 3.12. They are presented in WT-1316 as H + 1 hour contours but have been decayed to D + 1 day in this report (using appropriate decay for each shot as measured by SIO) for ease in comparison with the contours from the aerial surveys. Note that the later contours were not corrected for current.

Ship surveys indicated that Shot Cherokee produced so little fallout that isodose-rate contours could not be plotted. Only one small spot of water, 2 miles wide and of unknown length, was detectably above the normal oceanic background. No other fallout radioactivity was found, even though the local areas out to 300 miles from ground zero were investigated.

The dose-rate levels at any time are not a realistic indication of the fallout hazard that exists over the entire area, because fallout does not occur over most of the area at any one time. Therefore, isodose plots indicating the dose which would be accrued during the first 50 hours after detonation were also prepared. By application of measured decay constants, the actual ground level dose rates and their time of initial effectiveness on the ground were determined for the various positions within the fallout area. Integration of these determined ground dose rates from time of arrival to H + 50 hours resulted in the dose that a person in an unshielded position would sustain during the first 50 hours after a shot. The accumulated dose contours are presented in Figures 3.13 through 3.16.

Table 3.3 presents a summary of the extent of the fallout for the events in which ship survey data was obtained. For a comparison of the areas contaminated by the different shots, the total yield of each weapon, as presented in Table 3.3, was normalized to a 5-Mt detonation of 100 percent fission yield. To correct to 100-percent fission yield, the dose rates were divided by the fission fraction, and to normalize to the 5-Mt yields, dose

rates were assumed to increase with the cube root scaling law. The areas, following the same law, were increased by the square of the cube root of the yield. Figure 3.17 presents the results of this comparison. Predicted contour areas for a 5-Mt device have also been included in this figure (Reference 4). An apparent confirmation of scaling laws is indicated by Figure 3.17. By observing the critical dependence of the H+1 hour dose rates upon the decay used to convert readings back to this early time, it is possible to see that a slight variation of decay rates could modify the picture considerably. Even the variation of the decay rates measured in Project 2.63 from the ones used in Project 2.62 would be sufficient to open up the plots of Figure 3.17.

The contribution of sodium to the decay rates of Zuni and Navajo has not been evaluated. Other studies give varied estimates (Reference 3 and WT-1317). No effort was made to have the 3-foot land-equivalent dose contours corrected to represent the contours of a land surface burst. They are contours of bursts fired in the unique conditions present at Eniwetok (Table 1.1). The contribution of the radioactivity from the induced sodium should logically have placed

Dose-rate contours presented in Figures 3.9 through 3.12 have been decayed to H+24 hours for presentation for three reasons: (1) to permit ready comparison with the isodose contours measured by the aircraft in Project 2.62, (2) to reduce the effects of variations in decay rates used in several projects, and (3) to present the contours at a time when the induced sodium contribution to the dose rates observed for the clean shots is but a small fraction of the dose rate from the fission products.

Land Surveys. Helicopter probe-surveys of the islands of the Bikini Atoll were successfully accomplished by Project 2.65 following each of the events during which the fallout program participated. Fallout-produced gamma dose rates were measured 3 feet above the areas in which fallout contamination occurred. By application of the decay factors determined from the field decay rates observed by this project for each event, the land-surface observations were related to the common time of H+1 hour. These decay-corrected dose-rate values were then used to construct isodose-rate contour plots of the Bikini Lagoon area. Figure 3.18 shows the land-surface Zuni H+1 hour readings determined in this manner as well as the isodose-rate contours existing at that time. The Tewa data is presented in Figure 3.19. Again, no fallout was observed over Bikini Atoll following Shot Cherokee. The Bikini area isodose-rate contours for the water-surface detonations, Navajo and Flathead, are shown in Figures 3.20 and 3.21.

Although not specifically a part of the integrated fallout program, helicopter probe-surveys were also made in the vicinity of the craters resulting from the land-surface detonations, Lacrosse and Mohawk. The results are shown in Figures 3.22 and 3.23. These readings are of particular interest in that they were higher than any such readings previously reported.

3.4.2 Characteristics of Fallout Contaminant. Many studies were conducted on the physical, chemical, and radiochemical nature of the fallout debris collected at land and ocean stations.

Land-Surface Shots. The gross physical and chemical characteristics of the solid fallout from Shots Zuni and Tewa proved much the same as observed for Shot Mike during Operation Ivy and Shot Bravo during Operation Castle. The particles were irregular, spheroidal, and agglomerate types varying in color from white to yellow and ranging in size from less than 20 microns to several millimeters in diameter. The close-in

stations found most of the activity on particles larger than 210 microns in diameter. Most of the irregular particles consisted primarily of calcium hydroxide with a thin surface layer of calcium carbonate, although a few unchanged coral particles were present. The spheroidal particles consisted of calcium oxide and hydroxide, often with the same surface layer of calcium carbonate. The spherical particles were about 10 times as radioactive as the other types. Although the spheroidal particles accounted for no more than 15 percent of the total samples, they contributed 60 to 80 percent of the total activity on Zuni and 25 percent of the total activity of Tewa at H+ 240 hours. The agglomerates were also composed of calcium hydroxide with an outer layer of calcium carbonate. The particles almost certainly were formed by decarbonation of the original coral to calcium oxide in the fireball, followed by complete hydration in the case of the irregular particles, and incomplete hydration in the case of other particles. The surface layer, which may not have been formed by deposition time, resulted from reaction with carbon dioxide in the atmosphere. The densities of the particles were grouped around 2.3 and 2.7 gr/cm³. Radioactive, black, spherical particles, usually less than 1 micron in diameter, were observed in the fallout from Zuni but not in that from Tewa. Nearly all such particles were attached to the surface of irregular particles. They consisted partially of calcium iron oxide and could have been formed by direct condensation in the fireball. The radionuclide composition of the irregular particles varied from that of the spheroidal and agglomerated particles. The former tended to typify the cloud sample and distant fallout radiochemistry, while the latter were more characteristic of the gross fallout near ground zero. Project 2.63 found that the irregular particles tended to be enriched in Ba¹⁴⁰ and La¹⁴⁰, and slightly depleted in Sr⁸⁸. The spheroidal and agglomerated particles from ship samples were depleted in these nuclides, but were much higher in specific activity. The close-in land samples showed irregular particles depleted in Mo⁹⁸, Ce¹⁴⁴, Np²³⁸, and Ca⁴⁵ over the spherical particles and no difference in Sr⁹⁰ and Ba¹⁴⁰. It should be recognized that this classification by types may be an oversimplification and that a large sample of individual particles of all types might show a continuous variation of the properties described. The inference is strong, nevertheless, that the fractionation observed from point to point in the fallout field from Zuni was due to the relative abundance and activity contribution of various particle types at each location. The capture-to-fission ratios were smallest in the solid fallout samples and highest in the liquid samples. Cloud samples were in between.

The activities of the irregular particles varied roughly as their surface area, or diameter squared. On the other hand, essentially all of the spheroidal particles were radioactive throughout their volumes; they were formed in a region of high activity concentration in the cloud, with the activity diffusing into the interior while these particles were still in a molten state. Activity was not related to particle density, but varied with the weight of irregular particles in a manner consistent with a surface-area function.

Water-Surface Shots. The characteristics of the fallout resulting from the water-surface shots, Flathead and Navajo, differed considerably from those of the land-surface shots. For the land stations of the lagoon area, the Navajo fallout consisted of some solid particles: a rather dry, thin, misty slurry containing calcium carbonate and ferrous oxide particles, sodium chloride crystals, and liquid droplets. In the case of Flathead most of the activity at the land stations was associated with a wet slurry, or mud, containing calcium carbonate and ferrous oxide particles mixed with sodium chloride crystals. This slurry was deposited at an angle of at least 24 degrees from the horizontal. At the ship collecting stations, the fallout from these two events was made up entirely of slurry particles consisting of about 80 percent sodium chloride, 18 percent

water, and 2 percent insoluble solids composed primarily of oxides of calcium and iron. The individual, insoluble, solid particles were generally spherical and less than 1 micron in diameter, appearing to be the result of direct condensation in the fireball. The radionuclide composition of individual slurry drops could not be assessed because of insufficient activity, but the results of combining a number of droplets were similar to those obtained from gross fallout samples.

In general, much less fractionation of radionuclides was evident in the slurry from water shots than in the solid fallout from the land shots. The amount of chloride in a slurry drop appeared to be proportional to the drop activity for the ship stations at Flathead; however, variability was experienced for Navajo, and the relationship failed for both shots at close-in locations. Conflicting data was obtained concerning the contribution of the insoluble solids to the total drop activity. Although the slurry nature of the fallout and certain properties—drop diameters, densities, and concentrations—were adequately determined, further experimentation is required to establish the composition of the insoluble solids, and partition of activity among the components of the drop. The small amount of fallout that was deposited during Cherokee arrived as slurry particles, similar to those produced by Flathead and Navajo. The total amount deposited, however, was small and of no military significance.

Fractionation of radionuclides occurred in the fallout of all Redwing surface shots investigated. By several criteria, such as R-values and capture-to-fission ratios, Navajo was the least fractionated. Flathead ran a close second. Fractionation increased for Tewa and was greatest for Zuni. The R-values were generally higher at the distant stations, as were the activity concentrations and capture-to-fission ratios for particles of the same size fraction. This was probably due to the higher frequency of the spherical particles and a lower contribution of the Mo⁹⁹ at the distant stations. R-values of cloud samples increased for Sr⁸⁹ and Ba¹⁴⁰ with time after detonation, probable because of the increased relative contributions of both the smaller particles and the liquid phases. There was less fractionation between solid and liquid fallout samples from water-surface shots than from land-surface shots. The consideration of Flathead and Navajo as representative water-surface shots is not completely justified, because of the effects remaining in the lagoon from previous shots. The effects of the bottom material on the fallout characteristics have not been studied or evaluated.

The CWL evaluated the logic of using Mo⁹⁹ as the basis for R-values and concluded that Ce¹⁴⁴ appeared to be more representative of the fission products, and thus a better reference for at least the close-in stations. Project 2.65 also concluded that fractionation has no military significance, except for a possible ingestion hazard of specific nuclides, and is of interest only because it may indicate the mechanism of radioactive particle formation in the fireball, column, and cloud.

Cherokee fallout was relatively unfractionated with regard to radionuclide composition. For all shots the important nuclides that were deficient in the fallout were members of the decay chains of antimony, xenon, and krypton. Their rare-gas precursors do not combine easily with either condensing or unaltered carrier particles. Relations between R-values of common precursors were examined by Project 2.63 to estimate R-values of unmeasured isotopes. As yet, no method is known for predicting the extent of fractionation to be expected for specific yield and detonation conditions.

Decay of unfractionated fission products according to $t^{-1.2}$ was found to be adequate for planning and estimating purposes. However, if much fractionation exists or significant induced activities are present, an actual decay curve (measured with a counter having known response characteristics, or computed for the specific radionuclide

composition involved) should be used. The observed early-gamma-dose-rate decay exponents, as measured in lagoon-area land stations, are shown in Table 3.4. However, large errors can result from misapplication of the $t^{-1.2}$ rule in using standard computing methods to estimate radiological effects from fallout. Participation in the tests showed that field dose rates can be calculated from the gamma spectra of samples.

3.4.3 Characteristics of Arrival and Deposition of Fallout. The time of arrival, rates of deposition, and duration of fallout at the lagoon land stations varied for the different shots and with distances from ground zero. Project 2.63 concluded the time from fallout arrival to peak radiation rate was approximately equal to the time of arrival for all stations and events. Further, the shape of the activity arrival curve was not markedly different for solid- and slurry-particle shots (Figures 3.24 and 3.25). In both types of events, the time from the onset of fallout to the time when the radiation rate peaked was usually much shorter than the time required for the remainder of the fallout to be deposited. The concentrations of the smallest sizes remained almost constant with time. Particle diameters gradually decreased with time at each station during the slurry-particle shots, Flathead and Navajo, though remaining remarkably constant at about 100 to 200 microns in diameter on the ships during the entire fallout period.

At the lagoon land stations, the activity percent weight of fallout resulting from land-surface bursts was found to be higher at the more distant stations. Most of the radioactivity was associated with particles between 149 and 420 microns. Particle size distributions varied continuously with time at all stations during the solid-particle shots, Zuni and Tewa, with the activity arrival waves being characterized by sharp increases in the concentrations of the larger particles. Because of background dust and unavoidable debris on collection trays, correlation of the concentrations of smaller particles with radiological measurements was difficult.

In the vicinity of the ships, the gross body of fallout activity for the slurry-particle events penetrated to the thermocline from a depth of 10 to 20 meters at the rate of 3 to 4 m/hr. A considerable fraction of the activity for the solid-particle events penetrated to the thermocline at about the same rate. This activity remained more or less uniformly distributed above the thermocline up to at least 2 days after the shot and is presumed to have been in solution or associated with fine particles present either at deposition or produced by the breakup of solid aggregates in sea water. An unknown amount of activity, perhaps as much as 50 percent total, penetrated at a higher rate and may have disappeared below the thermocline during the land-surface shots. It is unlikely that any significant amount of activity was lost in this way during the water-surface shots. Fractionation of Mo^{99} , Np^{239} , and I^{131} occurred in the surface water layer following solid-particle deposition; a continuous variation in composition with depth was indicated. Only slight tendencies in this direction were noted for slurry fallout.

Although an attempt was made to determine the role played by the base surge in the transport of radioactive debris following water-surface bursts, the results obtained were inconclusive. The radioactive base surge from Shot Flathead, if one indeed was generated, did not reach the detection stations established for its documentation. Therefore, the significance of the base surge in transporting radioactive contamination in the vicinity of a water-surface burst could not be ascertained.

3.4.4 Fallout Prediction Correlations. Before and during the fallout events, successive predictions were made of the location of the boundaries and hot line of the fallout pattern for each event. The final predictions were superimposed on the measured fallout

patterns, as determined by the oceanographic surveys, and are shown in Figures 3.26 through 3.29. Allowance has been made for time variation of the wind during Shots Navajo and Flathead, and for time and space variations of the wind during Shots Zuni and Tewa. Comparison can be made with the H+24 hour contours obtained by aerial survey by referring to Figures 3.4 to 3.7 and converting for decay. Predicted and observed times of arrival at most of the major stations, as well as the maximum particle sizes predicted and observed at times of arrival, peak, and cessation, are compared in Table 3.5. In the majority of cases, agreement is close enough to justify the assumptions used in making the predictions; in the remaining cases the differences are suggestive of the way in which these assumptions should be altered.

The fallout prediction method used is described in Reference 5. Beginning with a vertical line source above the shot point and assuming all particle sizes to exist at all altitudes, the arrival points of particles of several different sizes (75, 100, 200, and 350 microns in diameter in this case), originating at the centers of successive 5,000-foot altitude increments, are plotted on the surface.

Size lines result from connecting surface arrival points for particles of the same size for increasing increments of altitude; height lines are generated by connecting the arrival points of particles of different sizes from the same altitude. These two types of lines form a network from which the arrival times of particles of various sizes and the perimeter of the fallout pattern may be estimated, once the arrival points representing the line source have been expanded to include the entire cloud diameter. This last step requires the use of a specific cloud model. The cloud model used to arrive at the results previously presented is shown in Figure 3.30. Particles larger than 1,000 microns in diameter were restricted to the stem radius or inner 10 percent of the cloud radius, while those from 500 to 1,000 microns in diameter were limited to the inner 50 percent of the cloud radius. All particle sizes were assumed to be concentrated primarily in the lower third of the cloud and upper third of the stem. The cloud and stem dimensions shown on the fallout-pattern figures were derived from empirical curves available in the field, relating cloud height and diameter to device yield; however, actual photographic measurements were used wherever possible for subsequent calculations leading to the results presented in Table 3.5.

The location of the predicted hot line follows directly from the assumed cloud model, being determined by the height lines from the lower third of the cloud, successively corrected for time and, sometimes, space variation of the winds. Time variation was applied in all cases, but space variation only in cases of gross disagreement.

Reasonable agreement between the predicted and observed perimeters and central axes of fallout patterns is indicated for Zuni and Tewa, when corrections are made for time and spatial variation of the winds. Rough agreement was also achieved for Flathead and Navajo by neglecting spatial variation of the winds, in spite of the gross differences in the character of the fallout. The reason for this agreement is not well understood. Predicted fallout arrival times were often less than the measured times by 10 to 25 percent, and the maximum particle sizes predicted at the times of arrival, peak, and cessation were usually smaller by 10 to 50 percent than measured sizes.

3.5 DISTRIBUTION OF ACTIVITY IN THE MUSHROOM

3.5.1 Rocket Data. Forty ASP (atmospheric-sounding projectile) rockets were successfully fired at the mushrooms resulting from Shots Cherokee, Zuni, Navajo, and Tewa. All rockets operated satisfactorily, and information was obtained concerning gamma

intensities within the mushrooms, from which spatial distribution of activity concentration within the cloud and stem could be determined. Figure 3.31 shows the planned rocket trajectories. At H+7 and H+15 minutes, two salvos of six rockets each were fired successfully during Shots Cherokee, Zuni, and Navajo. Four rockets were fired during Shot Tewa, 7 minutes after detonation. During Shot Cherokee, good signal strength was received on all channels, and despite the relatively high radiation fields encountered (3×10^4 r/hr), no serious attenuation of the telemetering signal was noted. The Zuni rockets gave good signal strengths on all channels. The radiation fields measured were lower than those encountered during Cherokee. Channels corresponding to rockets aimed at the lowest elevations had no data on the carriers. Figures 3.32 and 3.33 show the activity distribution for Shot Zuni in the planes of the rocket trajectories at H+7 and H+15 minutes, respectively, and are typical of the results achieved by the project.

Figure 3.33 includes the wind profile in the plane of the rocket trajectory, which is a projection, in this plane, of a zero-time vertical line above ground zero as it would have been distorted in 15 minutes by the prevailing winds. The wind profile provides a means of visualizing the amount of shear to be expected in the clouds.

The six rockets of the first salvo during Navajo were fired at the same quadrant elevation but at different azimuth angles to provide good assurance of intersecting the mushroom stem. From visual observation of the Navajo stem location, it appeared probable that at least three rockets of this salvo penetrated the stem at altitudes of approximately 25,000 feet. None of these rockets yielded data indicating gamma intensities in excess of 1 r/hr. The second salvo was fired in a vertical fan, similar to that used for Cherokee and Zuni, and the activity distribution within the cloud was successfully documented. The data obtained indicated that the gamma activity concentrations in the Navajo cloud were appreciably lower than those observed during Cherokee and Zuni. Of the four rockets fired during Tewa, only one produced useful radiological information; however, the data was consistent with similar data obtained along a comparable trajectory during Cherokee. When the values of total cloud activity, as determined from the rocket measurements, were compared with theoretical values, order of magnitude agreement was obtained.

3.5.2 Aircraft Data. Radiation dose rates, as recorded by penetration aircraft flying through the nuclear clouds, yielded activity concentrations which are in satisfactory agreement with those obtained by the rocket data. Table 3.6 gives the aircraft penetration data as recorded after Shot Zuni in B-57B aircraft.

The fourth column is the activity concentration at the time of aircraft penetration. This is converted from the dose rate readings by assuming an average effective energy of the photons and correcting for the altitude at which the measurements were taken. The fifth column shows the evaluated activity at H+15 minutes, using the activity at the time of penetration and a decay factor of $t^{-1.7}$. This decay factor was determined by the aircraft penetration experiment and accounted for both decay and dispersion of the cloud between H+15 minutes and the time of aircraft penetration.

By comparing the maximum activity encountered by the aircraft (evaluated to H+15 minutes) with the activity distribution plot of the H+15 minute Zuni rockets, presented in Figure 3.33, it is seen that there is reasonably good agreement. This correlation is adequate when it is considered: (1) that the decay factor of $t^{-1.7}$ accounts for both fission-product decay and the dilution of the activity because of the dispersion of the cloud, and (2) that the penetration aircraft did not fly in the plane of the rocket trajectories.

The cloud exposure rate data from the penetration aircraft could be fitted by the expression:

$$\bar{D} = 1.0 \times 10^5 \times f \times t^{-1.7}$$

Where: \bar{D} = average exposure rate, r/hr
 f = fractional fission yield
 t = time after detonation, minutes

The average exposure rate in the stem beneath the mushroom of clouds from water-surface bursts or airbursts was less than the exposure rate in the mushroom by a factor of 5 to 10. In terms of crew exposure, a high-performance aircraft could penetrate the cloud from any yield 100-percent-fission device at an altitude of 45,000 feet at H+20 minutes with an average mission dose of 25 r. At 30,000 feet, where the activity is less, a penetration could be made at H+10 minutes for a radiation dose of the same magnitude. In clouds from detonations in which the fission yield is some fraction of the total yield, the radiation dose rate is reduced proportionally.

An investigation of the internal radiation hazard encountered by flight crews during penetration indicated that it was insignificant when compared to the external hazard.

In summary, the radiation hazard in atomic clouds denies to aircraft only a small portion of sky for a very short period of time after detonation.

3.6 INITIAL RADIATION

3.6.1 Initial-Gamma Radiation. The initial-gamma time histories obtained indicated the influence of the hydrodynamic effect on the initial gamma dose. Figure 3.34 demonstrates the enhancement of the exposure rate during the approach and following the passage of the airblast shock front. The figure also shows that approximately two-thirds of the total initial-gamma exposure occurs after the passage of the shock front and that essentially all of the initial dose is delivered by 30 to 40 seconds after shot time. Curves of total initial-gamma exposures as a function of distance for Shots Flathead, Dakota, Navajo, and Tewa, as well as comparable prediction curves from Reference 4, are presented in Figure 3.35.

Because an analysis of the initial-gamma data obtained indicates that in all cases the exposures at distances in excess of 3 miles was less than 10 r, and in most cases less than 1 r, it is apparent that the initial-gamma exposure received by unprotected personnel during megaton-range detonations is of little significance when compared to airblast and thermal effects. Initial-gamma dose prediction curves indicate total exposure values that are too low for close-in stations while too high at the more remote stations, as shown in Figure 3.35.

3.6.2 Neutrons. Because the Cherokee air drop did not come sufficiently near the intended burst point to result in activation of the neutron detectors, no neutron data was obtained for this event. For this same reason, the primary soil-activation experiment failed to yield usable data.

Neutron data was successfully obtained for Shots Yuma, Kickapoo, Blackfoot, Erie, and Osage. Table 3.7 demonstrates the angular variation of the various energy fluxes measured during the firing of

Within the limits of accuracy of the threshold-detector system, measurements of the neutron energy spectrum indicated there was no detectable variation of the spectrum with distance. In other words, the measured absorption length, that is, e-fold distance, was

the same for the different detectors placed along an instrument line for distances in excess of 300 yards. Table 3.8 indicates the near constancy of the neutron spectrum even between differing shots.

The absorption lengths observed for the shots on which measurements were made are presented in Table 3.9. A part of the variation indicated in these absorption lengths was due to the effect of terrain, in that it affects the scattered flux. Surfaces covered with vegetation tended to increase the values of the absorption lengths measured over them, although the effect could not be evaluated quantitatively.

The neutron dose normalized to unit-kiloton yield for each of the shots on which neutron measurements were made is presented in Figure 3.36. It is to be noted that the dose versus distance curves for Yuma, Blackfoot, and Kickapoo are outside the stated limits of reliability for the prediction curve. There was an indication that correlation existed between implosive high-explosive thickness and the neutron flux from a weapon, although the data was insufficient to establish a quantitative relation.

Neutron shielding experiments, utilizing concrete boxes containing various admixtures of borax and sulfur, showed that there is little or no increase in the attenuation of fast neutrons by the addition of these substances to concrete. The thermal neutron flux, however, was attenuated by the addition of borax to the concrete. The neutron dose was found to be reduced by a factor of about 4 by a concrete box, 3 feet on a side and 6 inches thick, fabricated from a mixture containing 1.6 percent borax by weight. The gamma-ray dose inside this type structure, however, was found to be increased by a factor of approximately 3.

A limited soil-activation experiment performed during Yuma indicated that the activation of coral soil, sodium chloride, and magnesium oxide was approximately twice as great for a sample exposed from $\frac{1}{2}$ to 1 inch below the coral soil surface than for a sample exposed on the surface. The moderating effect of the soil results in the thermalization of a large number of neutrons, making them more available for capture by the Na^{23} and Mn^{55} .

3.7 CONTAMINATION-DECONTAMINATION

3.7.1 Building Materials. The contamination levels of the building materials exposed to fallout aboard the YAG's were too low to obtain the desired experimental results. Shots Cherokee and Navajo produced negligible contamination aboard the YAG's, whereas Zuni and Flathead contamination was so light as to yield only minimal data. Although Shot Tewa produced relatively high radiation levels on the decks of the ships, subsequent torrential rains removed the contamination to such a degree that the panel radiation levels were below the Site Elmer island background at time of recovery, making decontamination studies impractical.

The limited data obtained indicated that small-particulate contaminant resulted from Zuni, whereas Flathead produced a liquid contaminant. In the case of the particulate contaminant, the horizontal surfaces were the more heavily contaminated, whereas the liquid contaminant from Flathead produced the heaviest contamination on vertical surfaces. The heaviest contamination observed was on the asphalt-gravel built-up roofs, the roughest of all surfaces, following Zuni. Hosing of these panels was relatively ineffective, although scrubbing with detergents generally resulted in effective decontamination. Contamination levels of panels were generally reduced by factors of 2 to 4 by this decontamination procedure.

Unpainted wood surfaces allowed contamination to penetrate to depths of 1 to 2 mm, or more; however, most of the contaminant was retained in the outer 200 microns. On painted panels, the depth of contamination rarely exceeded the depth of the paint, which ranged from 180 to 300 microns.

3.7.2 Shipboard Materials. Materials tested under this category consisted of wire rope, manila line, canvas, firehose, and wood decking. The wire rope and canvas were tested both with and without various protective coatings, whereas the manila line and firehose were tested unprotected. The samples were exposed aboard the YAG-40 for Shots Zuni and Flathead, with the wood decking also being exposed during Tewa. In general, it was found that shipboard materials such as these contribute only a small amount to the total ship radiation hazard. Unprotected wire ropes and manila lines are rather difficult to decontaminate because of their inherent absorptiveness and the presence of many tiny crevices. Therefore, these materials may contribute to a long-term radiation hazard.

Protective coating reduces the initial contamination of shipboard materials by restricting the absorption of the contaminant. The coatings also increase the effectiveness of decontamination.

Ropes, lines, and hoses that become contaminated should be uncoiled to reduce the inherent radiation hazard. If this is not possible, they should be stored in an unfrequented location until the radiation has decayed below the hazardous level. Canvas, unless coated, should not be left open to fallout.

Contamination of wood decking appears to be mainly dependent on two factors: the nature of the fallout contamination, and the surface roughness of the wood deck. The surface roughness was a major factor in determining the initial contamination level. Penetration of fallout contamination into the wood beyond the rough surface layer was negligible, but decontamination to a residual of 2 percent would have required removal of approximately 2 mm of the surface layer because of roughness. The payed joints between the wooden planks presented no additional problem, as long as the joints were free of fissures and pockets.

3.7.3 Washdown Effectiveness. The washdown systems on the after portions of the YAG's 39 and 40 were operated during four fallout contaminating events, and the maximum levels of gamma radiation ranged from 266 mr/hr at 11 hours after Flathead to 21.2 r/hr at 4.6 hours after Tewa. These events produced two general types of fallout contaminant: a solid particulate material from the land-surface detonations, Zuni and Tewa, and a salt-water slurry following the water-surface bursts, Flathead and Navajo. The washdown systems were effective in reducing the total shipboard dose rates at end of washdown by 85 to 98 percent for slurry fallout and 85 to 95 percent for the particulate fallout. Reductions of the total accumulated dose to time of fallout cessation ranged between 95 and 97 percent for slurry material, and 76 to 86 percent for particulate material. Maximum washdown effectiveness was achieved by prompt activation of the washdown system at the start of the contaminating event and by continuous operation as long as possible after fallout had ceased. Washing after fallout cessation was particularly advantageous in the case of particulate fallout, because the washdown system is less effective in the removal of this type of contaminant. Overall effectiveness can be materially increased by smooth, well-drained ship weather-surfaces.

3.7.4 Shipboard Decontamination Procedures. Evaluation of various shipboard

decontamination procedures was detrimentally affected by the low, residual, contamination levels which existed on the test ships following their return to the Eniwetok Lagoon. The proof-testing of the standard ship recovery procedure, which consisted of firehosing, hand-scrubbing, and firehosing again, was carried out after Shot Tewa on a ship that had an average residual dose rate of 290 mr/hr. At the same time a second procedure, hot-liquid-jet cleaning, was investigated under like conditions. The tests indicated that, for nonwashdown areas, the two procedures were approximately equal in effectiveness with average fractions of contamination remaining being 0.33 for the standard recovery procedure and 0.41 for the hot-liquid-jet method. The hot-liquid-jet cleaning progressed at about twice the surface coverage rate of the standard recovery method; however, it was concluded that insufficient data was obtained to justify expenditure of large sums for the special equipment involved, based on this apparent greater operating rate.

Evaluation of a decontamination method involving removable, radiological, protective coating (RRPC) was conducted after Shots Zuni and Flathead. Removal of the RRPC in the nonwashdown shipboard areas after Zuni resulted in the removal of all but 0.5 to 8.0 percent of the contaminant, while firehosing alone left a residual of 6 to 28 percent. Firehosing plus RRPC removal eliminated 97 to 99.8 percent of the residual contamination. In the washdown area, the RRPC removal left 6 to 9 percent residual contamination, compared to 16 to 40 percent remaining after decontamination of an uncoated area by the hot-liquid-jet method. After Flathead, the removal of RRPC from a nonwashdown area was 97 percent effective as compared to the 82 percent effectiveness of a firehosing-plus-handscrubbing procedure. Removal of the coating in washdown areas, however, showed only a 20-percent reduction of the contamination, although the levels of contamination were actually too low to give reliable instrument readings. Comparison of manual and mechanical scrubbing indicated the mechanical method was slightly inferior; however, operators felt no fatigue and could have easily endured long scrubbing times.

3.7.5 Aircraft Contamination. Contamination studies conducted on the B-57B and F-84 aircraft used in early cloud penetrations indicated that the amount and distribution of the contamination that aircraft incur during flights through nuclear clouds is fairly uniform, considering the widely varying circumstances under which the contamination is incurred. There does not seem to be any significant variation in the contamination due to device yield or aircraft type.

The contact hazard that personnel experience when working on contaminated aircraft was also investigated. It was found that the contact hazard could be estimated by surveying the aircraft with a gamma survey meter (T1B) and applying a correction factor to the readings obtained. A factor 110 will convert the T1B readings to the approximate contact dose rate (rep/hr) to the skin in areas of direct impingement of the contaminant, i.e., leading edge of nose, wing, and the like, whereas a factor of 40 is applicable to the sliding surfaces, such as the sides of the fuselage. It was also found that gloves reduced the radiation intensity to the hands by at least 50 percent, in addition to preventing the direct contact of the contaminant with the skin. The wearing of gloves is, therefore, recommended when working on surfaces that show a gamma survey reading of 0.1 r/hr or more.

As the result of these findings, it was concluded that aircraft maintenance, refueling, and rearming personnel could begin work as early as H+2 hours and continue to work for a period of 8 hours on the most highly contaminated aircraft studied during Redwing, accumulating a total dose of 5 r of whole body gamma radiation. After H+24 hours, personnel could work for 10 days, at a rate of 8 hours per day, on these aircraft, and accumulate a total dose of less than 1.5 r.

3.7.6 Skin Decontamination. A study of the effectiveness of a water-repellent barrier cream in reducing the contaminability of hands yielded insufficient data to permit the drawing of any conclusions. Soap plus water and ammoniacal petroleum-based waterless cleansers proved equally effective in removing fission product contamination from the hands of personnel who participated in recovery operations. The geometric mean of hand contamination was observed to vary directly with the radiation field intensity in which these personnel conducted their recovery operations. No evidence of irritation was noted, even in cases where approximately 25 μc of mixed fission products were in contact with the hands for periods of 2 hours.

3.8 SHIP SHIELDING

Data on the air envelope, water envelope, and shipboard contamination gamma-source contributions to the total gamma field experienced aboard ships was obtained during Shots Zuni, Flathead, Navajo, and Tewa. The highest estimates of percent-air-envelope contribution were obtained from the Tewa results, which indicated that, for the washed portions of the ship, the air contributed between 32 and 95 percent of the dose rate during the period of maximum rate of fallout arrival and more than 10 percent of the dose rate between 12 and 20 hours after fallout began. In unwashed areas, the percent-air contribution would be less significant, because a greater portion of the radiation would come from the contamination retained on the weather surfaces of the ships.

The water-envelope contributions to the total shipboard gamma radiation fields was found to be significant only in compartments adjacent to the sea and well-shielded from contaminated weather surfaces. For an unwashed ship, the contributions to both dose and dose rate were estimated to be less than 11 percent in the lower hold, 3.5 percent in the upper hold, and 1 percent on the deck. The values on a washed ship could be as much as six times higher than those on an unwashed ship and would therefore be of significance in the shielded areas.

The relative contribution of contaminated weather-surfaces depended on the washdown situation aboard ship, and the greatest contribution, of course, occurred in the unwashed portions of the ships. The radiation from the weather surfaces became the primary contributor after passage of the primary fallout fronts and contributed in excess of 95 percent of the total dose accumulated during the first 25 hours in the nonwashed areas of the YAG-40 following Shot Tewa, and more than 80 percent in washed areas.

Gamma radiation attenuation offered by the ship's superstructures varied between shots and with locations within the ships. The ratios of the dose rates inside the various compartments to those existing on deck ranged generally from 0.001 to 0.02 for compartments beneath a washed deck and from about 0.03 to 0.2 for compartments below decks that were unwashed. Although the ratios reached values as high as 0.04 and 0.3, respectively, in exceptional cases, most of the values were of the order of 0.01 beneath washed areas and 0.1 beneath unwashed areas.

The values of combined absorption and scattering coefficients, as determined with cylindrical steel shields, were found to vary with time after a given shot and to vary from shot to shot. The combined coefficient increased with time after each shot, indicating that the same thickness of steel becomes more effective at later postshot times as would be expected as a consequence of the softening of the gamma ray spectra with time. The most extreme example of this change in shielding effectiveness was observed during Navajo, in which the combined gamma absorption and scattering coefficient for steel changed from a value of approximately 0.83 in^{-1} at H+10 hours to about 1.16 in^{-1} at H+30 hours.

3.9 EVALUATION OF DOSIMETERS

The gamma doses measured aboard ship during the fallout participation events by DT-60/PD (phosphate glass) and IM-107/PD (quartz fiber) dosimeters, mounted on the surface of masonite phantoms were compared with doses measured by phosphate-glass needles imbedded at depths of 3 to 5 cm in the phantoms, the latter dose being considered as a more satisfactory indicator for the evaluation of acute radiation effects to personnel than the air dose. Differences between the readings of the two dosimeter types, scatter in the doses measured by the same type dosimeters, and differences between the surface readings and the depth readings, indicated that the DT-60 and IM-107 dosimeters were not satisfactory in their present form for proper measurement and interpretation of the biologically significant radiation dose sustained by shipboard personnel above decks in a fallout field. Below decks, the external dosimeter doses showed fairly good correlation with the depth readings, indicating that the variations noted above deck were probably due to dosimeter beta-sensitivity or soft-gamma radiation effects.

TABLE 3.1. PROJECTS AND OBJECTIVES, PROGRAM 1


Project Number and Title	Objective	Methods	Results and Conclusions
2.1, Gamma Exposure versus Distance	<ol style="list-style-type: none"> 1. Initial gamma versus distance for high yield shots. 2. Check scaling of gamma exposure contours versus types of burst. 3. Residual gamma on islands. 	<ol style="list-style-type: none"> 1. and 2. Detection of gamma by various dosimeters at ranges of 1 to 4 miles. 3. Used residual radiation shielding for some dosimeters. 	<ol style="list-style-type: none"> 1. Initial gamma versus range for weapons tested showed higher doses close in and lower doses farther out than TM 23-200 predicted. 2. Residual gamma found on islands of lagoon.
2.2, Gamma Exposure Rate versus Time	<ol style="list-style-type: none"> 1. Initial gamma versus time. 2. Residual gamma versus time. 3. Feasibility of telemetering radiation readings. 4. Feasibility of thermal detector. 	<ol style="list-style-type: none"> 1. and 2. Recording by various detectors versus time. 3. Telemetered radiation readings. 4. Put thermal detectors in field. 	<ol style="list-style-type: none"> 1. Two-thirds of initial gamma received after shock front. 2. t^{-1} to $t^{-1.5}$ decay rates observed. 3. Good. 4. Good.
2.4, Decontamination and Protection	<ol style="list-style-type: none"> 1. Investigate contaminability of construction materials versus orientation and angle. 2. Investigate effectiveness of decontamination techniques. 	<ol style="list-style-type: none"> 1. Exposed panels to fallout on ships. 2. Evaluated controlled decontamination. 	<ol style="list-style-type: none"> 1. and 2. Little data, because of no fallout and weather.
2.51, Neutron Flux Measurement	<ol style="list-style-type: none"> 1. Measure neutron flux and spectrum. 2. Measure flux versus distance. 3. Measure spectrum versus distance. 4. Compare measuring devices of chemical and semiconductor dosimeters. 5. Effects of borax and sulfur on shielding effect of concrete. 	<ol style="list-style-type: none"> 1., 2., and 3. Used foils to measure flux at various distances and various energy levels. 4. Exposed dosimeters in field. 5. Exposed concrete slabs. 	<ol style="list-style-type: none"> 1. and 2.  3. No variation of neutron spectrum versus distance. 4. Chemical dosimeter poor; others, OK. 5. No added shielding effects from borax or sulfur.
2.52, Neutron-Induced Soil Radioactivity	<ol style="list-style-type: none"> 1. Measure induced activity in soils other than those at Nevada Test Site. 	<ol style="list-style-type: none"> 1. Exposed various soil samples. 2. Examined samples at various depths. 	<ol style="list-style-type: none"> 1. No induced activity, because air shot was not close enough. 2. Higher activity below surface in a specific case.
2.61, Rocket Determination of Activity Distribution Within the Stabilized Cloud	<ol style="list-style-type: none"> 1. Proof-test rocket system and telemetering to measure radioactivity in mushroom. 2. Measure gamma rates in stem and cloud at 7 and 15 minutes. 3. Measure contamination of rocket by cloud. 	<ol style="list-style-type: none"> 1. Used ASP rocket with radiation detectors and telemetering equipment. 2. Used rocketborne detectors. 3. Examined rockets after impact. 	<ol style="list-style-type: none"> 1. Good results. Rocket telemetering of radiation levels worked. 2. Almost all activity in mushroom cloud. 3. Contamination of rockets was slight.
2.62a, Fallout Studies by Oceanographic Methods	<ol style="list-style-type: none"> 1. Construct land equivalent fallout contours. 2. Improve technique for fallout measurement. 3. Perform radchem analysis in marine biosphere. 4. Perform deep moors. 	<ol style="list-style-type: none"> 1. Towed submerged detector below surface. 2. Reviewed efforts and theories. 3. Laboratory work aboard ship. 4. Used new techniques. 	<ol style="list-style-type: none"> 1. No significant fallout from air shot. Dose-rate levels scale as percent fission yield for surface shots. Cube root scaling OK. 2. Use scintillation devices. 3. Mn^{54}, Co^{58}, Co^{60}, and Zn^{66} were selectively absorbed. 4. Moorings worked.
2.62b, Oceanographic Surveys and Background Radioactivity	<ol style="list-style-type: none"> 1. Determine oceanography parameters effecting fallout area. 2. Predict radioactive behavior of lagoon. 	<ol style="list-style-type: none"> 1. Studied area prior to shots. 	<ol style="list-style-type: none"> 1. Currents were extremely variable. Thermocline varied 50 to 100 meters. Sound channel 1.3 to 1.5 times as deep as West Coast. 2. No rapid flushing of lagoon.
2.63, Characterization of Fallout	<ol style="list-style-type: none"> 1. Determine fallout time of arrival, rate of arrival and time of cessation; also size versus time and intensity versus time. 2. Determine particle size, and size versus time, shape, density, and radioactivity; and evaluate fallout models. Determine fallout radioactivity/area, mass/area, and chemical composition. 3. Determine radioactive decay rate and gamma energy spectrum. 	<ol style="list-style-type: none"> 1. Used specialized collectors and devices. 2. Collected fallout. 3. Laboratory analysis. 4. Measured rate of penetration of fallout in water and distribution with depth and decay versus time above water surface. 5. Measured rate of penetration of fallout in water and distribution with depth and decay versus time above water surface. 	<ol style="list-style-type: none"> 1. Much information obtained to support models. 2. Three types of particles: spheroidal, irregular, and agglomerates. Postulated chemical theory for particle formation. 3. Variable. <ol style="list-style-type: none"> 1. Above-water probe became contaminated. 5. Measured percent of weapon at intermediate ranges.

TABLE 3.1 CONTINUED

Project Number and Title	Objective	Methods	Results and Conclusions
	4. Obtain correlation points for air and water survey. 5. Obtain supplementary radiation contour data.	5. Coracles, total collectors, and time-of-arrival detectors.	
2.64, Fallout Location and Delineation by Aerial Survey	1. Make fallout contours from aircraft observations.	1. Mapped area, using detector inside aircraft at 300-foot altitude after fallout was down.	1. Constructed 3-foot land surface equivalent dose-rate contours.
2.65, Land Fallout Studies	1. Make radchemical and rad-physical analysis of fallout. 2. Make dose-rate contours for atoll area. 3. Evaluate roll of base surge.	1. Incremental samplers on islands and on 3 ships downwind. 2. Used probe suspended from helicopter to measure craters. 3. Photoelectric cells.	1. No significant fallout from airburst. Weathering and leaching was small. Water and land shots gave predominantly slurry and solid fallout respectively. Fireball chemistry was postulated. Fractionation measurements using Mo ⁹⁹ as a base is fair; Ce ¹⁴⁴ would be better. Bottom debris clouded water debris. Salting is ineffective. 2. Maximum dose observed 13,000 r/hr at H+1. 3. No definitive results.
2.66a, Early Cloud Penetration	1. Measure dose and dose rate for people flying through a nuclear cloud.	1. Flew planes straight in at 20 to 80 minutes after detonation.	1. Can fly through at 20 minutes at 45,000 or at 10 minutes at 30,000 feet.
2.66b, Contact-Radiation Hazard Associated with Aircraft Contamination	1. Examine correlation between aircraft contact-radiation hazard and dose rate measured on aircraft (by an ANPDR-39) surfaces. 2. Study contact radioactivity. 3. Study glove protection for radioactivity.	1. Surveyed plane and checked readiness versus hazard. 2. Measured decay. 3. Glove-versus-no-glove operations.	1. Established the calibrating or correcting factor. 2. Do not need to decontaminate aircraft. Decay was $t^{-1.5}$. Recommend using gloves to reduce contamination by 50 percent.
2.71, Ship Shielding Studies	1. Determine relative gamma field strength versus time: on ship weather surface, in surrounding air, and in surrounding water. 2. Determine characteristics of interaction gamma in steel.	1. Took total gamma readings and subtracted air and water readings. Used shielded detector on board two YAG's. 2. Detector inclosed in steel cylinders.	1. Deck gave 50 percent. Air contribution was about 50 ± 30 percent. Waterborne contamination contributed 11 percent of radiation in hold and 1 percent on deck. 2. Wide variations found versus time and type shot.
2.72, Evaluation of Standard Navy DT60/PD and IM107/PD in Residual Radiation Fields Aboard Ships	1. Evaluate Navy dosimeters' capability to read proper personnel depth dose.	1. Dosimeters and gamma detectors on phantoms.	1. Ineffective for topside use. 2. OK for below decks.
2.8, Shipboard Radiological Countermeasure Methods	1. Proof-test ship protection and decontamination procedures and recommend improvements	1. Test surfaces were exposed on YAG's to fallout under test conditions.	1. Procedures studied were very effective. Fallout on rough surface, lines, etc., posed long-term hazard. Zuni fallout more difficult to remove than Flathead because of mass involved.
2.9, Standard Recovery Procedure for Tactical Decontamination of Ships	1. Proof-test tactical decontamination of a ship. 2. Make operational decontamination of ships in port.	1. Decontaminate at Eniwetok. 2. Scrubbing evaluated.	1. Ships were not sufficiently hot. 2. Decontamination procedures are OK.
2.10, Verification of Shipboard Washdown Countermeasures	1. Verify effectiveness of ship washdown.	1. Compared gamma field in washdown area with non-washdown area of two YAG's.	1. Ninety-five percent reduction of slurry-type fallout. Eighty percent reduction of dry fallout.

TABLE 3.2 PERCENT OF FISSION FRAGMENTS

All numbers in percent.

Shot	Device Down			Na ²⁴ Na ²⁴		If Collimated, Fall-out Product Down	
	a	b	c	d	e	c/d	c/e
Flathead	29	15	90	17	7.8	50	55
Navajo	50	36.59	144.236	64	37	52/85	91/149
Tewa	28	24	96	17	4.5	80	91
Zuni	48	47	188	50	33	94	125

a These estimates of the percent down were obtained in an unusual manner (WT-1318).

b Summation within contours of WT-1318 gives percentages as listed in this column.

c Detector readings of WT-1318 corrected for collimation.

d The contribution of Na²⁴ (Reference 3).

e Calculations of Project 2.53 as to the contribution of Na²⁴.

c/d WT-1318 collimated readings modified by subtracting sodium contribution of Column d, to give the percent of fission products actually accounted for.

c/e WT-1318 collimated reading modified by subtracting sodium contribution of Column e, to give the percent of fission products actually accounted for.

TABLE 3.3 SUMMARY OF AREAL EXTENT OF FALLOUT

r/hr	Area Within Contour Lines, mi ²			
	Zuni	Flathead	Navajo	Tewa
H + 1 hour dose rate				
1,000	—	—	25	450
500	—	—	55	1,050
300	—	—	80	1,550
100	750	—	310	3,500
50	1,720	—	950	5,850
30	4,000	90	1,350	11,500
10	7,600	2,100	3,300	>29,000
5	10,800*	7,600	8,250*	—
3	>16,500	10,800	11,600*	—
1	>28,000	>20,000	—	—
Two-day accumulated dose roentgens				
1,000	—	—	20	520
500	—	—	30	1,050
300	—	—	45	1,500
100	1,450	75	350	3,000
50	2,750	425	770	3,900
30	4,300	800	1,300	5,450
10	7,900	2,700	2,150	13,600
5	11,400*	5,400	3,100	>22,000
3	>15,700	9,500	4,650*	—
1	>28,000	>18,000	11,700*	—
Total Yield, Mt	3.38		4.6	
Percent Fission Yield	—		—	

* Contour lines that have been closed by estimation.

TABLE 3.4 EARLY-GAMMA-DOSE-RATE DECAY SLOPES

	Shot*			
	Zuni	Flathead	Navajo	Tewa
Fallout on Land Stations				
Field gamma decay slope (H + 8 to H + 50 hours)	-0.92	-1.0	*	-1.08
Laboratory gamma decay slope (H + 20 to H + 50 hours)	-0.90	-1.2	-1.02	†
Laboratory gamma decay slope (H + 20 to H + 250 hours)	-1.2	-1.21	-1.6† -1.2 -2.5	—
Fallout on Ship Stations				
Doghhouse counter (times indicated)	-1.4 (70 to 2,500 hr)	-1.58 (55 to 3,000 hr)	-1.32† (55 to 3,000 hr)	-1.72† (100 to 1,500 hr)
Theoretical calculations for doghouse counter (H + 1 to H + 6,000 hours)	-1.25†	-1.23†	-1.19†	-1.20†

* Heavy rains prevented evaluation of field decay slope.
 † High background on Site Elmer prevented determination.
 ‡ The slopes changed with time. To find decay rate for any particular time period, it is necessary to refer to the measured decay curves.

TABLE 3.5 COMPARISON OF PREDICTED AND OBSERVED TIMES OF ARRIVAL AND MAXIMUM PARTICLE SIZE VARIATION WITH TIME

Shot*	Station	Time of Arrival		Maximum Particle Size (microns) at					
		TSD (hr)		Time of Arrival		Time of Peak Activity		Time of Cessation	
		Predicted	Observed	Predicted	Observed	Predicted	Observed	Predicted	Observed
Flathead	YFNB-13	†	0.35	—	—	—	—	—	—
	How I	†	1	—	—	—	—	—	—
	YAG-39	3	4.5	200	—	†	—	†	—
	YAG-40	9	8.0	125	—	70	120	< 70	—
	LST-611	6	6.6	120	112	†	—	†	—
Navajo	YFNB-13	< 0.5	0.20	> 1,000	—	> 1,000	—	—	—
	How I	1.5	0.75	500	—	500	—	†	—
	YAG-39	2	2.3	500	—	180	—	~ 100	—
	YAG-40	4	6.0	200	—	130	96	~ 75	84
	LST-611	3	3.0	300	—	180	166	—	—
Zuni	YFNB-13	< 1	0.33	500	1,400	500	695	500	545
	How I	< 1.5	0.38	> 500	—	> 500	365	> 500	—
	YAG-40	~ 6	3.4	†	325	150	300	125	245
	YAG-39	9	12	100	—	†	—	†	—
	LST-611	†	†	—	—	—	—	—	—
Tewa	YFNB-13	< 0.5	0.25	2,000	285	350	—	†	—
	YFNB-29	< 1	0.23	800	1,100	500	1,000	†	—
	How I	1	1.6	1,000	205	250	285	†	—
	YAG-39	2	2.0	500	—	180	395	†	—
	YAG-40	3.5	4.4	200	—	100	285	90	255
	LST-611	7	7.0	150	285	80	205	—	—

* The following cloud dimensions were used in the calculations:

	Flathead	Navajo	Zuni	Tewa
Top (x 1,000 ft)	65	85	80	90
Base (x 1,000 ft)	35	50	50	50
Diameter (naut mi)	6	40	40	60

† No fallout, or no fallout at reference time.
 ‡ Fallout completed by reference time.

TABLE 3.6 SHOT ZUNI CLOUD PENETRATION DATA (P-METER)

Time of Penetration (t)	Altitude	Maximum Dose Rate	Activity at Time t	Activity at H - 15 Minutes
min	ft	r/hr	mc/m ³	mc/m ³
H + 52	41,000	96	9.4	78
H + 68	44,000	108	9.5	123
H + 78	46,000	204	16.7	275

TABLE 3.7 ANGULAR VARIATION OF NEUTRON FLUX FOR SHOTS YUMA AND KICKAPOO

Shot	Detector	Flux × r ² 64° Line	Flux × r ² 85° Line
		Flux × r ² 0° Line	Flux × r ² 0° Line
Yuma	Pu	1.34	—
	U	1.91	—
	Au	1.18	—
Kickapoo	Pu	—	1.62
	U	—	1.70
	Au	—	1.22

TABLE 3.8 PERCENT OF TOTAL NEUTRONS IN EACH ENERGY INTERVAL

Energy Range	Kickapoo	Erie	Osage
10 kev to 0.63 Mev	28.8	25.4	29.2
0.63 Mev to 1.5 Mev	55.1	52.4	57.0
1.5 Mev to 3 Mev	14.9	19.4	12.8

TABLE 3.9 THE e-FOLD DISTANCES FROM SHOTS YUMA, KICKAPOO, BLACKFOOT, ERIE, AND OSAGE

Shot	e-Fold Distance
	yd
Yuma	
0°	215
45°	218
64°	210
Kickapoo	
0°	203
45°	203
85°	203
Blackfoot	230
Erie	200
Osage	190

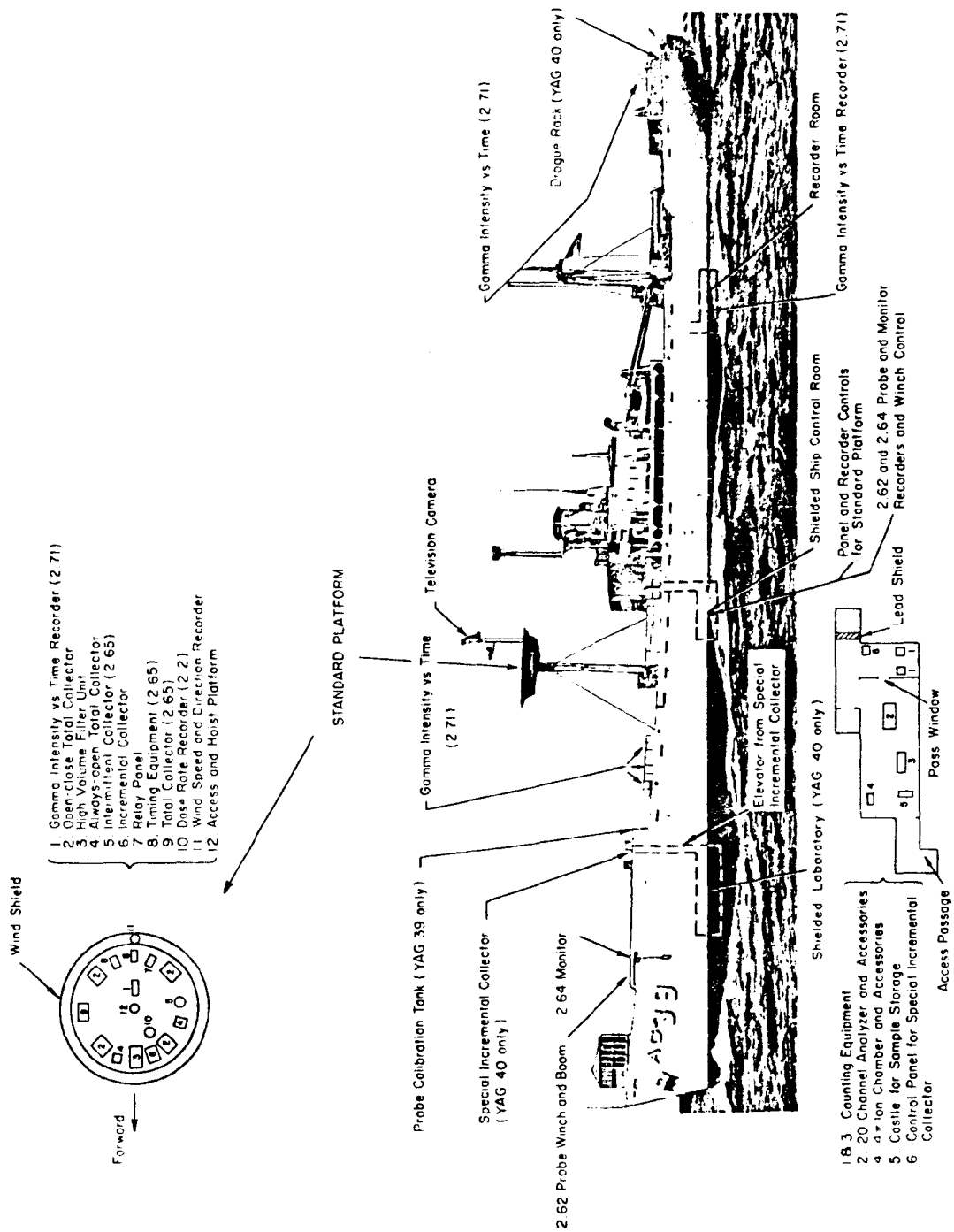


Figure 3.1 Granville S. Hall (YAG-39). Fallout instrumentation pertains to Project 2.63 unless otherwise noted.

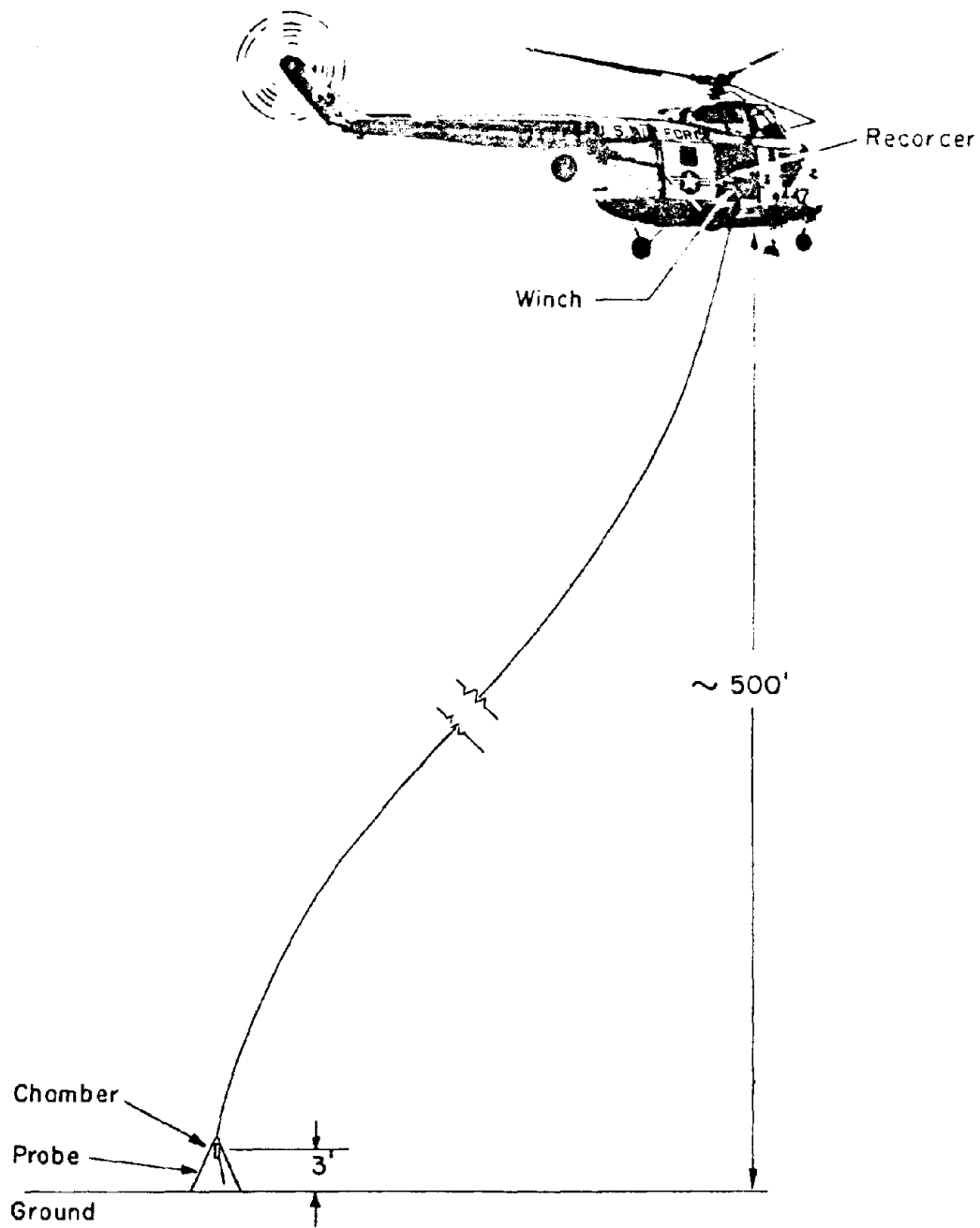


Figure 3.2 Project 2.65 helicopter probe survey technique.

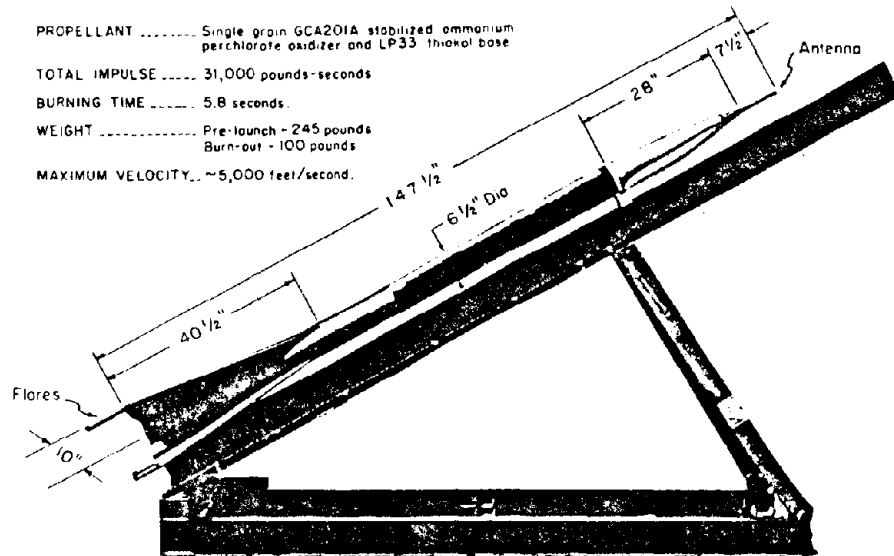


Figure 3.3 Project 2.61 ASP rocket on launcher.

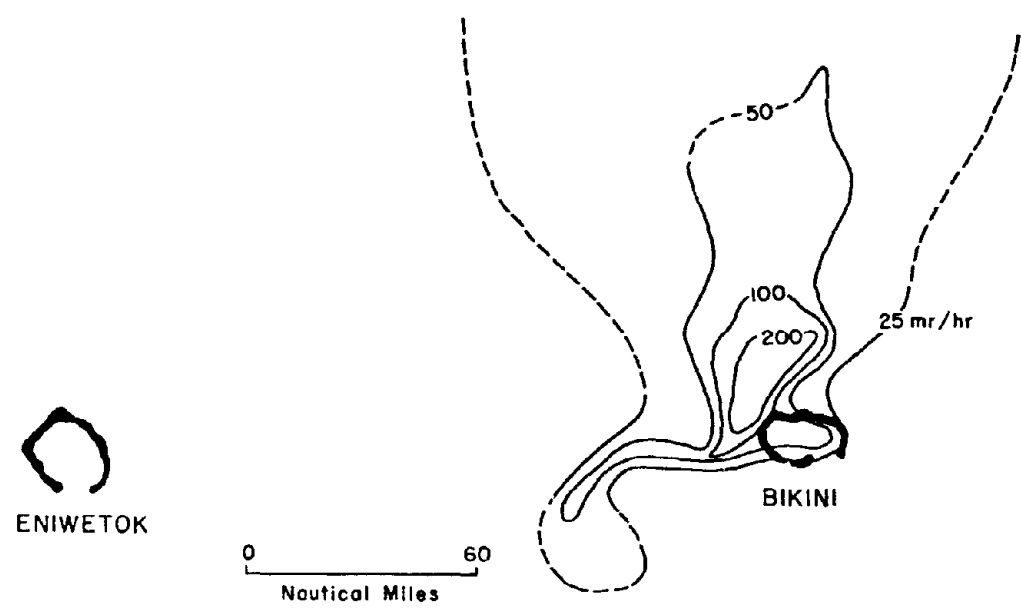


Figure 3.4 Contours on D+1 day at 3 feet above surface, Shot Flathead.

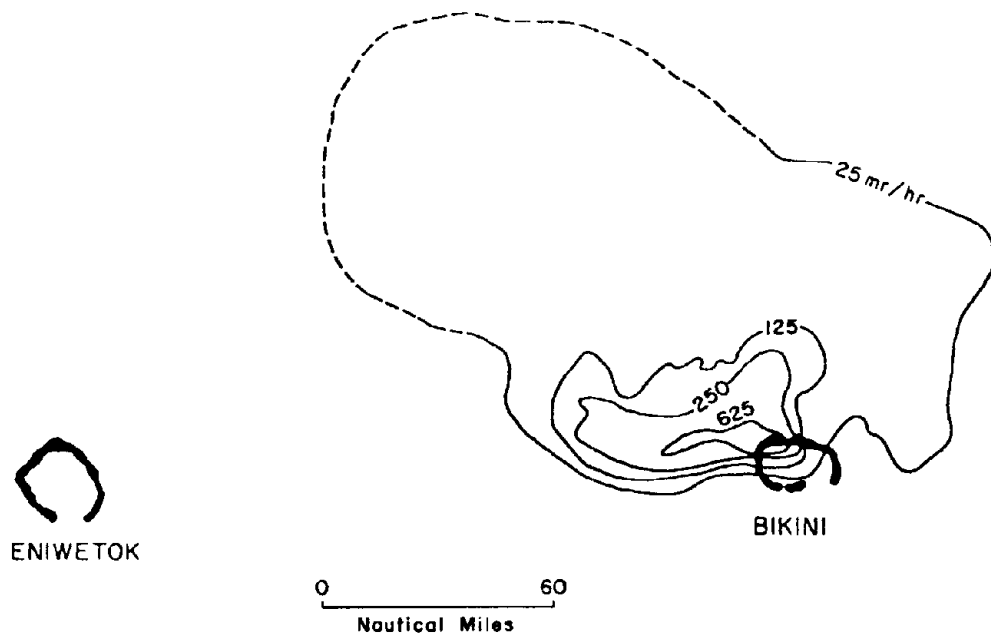


Figure 3.5 Contours on D+1 day at 3 feet above surface, Shot Navajo.

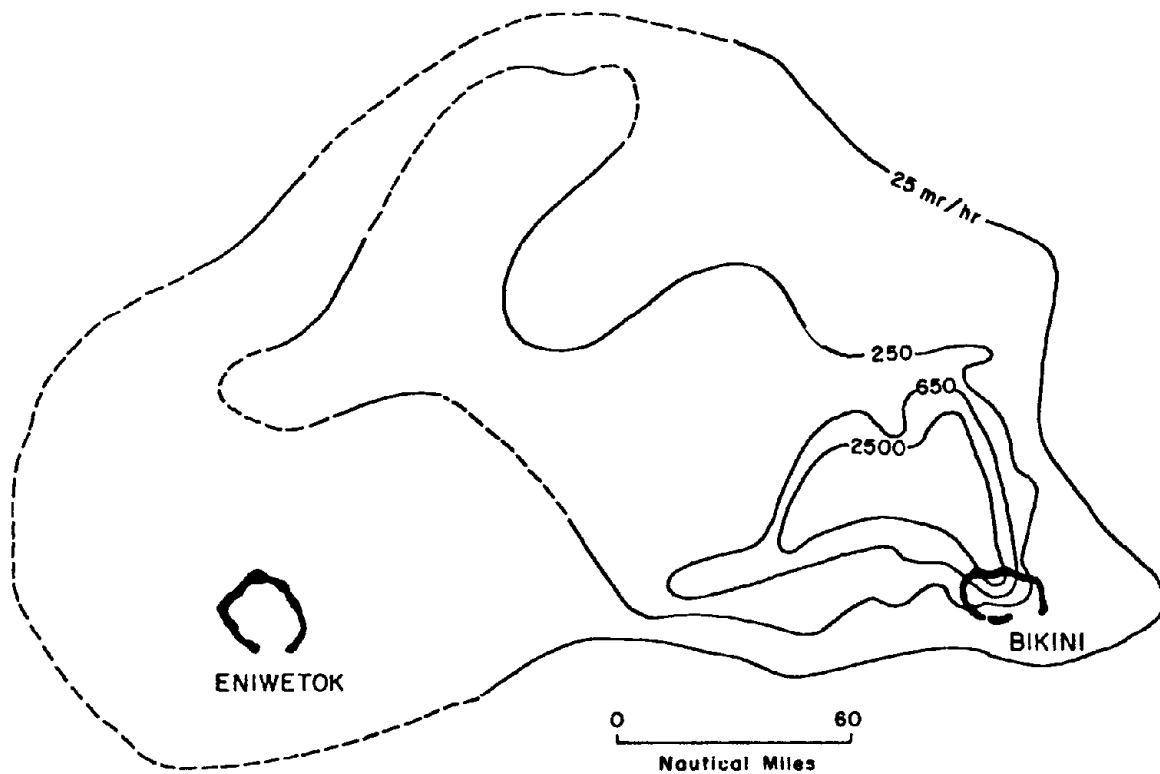


Figure 3.6 Contours on D+1 day at 3 feet above surface, Shot Tewa.

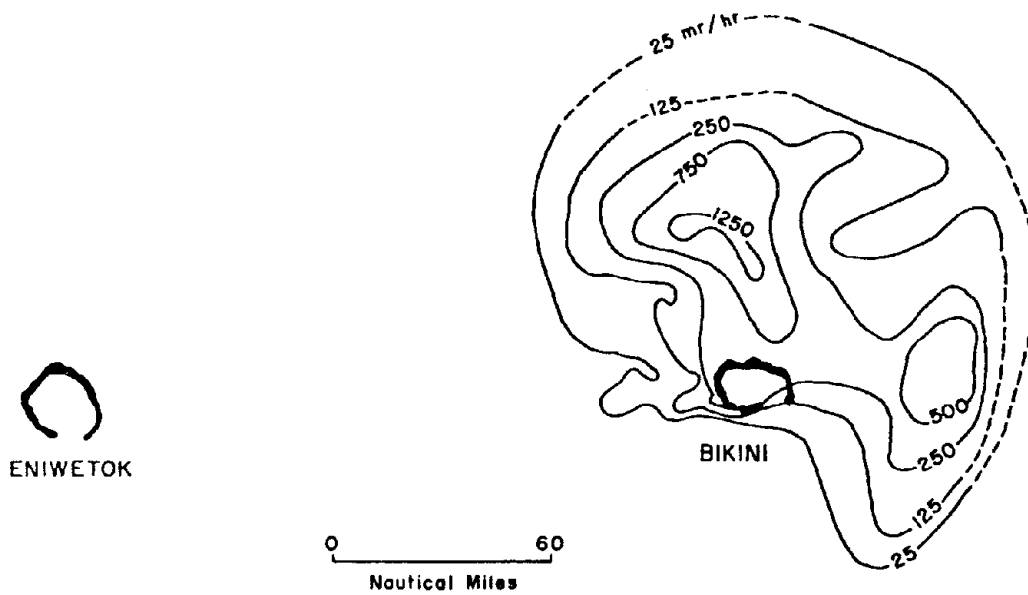


Figure 3.7 Contours on D+1 day at 3 feet above surface, Shot Zuni.

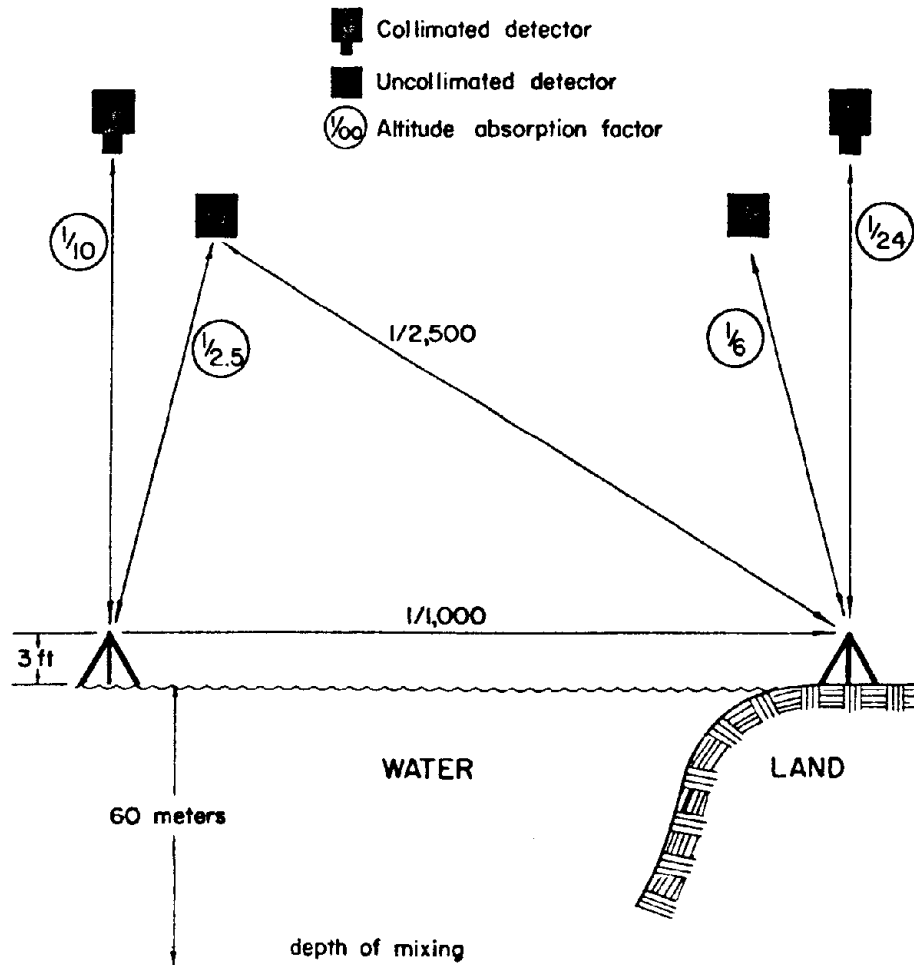


Figure 3.8 Diagram of conversion factors.

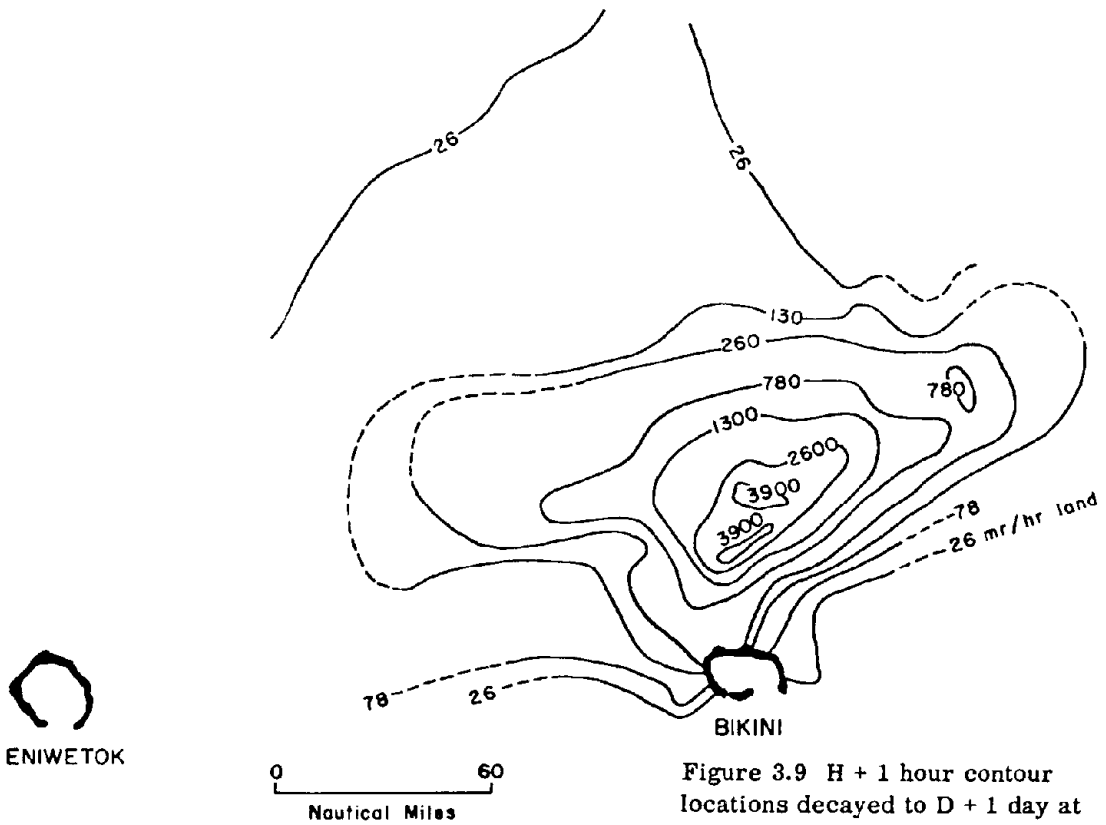


Figure 3.9 H + 1 hour contour locations decayed to D + 1 day at 3 feet above surface, Shot Zuni.

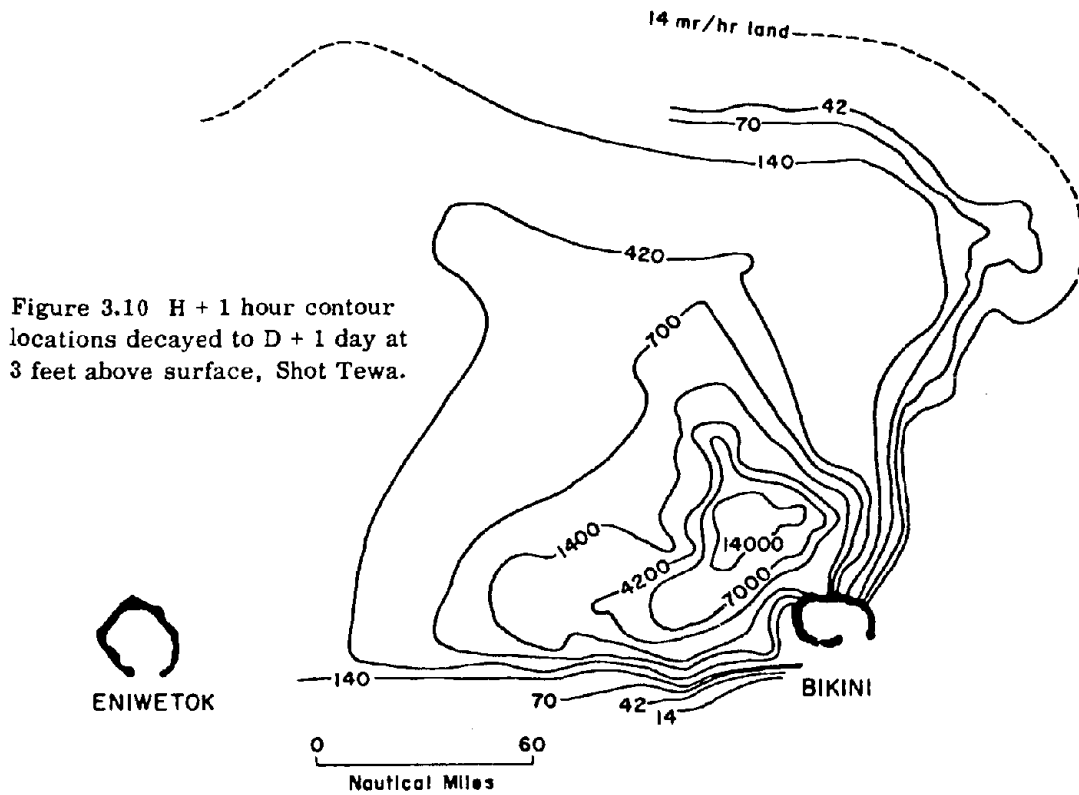


Figure 3.10 H + 1 hour contour locations decayed to D + 1 day at 3 feet above surface, Shot Tewa.

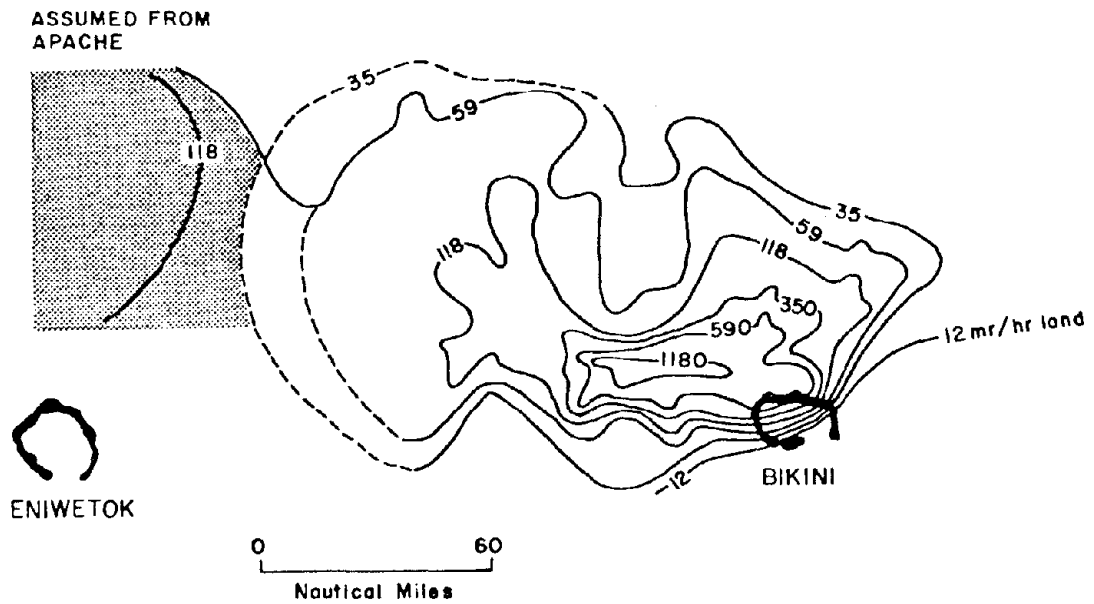


Figure 3.11 H+1 hour contour locations decayed to D+1 day at 3 feet above surface, Shot Navajo.

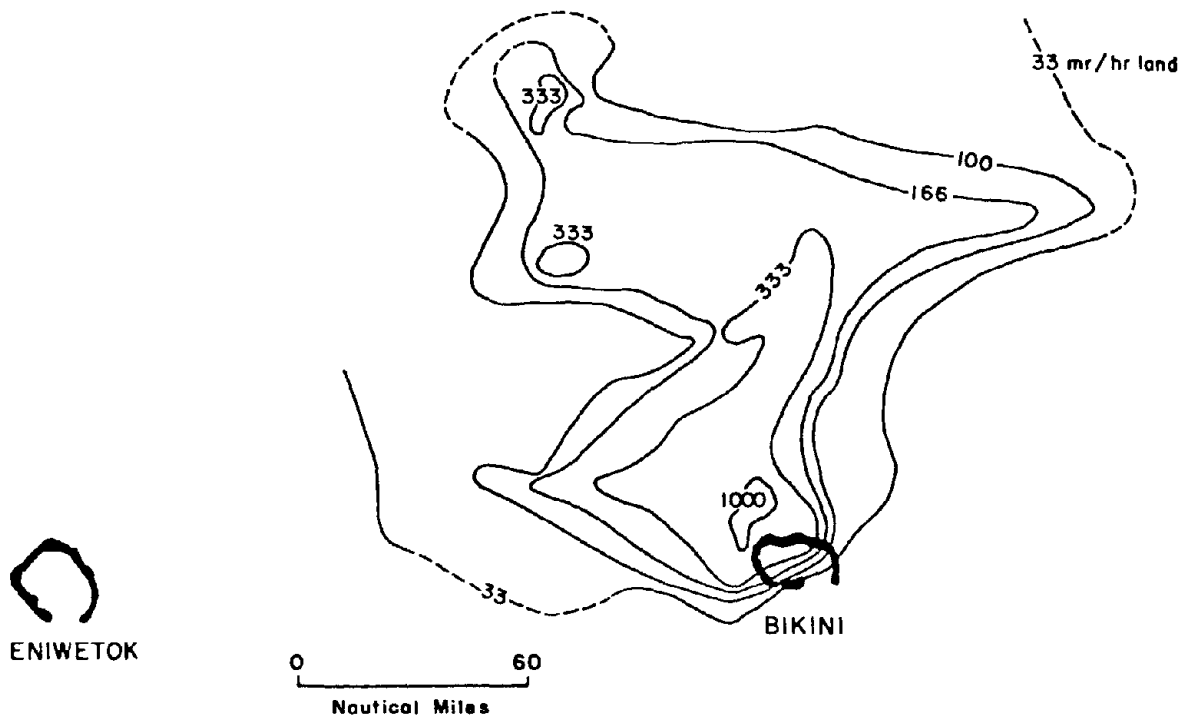


Figure 3.12 H+1 hour contour locations decayed to D+1 day at 3 feet above surface, Shot Flathead.

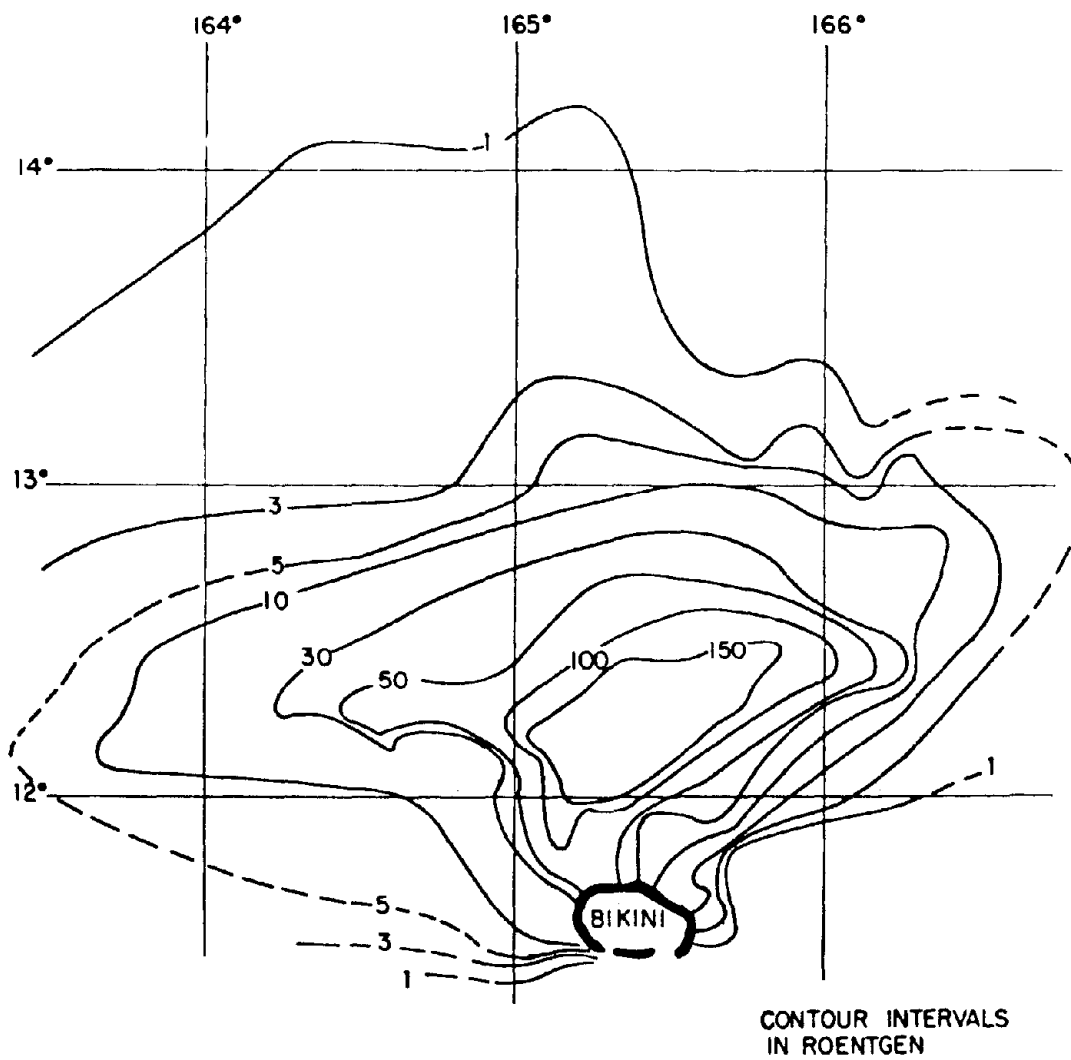


Figure 3.13 Accumulated dose (time of arrival to H + 50), Shot Zuni.

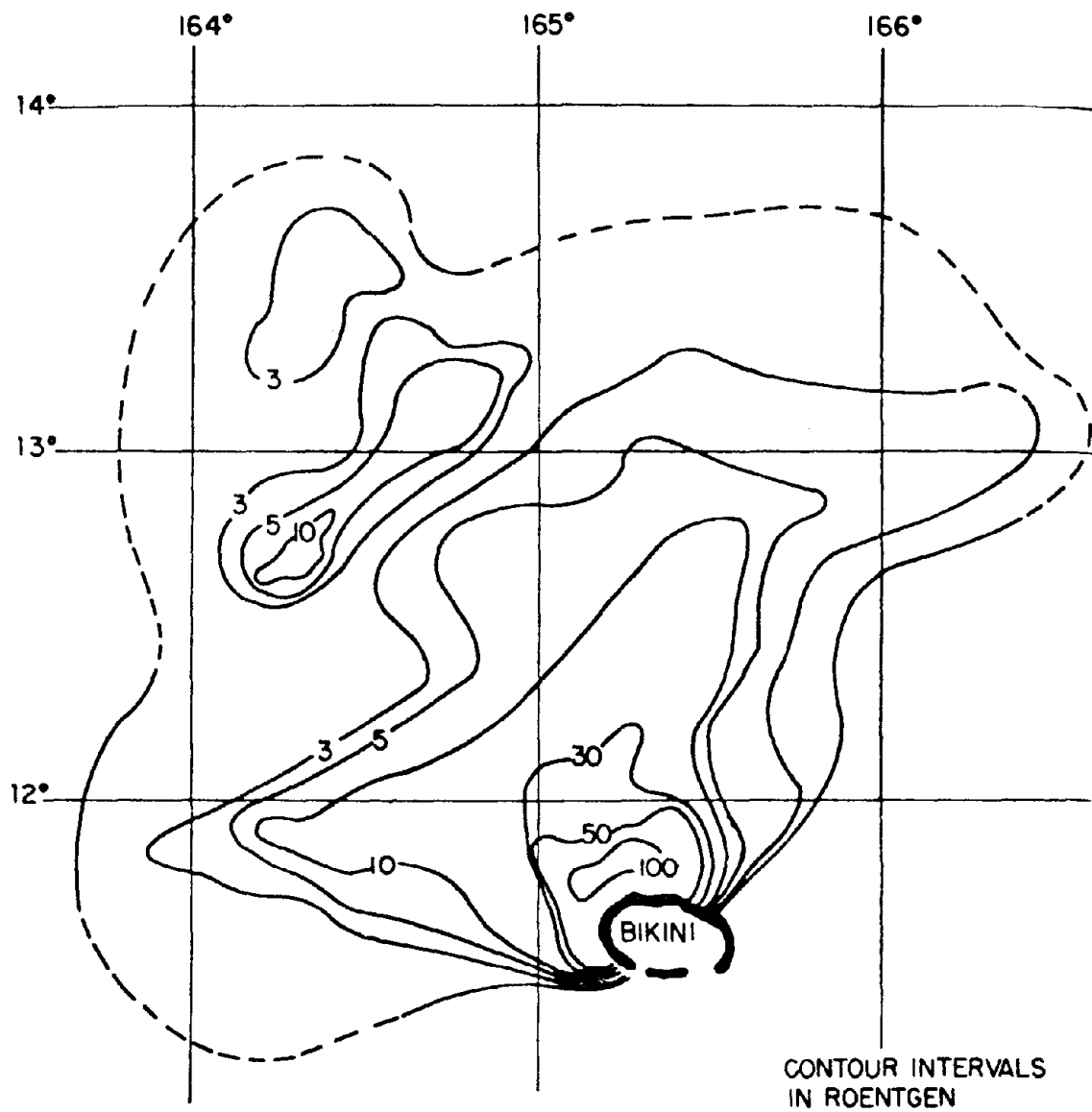


Figure 3.14 Accumulated dose (time of arrival to H + 50), Shot Flathead.

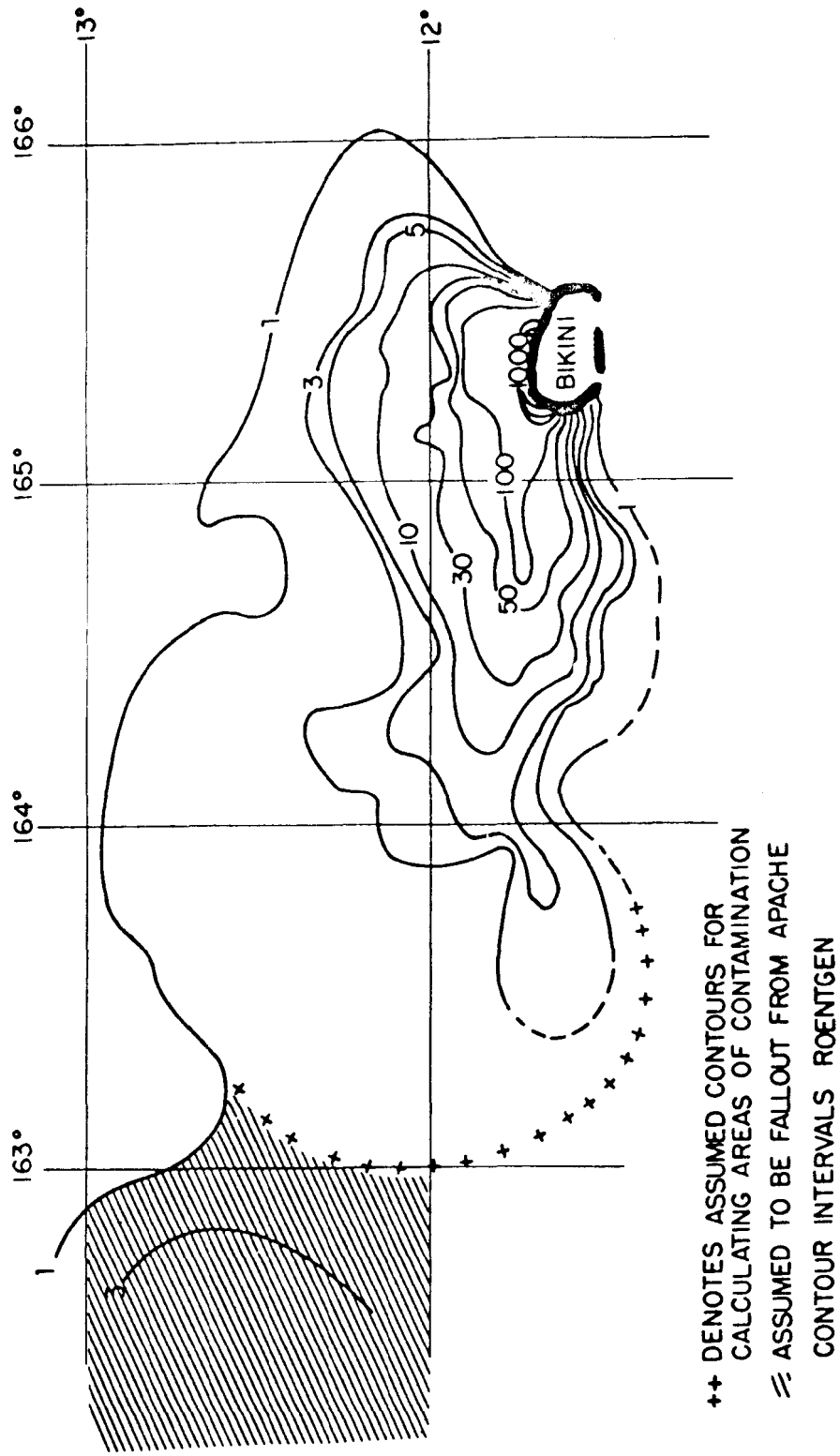


Figure 3.15 Accumulated dose (time of arrival to H + 50), Shot Navajo.

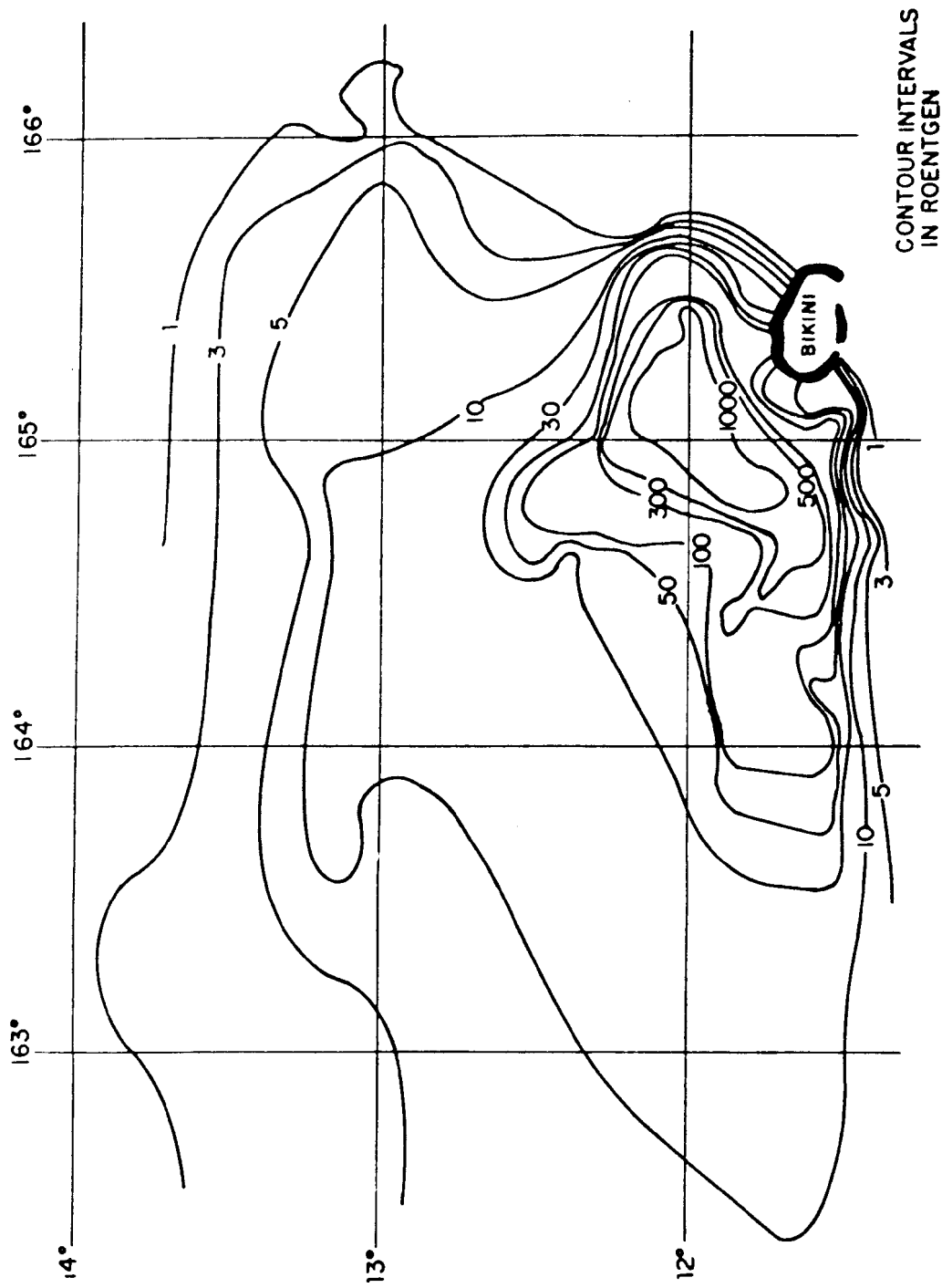


Figure 3.16 Accumulated dose (time of arrival to H + 50), Shot Tewa.

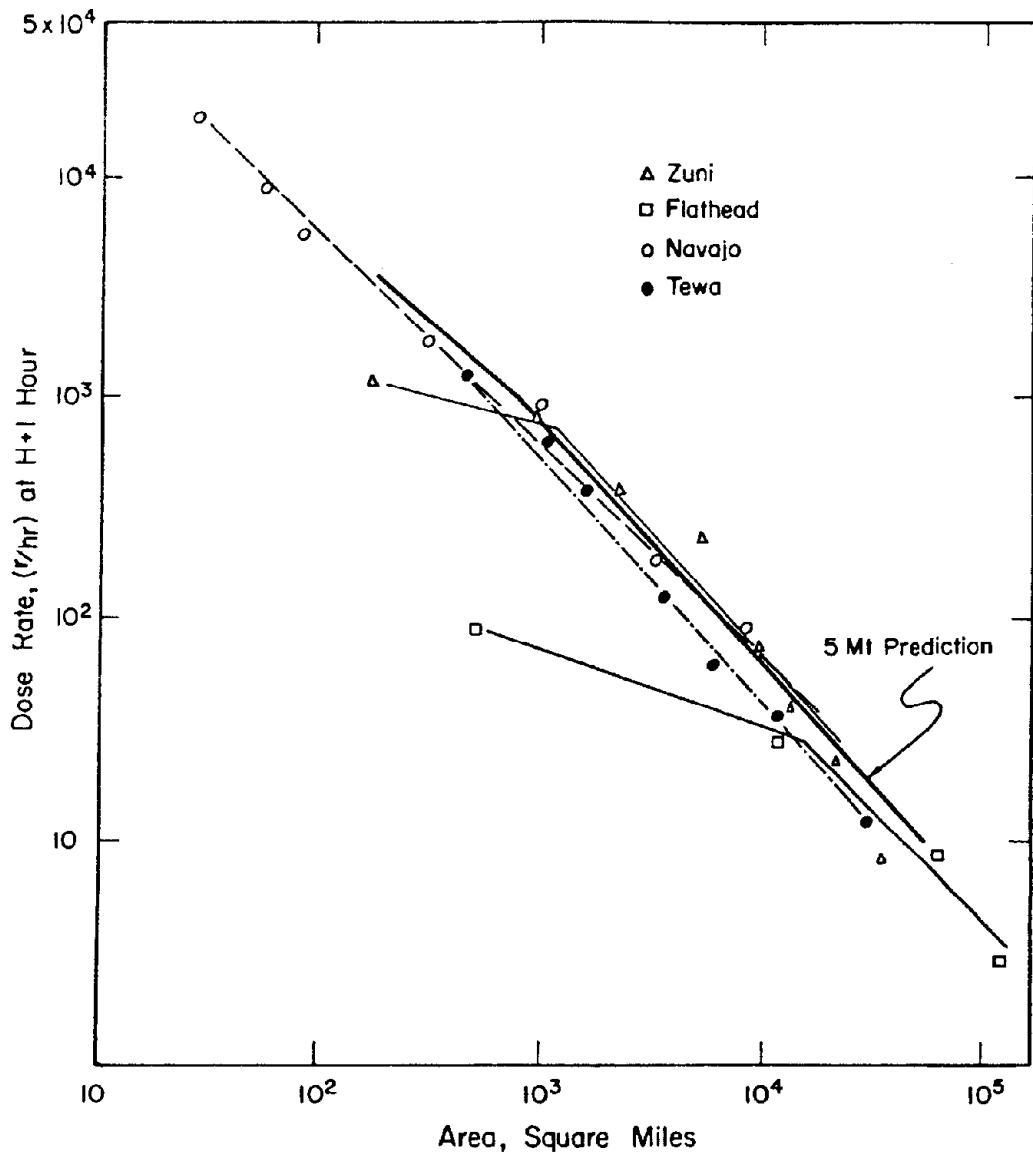


Figure 3.17 Areas of dose rate contours for Redwing shots normalized to 5-Mt 100-percent fission yield.

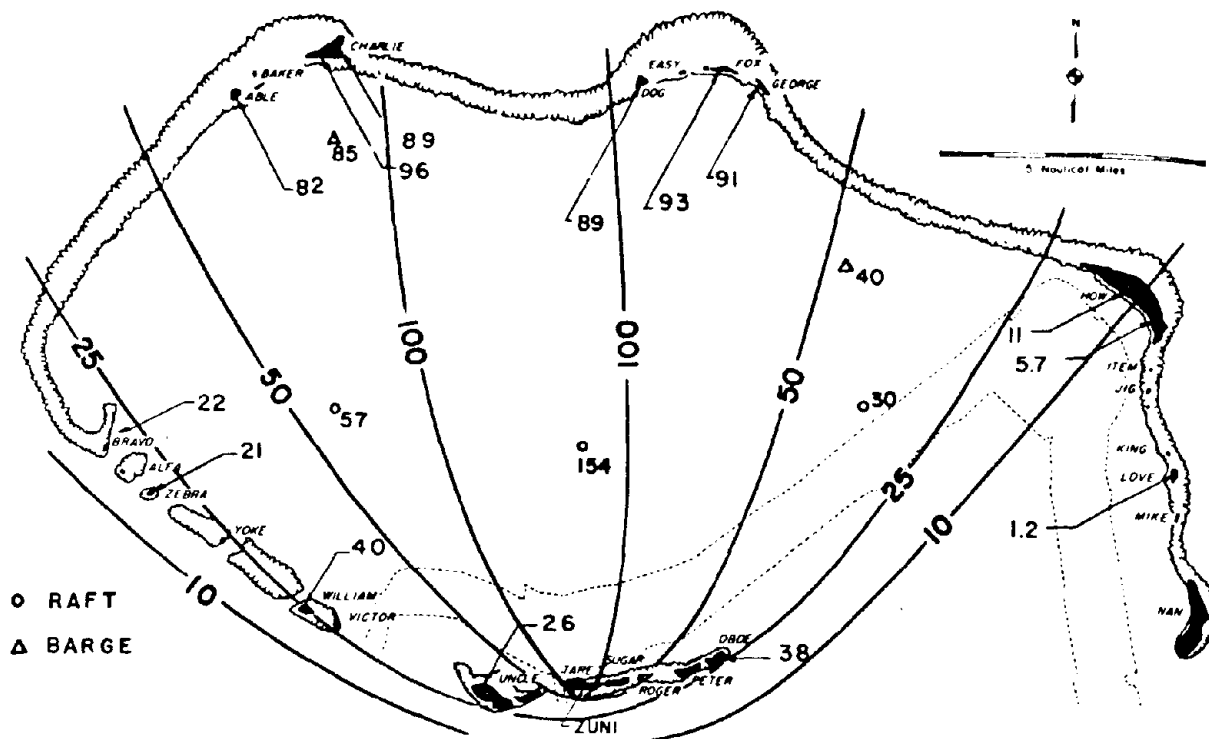


Figure 3.18 Aerial survey readings at 3 feet, corrected to H+1 hour in r/hr and dose rate contours, Shot Zuni.

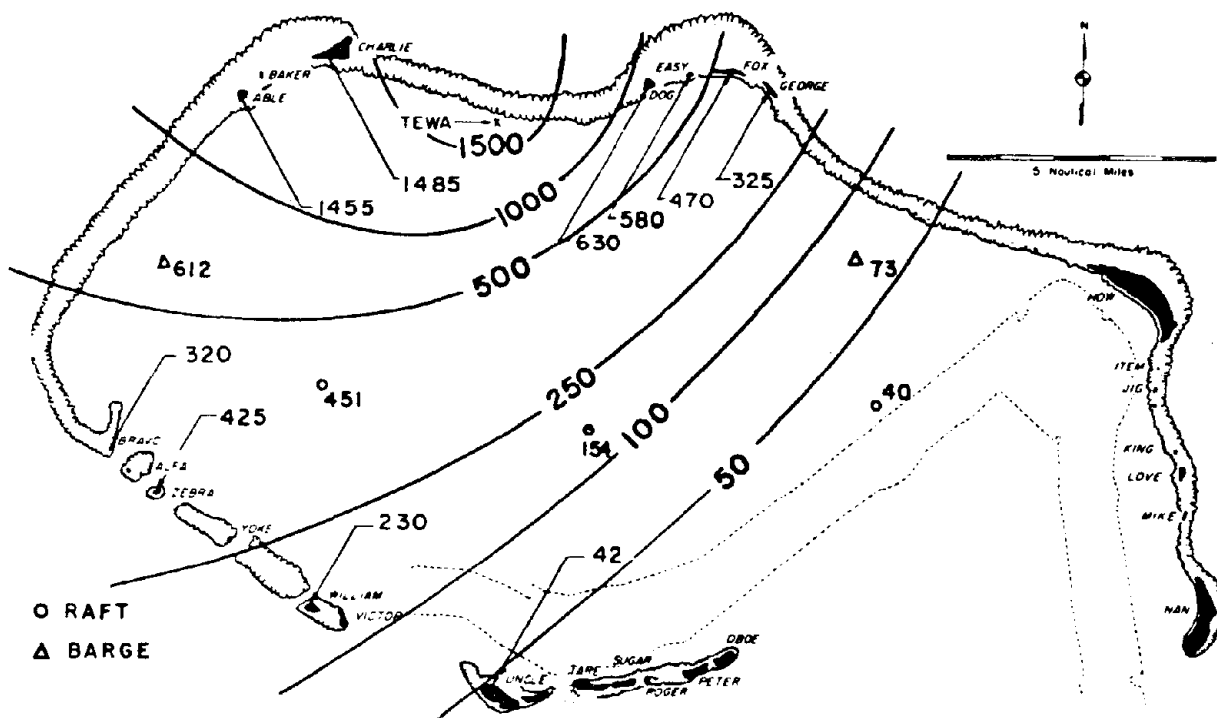


Figure 3.19 Aerial survey readings at 3 feet, corrected to H+1 hour in r/hr and dose rate contours, Shot Tewa.

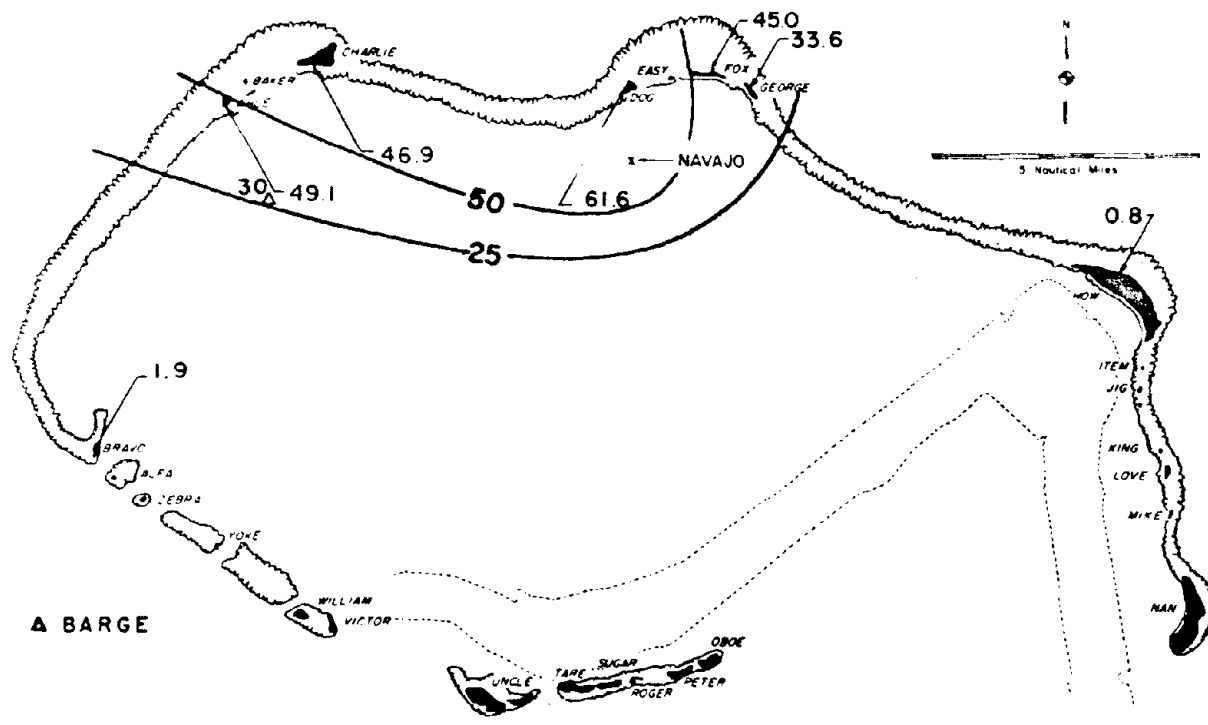


Figure 3.20 Aerial survey readings at 3 feet, corrected to H+1 hour in r/hr and dose rate contours, Shot Navajo.

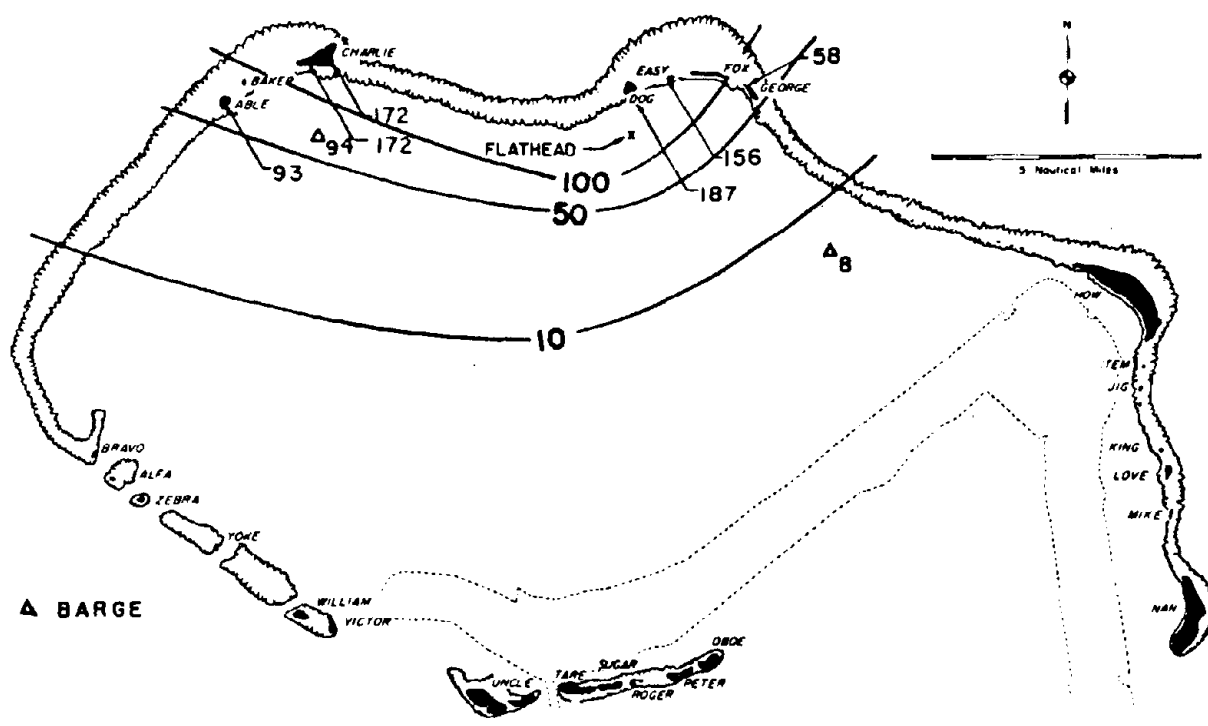


Figure 3.21 Aerial survey readings at 3 feet, corrected to H+1 hour in r/hr and dose rate contours, Shot Flathead.

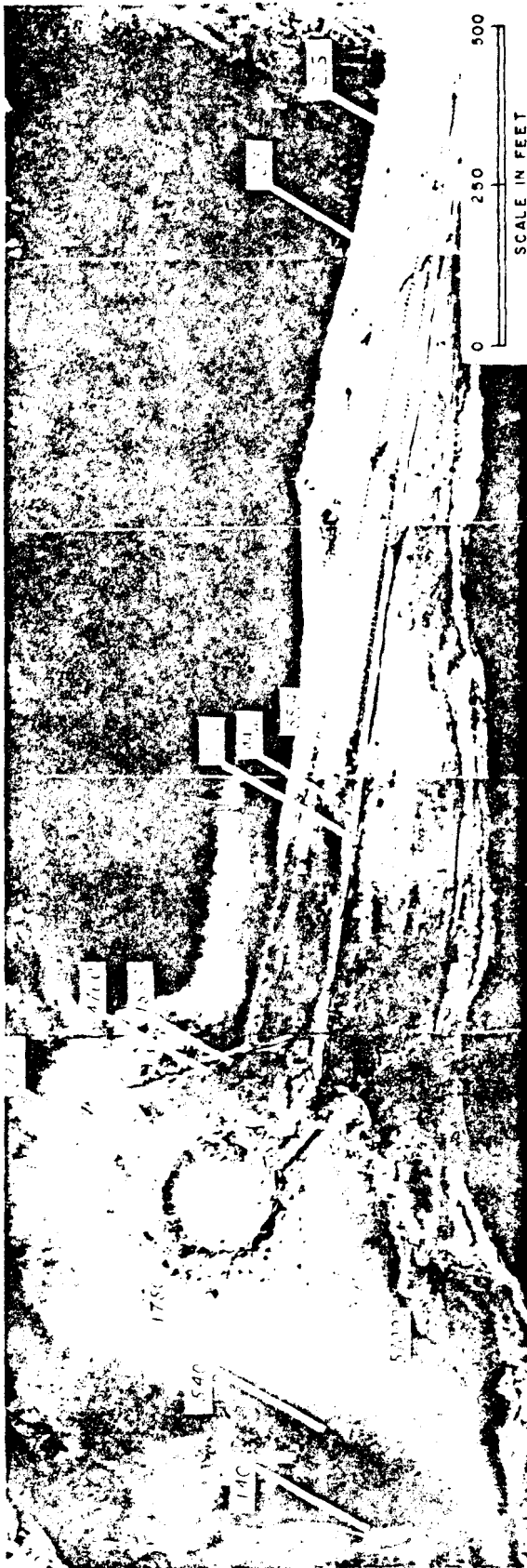


Figure 3.22 Aerial survey reading at 3 feet on Site Yvonne after Shot Lacrosse, corrected to H+1 hour in r/hr.



Figure 3.23 Aerial survey readings at 3 feet in the vicinity of the Shot Mohawk crater, corrected to H+1 hour in r/hr.

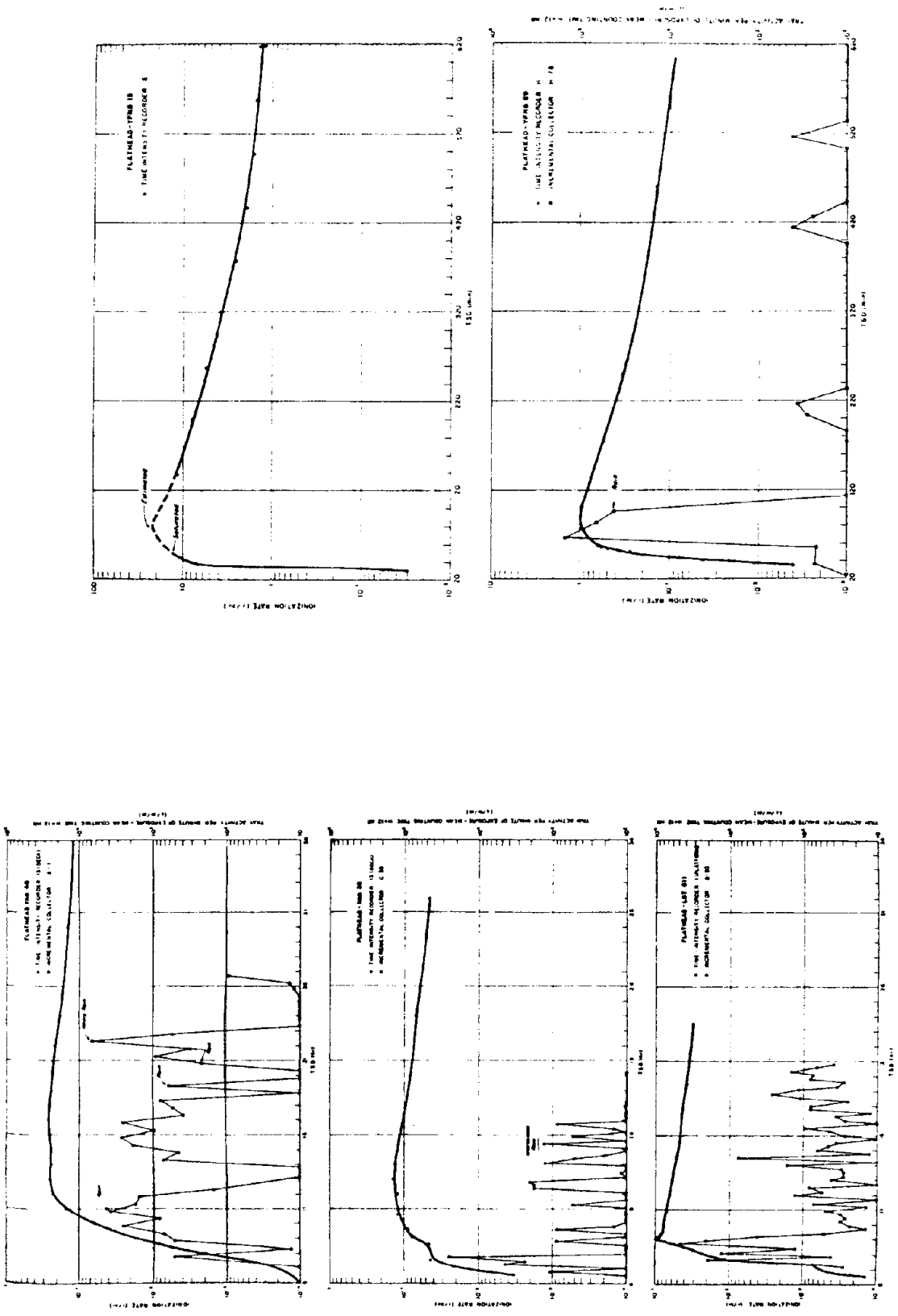


Figure 3.24 Rates of arrival at major stations, Shot Flathead.

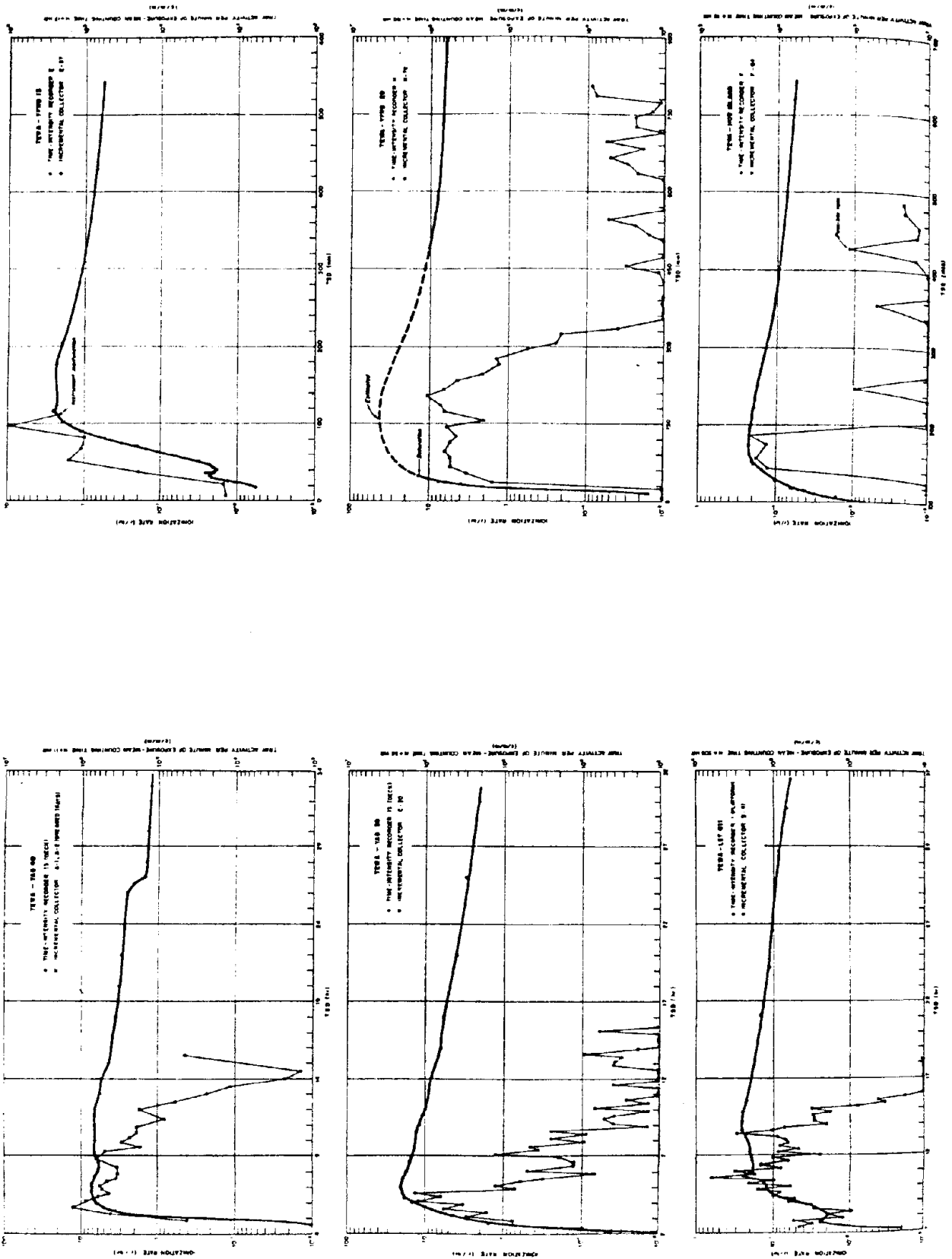
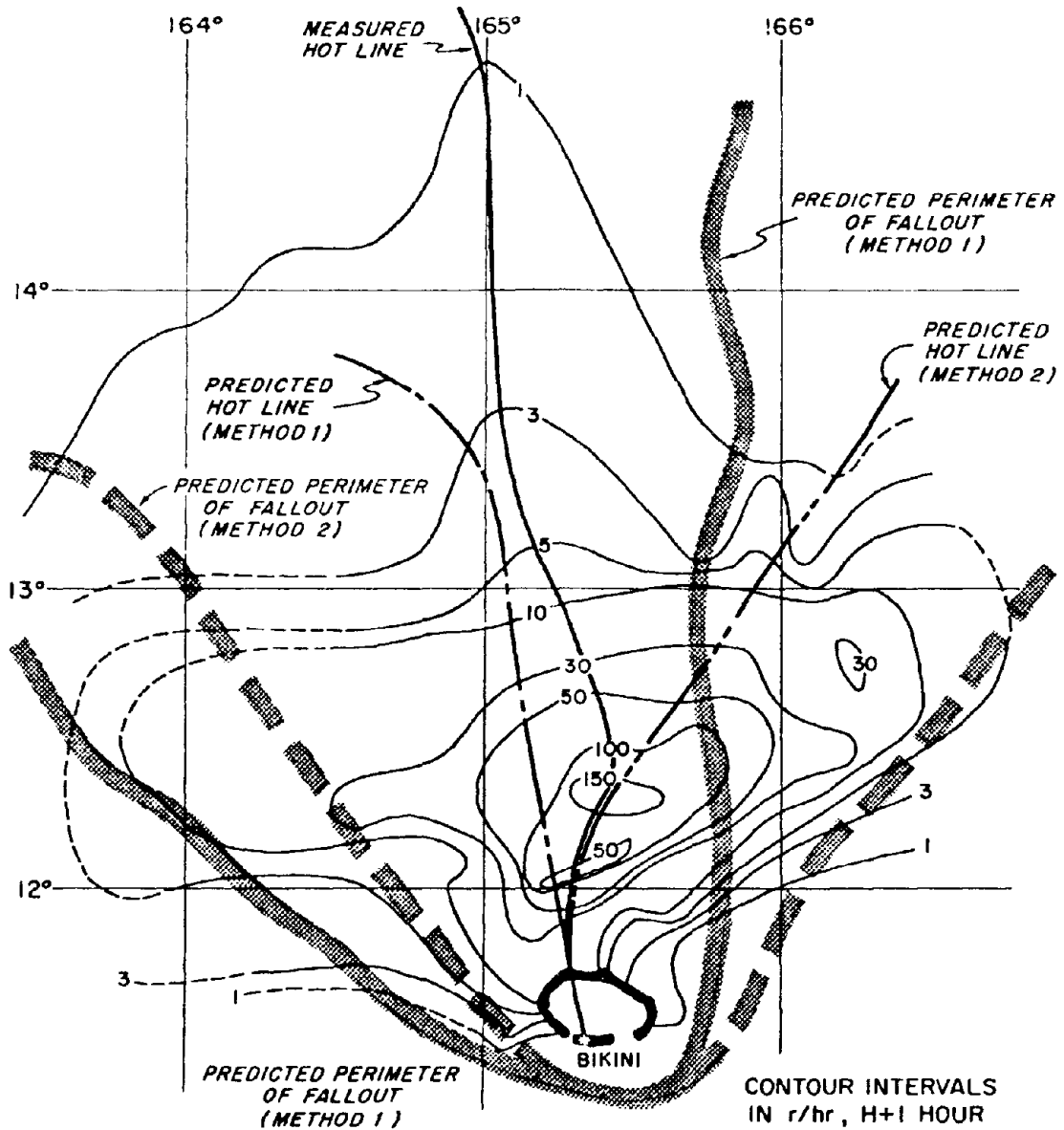


Figure 3.25 Rates of arrival at major stations, Shot Tewa.



Parameter assumptions used.

1. Cloud top: 85,000 ft.
2. Cloud base: 52,000 ft.
3. Cloud diameter: 50 naut mi.
4. Hot line fallout: from 60,000 ft.

Meteorological parameters:

- Method 1. Time variation of the wind field
 Method 2. Time and space variation of the wind field.

Figure 3.26 Predicted and observed fallout pattern, Shot Zuni.

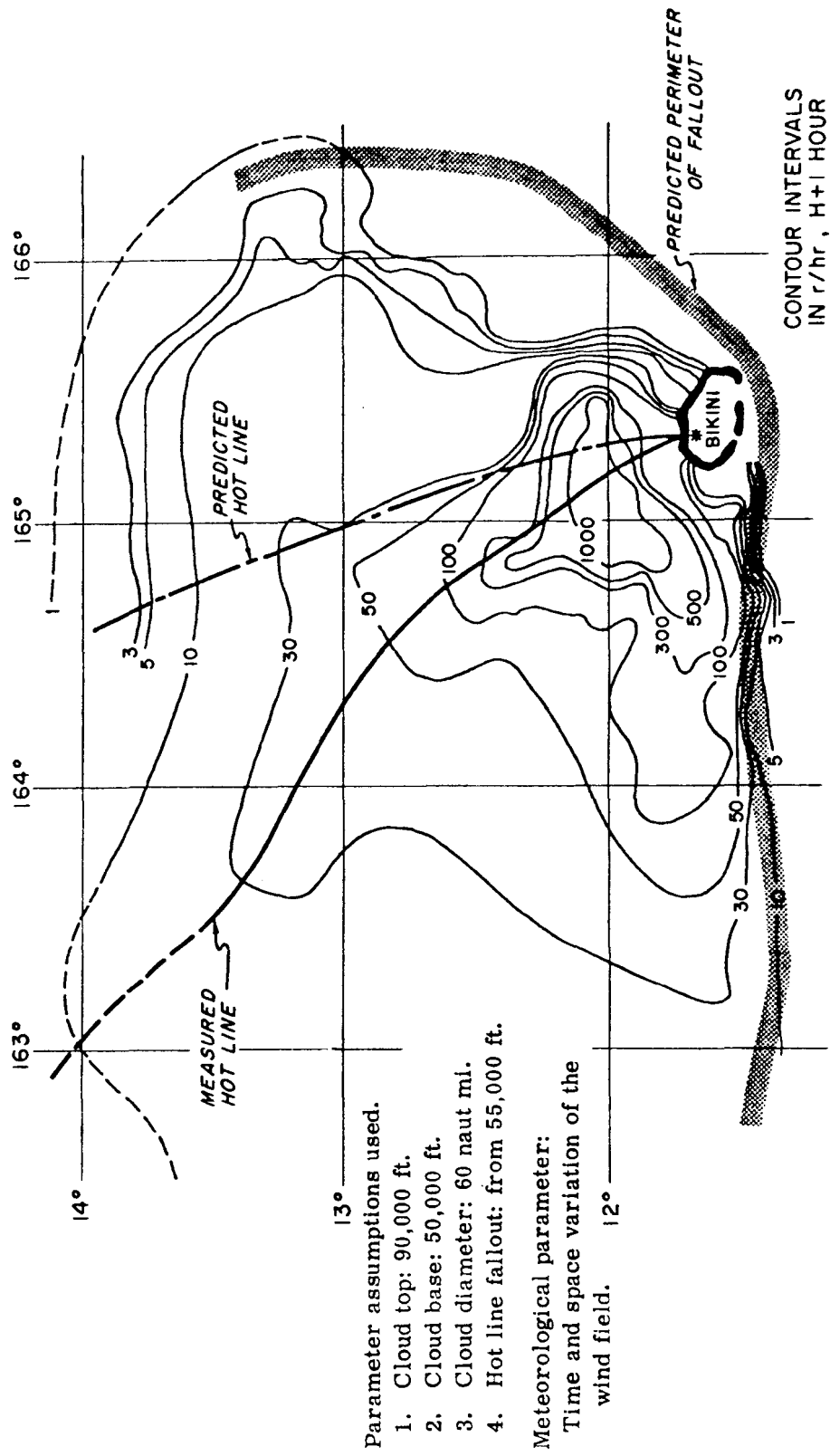


Figure 3.27 Predicted and observed fallout pattern, Shot Tewa.

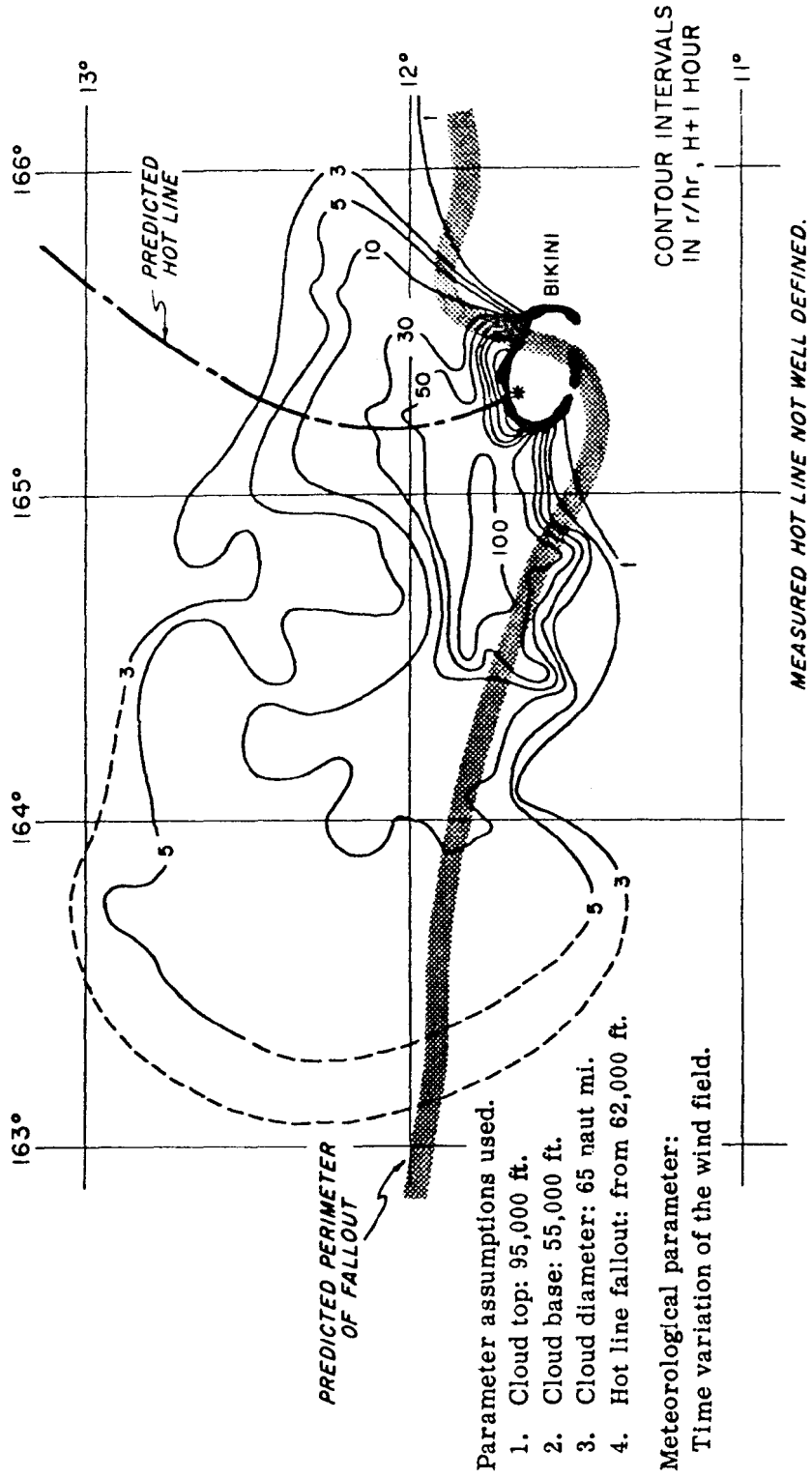
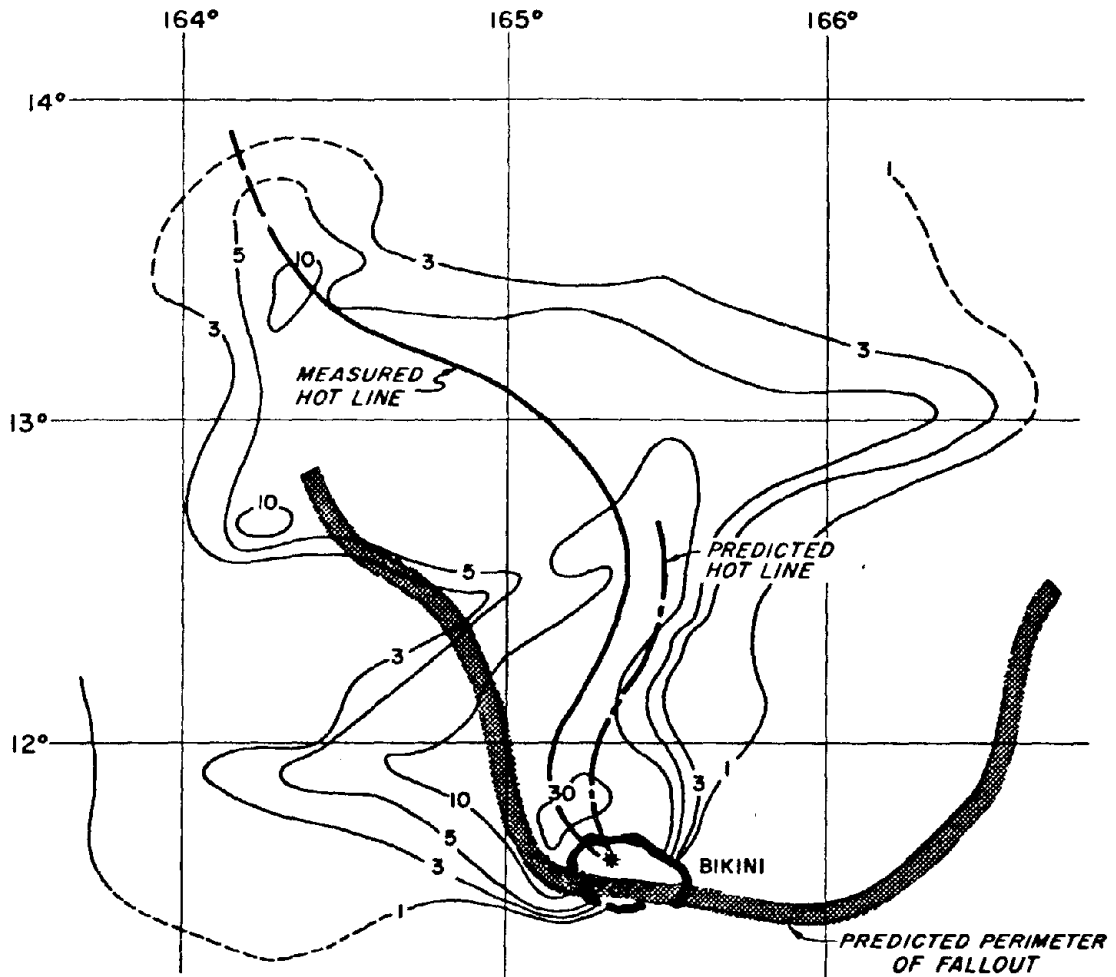


Figure 3.28 Predicted and observed fallout pattern, Shot Navajo.

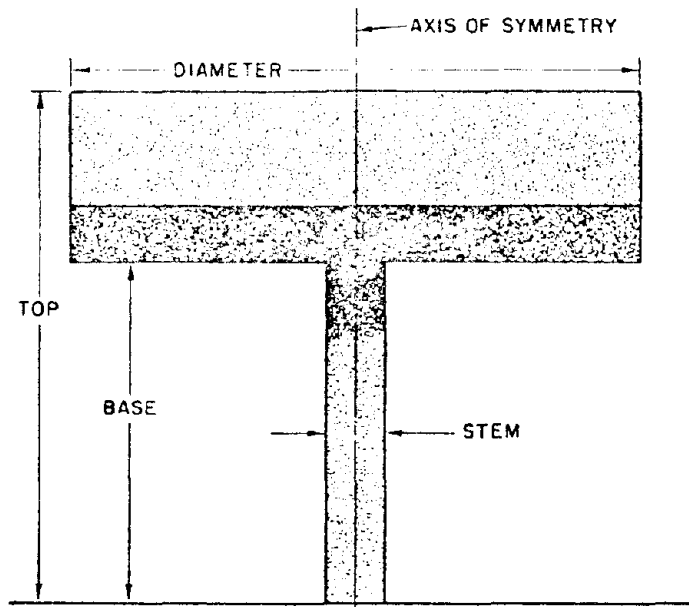


- Parameter assumptions used.
1. Cloud top: 60,000 ft.
 2. Cloud base: 40,000 ft.
 3. Cloud diameter: 14 naut mi.
 4. Hot line fallout: from 43,000 ft.

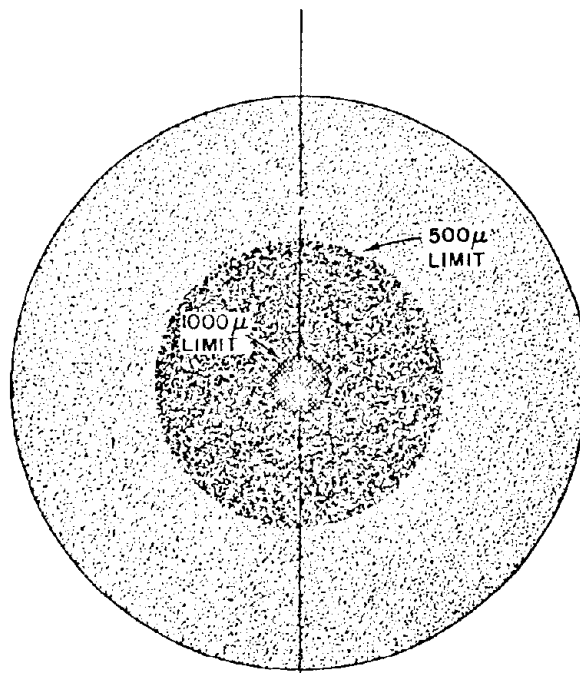
Meteorological parameter:
Time variation of the wind field.

CONTOUR INTERVALS
IN r/hr, H+1 HOUR

Figure 3.29 Predicted and observed fallout pattern, Shot Flathead.



ACTIVITY DISTRIBUTION



SIZE FRACTIONATION

Figure 3.30 Cloud model for fallout prediction.

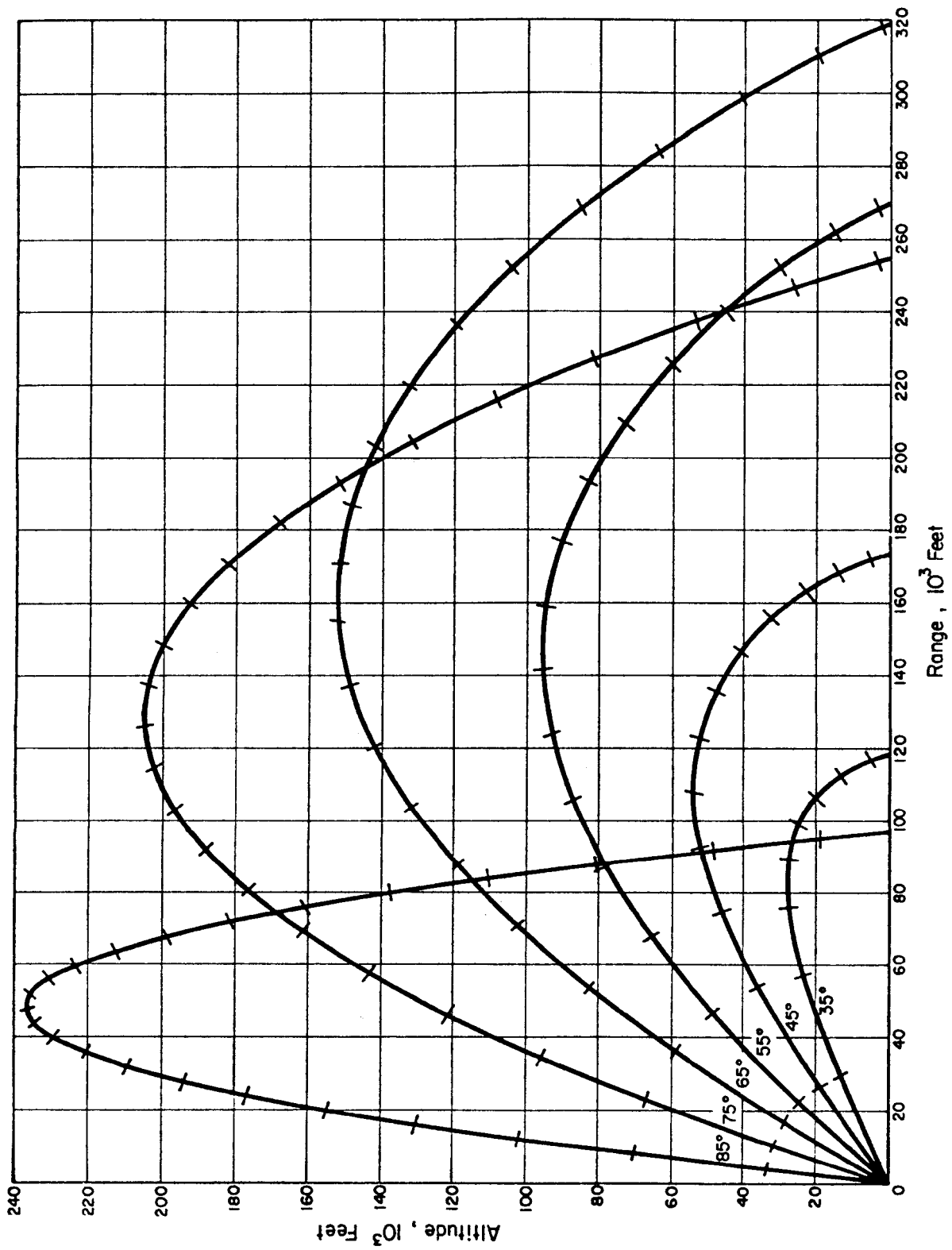


Figure 3.31 Trajectories of ASP rockets (mark on trajectories in 10-second intervals).

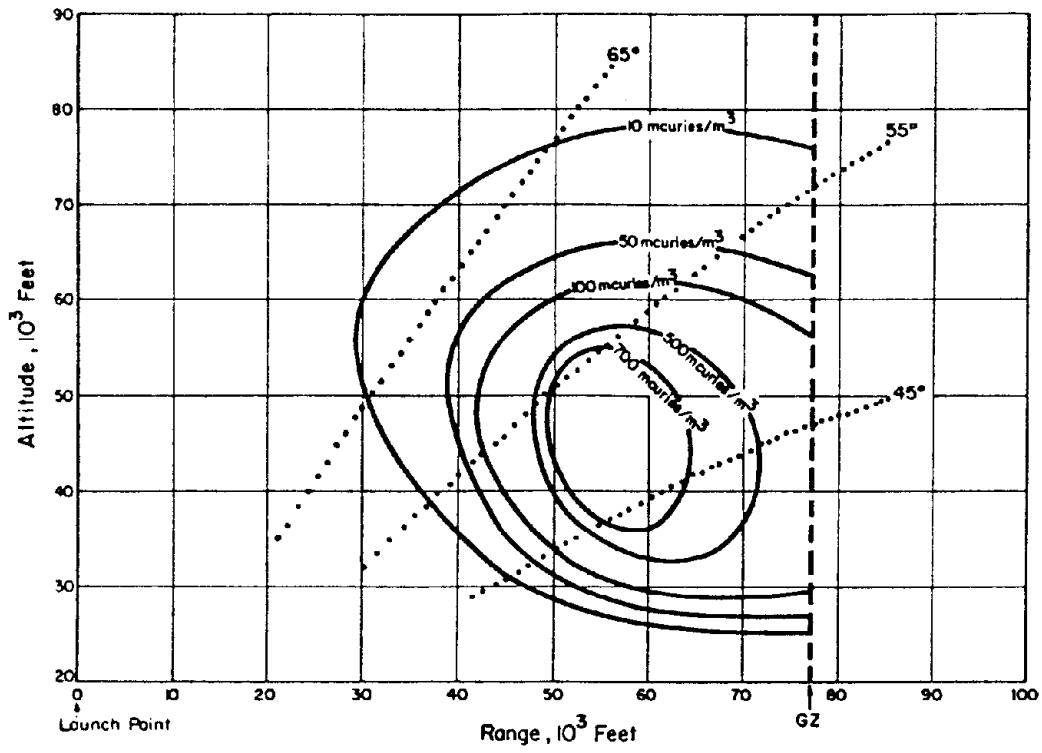


Figure 3.32 Activity distribution in the plane of rocket trajectories 7 minutes after Shot Zuni.

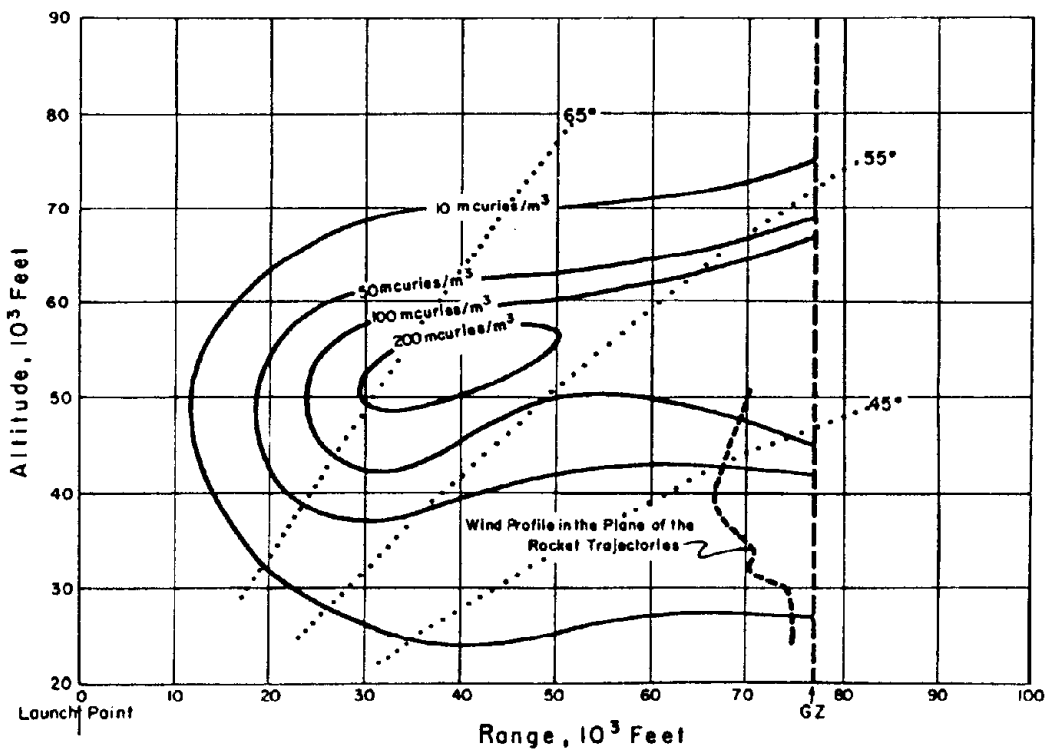


Figure 3.33 Activity distribution in the plane of rocket trajectories 15 minutes after Shot Zuni.

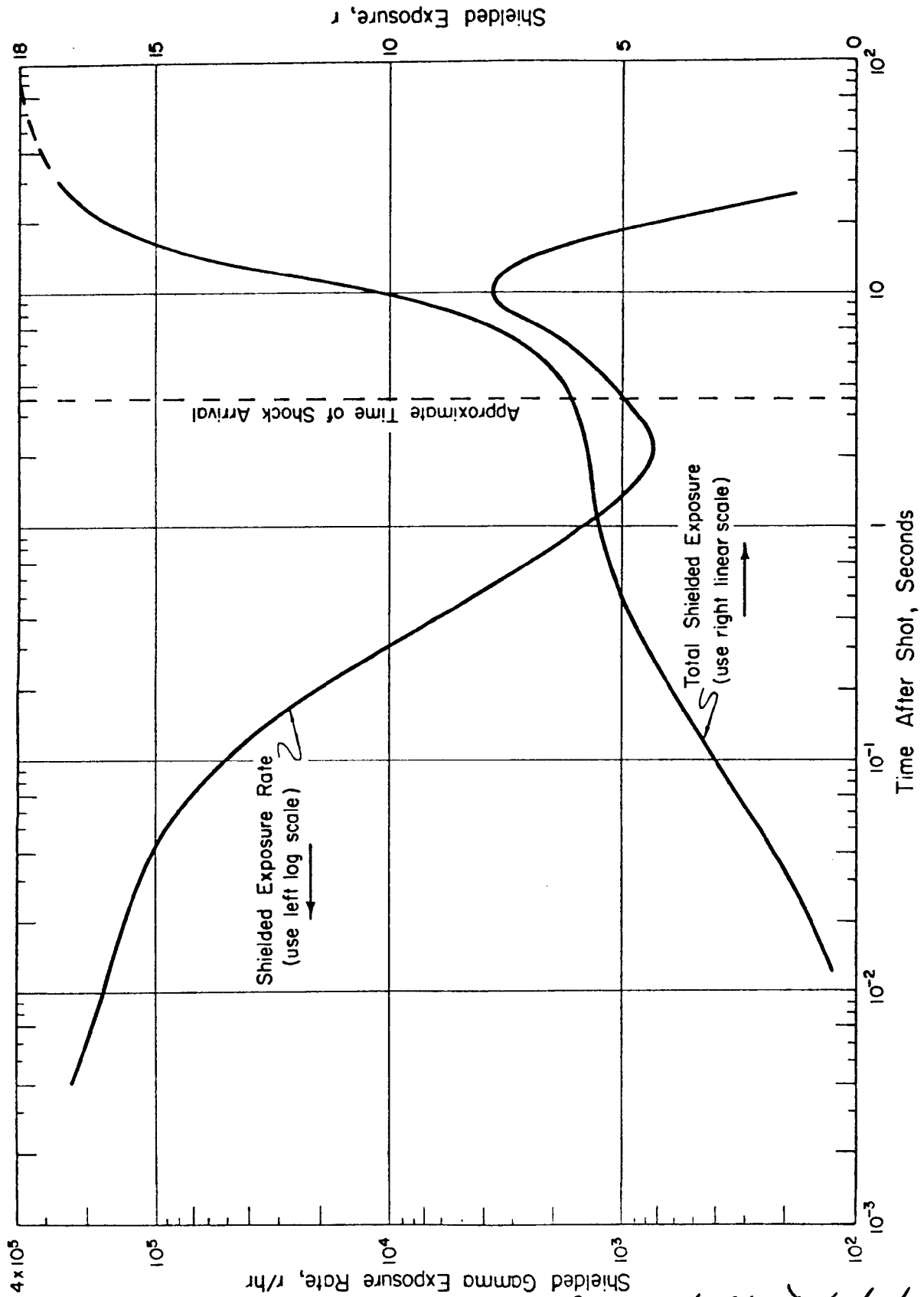


Figure 3.34 Shielded initial exposure rate within blast shield versus time for Shot Navajo; Station 221.05, range 13,170 feet. For unshielded rate multiply by 1.2.

Pgs. 175 & 176 Deleted.

Chapter 4

EFFECTS ON STRUCTURES

The efforts of Program 3, Effects on Structures, were concentrated in one relatively large project—Project 3.1. (See Section A.3 in the Appendix.)

4.1 OBJECTIVES

The primary objective was to obtain information regarding the effect of the duration of the positive phase of blast from nuclear detonations on the response of drag and semi-drag types of structures. The secondary objective was to study further the general problem of drag loading and response of structures to blast forces.

4.2 BACKGROUND

This project was the second part of a two-part program. The first part involved participation in Operation Teapot to study the response of four typical single-story steel-frame industrial buildings to the blast from a burst with a yield of approximately 22 kt. The second part, during Operation Redwing, involved a study of the response of identical industrial buildings to an airburst with a yield of approximately 3.7 Mt. Essentially, the first part was a test under a positive-phase blast with relatively short duration, whereas the second was a test under a positive-phase blast with relatively long duration.

To assure identical steel-frame structures for both parts of the program, all of the steel for the buildings tested during Operation Teapot and those tested during Operation Redwing were obtained at one time from the same mill rollings and were completely shop-fabricated by the steel fabricator during the same period in 1954, prior to Teapot. The complete shop-fabricated steel, i.e., roof trusses, columns, crane girders, and other structural components, for the six buildings to be tested during Redwing was stored for approximately a year at the USAF Air Materiel Command Depot, Stockton, California, prior to shipment to the Pacific Proving Grounds (PPG) for assembly. This procurement procedure insured, within practical limits, close identicalness of the structures tested at the Nevada Test Site (NTS) in 1955 and those tested at PPG in 1956.

4.3 PROCEDURE

Six steel-frame industrial buildings were tested during Redwing. The buildings were approximately 30 feet high, 40 feet in span, and 40 feet long (two 20-foot bays) for the three drag structures and 80 feet long (four 20-foot bays) for the three semidrag structures. The drag structures had light asbestos-sheet siding and roofing, which were expected to fail before much load could be transferred by it to the steel frame. The semidrag structures also had light asbestos-sheet roofing, but the walls were constructed of reinforced concrete with a window opening comprising about 30 percent of the full wall area.

The structures were located on three manmade islands along the shallow reef between Sites Charlie and Dog and on Site Dog at ranges of 20,500, 24,000, 29,000, and 35,600 feet from expected ground zero of Shot Cherokee. Each type of structure nearest expected ground zero was located so that, if the yield of the weapon were near the lower limit of its predicted range, the structure would undergo considerable inelastic deformation. Conversely, those structures farthest from ground zero were located so that, if the yield of the weapon were near the upper limit of its predicted range, they would be substantially deformed but would not collapse. The third building of each type was located at an intermediate point, so that the range in the degrees of damage suffered by the structures would be as large as possible.

The selection of the site locations of the six structures was made after careful consideration of all factors involved. The structures had to be placed in locations that would insure the best possible chance of getting a reasonable range in degree of damage for both types of structures. Furthermore, only three structures of each type were available. Because natural land areas are present only in the form of small islands in PPG, it became obvious in the early planning stage that only one, if any, of these natural islands would be so located with respect to ground zero that it could be used as a site location of one of the test structures. It was necessary, therefore, to place the other test structures on manmade islands located along the shallow reef connecting the natural islands of the Bikini Atoll. It was recognized, from the standpoint of economy, that it was extremely desirable to reduce the required number of manmade islands to a minimum. It was found that two of such manmade islands could be used to support one building of each type, without departing more than 500 feet from the ranges from ground zero that would have been preferred if no consideration had been given to the possibility of using double islands. Accordingly, the final layout provided for manmade Islands 1, 2, and 3 along the reef, at ranges of 20,500, 24,000, and 29,000 feet, respectively. Thus, a drag type structure was located on Island 1; a drag type and a semidrag type on each of Islands 2 and 3; and a semidrag type on Site Dog.

Shock-tube model studies conducted at the Ballistic Research Laboratories (BRL) in the early planning stages assisted in the determination of the minimum satisfactory size for the manmade islands. It was necessary that the size be sufficiently large so that a relatively nonturbulent, or smooth, airblast flow would occur at the front faces of the instrumentation (p_t and q gages) and building structures. These model studies resulted in the adoption of a rounded nosing on the front edge of the islands and a reduction in the overall length of the islands by 30 feet, or by about 20 percent. This, in turn, resulted in a reduction in the total construction costs. The final size determined necessary for Island 1 was 140 by 90 feet; for Islands 2 and 3, 140 by 210 feet. An island height of approximately 4 feet above high-tide level (10 feet above the reef level) was selected as adequate to protect the island surface from wave action

4.4 SITE CONSTRUCTION

Site construction began at PPG in November 1955 and was scheduled for completion by 1 April 1956. This allowed only approximately 5 months for construction of the manmade islands and erection of the building structures thereon. However, excessively high waves from a heavy mid-Pacific storm in December 1955 partially destroyed certain interisland causeways and damaged the partially completed islands at Bikini Atoll, all of which resulted in an unexpected delay in completion of about 3 weeks. Nevertheless, it may be stated that the design and construction of the manmade islands are considered to have been adequate for the purpose intended.

Construction of these islands and the erection of the structures thereon actually proved to be a major task and was often a challenge to the men, equipment, and material involved. This was largely because of the action of the intermittent tidal water flow over the reef sites. This flow alternately ranged in depth from approximately 7 feet maximum to 1 foot minimum, depending on the tidal stage, plus 1- to 3-foot waves, even at the shallow-reef locations selected. Extensive use of heavy construction equipment, such as bulldozers, earthmoving scrapers, and cranes, was possible on the reef only during low tide. Maximum use of the amphibious trucks (DUKWs) and helicopters, for the daily movements of working personnel and small equipment parts to the sites, contributed materially to expediting successful completion of this construction phase within the relatively short time schedule allowed.

4.5 INSTRUMENTATION

Instrumentation was provided by BRL, utilizing primarily electronic recording gages, but with supplementary backup free-field pressure instrumentation by BRL self-recording p_t and q gages. Instrumentation was provided to obtain transient structural deflections, strains, and accelerations, as well as the overpressure-versus-time and dynamic-pressure-versus-time relationships at the sites of each of the test structures.

Because the structures were identical to those used during Operation Teapot, the natural periods of vibration and the resistance functions as determined during Teapot from the pre- and post-test static pull tests were assumed to be correct. Accordingly, these measurements were not repeated.

4.6 RESULTS

Because of the delivery error of Shot Cherokee, all structures of this project were exposed to higher overpressures than planned. As a result, the planned gradation of damage was not achieved, and all structures collapsed (Figures 4.1 and 4.2).

The peak pressure intensities obtained from BRL self-recording gages of Project 1.1 at each structure were 8.5, 7.5, and 6.1 for the drag structures and 7.5, 6.1, and 5.0 psi for the semidrag structures. In addition to obtaining higher peak pressures than expected, the structures were oriented at incident angles varying from 58 to 33 degrees, as a result of the large change in ground zero (Figure 4.3). The results of the project are shown in Table 4.1 which compares the Teapot and Redwing results.

The comparison of results was seriously limited because of the collapse of all Redwing structures. Because the only reliable records obtained were surface overpressure records, and possibly some strain records, it was impossible to correlate the observed response with computed response except in a most general way. To make even a general study of the relationships between load and maximum response that existed in the field tests, it was necessary that supplementary information relative to the effects of orientation on the normal component of the load transmitted to each of the test structures be obtained. This supplementary information was obtained from a series of tests on various orientations of scaled models of the test structures in the AFSWP-USAF 6-foot-diameter shock tube operated by the Armour Research Foundation at Gary, Indiana.

By utilizing the available general knowledge of blast loadings on aboveground structures and extending specifically the methods employed satisfactorily during Operation Teapot, it was possible to estimate the probable loadings that would have acted on the structures if they had been oriented normal to the direction of blast propagation. The

loads thus estimated were adjusted on the basis of the model results to give probable loadings on the actual structures. The theoretical maximum responses of the structures to these probable loadings were then computed and compared with the observed collapsed condition of the structures.

4.7 CONCLUSIONS

The following qualified conclusions are based on the inadequate data:

1. There is a definite bonus effect to be derived from shock waves having long positive-phase lengths, compared to shock waves having the same peak pressure levels but shorter positive-phase lengths, when the structures being considered are sensitive primarily to drag loading. This is verified by the fact that, for the Redwing drag Structure 3.1-A-3, total collapse occurred under a peak overpressure of 6.1 psi, unreduced for the effect of orientation, whereas the Teapot drag Structure 3.7-A-1 experienced a maximum deflection of only 22 inches from a peak overpressure of 6.5 psi. Further verification exists if the measured overpressure of 8.0 psi at Teapot Structure 3.7-A-1 was correct, because Redwing Structure 3.1-A-2 collapsed under an overpressure of 7.5 psi uncorrected for the effects of orientation.

2. The data presented in Table 4.1 indicates that, for the drag structures tested, an overpressure of no more than 4.9 psi in a normally incident shock wave from a 3.8-Mt weapon would produce complete collapse, whereas an overpressure of 8.2 psi from a 22-kt weapon would be required. Thus the reduction in overpressure level required to produce collapse was estimated as at least 40 percent.

3. The data also indicates that, for the semidrag structures tested, an overpressure of no more than 4.2 psi in a normally incident shock wave from a 3.8-Mt weapon would produce complete collapse, whereas an overpressure of 5.5 psi from a 22-kt weapon would be required. Thus the reduction in overpressure level required to produce collapse was estimated as at least 24 percent.

4. Conclusions 2 and 3 are based on the assumption that the loads that acted on the Redwing structures were just large enough to produce collapse. An inspection of the collapsed structures indicated strongly that the loads were probably considerably larger than this. Therefore, the effectiveness of a long positive phase of blast wave, as given by the percentages in conclusions 2 and 3, is probably underestimated.

TABLE 4.1 COMPARISON OF RESULTS FROM OPERATIONS TEAPOT AND REDWING

	Drag Structures						Semidrag Structures					
	Teapot			Redwing			Teapot			Redwing		
	3.7-A-1	3.7-A-2	3.1-A-1	3.1-A-2	3.1-A-3	3.7-B-1	3.7-B-2	3.1-B-1	3.1-B-2	3.1-B-3		
Range, ft	3,600	4,350	19,900	21,200	24,000	5,000	5,750	21,200	24,000	26,800		
Observed peak overpressure, psi	6.5	4.7	8.5	7.5	6.1	3.4	2.7	7.5	6.1	5.0		
Positive phase duration, sec	0.88	0.89	4.0	4.2	4.7	0.95	1.01	4.2	4.7	4.8		
Observed maximum deflection, in	22	10.8	Collapse +	Collapse +	Collapse +	13	6.8	Collapse +	Collapse	Collapse +		
Collapse (TP) or orientation (RW) factor	1.26	1.75	0.34	0.48	0.64	1.53	2.15	0.55	0.68	0.79		
Equivalent peak overpressure, psi by p _r	8.2	8.2	—	—	—	5.2	5.8	—	—	—		
by p _d	—	—	—	—	—	—	—	4.1	4.2	4.0		
Average equivalent P _s	8.2	8.2	4.9	5.2	4.9	—	—	5.6	5.0	4.4		
Ratio RW equivalent P _s to TP equivalent P _s , pct	—	—	60	63	60	—	—	87	84	76		
Adjusted maximum deflection	Collapse	Collapse	Collapse +	Collapse +	Collapse +	Collapse	Collapse	Collapse +	Collapse +	Collapse +		

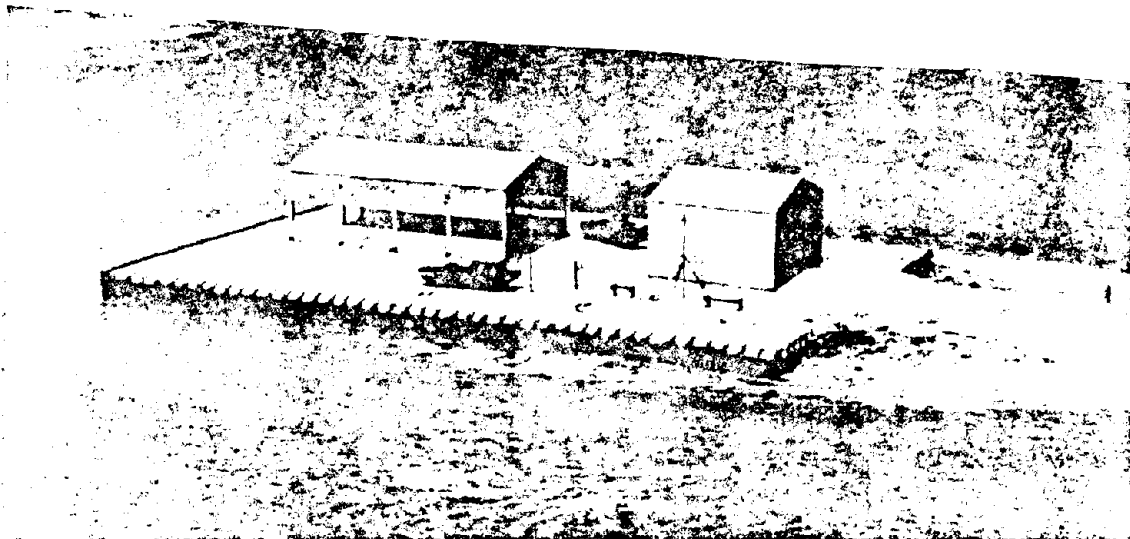


Figure 4.1 Air view of structures on manmade Island 2, before Cherokee (looking toward Site Dog).

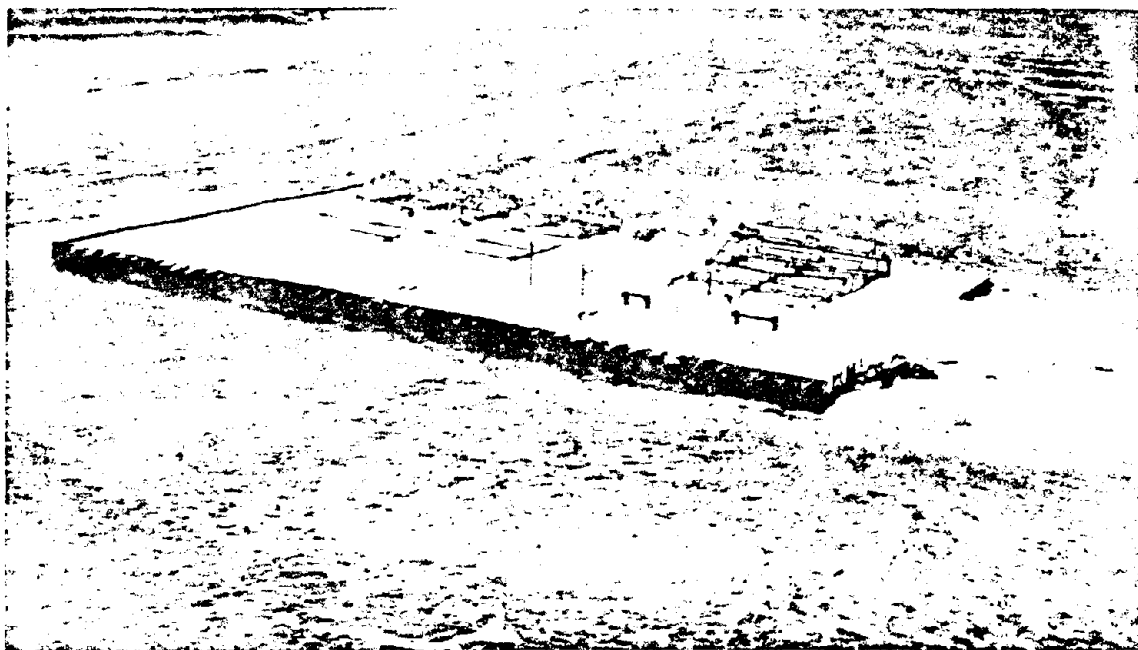


Figure 4.2 Air view of structures on manmade Island 2, after Cherokee (looking toward Site Dog).

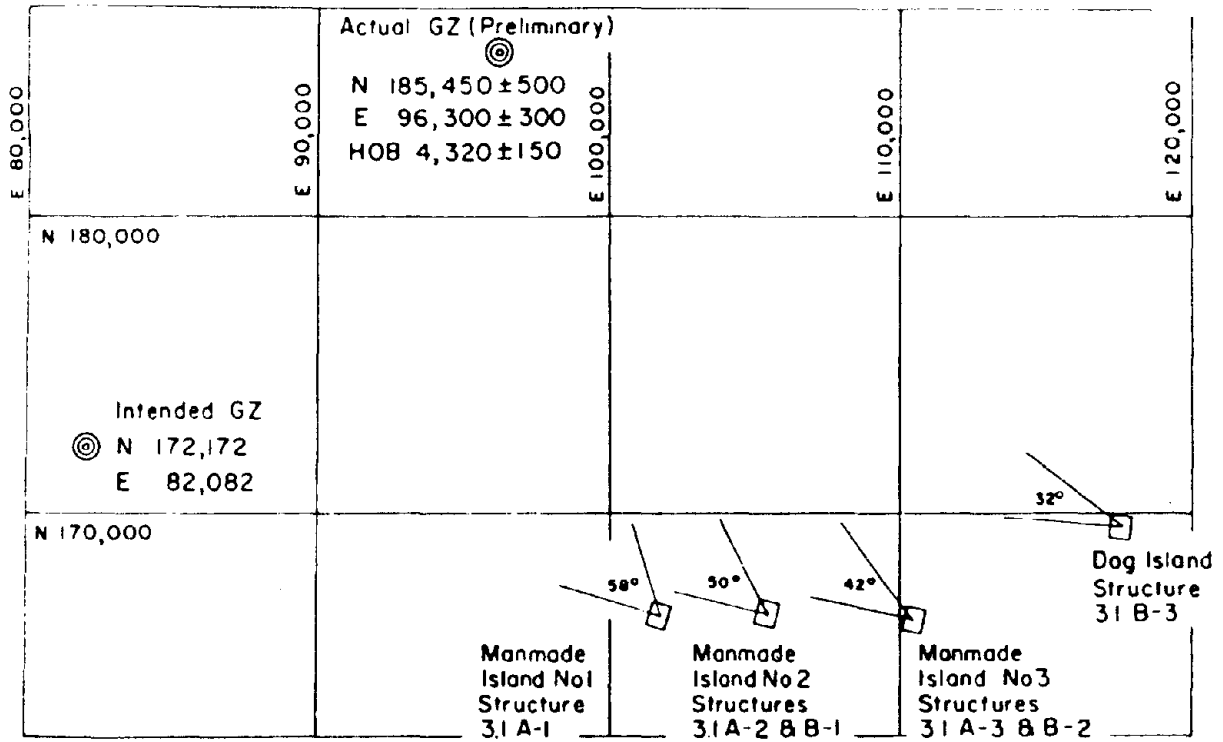


Figure 4.3 Location of structures with reference to intended and actual ground zeros with orientation angles.

Chapter 5

BIOMEDICAL EFFECTS

5.1 OBJECTIVES

The efforts of Program 4, Biomedical Effects, were concentrated in one project—Project 4.1—designed to furnish information on the requirements for protection against chorioretinal burns. (See Section A.4 in the Appendix.)

Rabbits and monkeys were exposed to the thermal pulse of Shots Lacrosse, Cherokee, Zuni, Erie, Mohawk, and Navajo with all exposure stations less than 22 miles from ground zero. Timing and shutter mechanisms for fractionating the light-pulse were used at the exposure stations, along with protective shutters and filters.

5.2 BACKGROUND

Previous experience indicated chorioretinal burns would be received at all exposure sites. Four cases of accidental human retinal burns had been produced at distances of 2 to 10 miles from a nuclear detonation. During Operation Upshot-Knothole, chorioretinal burns were produced in rabbits at distances from 2 to 42.5 miles. The atmospheric transmission of thermal energy in the hot, dry climate of the Nevada Test Site ranges between 95 and 97 percent per mile, while 80 to 85 percent transmission per mile usually is encountered at the Pacific Proving Grounds (PPG). The difference in transmission at the PPG is attributed to higher humidity and the prevalence of salt spray in the atmosphere. Irradiance (the rate at which thermal energy is received), as well as the total radiant exposure (total thermal energy received), must be considered in the prediction of burns from a nuclear detonation. Because the duration of the pulse for megaton-range devices is considerably longer than for kiloton-range devices, the irradiance, rather than the total thermal energy at the exposure site, could be the critical parameter.

5.3 RESULTS

5.3.1 Chorioretinal Burns. Only Shots Erie and Mohawk produced chorioretinal burns. The lack of these burns during Operation Redwing may partially be explained by climatic conditions and the characteristic parameters of the thermal pulse. For Shot Navajo, clouds and rain squalls evidently protected the animals.

The percentage of the total radiant exposure during the blink reflex time of animals was found to decrease with increasing yield. Table 5.1 gives a summary of the data obtained.

Measurements of the spectrum as a function of time were not made; the thermal data obtained either from other projects or calculated from available information. The calculated incident thermal energy at the exposure sites for Shots Cherokee and Zuni,

where no burns were received, was greater than the incident thermal energy at at least three of the exposure sites for Shot Erie, where burns were received. This supports the theory that the total thermal energy at the exposure site is not the critical parameter in the production of chorioretinal burns.

Where 60 mc cal/cm² was received during the blink reflex time, animals received lesions; where animals received 50 mc cal/cm² or less during the blink reflex time, no burns were received. However, there is insufficient data to establish conditions and energies that can be designated as a threshold value for chorioretinal burns.

Results from Shots Erie and Mohawk indicate that the burns are produced at distances greatly exceeding the limits for any other prompt significant biological effects of nuclear detonations. During Erie, 22 of 26 unprotected rabbits and 6 of 8 unprotected monkeys at various distances out to 8.1 miles received burns. During Mohawk, 6 of 8 unprotected rabbits and 8 of 8 unprotected monkeys on Site Yvonne, 7.5 miles from ground zero, also received burns. Smaller lesions were encountered at increasing distances from the fireball; and for Mohawk, at 14.4 miles, no burns were received. The blink reflex time for rabbits and monkeys is not sufficient to protect against the flash from devices. Exact reflex time for the animals was obtained from laboratory analysis of photographs made during Shots Erie and Mohawk.

5.3.2 Protective Devices. The test of developmental electromechanical shutters was inconclusive. During Erie, although there was equipment failure and shutters remained open, no burns were obtained. The high percentage of attenuation (60 to 65 percent) produced by the shutters in the open position may have been sufficient to reduce the radiant exposure on the cornea to a level below the burn threshold. The device for recording time of closure of shutters did not function properly on any test.

Electrophysical shutters were installed for Shots Cherokee, Zuni, and Navajo. Inasmuch as unprotected animals received no burns from these detonations, no conclusion can be made as to the effectiveness of the shutters for eye protection. This developmental device contained a small aperture with the field of view extremely constricted; in the open position, under conditions of this test, the device appeared to have sufficiently high attenuation to prevent burns.

Fixed-density optical filters reduced the radiant exposure and irradiance on the eyes and, therefore, either prevented or reduced the severity of chorioretinal burns. No conclusion can be reached regarding the relative effectiveness of filters having various spectral transmissions.

Two groups of time-fractionating shutters were used to evaluate the effectiveness of various parts of the thermal pulse as to its ability to produce chorioretinal burns. One group, opened at time zero, closed at increasing intervals of time. Shutters in the other group, closed at time zero, were opened for preselected time increments during the flash. Shutter opening and closing times were determined by laboratory evaluation of photographs of shutter operation. The data shows that only the second thermal pulse from the device produced chorioretinal burns, whereas both the first and second pulses from the device produced burns. During Shot Mohawk, about 25 percent of the animals exposed to the initial thermal pulse received burns. The time to second maximum for Erie was calculated to be 112 msec. In the delayed-opening shutters, 3 out of 10 rabbits received burns. The lesions were produced mostly in cases where the exposure included the maximum or near-maximum flux of the second pulse. Increments of the flash beyond 500 msec for Erie and 950 msec for Mohawk did not produce burns.

Although the results were not as successful as anticipated, information obtained from this study has proved valuable in the development of eye-protective devices that were tested in subsequent operations.

TABLE 5.1 SUMMARY OF DATA AT EXPOSURE SITES

Shot	Yield	Distance from Ground Zero	Incident Thermal Energy at Exposure Site	Time of T; MAX	Range of Blink Reflex Time (BRT)*	Percent of Incident Thermal Energy Radiated During BRT	Incident Thermal Energy Available During BRT	Effects†			
								Blink Reflex	Early Closing Shutter	Delayed Closing Shutter	Filter
Lacrosse	39.5	8.9	72	163	289 to 437	46 to 62	20 to 30	N	N	N	N
Cherokee†		21.6			250 to 454	1.0 to 1.7		N	N	N	N
Zuni†	3,380	12.9	1,600 to 2,000	1,900	250 to 454	0.5 to 1.5	20 to 30	N	N	N	N
Erie		2.7			289 to 437	62 to 76		B	-	-	N
Erie		3.0			289 to 437	62 to 76		B	-	-	B
Erie		3.8			289 to 437	62 to 76		B	-	-	B
Erie		4.9			289 to 437	62 to 76		B	-	-	N
Erie		8.1			289 to 437	62 to 76		B	B	-	N
Mohawk†		7.5			250 to 454	15 to 28		B	B	B	B
Mohawk		14.4			250 to 454	15 to 28		N	-	-	N
Navajot		10.6			250 to 454	1.0 to 2.0		N	N	N	N
Navajot		16.1			250 to 454	1.0 to 1.5		N	-	-	N

* BRT measured for Erie assumed for Lacrosse; BRT measured for Mohawk assumed for multimegaton shots.

† N = No burns produced; B = burns produced; - = no exposures.

Chapter 6

EFFECTS ON AIRCRAFT STRUCTURES

6.1 OBJECTIVES

Seven of the nine projects in Program 5 were primarily concerned with the determination of the capability of six Air Force and one Navy aircraft to deliver nuclear weapons. The projects identifying the specific aircraft were as follows: Projects 5.1, B-47; 5.2, B-52; 5.3, B-66; 5.4, B-57; 5.5, F-84F (two); 5.6, F-101A; and 5.8, A3D-1.

The secondary objectives of the aircraft projects were to: (1) obtain basic design research data for future aircraft and (2) verify or correct the present analytical methods for the prediction of weapon-effect input data and the resultant responses of the aircraft structures.

Project 5.7 was to obtain experimental data with airborne instrumentation of basic thermal phenomena associated with nuclear explosions, and to provide supporting thermal measurements to Projects 5.1, 5.2, 5.3, and 5.4.

Project 5.9 was designed to investigate the vulnerability of basic missile structures and materials to fireball and associated phenomena of a nuclear detonation.

The project abstracts are given in Section A.5 of the Appendix.

6.2 BACKGROUND

These Redwing projects were a continuation of studies made on a B-36 during Operations Ivy, Upshot-Knothole, and Castle; on a B-47 during Ivy and Castle; and on F-84F fighters and QF-80 drone aircraft during Operation Teapot. All of these projects were conducted by the Aircraft Laboratory of Wright Air Development Center. The previous tests indicated the critical importance of thermal effects on the aircraft structures with respect to subsequent loading of the heated structure by blast (both gust and overpressure).

6.3 OPERATIONS

6.3.1 Aircraft-Positioning Reports. Aircraft effects data from Operations Ivy, Upshot-Knothole, Castle, and Teapot provided check points for the analytical studies by the Air Force and Navy to predict input data and the resulting aircraft response. As more was learned about the effects of nuclear devices on aircraft, test aircraft were positioned with greater confidence in the safety of the crew and aircraft and with more assurance of obtaining the required data.

As a result of a canvass of the various agencies involved, a flight-path-and-positioning report was required from each aircraft project officer before the Redwing field-operational phase. In essence, these reports contained detailed methods used to compute the weapon-effect input data at points in space, plus a dissertation on the anticipated responses of the aircraft structures to the basic inputs. The material was augmented by sample situations

and complete flight-path planning charts from time of takeoff to time of landing. In case aircraft were not in the desired position at zero time, necessary abort procedures were outlined.

During the operational phase of the test series, the projects submitted detailed position reports for examination by TU-3 and a board convened by CTG-7.4 (see Section 1.5) to determine ultimate operational safety of the project aircraft. To assist in safety considerations, a policy directive was published; it set forth experimental limits and provided controlled procedures in case it was desired to exceed the limits during the test series.

In general, gust response limits were set at 80 percent of design limit for Shot Cherokee, 85 percent of limit for Shot Zuni, and 95 percent of limit for other shots. Over-pressure limits were imposed to prevent canopy, radome, or skin damage that could affect safe flight. Thermal-effect responses were limited to total temperatures in thin skins of 500 degrees F. Radiation dosage was limited to a total of 3.9 r.

Exceptions to the above criteria were made toward the end of the test series. Project Officers were required to submit, in writing, complete justification for each exception, with their best estimate of the effect of the exception on the safety of the aircraft. After approval both from the technical and safety standpoints, the proposed positions were submitted to the TG-7.4 Safety Board for consideration. Responsibility for ultimate aircraft safety lay with CTG-7.4, as operational commander for all air operations in the PPG.

These detailed procedures resulted in complete success of the aircraft projects in obtaining desired technical data with controlled safety of flight.

6.3.2 Aircraft-Positioning Systems. To position the aircraft at the precise locations in space and to have a complete record of the flight paths at time zero and at time of shock arrival, various aircraft and ground electronic positioning systems were utilized.

For all program aircraft on Bikini events, an electronic tracking system—the Raydist navigation system by Hastings Corporation of Hampton, Virginia—was used to determine actual positions. The F-84F's, F-101A, and A3D-1 also used Raydist to position the aircraft at Bikini, whereas the B-47, B-52, B-66, and B-57 used their aircraft radar bombing systems to attain desired flight paths and positions.

The Raydist system involved ground master, relay, and reference stations to provide intersecting fields of hyperbolic functions (similar to Loran and Shoran) in conjunction with aircraft transponders to measure ultimately the path of the aircraft with respect to the Raydist electronic fields. In the case of the fighters and the A3D-1, the flight paths were then compared at the master station with a desired flight path tape and corrections were telemetered to each aircraft. Indications in the cockpit then relayed flight path information to the pilot. The Air Force bomber aircraft made visual and radar bombing runs to attain desired tracks and positions.

Task Group 7.4 maintained surveillance over each aircraft through Identification Friend or Foe (IFF) indicator scopes in the Combat Information Center (CIC) on board the USS Estes off Bikini. Aircraft out of position along their tracks were advised by the CIC controllers. In critical situations, the aircraft were aborted before time zero.

At Eniwetok, all bomber aircraft positioned themselves by the aircraft radar bombing systems and photo records of bombing-system coordinates. Scope photographs provided records of actual positions at all critical times. Fighter aircraft at Eniwetok were both positioned and tracked by MSQ-1A radar control systems in conjunction with Boeing data-recorded vans. The radar control systems were similar to Ground Controlled Approach

(GCA) radar equipment. The Boeing data recorders provided, after each event, positions at time zero and time of shock arrival.

Again, a surveillance system of IFF scopes was set up at the Air Operations Center (AOC) on Eniwetok by TG-7.4. Position advice and, when necessary, abort directives were given verbally to the pilots.

6.3.3 Positioning Yields. With the problems inherent in position planning and attainment described above, a real cause for concern in the attempt to obtain desired technical information was the uncertainty of predictable yield figures for the various events. For the purpose of Program 5 aircraft requirements, the scientific laboratories were asked to specify an aircraft-positioning yield as a value that would be safe to use. This positioning yield took into account the maximum unknowns of device performance and was used as a basis for positioning aircraft from the standpoint of prediction of weapon effects. Table 6.1 gives this positioning-yield information.

In most cases, especially with the multimegaton devices, the resultant actual yields were approximately 35 to 70 percent of the positioning yields. The consistently wide variation in the two yields made it extremely difficult to obtain inputs and responses in the desired range. Sound experimental procedures would not allow aircraft to be positioned to obtain near-destructive responses at positioning yields in order to get desired responses at expected (actual) yields. The problem was discussed with the scientific personnel of the laboratories, and the positioning yields of Shots Dakota and Huron were lowered toward more realistic values. These two shots, in general, provided the best results for participating aircraft in the series. In the case of Dakota, although the actual yield was higher than the preshot positioning yield, inherent safety in program and project positioning methods and philosophies obviated any dangerous responses.

6.4 RESULTS

In general, the objectives of the program were realized. There should be no requirement to retest any of the project aircraft in subsequent test series. The analytical methods to predict blast phenomena were verified within the accuracies of yield determination and instrumentation results. However, a real conservatism in the prediction methods for thermal inputs was noted. Predicted values were usually significantly higher than measured values. Consequently, lower radiant exposures resulted in smaller temperature rises in structural members. The various white protective paints used, with their low absorptivities (0.15 to 0.25), also proved to be excellent protection against temperature rises. Toward the middle of the operation, a modification of the methods of prediction of thermal inputs plus the use of gray and black panels resulted in obtaining thermal exposures in the desired range. A more precise method of prediction of thermal input and response mechanisms resulted from Operation Redwing.

Conservatism was also noted in the prediction methods of total dosage from nuclear radiation. Aircrews received about half of the predicted doses. With delivery of lower yield kiloton-range weapons by high-speed fighter-type aircraft, the importance of being able to predict radiation fields becomes paramount.

In obtaining the energy inputs and noting the resultant responses during Redwing, it became evident the primary structural components were not always the limiting items on the aircraft. Results indicate that secondary structural items and miscellaneous non-

load-carrying items of the aircraft restrict the delivery capability of the aircraft. The bomb-bay doors and the forward-wheel well doors of the B-47E were moderately damaged at 0.84 psi during Shot Dakota. The B-52 bomb-bay doors and various aerodynamic seals were damaged by both the thermal input and an overpressure of 0.87 psi on the same shot. The B-47 and B-57 both sustained wrinkled control surfaces (thin-skin structure) because of high thermal inputs. The honeycomb skin in the F-101A was a thermal limiting item, with the skin on the stabilator and wing becoming unbonded with a temperature rise of approximately 450 degrees F. At higher temperatures the material may deteriorate rapidly, with consequent control problems. Minor items of the aircraft, such as inspection doors and tailpipe braces, also failed. These findings have been considered in later aircraft design and have resulted in modification of more advanced models.

Tables 6.2 through 6.9 give information on the positioning of the aircraft for the various shots and the amount of thermal radiation and blast overpressures actually received.

Project 5.7 obtained data from cameras, radiometers, and calorimeters mounted on four project aircraft. The parameters of significance in the prediction of thermal radiant exposure at a point in space as a result of a nuclear detonation included fireball size, shape, rate of rise, color temperature, black-body quality, albedo effects, and the variation of spectral distribution as a function of time.

Radiant exposure and irradiance were measured for 10 events and spectra for 11 events. Filters were used with many of the instruments, isolating various parts of the visible and near-infrared spectrum. Records were obtained from the calorimeters and instruments aimed directly at the fireball, toward the water beneath the aircraft, and pointing away from the fireball. The purpose of the latter was to measure the back scattered radiation.

The thermal records reaffirm the reduced transmission of radiant energy in the near infrared because of absorption by water vapor and carbon dioxide.

The equation developed in Reference 6 for predicting the radiant exposure on a horizontal surface and its modification to a surface oriented normal to the fireball was tested against the Redwing data and was found to satisfactorily predict the radiant exposure.

Comparison between the air drop event, Cherokee, and a surface shot of similar yield, Zuni, indicated no significant differences in the irradiances or radiant exposures measured at the aircraft.

Measurements of the back-scattered radiation, where available, were found to be two or three orders of magnitude lower than the radiant energy received directly from the fireball. Tables 6.10 and 6.11 show the effectiveness of thermal instrumentation and the summary of the thermal exposure and maximum irradiance.

The photographic records of the Redwing series were taken at 64 frames/sec on 16-mm high resolution emulsions, from aircraft at slant ranges on the order of several kilometers from ground zero. Tables 6.12 and 6.13 show the effectiveness of photographic instrumentation and the aircraft positions at T_0 .

Such ancillary features as the Wilson cloud, plume, and bright spots appearing near shock wave breakaway, were found to perturb the thermal output by less than 15 percent. The air shock appears to attenuate the blue light; the shocked volume is visible in the infrared because of scattering from the denser air. No polarization phenomena, other than the expected difference in specular scattering from the undisturbed ocean surface, were resolved.

It was found that an attenuating mantle—absorption shell—surrounds the fireball from after breakaway until the end of the thermal pulse. This shell develops to a thickness of about a fourth of the fireball radius; it is somewhat more strongly attenuating in the blue than the infrared.

The spectral histories of all events appear quite similar, regardless of the yield; a large amount of NO_2 is formed quite early in the bomb history and persists throughout the entire event.

Aureole (air-scattered) light was found to be an order of magnitude more intense than the albedo of the unshocked water surface, for the typical moist atmospheric conditions of the Pacific Proving Grounds. This aureole is white and unpolarized. The shock froth albedo is about 12 times the unshocked water albedo. In general, the total red albedo entering typical camera fields of view, which is scattered from aureole, clouds, and water, is about equal to the direct flux from the fireball. The blue albedo is lower, presumably because of the air shock attenuation. Furthermore, the blue fireball shows considerably more limb darkening.

Both air shock and fireball dimensions were found to obey the expected scaling laws. There is evidence that the fireball surface temperature is not symmetric with azimuth in some cases, because the thermal flux appears higher from certain (large) regions.

Project 5.9 mounted 103 specimens for Shots Erie and Mohawk; 88 were recovered. Results of the material evaluation studies showed that 8-inch diameter spheres of stainless steel, molybdenum, and titanium sustained approximately equal mass ablation of 0.08 lb/in^2 at 100 feet and 0.06 lb/in^2 at the 200-foot range. Copper sustained two to four times the mass ablation of the above three metals, and plastic experienced substantially less than any of the metals for the exposure conditions on Shot Erie. It was shown that removal of a molten layer by spinning off drops of the material could lead to total ablation and would be important in ICBM destruction if the missile has an appreciable angular velocity. Table 6.14 summarizes the test specimen exposures.

TABLE 6.1 POSITIONING YIELD INFORMATION

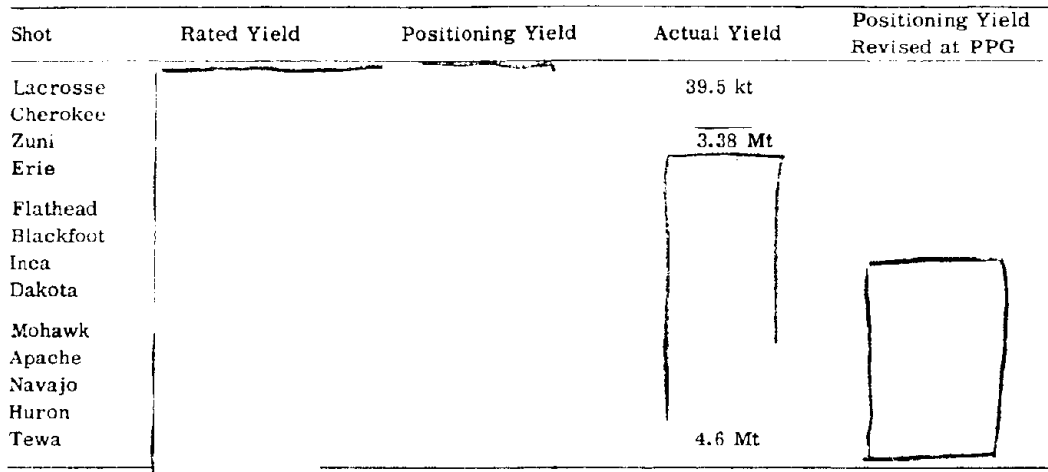


TABLE 6.2 SUMMARY DATA ON PROJECT 5.1

T_0 is time of detonation. T_{sa} is time of shock arrival.

Shot	Absolute Altitude feet	Horizontal Range at T_0 feet	Horizontal Range at T_{sa} feet	Radiant Exposure cal/cm ²	Peak Overpressure psi	Percent of Design Limit
Cherokee	38,000	53,800	156,700	10.19	—	39 Wing
Zuni	31,000	32,500	82,500	21.28	0.40	54 Wing
Flathead	38,000	3,400	33,300	3.64		82 Wing
Dakota	24,100	10,400	29,400	21.20		95 Wing
Huron	22,500	46,000	39,000	—		61 Wing
Mohawk	37,000	51,000	42,300	—		63 Wing
Apache	30,000	29,000	79,500	9.03		48 Wing
Navajo	33,800	33,300	88,900	20.69		59 Wing
Tewa	34,200	25,600	69,600	24.46	0.57	68 Wing

TABLE 6.3 SUMMARY DATA ON PROJECT 5.2

T_0 is time of detonation. T_{sa} is time of shock arrival.

Shot	Absolute Altitude feet	Horizontal Range at T_0 feet	Horizontal Range at T_{sa} feet	Radiant Exposure cal/cm ²	Peak Overpressure psi	Percent of Design Limit
Cherokee	31,000	35,800	85,200	34.6		55 Wing
Zuni	32,000	23,800	62,400	34.9	0.55	63 Wing
Dakota	22,000	11,500	32,700	28.6		87 Hor. Stab.
Mohawk	25,000	8,200	33,400	9.0		63 Wing
Apache	34,000	18,600	53,800	15.6		62 Wing
Navajo	38,000	18,300	53,300	41.9		95 Hor. Stab.
Tewa	41,000	26,700	81,000	21.5	0.36	55 Wing
Huron	20,000	5,700	23,200	8.2		64 Hor. Stab.

TABLE 6.4 SUMMARY DATA ON PROJECT 5.3

T₀ is time of detonation. T_{sa} is time of shock arrival.

Shot	Absolute Altitude feet	Horizontal Range at T ₀ feet	Horizontal Range at T _{sa} feet	Radiant Exposure cal/cm ²	Peak Overpressure psi	Percent of Design Limit
Cherokee	34,000	47,758	139,571	34.0	0.400	52 Wing
Zuni	14,000	27,000	97,760			
Flathead	16,000	17,800	59,100			
Dakota	16,000	13,100	35,050			
Apache	8,000	23,500	60,500			
Navajo	—	—	—			
Huron	9,894	8,768	23,386			
Tewa	19,000	27,250	65,750	0.900	65 Wing	

TABLE 6.5 SUMMARY DATA ON PROJECT 5.4

T₀ is time of detonation. T_{sa} is time of shock arrival.

Shot	Absolute Altitude feet	Horizontal Range at T ₀ feet	Horizontal Range at T _{sa} feet	Radiant Exposure cal/cm ²	Peak Overpressure psi	Percent of Design Limit
Lacrosse	13,700	6,750	28,200	1.17	0.283	35 Wing
Zuni	16,900	34,000	—	10.55		
Erie	10,450	3,829	14,000	10.55		
Flathead	25,700	13,466	44,659			
Inca	9,815	2,624	11,572			
Dakota	17,650	16,960	43,630			
Apache	10,200	28,516	45,375			
Huron	16,200	10,000	31,493	40 Wing		

TABLE 6.6 SUMMARY DATA ON PROJECT 5.5 CAPABILITIES AIRCRAFT (F-84F)

T₀ is time of detonation. T_{sa} is time of shock arrival.

Shot	Absolute Altitude feet	Horizontal Range at T ₀ feet	Horizontal Range at T _{sa} feet	Radiant Exposure cal/cm ²	Peak Overpressure psi	Percent of Design Limit
Lacrosse	15,200	8,640	600	1.65	0.80	51 Wing
Flathead	21,000	900	14,935			
Dakota	20,374	300	11,065			
Mohawk	19,920	3,729	19,700			
Apache	31,614	18,614	64,300			
Navajo	16,865	25,200	57,400			
						10 Wing

TABLE 6.7 SUMMARY DATA ON PROJECT 5.5 RESEARCH AIRCRAFT (F-84F)

T₀ is time of detonation. T_{sa} is time of shock arrival.

Shot	Absolute Altitude feet	Horizontal Range at T ₀ feet	Horizontal Range at T _{sa} feet	Radiant Exposure cal/cm ²	Peak Overpressure psi	Percent of Design Limit
Lacrosse	10,200	26,100	22,900		—	—
Cherokee	28,000	135,500	103,700			43 Side
Zuni	33,000	215,100	160,200		0.10	15 Side
Erie	6,100	14,500	12,300			70 Side
Flathead	18,000	40,400	33,100			60 Side
Dakota	23,400	39,900	30,400			69 Side
Mohawk	23,300	27,800	22,800			49 Side
Apache	35,649	44,000	35,000			52 Side
Navajo	32,047	90,500	74,000			52 Side
Huron	17,900	13,300	9,500			60 Side

TABLE 6.8 SUMMARY DATA ON PROJECT 5.6

T₀ is time of detonation. T_{sa} is time of shock arrival. Negative values indicate position short of ground zero; positive values beyond ground zero.

Shot	Absolute Altitude feet	Horizontal Range at T ₀ feet	Horizontal Range at T _{sa} feet	Radiant Exposure cal/cm ²	Peak Overpressure psi	Percent of Design Limit
Lacrosse	12,000	-3	+10,660	<u>2.53</u>	0.68	75 Stab.
Erie	11,850	-7,500	-346			41 Stab.
Flathead	26,800	-330	+22,628			27 Stab.
Kickapoo	7,700	-1,600	+3,950			17 Stab.
Inca	9,000	-5,780	+580			85 Stab.
Dakota	26,000	-900	+16,770			62 Stab.
Mohawk	21,950	+8,050	Outran shock			—
Apache	14,900	+20,000	+89,500			10 Stab.
Navajo	14,700	+24,000	+54,700			15 Stab.

TABLE 6.9 SUMMARY DATA ON PROJECT 5.8

T₀ is time of detonation. T_{sa} is time of shock arrival.

Shot	Absolute Altitude feet	Horizontal Range at T ₀ feet	Horizontal Range at T _{sa} feet	Radiant Exposure cal/cm ²	Peak Overpressure psi	Percent of Design Limit
Cherokee	34,100	57,500	190,000			—
Zuni	28,170	32,059	96,474	<u>23.7</u>	<u>0.34</u>	41 Gust
Flathead	14,050	12,738	32,440			61 Gust
Apache	26,000	26,000	81,500			—
Navajo	36,100	26,170	79,665			—
Tewa	36,310	30,000	96,700	<u>23.0</u>	<u>0.32</u>	—
Huron	12,050	16,800	48,000			54 Gust

TABLE 6.10 EFFECTIVENESS OF THERMAL INSTRUMENTATION

Shot	Participation	Sensors Pointed at Ground Zero		Sensors Pointed Vertically Down		Sensors Oriented for Back-scatter		Total Number of Sensors		Percent Effective
		Number Operated	Usable Records Obtained	Number Operated	Usable Records Obtained	Number Operated	Usable Records Obtained	Number Operated	Usable Records Obtained	
Lacrosse	B-57	18	15	3	3	0	0	21	18	85
	B-66	18	0	3	0	0	0	21	0	0
	Total	36	15	6	3	0	0	42	18	43
Cherokee	B-47	18	18	3	3	6	1	27	22	81
	B-52	18	17	3	3	2	2	23	22	96
	B-57	18	0	3	0	0	0	21	0	0
	B-66	18	12	3	3	0	0	21	15	80
	Total	72	47	12	9	8	3	92	59	64
Zuni	B-47	18	18	3	3	6	2	27	23	85
	B-52	18	16	3	3	2	2	23	21	91
	B-57	18	16	3	2	0	0	21	18	86
	B-66	18	18	3	3	0	0	21	21	100
	Total	72	68	12	11	8	4	92	83	90
Erie	B-57	18	15	3	3	0	0	21	18	85
	B-66	18	0	3	0	0	0	21	0	0
	Total	36	15	6	3	0	0	42	18	43
Flathead	B-47	18	18	3	3	6	6	27	27	100
	B-52	18	0	3	0	2	0	23	0	0
	B-57	18	17	4	4	0	0	22	21	95
	B-66	18	18	3	3	0	0	21	21	100
	Total	72	53	13	10	8	6	93	69	74
Inca	B-57	18	0	4	0	0	0	22	0	0
	B-66	18	0	3	0	0	0	21	0	0
	Total	36	0	7	0	0	0	43	0	0
Dakota	B-47	18	15	3	3	6	5	27	23	85
	B-52	18	14	3	3	2	2	23	19	82
	B-57	18	16	4	4	0	0	22	20	91
	B-66	18	14	3	2	0	0	21	16	76
	Total	72	59	13	12	8	7	93	78	84
Mohawk	B-47	*	*	3	1	6	6	9	7	78
	B-52	18	17	3	3	2	2	23	22	95
	B-57	18	0	4	0	0	0	22	0	0
	B-66	18	0	3	0	0	0	21	0	0
	Total	54	17	13	4	8	8	75	29	39
Apache	B-47	18	17	3	3	6	3	27	23	85
	B-52	18	18	3	3	2	2	23	23	100
	B-57	18	17	4	4	0	0	22	21	95
	B-66	18	14	3	3	0	0	21	17	78
	Total	72	66	13	13	8	5	93	84	90
Navajo	B-47	18	18	3	3	6	5	27	26	96
	B-52	18	17	3	3	2	2	23	22	96
	B-66	18	0	3	0	0	0	21	0	0
	Total	54	35	9	6	8	7	71	48	68
Tewa	B-47	18	18	3	3	5	4	26	25	96
	B-52	18	17	3	3	2	2	23	22	96
	B-66	18	14	3	3	0	0	21	17	81
	Total	54	49	9	9	7	6	70	64	91
Huron	B-47	†	†	3	2	6	6	9	8	89
	B-52	18	18	3	3	2	2	23	23	100
	B-57	18	18	4	4	0	0	22	22	100
	B-66	18	14	3	3	0	0	21	17	81
	Total	54	50	13	13	8	8	75	70	93

* In this shot, the B-47 was positioned for side loads. None of the tail instrumentation was operated.

† In this shot, the B-47 was positioned for side loads. Only one very sensitive instrument was operated in the tail instrument position and was a back-scatter instrument. The output of this instrument was simultaneously recorded on an oscillograph and on frequency-modulated magnetic tape.

TABLE 6.11 THERMAL EXPOSURE AND MAXIMUM IRRADIANCE

Shot	Instrument, Field of View - Filter	Aircraft, Station, Orientation	Slant Range, D km	Radiant Exposure, D cal/cm ²	Maximum Irradiance, Q cal/cm ² -sec	$E = \frac{QD^2}{W}$ cal-km ² cm ² -kt	$\frac{D}{Q\sqrt{A}}$ cal/cm ²	$E = \frac{Q\sqrt{D^3}}{WA}$ cal-km ² cm ² -kt
Lacrosse	C-90-Q	57-1-F	4.68	1.42		0.78		
	C-160-A	57-2-V		0.84			0.94	0.53
	C-160-Q	57-1-F	(15,350 ft)	1.34		0.75		
	C-160-Q	57-2-V		1.21			1.36	0.75
	C-90-A	57-1-F		1.03				
	C-90-B	57-1-F		0.50				
	C-90-E	57-1-F		1.17				
	R-90-Q	57-1-F		1.42	2.39	0.78		
	R-90-Q	57-1-F		1.57	2.48	0.88		
	B-47 No results							
	B-66 No results							
Cherokee	C-90-B	47-1-F						
	C-160-A	47-2-V						
	C-90-A	47-1-F						
	C-160-Q	47-1-F						
	C-90-D	47-1-F						
	C-90-E	47-1-F						
	R-90-Q	47-1-F						
	R-90-Q	47-1-F						
	R-90-Q	47-1-F						
	B-57 No results							
	C-160-Q	66-1-F						
	C-90-Q	66-1-F						
	C-45-Q	66-1-F						
	C-160-Q	66-2-V						
	C-160-B	66-1-F						
	R-90-Q	66-1-F						
	R-90-Q	66-1-F						

TABLE 6.11 CONTINUED

Shot	Instrument Field of View - Filter	Aircraft, Station, Orientation	Slant Range, D km	Radiant Exposure, Q cal/cm ²	Maximum Irradiance, H cal/cm ² -sec	E = $\frac{QD^2}{W}$ cal-km ² cm ² -kt	Q _v A cal/cm ²	E = $\frac{Q_v D^3}{WA}$ cal-km ³ cm ² -kt	
Zuni	C-160-Q	47-2-V	13.99	18.6			27.6	1.54	
	C-160-A	47-2-V		13.0			14.3	1.08	
	C-90-Q	47-1-F	(45,910 ft)	27.3		1.53			
	C-90-D	47-1-F		26.6					
	C-90-E	47-1-F		23.5					
	C-90-F	47-1-F		23.8					
	C-90-B	47-1-F		9.17					
	C-90-B+Ge	47-1-F		9.76					
	C-90-Q	47-1-F		29.5		1.64			
	R-90-Q	47-1-F		20.1	5.13	1.13			
	R-90-Q	47-1-F		35.5	8.62	1.99			
	R-90-Q	47-1-F		35.7	8.65	1.99			
	B-57 No results								
	C-90-A	66-1-F		11.97	21.3				
	C-160-Q	66-1-F			29.9				
	C-160-Q	66-2-V	(39,260 ft)		18.7		1.23	38.8	1.58
	C-90-Q	66-1-F			30.3		1.24		
C-90-F	66-1-F			23.7					
C-45-Q	66-1-F			28.6		1.16			
C-160-A	66-2-V			10.9			22.5	0.92	
C-21-Q	66-1-F			14.6		0.58			
C-90-B	66-1-F			9.30					
C-90-D	66-1-F			27.1					
C-90-E	66-1-F			3.31					
C-90-A	66-1-F			21.2					
C-90-D	66-1-F			27.1					
R-90-Q	66-1-F			15.0	4.57	0.61			
R-90-Q	66-1-F			29.8	7.75	1.21			
Erie									
B-47 No results									
C-90-Q	57-1-F		3.41						
C-160-Q	57-2-V	(11,170 ft)							
C-90-B	57-1-F								
C-160-Q	57-1-F								
C-160-A	57-1-F								
C-90-A	57-2-V								
C-90-B	57-1-F								
C-90-E	57-1-F								
C-90-D	57-1-F								
R-90-Q	57-1-F								
R-90-Q	57-1-F								

Shot	Instrument, Field of View - Filter	Aircraft, Station, Orientation	Slant Range, D km	Radiant Exposure, Q cal/cm ²	Maximum Irradiance, H cal/cm ² -sec	$E = \frac{QD^2}{W}$ cal-km ² cm ² -kt	$\frac{D}{Q\sqrt{A}}$ cal/cm ²	$E = \frac{Q\sqrt{D^3}}{WA}$ cal-km ² cm ² -kt	
	B-66 No results								
Flathead	C-160-Q	47-1-F	11.64 (38,190 ft)						
	C-160-Q	47-2-V							
	C-160-A	47-2-V							
	C-90-Q	47-1-F							
	C-90-D	47-1-F							
	C-90-F	47-1-F							
	C-90-F	47-1-F							
	C-90-B	47-1-F							
	C-90-B	47-1-F							
	C-90-A	47-1-F							
	C-90-A	47-1-F							
	C-45-Q	47-1-F							
	C-21-Q	47-1-F							
	C-90-Q	47-1-F							
	C-90-E	47-1-F							
	R-90-Q	47-1-F							
	C-90-Q	57-1-F		8.91 (29,240 ft)					
	C-160-Q	57-2-V							
	C-160-Q	57-1-F							
	C-160-A	57-2-V							
	C-90-Q	57-1-F							
	C-90-A	57-1-F							
	C-90-B	57-1-F							
	C-90-D	57-1-F							
	C-90-E	57-1-F							
	R-90-Q	57-1-F							
	R-90-Q	57-1-F							
	C-90-A	66-1-F	7.41 (24,310 ft)						
	C-160-Q	66-2-V							
	C-160-Q	66-1-F							
	C-90-E	66-1-F							
	C-90-Q	66-1-F							
	C-90-B	66-1-F							
	C-21-Q	66-1-F							
	C-160-A	66-2-V							
	C-90-D	66-1-F							
	R-90-Q	66-1-F							
	R-90-Q	66-1-F							
Dakota	C-160-Q	47-1-F		8.09 (26,550 ft)					
	C-160-Q	47-2-V							
	C-160-Q	47-2-V							

TABLE 6.11 CONTINUED

Shot	Instrument Field of View - Filter	Aircraft, Station, Orientation	Slant Range, D km	Radiant Exposure, Q cal/cm ²	Maximum Irradiance, H cal/cm ² -sec	$E = \frac{QD^2}{W}$ cm ² -kt	$E = \frac{QD^2}{WA}$ cal/cm ²	$E = \frac{Q_v D^3}{WA}$ cal-km ² cm ² -kt
Dakota	C-160-A	47-2-V						
	C-90-Q	47-1-F						
	C-90-Q	47-1-F						
	C-90-Q	47-1-F						
	C-90-D	47-1-F						
	C-90-E	47-1-F						
	C-90-A	47-1-F						
	C-90-A	47-1-F						
	C-90-B	47-1-F						
	C-160-Q	47-1-F						
	C-45-Q	47-1-F						
	C-90-B+Ge	47-1-F						
	C-21-Q	47-1-F						
	C-90-Q	47-1-F						
	R-90-Q	47-1-F						
	R-90-Q	47-1-F						
	C-90-Q	57-1-F	7.63					
	C-90-C	57-1-F						
	C-90-Q	57-2-V	(25,020 ft)					
	C-160-Q	57-2-V						
	C-160-A	57-2-V						
	C-90-A	57-1-F						
	C-90-B	57-1-F						
	C-90-D	57-1-F						
	C-90-E	57-1-F						
	R-90-Q	57-1-F						
	R-90-Q	57-1-F						
	C-90-A	66-1-F	6.47					
	C-160-Q	66-2-V						
	C-160-Q	66-1-F	(21,210 ft)					
	C-90-E	66-1-F						
	C-90-Q	66-1-F						
	C-90-B	66-1-F						
	C-21-Q	66-1-F						
	C-160-A	66-2-V						
	C-90-D	66-1-F						
	R-90-Q	66-1-F						
	R-90-Q	66-1-F						

Shot	Instrument, Field of View - Filter	Aircraft, Station, Orientation	Slant Range, D km	Radiant Exposure, Q cal/cm ²	Maximum Irradiance, H cal/cm ² -sec	$E = \frac{QD^2}{W}$ cal-km ² cm ² -kt	$Q_v \frac{D}{A}$ cal/cm ²	$E = \frac{Q_v D^3}{WA}$ cal-km ³ cm ² -kt
Apache	C-160-Q	47-1-F	12.95 (42,490 ft)					
	C-160-Q	47-2-V						
	C-90-Q	47-2-V						
	C-90-Q	47-1-F						
	C-90-F	47-1-F						
	C-90-E	47-1-F						
	C-90-F	47-1-F						
	C-90-A	47-1-F						
	C-160-Q	47-1-F						
	C-90-Q	47-1-F						
	C-90-B	47-1-F						
	C-90-D	47-1-F						
	R-90-Q	47-1-F						
	C-90-C	57-1-F						
	C-160-Q	57-2-V						
	C-160-Q	57-1-F						
	C-160-A	57-2-V						
	C-90-Q	57-1-F						
	C-90-A	57-1-F						
	C-90-D	57-1-F						
C-90-E	57-1-F							
R-90-Q	57-1-F							
R-90-Q	57-1-F							
Navajo	C-160-Q	66-1-F	7.87 (25,820 ft)					
	C-90-Q	66-1-F						
	C-90-B	66-1-F						
	C-45-Q	66-1-F						
	C-160-Q	66-2-V						
	C-160-A	66-2-V						
	C-21-Q	66-1-F						
	C-90-D	66-1-F						
	R-90-Q	66-1-F						
	C-160-Q	47-1-F						
	C-160-Q	47-2-V						
	C-90-Q	47-2-V						
	C-160-A	47-2-V						
	C-90-Q	47-1-F						
	C-90-F	47-1-F						
C-160-Q	47-1-F							
C-45-Q	47-1-F							
C-21-Q	47-1-F							
C-90-Q	47-1-F							

TABLE 6.11 CONTINUED

Shot	Instrument, Field of View - Filter	Aircraft, Station, Orientation	Slant Range, D km	Radiant Exposure, Q cal/cm ²	Maximum Irradiance, H cal/cm ² -sec	$E = \frac{QD^2}{W}$ cal/km ² cm ² -kt	$Q_v \frac{D}{A}$ cal/cm ²	$E = \frac{Q_v D^2}{WA}$ cal-km ² cm ² -kt
	C-90-A	47-1-F		28.2				
	C-90-D	47-1-F		26.4				
	C-90-E	47-1-F		22.6				
	C-90-B	47-1-F		10.5				
	R-90-Q	47-1-F		37.5				
	R-90-Q	47-1-F		25.8				
	B-57 No results							
	B-66 No results							
Tewa	C-160-Q	47-1-F	13.30	21.8		0.78	32.7	1.24
	C-160-Q	47-2-V		25.5			25.9	0.92
	C-160-A	47-2-V	(43,640 ft)	20.2				
	C-90-Q	47-1-F		29.5		1.05		
	C-90-D	47-1-F		29.0				
	C-90-E	47-1-F		29.2				
	C-90-F	47-1-F		27.6				
	C-90-F	47-1-F		24.8				
	C-90-A	47-1-F		12.7				
	C-160-Q	47-1-F		32.6		1.14		
	R-90-Q	47-1-F		35.6	8.63	1.26		
	R-90-Q	47-1-F		35.0	9.34	1.23		
	B-57 No results							
	C-160-Q	66-1-F	10.52	40.9		0.91	10.8	0.24
	C-90-Q	66-2-V		5.92				
	C-90-Q	66-1-F	(34,500 ft)	42.3		0.94		
	C-90-D	66-1-F		38.1				
	C-45-Q	66-1-F		37.4		0.84		
	C-160-Q	66-1-F		26.3		0.59		
	C-160-A	66-2-V		17.9			32.51	0.73
	C-21-Q	66-1-F		20.3		0.45		
	R-90-Q	66-1-F		50.1	11.2	1.11		
	R-90-Q	66-1-F		54.5	12.8	1.21		
Huron	B-47 No results							
	C-160-Q	57-2-V	5.92					
	C-90-Q	57-1-F						
	C-90-C	57-1-F	(19,410 ft)					
	C-90-Q	57-2-V						
	C-160-Q	57-1-F						
	C-160-A	57-2-V						

TABLE 6.11 CONTINUED

Shot	Instrument, Field of View - Filter	Aircraft, Station, Orientation	Slant Range, D km	Radiant Exposure, Q cal/cm ²	Maximum Irradiance, H cal/cm ² -sec	E = $\frac{QD^2}{W}$ cal-km ² cm ² -kt	$\frac{D}{QVA}$ cal/cm ²	E = $\frac{QVD^3}{WA}$ $\frac{\text{cal-km}^2}{\text{cm}^2\text{-kt}}$
C-90-Q		57-1-F						
C-90-A		57-1-F						
C-90-B		57-1-F						
C-90-D		57-1-F						
C-90-E		57-1-F						
R-90-Q		57-1-F						
R-90-Q		57-1-F						
C-160-Q		66-1-F	4.12					
C-90-A		66-1-F						
C-90-Q		66-1-F	(13,520 ft)					
C-90-F		66-1-F						
C-45-Q		66-1-F						
C-90-B		66-1-F						
C-90-D		66-1-F						
R-90-Q		66-1-F						
R-90-Q		66-1-F						

* Radiometer data inconsistent. † Large contribution from the tail of the radiometer trace. ‡ Radiometer trace fell off very slowly after second maximum.

TABLE 6.12 EFFECTIVENESS OF PHOTOGRAPHIC INSTRUMENTATION

Shot	Participation	Backscatter		Albedo		Red Filtered Fireball		Blue Filtered Fireball		Polaroid		Total	
		Number Operated	Records Obtained	Number Operated	Records Obtained	Number Operated	Records Obtained	Number Operated	Records Obtained	Number Operated	Records Obtained	Number Operated	Records Obtained
Erie	B-57	0	0	2	2	1	1	1	0	0	0	4	3
	B-66	0	0	2	0	2	0	2	0	2	0	8	0
	Total	0	0	4	2	3	1	3	0	2	0	12	3
Lacrosse	B-57	0	0	2	2	1	0	1	1	0	0	4	3
	B-66	0	0	2	0	2	0	4	0	0	0	8	0
	Total	0	0	4	2	3	0	5	1	0	0	12	3
Huron	B-47	1	1	2	2	0	0	0	0	0	0	3	3
	B-52	1	1	1	1	2	2	1	1	0	0	5	5
	B-57	0	0	2	2	2	2	2	2	0	0	6	6
	B-66	0	0	4	3	1	1	1	1	0	0	6	5
	Total	2	2	9	8	5	4	4	4	0	0	20	19
Mohawk	B-47	1	1	2	0	0	0	0	0	0	0	3	1
	B-52	2	1	2	2	2	1	2	1	0	0	8	5
	B-57	0	0	2	0	1	0	1	0	0	0	4	0
	B-66	0	0	4	4	1	1	1	1	0	0	6	6
	Total	3	2	10	6	4	2	4	2	0	0	21	12
Flathead	B-47	1	1	2	1	2	1	2	2	0	0	7	5
	B-52	2	0	2	0	2	0	2	0	0	0	8	0
	B-57	0	0	2	2	1	1	1	1	0	0	4	4
	B-66	0	0	4	3	1	1	1	1	2	2	8	7
	Total	3	1	10	6	6	3	6	4	2	2	27	16
Dakota	B-47	1	1	2	2	2	1	2	2	0	0	7	6
	B-52	2	2	2	1	2	2	2	1	0	0	8	6
	B-57	0	0	2	2	1	1	1	1	0	0	4	4
	B-66	0	0	2	1	2	2	2	2	2	2	8	7
	Total	3	3	8	6	7	6	7	6	2	2	27	23
Apache	B-47	1	0	2	2	2	2	2	1	0	0	7	5
	B-52	2	0	2	2	2	2	2	1	0	0	8	5
	B-57	0	0	2	2	0	0	0	0	2	2	4	4
	B-66	0	0	6	6	1	1	1	1	0	0	8	8
	Total	3	0	12	12	5	5	5	3	2	2	27	22
Zuni	B-47	1	1	2	2	2	2	2	2	0	0	7	7
	B-52	2	1	2	2	2	2	2	2	0	0	8	7
	B-57	0	0	2	2	1	1	1	1	0	0	4	4
	B-66	0	0	6	6	1	1	1	1	0	0	8	8
	Total	3	2	12	12	6	6	6	6	0	0	27	26
Cherokee	B-47	1	0	2	0	1	0	1	0	3	0	8	0
	B-52	2	1	2	2	1	1	1	0	3	3	9	7
	B-57	0	0	2	0	1	0	1	0	0	0	4	0
	B-66	0	0	6	6	1	1	1	1	0	0	8	8
	Total	3	1	12	8	4	2	4	1	6	3	29	15
Tewa	B-47	1	1	2	2	2	2	2	2	0	0	7	7
	B-52	1	1	1	1	2	2	1	1	0	0	5	5
	B-66	0	0	6	6	1	1	1	1	0	0	8	8
	Total	2	2	9	9	5	5	4	4	0	0	20	20
Navajo	B-47	1	1	2	1	2	2	2	2	0	0	7	6
	B-52	1	0	2	2	1	1	2	0	0	0	7	3
	B-66	0	0	5	4	1	0	1	1	0	0	7	5
	Total	2	1	9	7	5	3	5	3	0	0	21	14
Inns	B-57	0	0	2	2	1	1	1	1	0	0	4	4
	B-66	0	0	2	0	2	0	2	0	2	0	6	0
	Total	0	0	4	2	3	1	3	1	2	0	10	4

TABLE 6.13 AIRCRAFT POSITIONS AT TIME ZERO

Shot and Aircraft	Horiz. Range GZ to A/C ft	Absolute Altitude ft	Ground Speed ft/sec	Aircraft Course deg	Azimuth from GZ deg
Erie					
B-57	3,829	10,450	681	050	052
Lacrosse					
B-57	6,751	13,700	817	137	136
Huron					
B-47	45,974	22,150	744	003	123
B-52	5,700	20,000	753	110	116
B-57	10,223	16,200	775	051	048
B-66	8,768	9,894	771	040	040
Mohawk					
B-47	51,000	37,000	786	021	155
B-52	8,200	25,000	765	136	136
Flathead					
B-47	3,410	38,000	716	306	290
B-57	13,462	25,700	754	119	128
B-66	17,804	16,000	819	118	118
Dakota					
B-47	10,382	24,100	724	272	270
B-52	11,550	22,000	776	282	285
B-57	16,955	17,650	761	119	126
B-66	13,101	16,000	781	127	127
Apache					
B-47	29,000	30,050	745	325	322
B-52	18,550	34,000	746	111	120
B-57	28,517	10,200	492	050	051
B-66	23,500	8,000	748	080	080
Zuni					
B-47	32,500	31,000	750	258	250
B-52	23,850	32,000	763	248	263
B-57	35,460	16,900	807	073	073
B-66	27,000	19,000	843	070	070
Tewa					
B-47	25,640	34,200	736	269	270
B-52	26,700	41,000	760	106	102
B-66	27,243	19,000	779	121	121
Navajo					
B-47	33,342	33,800	758	264	263
B-52	18,300	38,000	758	283	281
B-66	57,552	21,000	770	254	254

TABLE 6.14 SUMMARY OF TEST SPECIMEN EXPOSURE

Shot Erie										
Code	Specimen	Material	Station						Total	
			25	50	100	150	200	250		300
A	Composite specimen	Steel	1	3	2	2	2		10	
B	Composite specimen	Aluminum		1	1	1	1		4	
C	Composite specimen-shielded	Aluminum				1	2		3	
D	Flat plate-grooved-transverse	Steel		1	1	1	1		4	
E	Flat plate-grooved-transverse	Aluminum				1			1	
F	Flat plate-grooved-parallel	Steel				1			1	
G	Sphere	Plastic		1		1		1	4	
H	Sphere	Graphite		1		1		1	3	
I	Sphere	Moly	1		1		1		3	
J	Sphere	S. Steel	1		1		1		3	
K	Sphere	Titanium	1		1		1		3	
L	Sphere	Copper	1	1	1	1	1	1	6	
M	Sphere 32"	Steel		1					1	
N	Sphere 10"	Steel	1	1	1				3	
O	Sphere 8"	Steel		1					1	
P	Sphere 6"	Steel		1					1	
Q	Sphere 4"	Steel		2					2	
R	Cylinder	Plastic		1		1			2	
S	Cylinder	Tantalum	1		1		1		3	
T	Laminated cylinder	Aluminum			3	3			6	
U	Dynamic pressure cylinder	Steel		1		1		1	3	
V	Hollow cylinder (pointed)	Steel		1					1	
W	Hollow cylinder (blunt end)	Steel		1					1	
X	Instrumented sphere 12"	Steel			1	1	1	1	5	
Y	Instrumented sphere 16"	Steel		1					1	
Z	Overpressure sphere	Steel		1	1	1	1	1	6	
AA	Dynamic pressure cylinder (w/plastic insert)	Steel				2			2	
BB	Ballistic cylinder	Steel			1				1	
CC	Ballistic cylinder (w/plastic insert)	Steel			2				2	
DD	Bakelite cylinder	Bakelite			1		1		2	
EE	Cylinders with ceramic inserts	Steel	1	2	1		2		6	
		Totals	8	22	20	19	16	6	3	94
Shot Mohawk										
Code	Specimen	Material	Elevation		Total					
			70 Feet	150 Feet						
N	Sphere 10"	Steel	2		4					
O	Sphere 8"	Steel		2	2					
FF	Spheres with ceramic inserts	Steel		2	2					
GG	Sphere 10"	Aluminum		1	1					
		Totals	2	7	9					

Chapter 7

ELECTROMAGNETIC EFFECTS

7.1 OBJECTIVES

Program 6 consisted of five projects with more activity outside the Pacific Proving Grounds than the other DOD programs. Stations for these projects extended from Hawaii and the western Pacific all the way to the eastern United States.

The objectives of these projects were to: (1) determine the accuracy with which the ground zero of a nuclear detonation could be located by utilizing the generated electromagnetic pulse and to obtain yield data if possible by analysis of the pulse waveform; (2) determine the ionospheric effects of a nuclear detonation; (3) test an airborne fiducial antenna system to be used in a developmental type bhangmeter; (4) measure the radio frequency of electromagnetic radiation from a nuclear detonation; and (5) determine the attenuation of super-high-frequency (SHF) and ultra-high-frequency (UHF) radio waves in the ionized region produced by nuclear explosions.

The project abstracts are given in Section A.6 of the Appendix.

7.2 DETERMINATION OF GROUND ZERO USING ELECTROMAGNETIC PULSE GENERATED BY NUCLEAR DETONATION

This project was implemented by installing two short-baseline Narol (inverse Loran) systems—one in the Hawaiian Islands, about 2,000 nautical miles from ground zero, and one in California, about 4,400 nautical miles from ground zero. Two long-baseline (inverse hyperbolic) systems were established—one in the Hawaiian area, and one deep in the continental United States about 5,800 nautical miles from ground zero.

7.2.1 Short-Baseline System. In normal operations, two short-baseline Narol nets would be required to determine actual ground-zero fixes, but during Redwing each net determined a line of position (LOP) and demonstrated the feasibility of the system. The ability to isolate the bomb pulse from sferics and background noise determines the operational range of the system. The Hawaiian net, located at a distance greater than its estimated operational range, detected and reported each shot before postshot confirmation, and by the end of the operation it was determining and reporting line of position within a half hour after shot time. More difficulty was experienced by the California net. There the exact shot time was needed to identify the bomb pulse on the film record.

Of the 17 shots in the Redwing test series, the Hawaiian net was alerted for 15 and the California net for 14. The equipment operated and recorded data at all stations for these shots. With one exception, lines of position were determined successfully for each shot by the Hawaiian and California nets.

The lines of position determined at the Hawaiian net had an average error of 1.4 nautical miles, while those determined at the California net had an average error of 5.4 nautical miles.

7.2.2 Long-Baseline System. The two inverse-hyperbolic atomic strike recorder networks employed Cytac, a low-frequency, Loran-type, pulsed-signal system operating on 100 kc. The Cytac equipment was used for a fine-measurement synchronizing signal (tenths of a microsecond), and National Bureau of Standards time stations, WWV and WWVH, were used for coarse synchronizing signals (milliseconds). Data was recorded photographically and sent for analysis to a net control station. Information was interchanged between shots, with preliminary data bulletins being issued immediately after each shot.

Of the 17 shots, the Pacific net recorded data on 14 and the continental net recorded data on 11 of them. The average fix error at 2,000 nautical miles was about 5.5 miles with a standard deviation of 4 miles. At 5,800 nautical miles, the average LOP error was about 4 miles with a standard deviation of about 15 miles for the three LOP's used. Fix errors for the continental net, resulting from the poor geometry of the system, averaged 93 and 116 miles. Longer baselines and optimum station configuration with respect to shot location would improve the fix accuracy by a factor of seven.

7.2.3 Results. It has been demonstrated that operationally usable lines of position can be measured from the bomb pulse. Table 7.1 gives a comparison of long- and short-baseline position errors. At 2,000 miles, the large amplitudes and characteristic shapes of the electromagnetic radiations from the nuclear shots were clearly distinguishable from spherics resulting from weather. At greater distances it becomes more difficult to make a determination, because signals and propagation effects tend to obscure distinctive characteristics. The ability of the system to isolate bomb pulses from lightning transient noise will determine the reliability and ultimate operational range of the completed system.

7.3 IONOSPHERIC EFFECTS OF NUCLEAR DETONATIONS

The study of ionospheric effects of nuclear detonations was a research project with no immediate direct military application. A better understanding of the basic laws pertaining to ionospheric phenomena may lead to the improvement of communication systems and may aid in the development of guidance systems for long-range missiles.

The major objectives of this experiment were to investigate the area of absorption believed to be due to radioactive particles from large nuclear detonations and to study the effects of orientation of the path from the blast site to the observer relative to the geomagnetic field upon F2-layer effects of such detonations. Other objectives concerned distant effects, boundaries of rising air thought to result from strong shock waves, and accumulation of other ionospheric data.

The ground stations located at Eniwetok Island, Rongerik Atoll, and Lele Island, Kusaie, Caroline Islands, employed automatic ionospheric recorders, Model C-2. A Model C-3 recorder was installed in a C-97 airplane based at Eniwetok. The performance of both types of recorders was similar. The station at Rongerik was some 240 km east of Bikini, and that at Kusaie was about 740 km to the south. The aircraft operated within about 400 km of ground zero.

The ground recorder stations operated on a routine schedule throughout the operation to determine the normal ionospheric conditions. Periodic flights were conducted. The schedule was accelerated for high-yield weapons and for the times that abnormal conditions existed in the ionosphere.

Strong radio-wave absorption was experienced at the aircraft when underneath the radioactive cloud. The horizontal extent of the region responsible for significant radio-wave absorption is substantially identical to the extent of the visible radioactive cloud. A theory has been developed which shows that, for megaton shots, the level of maximum absorption occurs where the collision frequency is twice the operating frequency. The absorption is proportional to $Y^{0.7}$ and $t^{-0.85}$ and is roughly inversely proportional to operating frequency. Specifically, the total one-way vertical absorption (attenuation) at 5 Mc 1 hour after a 1-Mt detonation would be about 2 nepers. These partially empirical and partially theoretical findings are considered to be valid from 1 to 30 Mt.

Following large detonations near the geomagnetic equator, F2-layer effects occur to the south, which differ decidedly from those to the east. The effects observed to the south are much more pronounced, longer lasting, and include discrete moving disturbances attributable to the arrival of compressional and hydromagnetic waves. Pulse return phenomena for Shot Zuni are shown in Figure 7.1. No distant ionospheric effects were noted during Operation Redwing. The apparent rise of the F2-layer that has been attributed to large-scale convection was not observed. A theory has been developed to explain the fact that this convection occurs only in connection with shots of about 10 Mt and greater. The rise is now considered to be an actual vertical flow of electrons.

7.4 AIRBORNE ANTENNAS AND PHOTOTUBES FOR DETERMINATION OF NUCLEAR WEAPON YIELD

A nuclear detonation generates three categories of characteristic phenomena that can be measured from a high-speed aircraft: (1) low-frequency electromagnetic radiation, which can be received by an electromagnetic antenna; (2) thermal radiation detectable by phototubes; and (3) pictorial characteristics, which can be photographed. Based upon these characteristics, the objectives of this project were to: (1) determine the effectiveness of flush-mounted airborne antennas and phototubes at various ground-to-air ranges in detecting characteristic low-frequency electromagnetic radiation and visible radiation, respectively; (2) determine the temporal and amplitude characteristics of the low-frequency electromagnetic radiation at various ground-to-air ranges; (3) determine the temporal and intensity characteristics of visible radiation at various ground-to-air ranges; and (4) determine the effects of ambient conditions upon the satisfactory measurement of the parameters specified in (1) and (2) above.

Airborne equipment has been designed for determining the location and yield of a nuclear detonation. This equipment for indirect bomb damage assessment (IBDA) determines yield from a measurement of the interval between the time of the burst and the time of the second peak in the thermal radiation intensity curve. Three categories of equipment were used: (1) For the measurement of the very-low-frequency (VLF) electromagnetic signal, a specially designed flush-mounted antenna was utilized, along with associated amplification and presentation equipment. (2) The measurement of the thermal radiation from the detonation was by means of phototubes with their associated electronic and recording equipment. (3) A sequence camera was used to photograph the burst itself with its fireball and to photograph the nuclear cloud.

Flush-mounted ferrite-core magnetic loop antennas, for use in detecting the electromagnetic signal and thus fixing the time of burst, performed successfully during Operation Redwing. Two kinds of phototubes for detecting the second thermal peak were tested and were found about equally satisfactory. One was a 1P39 phototube and the other was a 6570 phototube. The determination of yield using $Y = 0.92T^2$ (where Y is the yield in

megatons and T the time in seconds between the beginning of the first thermal peak and the top of the second thermal peak) gave results accurate to ± 16 percent for five shots with yields in the range from _____ Tables 7.2 and 7.3 list the yield determinations using electromagnetic signal and photohead data, respectively.

A detailed study of the collected data showed that the electromagnetic signal, consisting of a direct pulse followed by a series of ionosphere-reflected sky waves, could be used in many ways to give information concerning the detonation and the ionosphere. From the time intervals between the ground wave and sky waves, it was found possible to compute both the distance between burst and receiver and the height of the reflecting ionosphere layer. From the oscillatory period of the individual sky waves or ground wave, the yield could be estimated. The waveform of a sky wave could be used for an estimate of the height of the receiving equipment. The amplitudes in a sequence of sky waves could be used to give the radian frequency ω_r characterizing the ionosphere, and to extrapolate to the amplitudes of other sky waves or the ground wave.

For a number of test shots, the thermal radiation intensity data was compared with the expected irradiance to give estimates of atmospheric attenuation due to clouds and haze. Measurements of ambient light intensity and of the variability of ambient light were also made, to aid in the evaluation of the IBDA system.

On the sequence photographs the position of the burst could be determined from: (1) the intersection of bright radial lines, (2) the center of symmetry of the condensation dome, (3) the fireball itself, or (4) the stem of the nuclear cloud. When the fireball was visible, its radius could be used as a measure of yield, provided that the timing of the picture and the range between burst and camera were known. The condensation dome, produced in humid air by the rarefaction phase of the shock wave, appeared in all burst sequences and was found useful in determining a rough value of the range and of the time of the burst relative to the timing of the photographs.

With some modification, the electromagnetic fiducial pulse system and the photocell combination will meet the requirement for yield determination in modern aircraft for ranges out to 135 nautical miles. Although not tested in this experiment, there is an additional expectancy of obtaining satisfactory results in clear weather out to ranges of approximately 250 miles.

7.5 MEASUREMENT OF RADIOFREQUENCY ELECTROMAGNETIC RADIATION FROM NUCLEAR DETONATIONS

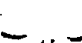
The objectives of this project were: (1) to obtain oscillographic waveforms of the electromagnetic radiation generated by nuclear detonations and (2) to analyze the waveform to determine field strength, time for first and second crossover, and time to initial peak.

The electromagnetic pulse generated by a nuclear detonation, under the conditions of this test (in which time and yield were known), was detected and waveforms recorded at stations located in areas from the test site to Forestport, New York. This project had stations on Site Elmer, Eniwetok Atoll, and on Kwajalein. The Site Elmer station recorded waveforms for 11 of the 17 detonations, and the station on Kwajalein recorded them on 7. At these close-in stations, where records were made with the oscilloscopes set at horizontal sweeps of approximately 30, 10, and 1 $\mu\text{sec/cm}$, the pulse waveform was shown with much detail.

Sferics and background noise interfered with recording and isolating the bomb pulse, even at the close-in stations where the field strength of the pulse was several volts per meter. However, oscillographic waveforms recorded at various speeds showed details of the initial portion of the signal as well as the complete signal and an ionospheric reflection. The characteristic waveform near ground zero consisted of an initial negative half-cycle with a sharp leading edge, a low-amplitude positive half-cycle, and a relatively high-amplitude negative third half-cycle.

Waveforms were analyzed to determine peak field strength, times to peak negative and positive deflections, and times to zero crossings. Fourier integral analyses were performed to obtain the frequency spectrum of each waveform. Analysis revealed that correlations existed between yield and each of the waveform duration characteristics, and also between yield and the frequency corresponding to the spectrum peak amplitude in the VLF region. Changes in the waveforms observed at different distances are attributed to effects of propagation. Correlations of field strength with yield and with distance were found to exist for kiloton-range devices. However, no such correlations could be found for megaton-range devices. Field strengths were lower than observed for devices of comparable yield during Operation Teapot. Figure 7.2 shows yields versus first crossover point in microseconds. Figure 7.3 presents waveforms as received from Shot Dakota.

The single waveform recorded from Shot Cherokee exhibited a variation in waveform characteristics that distinguished it from all ground-based shots of comparable yield. The recorded waveforms known to result from sferics did not exhibit the characteristics observed for detonation-generated waveforms.

Approximate distances to the source were obtained from a single station by utilizing sky wave delay. Tests indicated that time of signal arrival could be measured with 0.1- μ sec resolution and that signals from a  device could be detected at 420 miles.

Waveforms should provide valuable information for the development of systems to detect and to locate the source of nuclear explosions. However, for a practical detonation-location system, it still remains to be proved that the electromagnetic radiation from a nuclear detonation can be isolated with sufficient confidence from lightning transient noises when time, yield, and relative location of the detonation are not previously known.

7.6 ELECTROMAGNETIC WAVE ATTENUATION AT SUPER-HIGH AND ULTRA-HIGH FREQUENCIES RESULTING FROM NUCLEAR EXPLOSIONS

This project was designed to experimentally determine whether an instantaneous telemetry link was possible for early time transmission of technical information. Measurements of microwave attenuation as a function of time were made in the ionization region resulting from a nuclear detonation. Because most of the attenuation results from the presence of electrons, it was desirable to obtain values for the relevant parameters, to permit calculation of the microwave attenuation.

Measurements were made to determine the attenuation of UHF (9,450 Mc) and SHF (2,160 Mc) for three shots, Blackfoot, Osage, and Inca. In each instance the transmitter was placed near ground zero and the receiver was placed at a greater distance on the same radial as the transmitter. A typical example of attenuation versus time is delineated in Figure 7.4 as determined from an oscilloscope recording for Shot Blackfoot, where the transmitter was 5,300 feet from ground zero.

The data from Osage and Blackfoot indicates that the signal level dropped approximately 6 db at zero time and took on the order of 10 μ sec to recover completely. The measured attenuation agrees with the attenuation calculated for these shots.

The information obtained by this project indicates that instantaneous telemetering links are subject to blackout during early times. It appears advisable to provide for the storage of information during the first 10 to 20 μ sec following a detonation, when the transmitters are in relatively close proximity to ground zero. Thereafter, it appears feasible to telemeter technical information, using UHF or SHF.

TABLE 7.1 COMPARISON OF LONG- AND SHORT-BASELINE POSITION ERRORS

Shot	Short Base Line			Long Base Line						
	Hawaiian Net		California Net	Hawaiian Net (Lahaina - Palmyra)			Continental U. S. Net			
	Calculated Time Error	LOP Error	LOP Error	Calculated Time Error	LOP Error	Fix Error	Blytheville Harlingen	Blytheville Kinross	Harlingen Freeport	
	μ sec	naut. miles	naut. miles	μ sec	naut. miles	naut. miles	LOP Error naut. miles	LOP Error naut. miles	LOP Error naut. miles	
Lacrosse	-0.6	-2.4	+2.2							
Cherokee	+0.7	+2.5	-4.2	-12.4	-4.42					
Zuni	-0.3	-1.4	-3.5	-1.2	-0.43	1.24	+11.4	+26.6	+13.7	
Yuma	-0.6	-2.3	+3.0	-1.6	-1.0	1.85				
Erie	+0.3	+1.6	-4.2	-0.4	-0.15	0.31				
Flathead	+0.5	+1.8	-2.0	-2.2	-0.82	1.77	+6.4	-13.0	+21.0	
Blackfoot	-0.5	-1.8	-4.0	-0.1	-0.04	3.05	+9.1	-8.3	+4.9	
Inca	-0.6	-2.3	-5.0						+13.5	
Dakota	-0.5	-1.8	-8.5	-0.3	-0.11	0.77	+10.8	-18.3	+2.3	
Mohawk	-0.2	-0.8	-8.5	-2.7	-1.05	2.25	+9.1	-25.7	+1.6	
Apache	-0.2	-0.8	-6.5	-8.9	-3.44	15.3	+3.3	+2.5	+3.7	
Navajo	+0.1	+0.4	-9.0	-11.8	-4.21	14.0	+11.0	-15.7	+6.7	
Tewa	-0.4	-1.2	-5.6	-2.0	-0.58	1.6	-2.9	-4.3	+3.5	
Huron	-0.2	-0.8	-8.0	-5.4	-1.08	2.1	+5.0	-2.5		

TABLE 7.2 YIELDS FROM ELECTROMAGNETIC SIGNALS

Shot	Observed Time for First Cycle	Yield from Signal	Actual Yield
μ sec			
Kickapoo	29		
Mohawk	62		
Dakota	75		
Apache	50		
	93		
Navajo	70		
	92		

TABLE 7.3 PHOTOHEAD YIELDS

1P39: Blue-Green 6570: Infrared

Shot	Type Photohead	Calculated Yield	Actual Yield
Osage	1P39		
	6570		
Mohawk	1P39		
	6570		
Dakota	1P39		
	6570		
Apache	1P39		
	6570		
Tewa	1P39	5.52 Mt	4.6 Mt
	6570	5.52 Mt	4.6 Mt
Huron	1P39		
	6570		

* No data because of miscalibration of channel in recorder.

Pgs. 214 thru 216 Deleted.

Chapter 8

THERMAL RADIATION

8.1 OBJECTIVES

Program 8 participated in a total of five shots, during which its efforts were directed toward: (1) making basic thermal radiation measurements, (2) testing three new types of thermal measuring devices, and (3) exposing instrumented aircraft structural panels for the purpose of obtaining data to be used as a basis for additional laboratory studies. Abstracts of specific projects are contained in Section A.7 of the Appendix.

8.2 BASIC THERMAL MEASUREMENTS

Basic thermal measurements further the understanding of the mechanisms important in a nuclear explosion. The Redwing experiments of this nature included determination of irradiance in narrow spectral bands versus time, fireball radius versus time, spectral distribution of radiated energy versus time, color temperature, pulse shapes, and total thermal output.

The principal efforts were directed toward general documentation of thermal outputs of large weapons, comparing the thermal characteristics of an airburst to those of a surface burst, and comparing measurements made at a ground station with those made simultaneously at an airborne station.

Data obtained on previous operations (Ivy, Castle, Teapot) was inconsistent, much of it disagreeing with accepted scaling laws. Study of available data indicated several probable causes of experimental differences, particularly the following: (1) Attenuation of the thermal pulse by the normal components of the atmosphere. In the Pacific Proving Grounds (PPG), this effect is large, unknown, and spectrally selective. (2) Attenuation by clouds in the line of sight of the thermal instruments. (3) Reflection by clouds not in the line of sight of the instruments. (4) Attenuation and scattering from the Wilson cloud produced by the shock wave. (5) Attenuation by smoke generated by the bomb pulse. (6) Large and spectrally selective reflection from the ground or water to airborne instruments. (7) Distortion of the fireball (of an airburst) by shock waves reflected from the ground.

The effects of the above variables were most noticeable in the comparison of the data from ground and airborne stations. In such cases, the difference between the aerial and ground geometry was sufficient to cause serious inconsistencies in measured times to peaks and minimums and apparent yield, as well as in irradiance and spectral distribution.

During Operation Redwing, thermal measurements were made on Shots Cherokee, Zuni, Lacrosse, Erie, and Flathead. The station locations are listed in Table 8.1.

There were simultaneous measurements from ground and airborne stations during Shots Cherokee, Lacrosse, and Zuni. The airborne station was positioned over the most distant ground stations in order to maximize the scattering, attenuation, and reflection

effects that were believed to be the cause of differences in airborne and ground station measurements.

Participation during Shot Erie was an attempt to view an airburst from directly overhead, with the intention of seeing the fireball undistorted by the shock wave reflected from the ground.

Extensive photographic coverage was included for all shots on which thermal measurements were made, with the hope of being able to determine the degree, if any, of obscuration by clouds in the line of sight to the fireball, or reflection by clouds nearby.

Measurements included total energy as a function of time, broad-band spectral data, narrow-band spectral data, irradiance as a function of time, photographic data, and field-of-view data. The data was analyzed to obtain fireball radii versus time, color and power temperatures versus time, and (estimated) thermal yields. Irradiance versus time measurements were made by use of radiometers. Fireball radius versus time was determined by high-speed photography.

The thermal yield of a bomb is defined as the best estimate of the total energy radiated by the bomb in the form of thermal radiation, i. e., radiation for which the wavelength is between 2,000 Å and 100,000 Å (10 μ).

Thermal yield was determined by the relationship

$$Q = 4\pi D^2 \sum_j \left(\frac{\beta_i \Delta q}{\beta_W T} \right)_j$$

Where: β_i = the idealized area of the fireball, without obscuration, for the j'th time interval.

β_W = the estimated area of the fireball, for the j'th time interval, after the area of clouds and opaque objects have been deducted.

Δq = the measured value of energy received during the j'th time interval (cal/cm²).

T = the transmission of the instrument filter and the atmosphere (a combined correction) as estimated for the j'th time interval.

D = the slant range in centimeters.

Thermal power was determined by dividing the thermal yield for each time interval by the length of time interval. Figures 8.1, 8.2, and 8.3 show plots of total thermal power versus time.

Power temperature was computed from the relationship

$$\psi_{\Delta t} = \sqrt[4]{\frac{\pi D^2 \frac{\Delta q_m}{\Delta t}}{h \epsilon \beta_W T}}$$

Where: $\psi_{\Delta t}$ = Power temperature (°K) for the time increment Δt .

h = Stefan's constant (1.356×10^{-12} cal/cm² sec⁻¹ deg⁻⁴).

ϵ = the average emissivity of the fireball.

Δq_m = measured energy (cal/cm²).

Average emissivity was chosen as 1.0 since its actual value is not known. This leads to a minimum value of power temperature.

The color temperature of a fireball can be defined as the temperature of the black-body source whose spectral distribution most nearly matches that of the fireball at all wavelengths in the spectral regions 3,650 Å to 42,000 Å (4.2 μ). The color temperatures

shown in Figures 8.4, 8.5, and 8.6 were calculated (for each short time interval) by comparing the ratio of the change in reading of two calorimeters having different color filters.

The only major failure of the thermal program was associated with the bombing error of Shot Cherokee. The fireball was either out of the field of view of some instruments or obscured by clouds. The general result was a serious degradation of the Cherokee data, making the measurements essentially impossible to interpret.

A typical irradiance-versus-time record is shown in Figure 8.7. Spectral distribution of the irradiance (for Shot Zuni only) is shown in Figure 8.8. From these and other data, power and color temperatures, radius versus time and thermal yield can be derived.

Figures 8.4 through 8.11 shows the results of the analysis of the thermal data.

The irradiance-versus-time curves show the radiant energy (in cal/cm²) incident on the thermal instruments as a function of time. As previously mentioned, these values are strongly influenced by extraneous factors such as cloud cover. The records have had no corrections applied, although the fireball photograph shown in Figure 8.12 indicates that the obscured irradiance must have been considerably reduced by clouds, in addition to the normal atmospheric attenuation always present in the PPG. The spectral distribution curve (Figure 8.8) shows the effects of attenuation and indicates that a large portion of the energy is in the infrared region of the spectrum.

In the absence of attenuation, it would be expected that the spectral distribution would appear as a black-body spectrum.

Figures 8.9, 8.10, and 8.11 show fireball radius versus time as measured from photographic data.

Simultaneous measurements by ground and airborne stations were successful on Shots Zuni and Lacrosse. Comparisons are listed in Table 8.2. It is immediately seen that no simple explanation can account for the differences in the ground and airborne stations, because the ground station reading is higher than the airborne station by a factor of 3 on one shot, and lower by a factor of 2.5 on the other shot. Fireball photography (Figure 8.12) shows appreciable obscuration of the fireball on both shots.

8.3 CRITICAL IGNITION ENERGIES OF MATERIALS AND DEPTH OF CHAR IN WOOD

Measurements to determine critical ignition energies for various materials and depth of char in wood were made during Shot Cherokee from stations on Sites Dog and George. In addition, various natural kindling fuels on several islands were studied prior to and after the detonation. The objective was to obtain data from a nuclear device in the megaton range, which could be correlated with data from laboratory experiments.

Because of the bombing error of Shot Cherokee, the thermal radiation from the fireball entered the specimen containers at an appreciable angle, irradiating only a small portion of each specimen on Site George and missing entirely the specimens on Site Dog. Table 8.3 gives the estimates of critical ignition energy values for the various materials exposed, based on the observed results. The wood specimens on Site George were charred to depths depending on their densities and the transmission of attenuating filters. Some of the specimens of black and gray alpha-cellulose papers, newspapers, and pine needles were ignited, giving a good bracket on their critical ignition energies. None of the grass, cotton denim, rayon cloth, or white alpha-cellulose papers were ignited. Corrugated fiberboard was burned on Site Dog by the radiation. Many samples that were

not ignited were somewhat charred or discolored. Radiant exposure on Site Dog was indicated by Instruments of Projects 8.1 and 8.3 to be 73 to 75 cal/cm², whereas on Site George it was 21 cal/cm².

8.4 TESTS OF NEW TYPES OF THERMAL INDICATORS

Two self-recording calorimeters (Types 1 and 2), similar in principle to one used during Operation Teapot but of modified design, were scheduled for test by Project 8.3 during Shots Cherokee and Blackfoot. The two instruments utilized the same principle but were of different design. In addition, the Kidde pulse recorder, a commercial item that is suitable only for measurements of thermal energy in short pulses, was to be tested during Blackfoot.

Because of a high level of residual nuclear radiation remaining at the instrumentation stations after Shot Erie, it was not feasible to carry out the Blackfoot tests. No other suitable shot was scheduled. As a result, the two self-recording calorimeters were tested only on the long-duration pulse of Cherokee, whereas the Kidde instrument was not tested. The long-duration pulse provides most-severe test of these instruments; therefore, the Cherokee test may be considered sufficient. Both of the calorimeters had a field of view of 180 degrees and were able to obtain data despite the large angle of incidence resulting from the bombing error.

Table 8.4 contains a comparison of the uncorrected results obtained by the self-recording calorimeter (Type 2) with that obtained by the thermistor calorimeter used as a relative standard and with that obtained by the 90-degree-field-of-view disk calorimeters of Project 8.1. The results from the Type 2 calorimeter and the thermistor calorimeter compared favorably with those from the disk calorimeter. On the other hand, the data from the Type 1 calorimeter was erratic. Because both types utilize the same principle, it was concluded that the principle was proved by the Type 2, and the erratic results from the Type 1 were attributed to imperfections resulting from fabrication difficulties.

8.5 TEST OF AIRCRAFT STRUCTURAL PANELS

Project 8.4 measured the response of various types of aircraft structural panels exposed to the thermal pulse from Shot Cherokee. Test specimens were sandwich-type structural panels having various types of construction materials and facing thicknesses. Instrumentation consisted mainly of thermocouples embedded in the structural panels to provide temperature-versus-time histories at various points in the panels. Figure 8.13 shows the 40 test panels exposed during Shot Cherokee. In addition to these, two FJ-4 elevators were used at the same station, and small groups of similar specimens were mounted in the Project 5.8 effects aircraft.

Recorded peak surface temperature rises at the ground station were in the range from 100 to 350 degrees F, less than half of the expected and desired range. The peak temperatures were low, because smoke from the gray paint on some of the samples obscured the test array from some of the thermal pulse; the rate of heat conductivity was much higher than was originally expected. Figure 8.14 shows the thermal input to the test panels. Figure 8.15 shows a typical record from one of the aluminum honeycomb samples. Effect of the smoke can be seen in the divergence of the calculated and measured curves at about 3 seconds; the rapid decay after 4 seconds indicates a rapid conduction of heat from the surface to the interior of the panel. Figure 8.16 shows a

calculated response with smoke obscuration taken into account. Analysis of the test measurements and subsequent laboratory heating tests were successful in mathematically defining the response of sandwich-type structural panels to thermal inputs.

Post-exposure mechanical tests were also made on the test panels, to determine if any noticeable change in structural properties was caused by the thermal input. The samples mounted in an unstressed position showed no significant change in strength characteristics as a result of the radiant exposure. However, tests conducted on similar specimens in a prestressed condition show that structural failure will occur at temperatures well within the range encountered during Shot Cherokee.

8.6 AIRBORNE SPECTROSCOPY

Airborne spectroscopy measurements were made by Project 8.5 during Shots Lacrosse, Cherokee, Zuni, Erie, and Flathead (Table 8.5 and Figure 8.17).

For Shot Lacrosse, the light source failed to operate at H-hour; therefore, no atmospheric-transmission data was obtained. Spectrometer data was obtained on most channels. Most of the channels required filtering techniques in the laboratory to separate the useful data from the noise in the system; however, critical times which could be measured are shown in Table 8.6. Figure 8.18 shows a plot of the variation of t_{\max_2} as a function of wavelength.

No transmission measurements were attempted at H-hour for Shot Cherokee, because this was an airburst.

For Shot Zuni, the light source malfunctioned during an interference test on D-2 days and was evacuated on D-1 day; hence, again no transmission measurements were made at H-hour. The spectrometer obtained excellent data on this shot. This data is tabulated in Table 8.7. Figure 8.19 shows a plot of time to second maximum as a function of wavelength.

During Shot Erie, the project was successful, obtaining both transmission data at H-hour and good spectrometer data. In addition, the aircraft was looking almost down on this detonation; the view of the fireball was unperturbed by the reflected shock wave. Data for this shot is listed in Table 8.8, and a plot of time to second maximum as a function of wavelength is shown in Figure 8.20.

The project participated during Shot Flathead, where the light source functioned well, but as the result of a 20-minute postponement in shot time the transmissometer was saturated with sunlight, so that no useful transmission data was obtained. The spectrometer was successful, however, and the data is listed in Table 8.9.

It is interesting to note the variation of time to second maximum with wavelength shown in Figures 8.18 through 8.20. An examination of these curves suggests two findings worthy of further analysis:

First, the broad-spectrum instruments and instruments sensitive mostly in the blue region that are used to determine time to second maximum for use in calculating yields may be subject to considerable dispersion in readings of time to second maximum and, thereby, to substantial error. This results from the rather abrupt variation of time to second maximum in the blue region of the spectrum, indicated in Figures 8.19 and 8.20. It may be noted in these few samples that the time to second maximum appears to have a minimum in the region of 0.5 to 0.7 microns and to increase toward both the blue and the red regions of the spectrum, the increase being exceptionally rapid. This would seem to suggest that the most accurate results for yield determination should be obtained from an instrument operating in a limited region 0.5 to 0.7 microns.

Second, it may be noted that this minimum appears to be in the vicinity of 0.5 microns for airbursts, and 0.7 microns for surface bursts, suggesting a slightly different scaling relationship of yield as a function of time to second maximum for airbursts and surface bursts. This probably results from a difference in apparent color temperature.

TABLE 8.1 STATION LOCATIONS

Shot	Site	Horizontal Range ft	Instruments	Project	
Cherokee	Dog	26,380	Radiometer	8.1	
			Calorimeter		
	George	38,837	Cellulosic samples	8.2	
			Radiometer	8.1	
			Calorimeter		
			Bolometer Spectrometer		
How	84,406	Cellulosic samples	8.2		
		Aircraft structural panels	8.4		
		Radiometer	8.1		
		Calorimeter			
P2V aircraft	84,400 23,000 altitude	Bolometer	8.4		
		Spectrometer			
Zuni	Obce	17,005	Radiometer	8.1	
			Calorimeter		
	William	32,073	Bolometer	8.1	
			Spectrometer		
			Radiometer		8.1
			Calorimeter		
Nan	68,580	Bolometer	8.1		
		Spectrometer			
P2V aircraft	69,330 22,000 altitude	Airborne station	8.5		
		Yvonne	8,121	Radiometer	8.1
Calorimeter					
Bolometer					
Spectrometer					
Wilma	15,600 SSW	Radiometer	8.1		
		Calorimeter			
		Bolometer			
P2V aircraft	14,392 23,000 altitude	Airborne station	8.5		
Erie	P2V aircraft	1,560 22,000 altitude	Airborne station	8.5	
		P2V aircraft	41,950 23,000 altitude	Airborne station	8.5
Flathead	P2V aircraft	41,950 23,000 altitude	Airborne station	8.5	

TABLE 8.2 COMPARISON OF TOTAL THERMAL ENERGY RECEIVED AT GROUND AND AIRBORNE STATIONS

	Lacrosse	Zuni
Airborne station	0.432 calories/cm ²	5.0 calories/cm ²
Ground station	1.4 calories/cm ²	2.1 calories/cm ²

TABLE 8.3 CRITICAL IGNITION ENERGY VALUES ESTIMATED FOR VARIOUS MATERIALS EXPOSED TO SHOT CHEROKEE

Values shown are cal/cm².

Material	Minimum Thermal Ignition Energy	
	Low Moisture Content	High Moisture Content
White alpha-cellulose paper	>21.0	>21.0
Blue cotton denim	>21.0	>21.0
Charcoal-gray rayon	>21.0	>21.0
Newspaper *	12.7	9.8
Corrugated fiberboard	>13.9	>10.2
Yellow grass	>13.9	>13.9
Pine needles *	18.5	18.5

* The values for newspaper and pine needles were estimated by considering the effects of radiation somewhat insufficient to cause sustained flaming.

TABLE 8.4 COMPARISON OF RADIANT EXPOSURE VALUES AS MEASURED BY THE THREE TYPES OF CALORIMETERS

Station	Ground Zero Range ft	Type 2 Self-Recording Calorimeter cal/cm ²	Thermistor Calorimeter cal/cm ²	NRDL Disk Calorimeter cal/cm ²
Dog (830.01)	26,000	75.4	70.0 75.6	70.7
Dog (830.02)	26,000	—	73.3	—
George (830.03)	38,500	24.5	24.2 22.0	19.0
George (830.04)	38,500	24.5	24.2	—
How (830.05)	84,000	Below Range	0.5	1.75

TABLE 8.5 AIRCRAFT POSITIONS FOR PARTICIPATING EVENTS, PROJECT 8.5

Shot	Horizontal Range		Altitude		Slant Range	
	Desired	Actual	Desired	Actual	Desired	Actual
	feet	feet	feet	feet	feet	feet
Lacrosse	15,000	15,600 ± 400	23,000	23,000	27,600	27,830
Cherokee	92,620	84,400 ± 500	23,000	23,000	94,400	86,400
Zuni	68,430	69,330 ± 600	22,000	22,000	72,000	72,610
Erie	0	1,560 ± 50	22,000	22,000	22,000	22,090
Flathead	40,000	41,950 ± 500	23,000	23,000	45,700	47,900

Pg. 226 Deleted.

7

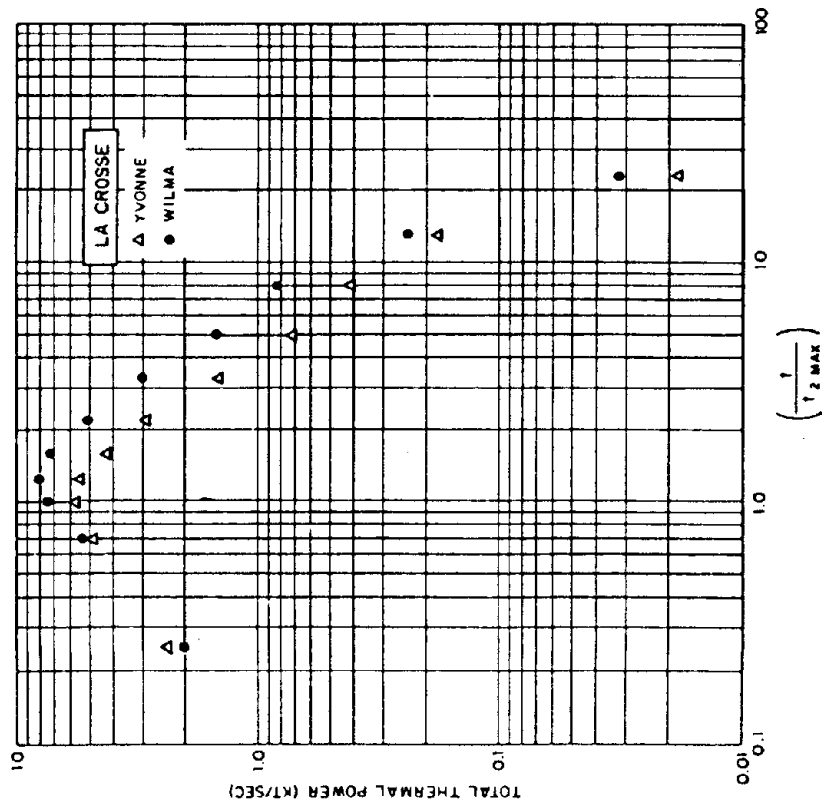


Figure 8.1 Total thermal power versus time, Shot Lacrosse.

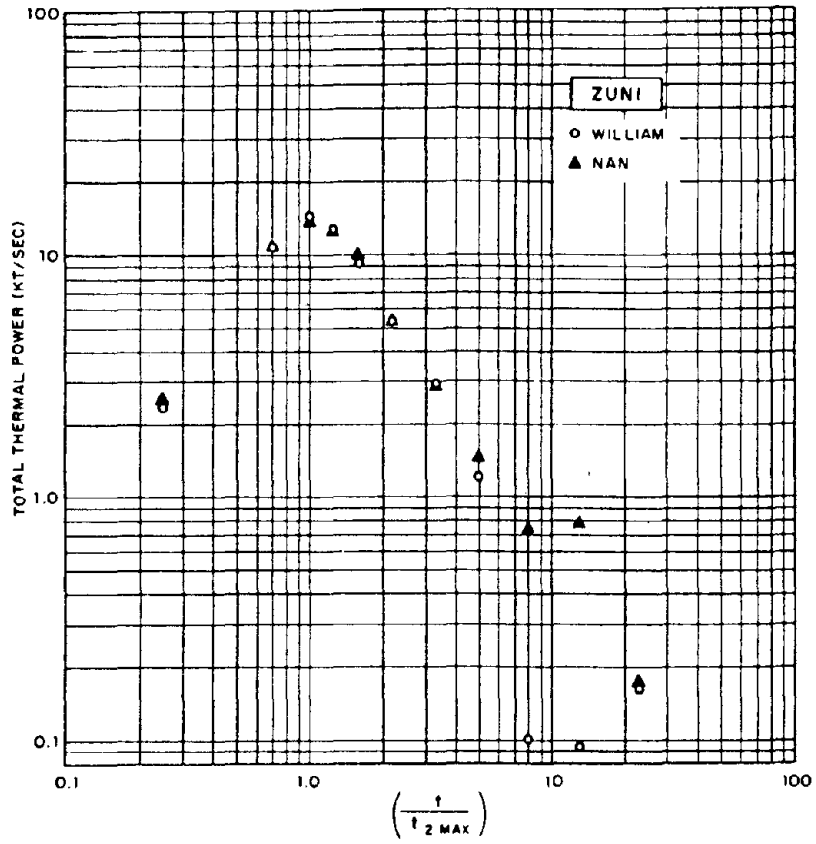


Figure 8.3 Total thermal power versus time, Shot Zuni.

Pgs. 229 & 230 Deleted.

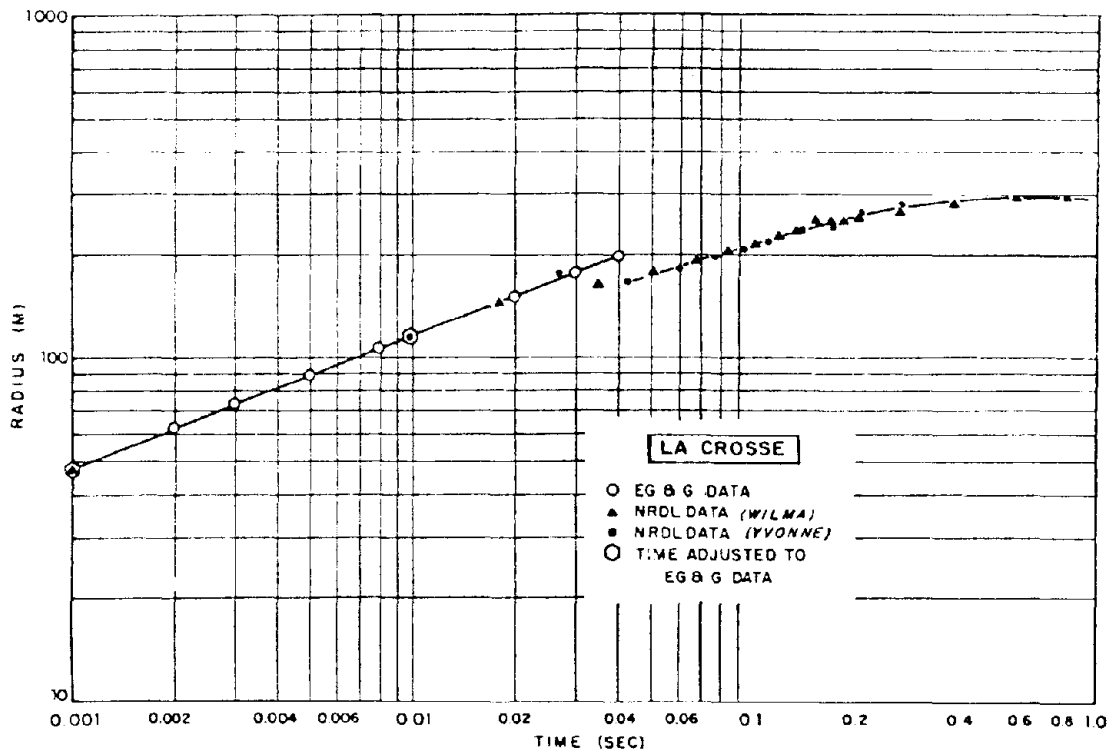


Figure 8.9 Shot Lacrosse fireball radius versus time.

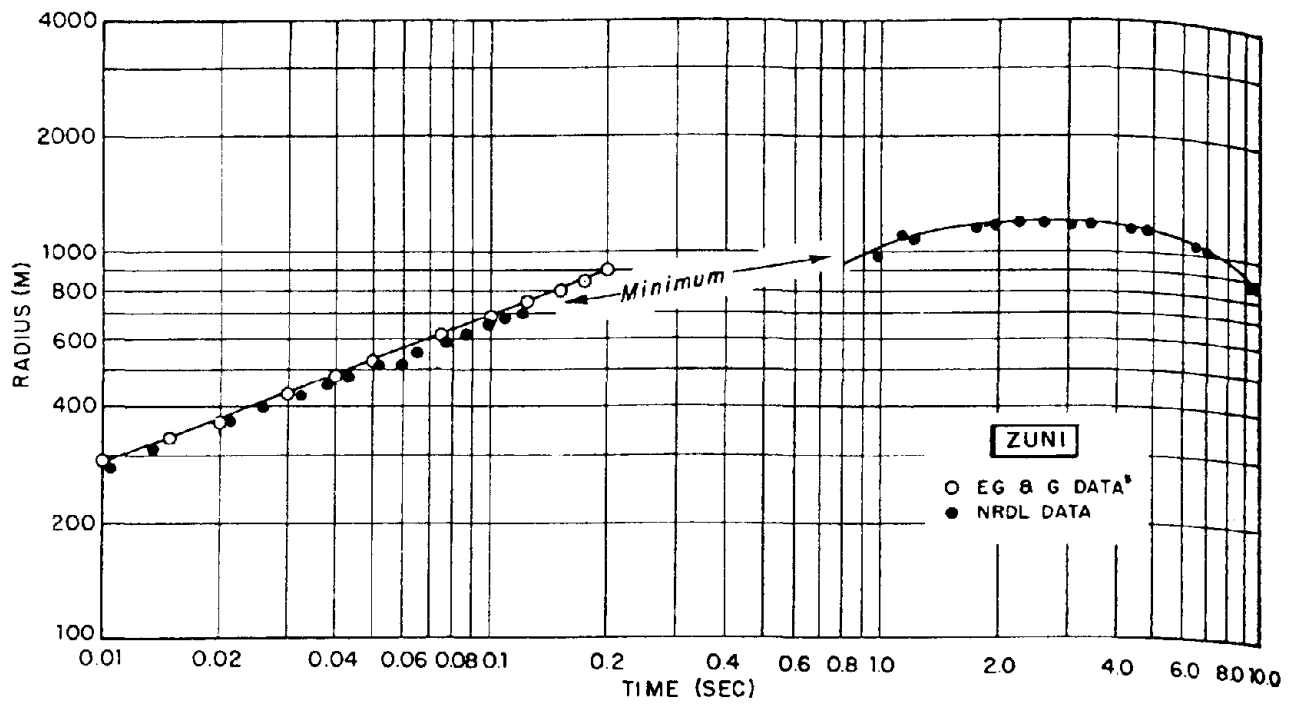


Figure 8.11 Shot Zuni fireball radius versus time.

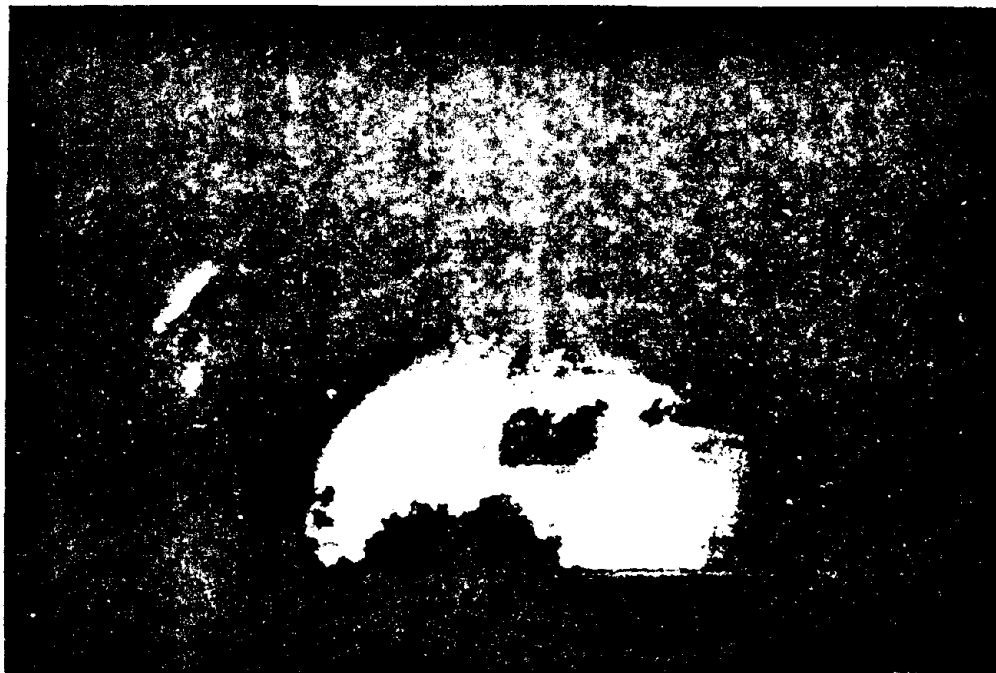


Figure 8.12 Shot Zuni from Site Nan at 1.95 seconds.

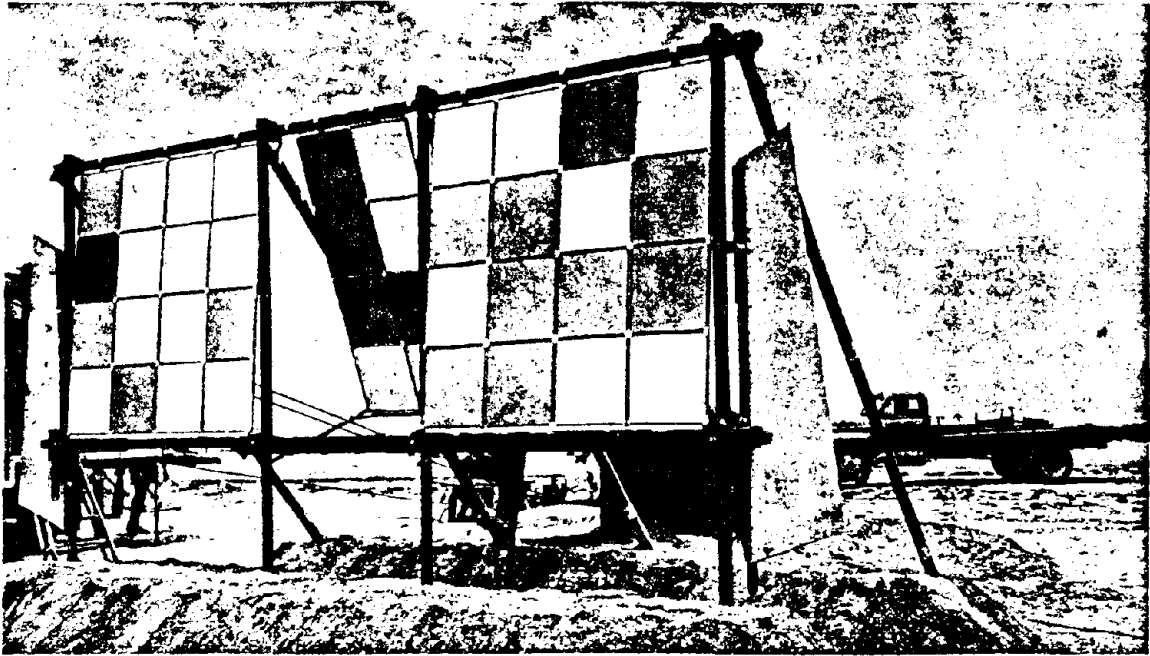


Figure 8.13 Specimen array at Project 8.4 test site.

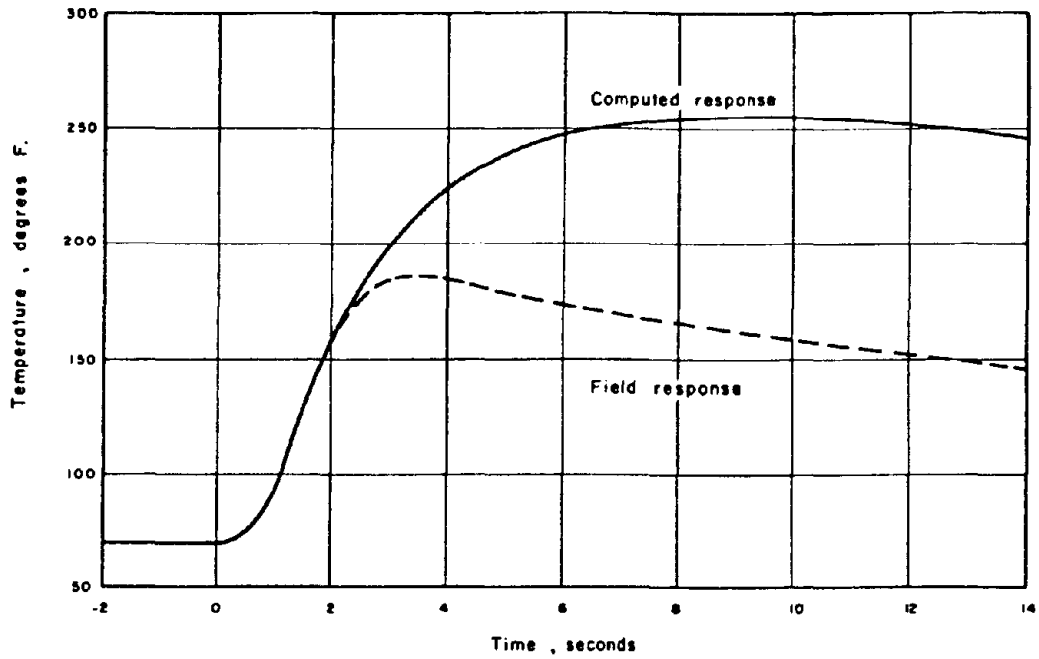


Figure 8.15 Exposed facing temperature-time histories of GLM specimen with 0.016-inch white-painted skin. (Computed peak temperature: 255°F.)

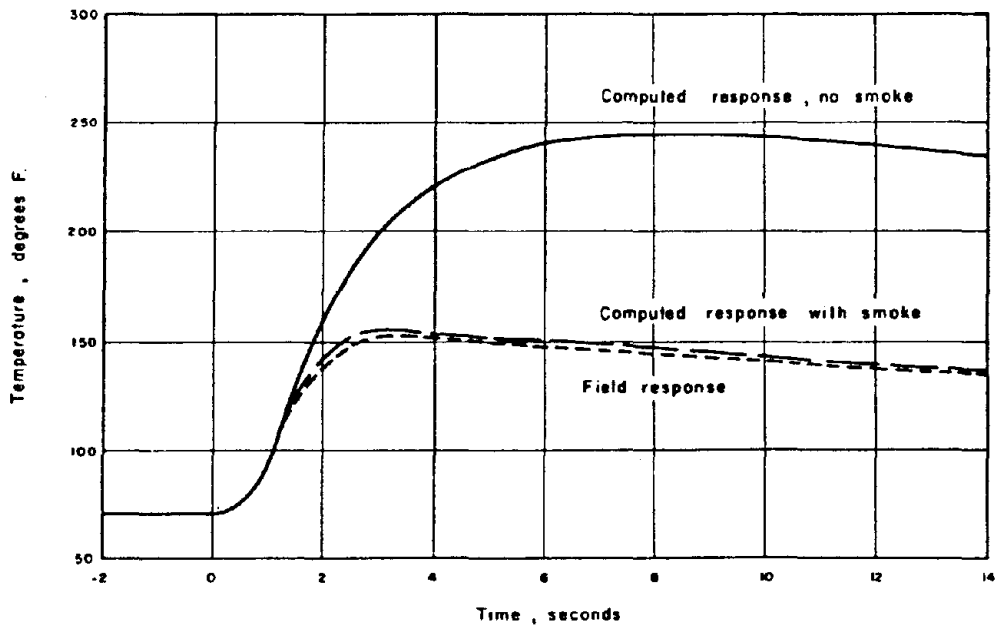


Figure 8.16 Exposed facing temperature-time histories of NAA specimen with $\frac{1}{8}$ -inch cell size and 0.016-inch white-painted skin. (Computed peak temperature: 243° F.)

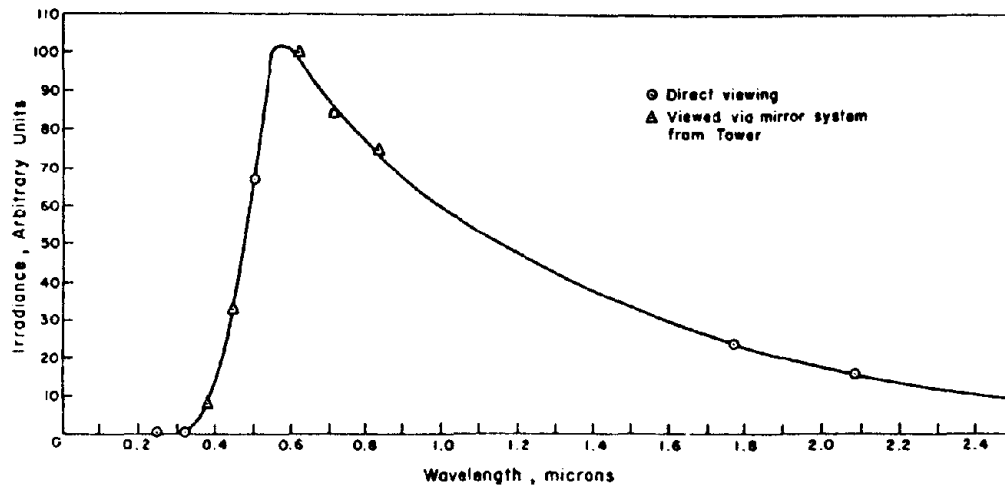


Figure 8.17 Relative spectral distribution of irradiance at t_{\max_2} , Shot Zuni, Site Nan, composite, Project 8.1.

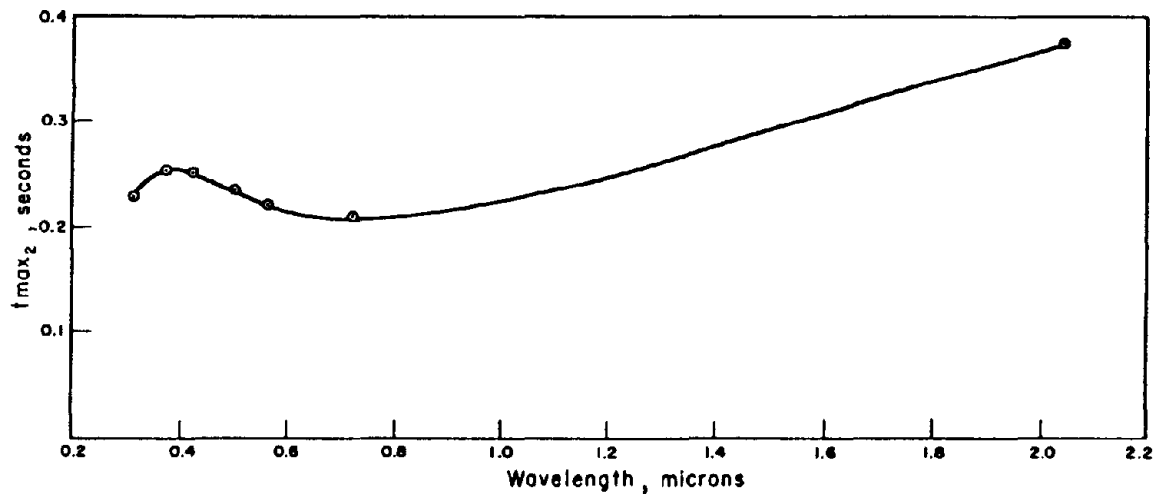


Figure 8.18 Time to second maximum versus wavelength, Shot Lacrosse, P2V-2 airborne station, Project 8.5.

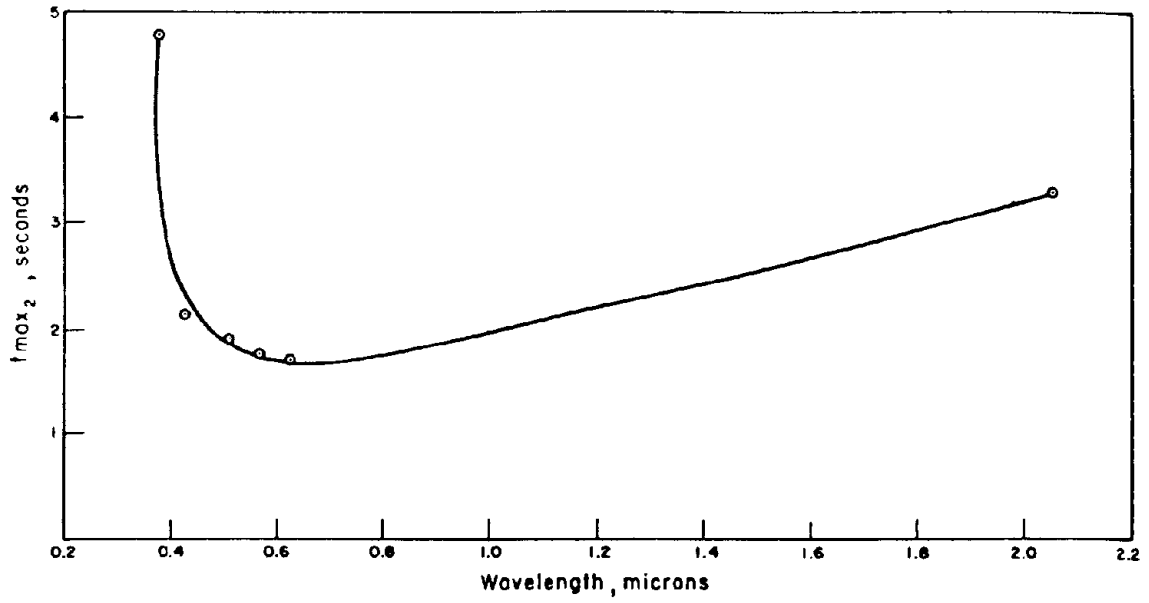


Figure 8.19 Time to second maximum versus wavelength, Shot Zuni, P2V-2 airborne station, Project 8.5.

Chapter 9

SUPPORT PHOTOGRAPHY

9.1 OBJECTIVES

This program was primarily of a support nature and consisted of two projects. Project 9.1a had the mission of documenting, by photographic means, the various parameters of the nuclear clouds as a function of time and attempted to establish approximate scaling (yield) relations. Project 9.1b was concerned with the broad function of providing general technical photographic support to the military-effect programs, including the production of a documentary motion picture.

The project abstracts are given in Section A.8 of the Appendix.

9.2 BACKGROUND

Collection of cloud-rise and height data was attempted as far back as Operation Sandstone (April 1948) by means of manually controlled theodolites. All measurements were taken with ground-based cameras until Operation Ivy, when the first attempt at aerial documentation was made. The data obtained was far from perfect but provided invaluable experience in planning subsequent tests. Essentially the same statement can be made concerning Castle results.

Redwing Project 9.1a was concerned with observing and documenting the cloud phenomena, not with explaining them; hence, any detailed theoretical development was not a part of this project. The simple optical relationships between object and image were used.

9.3 INSTRUMENTATION AND OPERATIONS

To overcome difficulties encountered on previous operations, use was made during Operation Redwing of the gyro-camera mount. With this stabilized table, the angle of tilt in aiming the camera was known, and film measurements were made relative to a fiducial or other artificial reference points when no natural reference appeared in the photograph. However, to investigate such subjects as the near edge of the cloud, more information was needed, such as a second picture from another location. If the object was identified clearly in both pictures and if the camera aiming angles were clearly known, the position of the object was computed by triangulation.

Three RB-50E aircraft were equipped with identical camera assemblies on A-28 gyro-stabilized mounts located in the aft section of the aircraft. Each mount held an Edgerton, Germeshausen and Grier 70-mm cloud camera, an Eclair 35-mm motion-picture camera (one frame every 15 seconds) and a gun sight aiming point 16-mm motion-picture camera. The three aircraft were positioned in the east, west, and south quadrants, respectively, at ranges of 70 nautical miles from ground zero on all kiloton-range shots and 110 nautical miles from the megaton-range shots.

9.4 RESULTS

Project 9.1b fulfilled its overall mission of providing technical photographic support to the various projects. A documentary color motion picture was produced and distributed.

The cloud photography obtained by Project 9.1a is superior to that from previous operations (Figure 9.1). The value of the fiducial-mark system of referencing data was again demonstrated. Both aircraft positioning and the recording of navigational data were excellent. The data has confirmed and extended previous knowledge of nuclear cloud growth.

9.5 CONCLUSIONS

It is now possible to predict cloud growth and rise and its dissipation during the first 20 minutes after detonation with a high degree of accuracy. Further documentation of cloud behavior during this time period now seems unnecessary. The precision of cloud measurement could be improved slightly by undertaking a vastly expanded program, but the cost of the program would be entirely out of proportion to the increase in accuracy of the data so obtained.

Pg. 239 Deleted.

Appendix

PROJECT ABSTRACTS

A.1 PROGRAM 1: BLAST MEASUREMENTS

A.1.1 Project 1.1. Basic Surface Blast Measurements. Agency: Ballistic Research Laboratories. Report Title: Ground Surface Air-Blast Pressure versus Distance, WT-1301. Project Officer: C. N. Kingery.

General objectives of this project were: (1) to instrument certain shots during Operation Redwing and obtain basic information of the propagation of blast waves over different surfaces from various yields and heights of burst; and (2) supply measurements of overpressure and dynamic pressure at certain locations in support of other projects.

The specific objective of the project was to determine the pressure versus time and dynamic pressure versus time variations with distance from ground zero on five shots during Operation Redwing. These shots were: (1) Lacrosse, a medium kiloton-range surface burst; (2) Cherokee, a megaton-range airburst; (3) Zuni, a megaton-range surface burst; (4) Yuma, a [redacted] power shot; and (5) Inca, a small kiloton-range tower shot.

The project had the prime responsibility for basic airblast instrumentation on Shots Cherokee, Zuni, and Yuma. On Shots Lacrosse and Inca the project participated to provide back-up instrumentation for the electronic recording system used by Projects 1.2, 1.10, and 30.2 of Sandia Corporation (SC).

The secondary specific objectives of this project were to: (1) record the diffraction phenomenon over the manmade islands for Project 3.1; (2) furnish dynamic pressure measurements to Project 1.5 for evaluation of vehicle damage; and (3) furnish water pressure measurements to Project 1.9 for wave height studies from Shot Zuni.

Shot Lacrosse afforded an opportunity to instrument a medium yield (39.5 kt) surface burst. Ground surface airblast gages recorded a precursor type shock wave at a station 1,180 feet from ground zero and a clean or classical type wave at a station 1,950 feet from ground zero. Correlation of airblast data with Projects 1.2 and 30.2 of SC electronically recorded blast measurements was excellent.

Shot Cherokee was a high yield ([redacted]) airburst. It had the largest instrumentation participation of the series, but unfortunately the device did not detonate over the intended ground zero. This caused the loss of many records and a reduction of the accuracy of many because the range of the pressure transducers at some stations was as much as 40 times greater than the actual pressure measured. A difference in the overpressure and wave shape was noted on records obtained from the manmade islands and those obtained from the reef stations east of Site Charlie. Scaled models of these stations were fired on in the BRL shock tube and, based on these experiments, the difference in wave shape and 20 percent or more degradation in pressure may be attributed to the type gage mount used for the reef stations.

Shot Zuni was the first high yield (3.38 Mt) surface burst that afforded a land-surface blast line from ground zero to the gages. Two blast lines, approximately 180 degrees apart, were instrumented for this shot. One blast line was along the Tare Complex where nonideal (precursor type) shock waves were recorded out as far as 8,300 feet. The second blast line was on Site Uncle where nonideal shock waves were recorded as far out as 9,880 feet.

Participation in Shot Yuma gave an opportunity to record airblast data from a [redacted] device detonated from a tower. Basic blast data were recorded which will be used to validate or modify the height of burst curves for use with [redacted] yields.

Shot Inca was the last shot in which Project 1.1 participated. Two blast lines were instrumented on the same island, one over a cleared area and the other over a vegetated area. Records were obtained from both blast lines, but some accuracy was lost because the actual yield [redacted] was more than double the predicted yield [redacted] and some of the pressure-sensing capsules were overstressed beyond their intended range.

A.1.2 Project 1.2. Surface Blast Measurements of Static and Dynamic Pressures. Agency: Sandia Corporation. Report Title: Blast Measurements on a Medium-Yield Surface Burst, WT-1302. Project

Officer: C. D. Broyles.

The objective of this project was the measurement of overpressure and dynamic pressure as a function of time and distance from a surface burst of a medium-yield atomic device, a yield range not previously examined experimentally for this type burst.

Overpressure and dynamic pressure were measured as a function of time and distance (690 to 3,250 feet) on a surface burst of a medium yield (40 kt) nuclear device on Site Yvonne, Eniwetok. Overpressures were measured with ground baffles and pitot-static gages. A precursor formed but died out at an unusually high overpressure of between 35 and 55 psi. The usual high dynamic pressures associated with precursors were observed. Outside of the limited region in which the precursor existed, the overpressure and dynamic pressure measurements were in agreement with previous measurements on surface bursts. They were consistent with the free-air values for 1.6 times the actual yield of 39.5 kt.

A.1.3 Project 1.3. Blast Measurements by Shock Photography. Agency: U. S. Naval Ordnance Laboratory. Report Title: Air Blast and Shock Phenomena by Photography, WT-1303. Project Officer: L. J. Belliveau.

The primary objective of this project was to obtain blast measurements vertically above and at horizontal ranges from specific shots. Of highest priority was the measurement vertically above the high-yield airburst to document the propagation of the blast wave through a nonhomogeneous atmosphere. Other objectives included study of the effects of the ground or water surface on the blast wave and, basically, to determine the peak overpressure as a function of distance relation for the various shots.

The project participated in Shots Cherokee, Lacrosse, Zuni, Inca, Mohawk, and Seminole. No shock photography data were obtained from Cherokee as the result of a bombing error. The smoke-rocket technique was used during Zuni and Lacrosse and usable data were obtained. Direct-shock photography was used during Inca, Mohawk, and Seminole. Only fragmentary shocks were observed on Inca and Mohawk films, and no shock was observed in Seminole films.

Shot Zuni was a ground-surface burst of 3.38 Mt. Pressure-distance data were obtained over the surface (water) and above ground zero to distances of 14,000 and 13,000 feet, respectively. The surface data were compatible with the data obtained from previous operations. The pressure-distance data obtained above ground zero is not in agreement with available methods of predicting peak overpressures above ground zero. However, a qualitative picture can be given in terms of phenomena observed on high-explosive tests and on theoretical predictions based on the effects of atmospheric nonhomogeneity.

Shot Lacrosse was a surface burst with a recommended yield of 39.5 kt. Peak-shock overpressure-distance data was obtained along the surface to a distance of 3,250 feet. This data was obtained over a water surface, and it was noted that there were no significant differences between the data and that obtained by other agencies over a land surface. No data was obtained above ground zero. The cameras did not operate at Station 1514 (Mack Tower); consequently, a study of the thermal effects over the land surface cannot be made.

Shot Inca was a _____ shot detonated on a 200-foot tower. Pressure-distance data was obtained to a distance of 1,050 feet along the surface. No angles for the precursor could be reliably read from the films.

Shot Mohawk was a _____ device detonated on a 300-foot tower. Only a fragment of a shock wave was observed on the films. This fragmentary shock occurred along a radial line approximately 10 degrees above the horizontal that passed through a protrusion from the fireball. Because of the asymmetric configuration, the data obtained did not compare with scaled data from other shots.

Shot Seminole was a device detonated at the surface in a large tank of water with a yield of _____ No shock wave was visible in the films examined. Some explosion profiles with time are presented in three views of the shot location.

A.1.4 Project 1.4. Free-Air-Pressure Measurements at Altitude. Agency: Air Force Cambridge Research Center. Report Title: Measurement of Free-Air Atomic-Blast Pressures, WT-1304. Project Officer: N. A. Haskell.

The objective of the project was to measure free-air peak overpressure and overpressure versus time vertically above an airburst of more than a megaton yield. These data were desired so that a comparison could be made between the overpressures actually observed and those calculated by various approximate methods of correcting for altitude effects.

A vertical array of 12 parachute-borne, telemetering, blast-pressure canisters was deployed by drop from a B-36 aircraft above intended ground zero for Shot Cherokee. Due to a large horizontal error in the actual point of burst, the array was not directly above the burst; 10 of the 12 canisters were in the free-air region, and two were below the path of the triple point in the Mach region. The range of altitude covered was 850 to 33,800 feet. Data were received from all units.

Observed peak overpressures were in satisfactory agreement with those calculated according to the Theilheimer-Rudlin theory, provided the integration of the Theilheimer-Rudlin equation is started with an appropriate initial condition. There are indications that the appropriate initial condition is a slowly varying function of yield.

Observed positive-phase durations suggest a slight upward revision of the currently accepted standard curve for this quantity.

Measured values of the time of arrival and amplitude of the reflected shock were in general agreement with previous data obtained at shots of smaller yield.

A.1.5 Project 1.5. Transient Drag Loading of Actual and Idealized Shapes. Agency: Ballistic Research Laboratories. Report Title: Transient Drag Loading of Actual and Idealized Shapes from High-Yield Detonations, WT-1305. Project Officer: H. S. Burden.

This project consisted of five parts. The objectives and results are briefly stated as follows:

Part 1. Investigation of aerodynamic-drag characteristics by measurements on full-scale beams (8WF67) and angles (8L56.9) were made at various pressure levels from Shot Cherokee. Drag and lift coefficients were obtained although the flow was not normal to the beams. Resolution of the flow was determined. Drag coefficients for the WF beams varied from 2.44 to 2.82 which was somewhat higher than steady-state data, which is usually given at 2.03. The drag coefficient for the angles varied from 2.11 to 2.61, whereas the steady-state value was 1.83. The lift coefficient for the angles varied from 2.28 to 2.73, and the steady-state value was 2.07.

Part 2. A description of an experiment for determining drag coefficients for spherical shapes as a function of the dynamic pressure of the flow following blast wave fronts is given. Two sizes of spherical shell (3 and 10 inch diameter) were used in conjunction with three-dimensional, force-sensing mechanisms. The sensing mechanisms and calibration procedure are described. The objectives were not achieved because of a serious error in the position of the detonation and because of some dubious behavior by the gages. Speculative, rather than authoritative, values of peak drag coefficient are listed as deduced from the experiment. The results are briefly compared with those for gages used in a similar pressure range on Operation Teapot.

Part 3. Investigation of the response of drag-type targets and continuation of the statistical evaluation studies on military vehicles were made by the exposure of $\frac{1}{4}$ -ton trucks (jeeps) on Shots Lacrosse, Zuni, and Yuma. Ground ranges were selected to give further data for predicting damage to vehicles under different blast conditions than those previously tested. Analysis of the data indicated an appreciable reduction in damage radii for nonprecursor conditions below that for precursor conditions. There was further indication that displacement, like damage, resulting from exposure to a blast wave of classical shape was significantly reduced as compared to the displacement received from a nonclassical or precursor wave.

Part 4. Airblast diffraction and drag loading measurements were made at a limited number of positions on a concrete cubicle during Shot Zuni. The target structure was 6 by 12 feet and located in a pressure region of 23 psi with a duration of approximately 2 to 5 seconds. The objective was achieved, in that successful records were obtained on representative locations on the various faces of the structure, but since the observed wave was nonideal in character, it was not possible to correlate the actual loading with that predicted from a scaled shock tube model.

For comparison, the actual field records and predicted records are both presented in the body of the report. Although the free-stream record was only slightly rounded, the reflected pressure over the front of the structure remained high and did not decay as predicted.

Part 5. Electronic recording instrumentation was provided for Project 1.5 on Shots Cherokee and Zuni and recording and structure instrumentation for structural-response Project 3.1 on Shot Cherokee. A multi-channel magnetic tape recording system was utilized to record 160 data channels. The objective was not fully satisfied on Shot Cherokee because of the delivery error, even though most of the instrumentation functioned satisfactorily. This error adversely affected the data records obtained from the unidirectional electronic pitot-static q and other gages. The objective was satisfactorily met on Shot Zuni.

A.1.6 Project 1.6. Drag Loading on Model Targets. Agency: U. S. Naval Ordnance Laboratory. Report Title: Drag Loading on Model Targets, WT-1306. Project Officer: Joseph Petes.

The specific and immediate objectives of this project were to: (1) measure transient drag forces as functions of time on representative model targets in regions of high- and low-dynamic pressures resulting from a medium-yield land surface burst; (2) correlate drag forces and drag coefficients experienced by model targets exposed to atomic weapon blast with drag forces and coefficients obtained on the same model in the shock tube and wind tunnel, on similar scale models previously tested in the shock tube and on high-explosive (chemical) tests, and on full-scale models tested on atomic weapons tests; and (3) compare drag

forces on models located in precursor and nonprecursor regions at approximately the same dynamic-pressure levels, utilizing data obtained on Shot 12 of Operation Teapot.

Objective 1 defined the field phase of the project's work. The drag-force measurements made on the model targets (which included sphere, cubes, cylinders, and parallelepipeds) formed the basis for meeting the other objectives. Successful attainment of Objective 2 would be a major step toward the goal of establishing realistic and reliable criteria for predicting drag forces on full-scale targets in clean Mach regions for atomic detonations on the basis of laboratory work. Attainment of Objective 3 would help in determining the role of the precursor and dust-loaded air in modifying drag forces on targets. This latter objective will help answer an immediate military need-to-know in the problem of determining the importance of the precursor phenomenon as a damage-producing mechanism.

Model targets consisted of 4-inch and 10-inch spheres, 4-inch and 10-inch cubes, $6\frac{5}{8}$ -inch-diameter cylinders, and $6\frac{5}{8}$ -by- $6\frac{5}{8}$ -inch cross-section parallelepipeds. The sphere models were mounted on stings (a configuration used previously during Operation Teapot), and the cubes were mounted on an elevated artificial ground plane. The cylinders and parallelepipeds consisted of 6-inch-long model test sections located centrally in 7-foot-long, constant cross-section mounts supported horizontally between vertical end posts approximating a two-dimensional configuration. Subsequent to the field test, the same models, similarly mounted, were tested in the wind tunnel at Mach numbers from 0.2 to 0.5 and in the shock tube at shock overpressures from 3 to 30 psi.

From the force measurements and measurements of the free-stream parameters of side-on and dynamic pressures, drag coefficients were obtained for each of the model configurations under each of the test conditions. Reasonable drag-coefficient correlation was obtained for all of the test models (except spheres) for the field and wind tunnel data. Hence, it was concluded that, for the model sizes used, the field flow conditions approached the steady-state flow conditions of the wind tunnel. The short-duration flow in the shock tube and the flow blockage resulting from the model size obviated the establishment of steady drag conditions in this facility. Thus, only extrapolations can be made to wind-tunnel and field conditions. The differences in the drag coefficients obtained in the various test facilities were attributed primarily to differences in wave shapes (particularly for the two-dimensional models), differences in boundary layers on the surfaces on which the cubes were mounted, and indeterminate parameters such as inhomogeneities of the medium during the field test.

The effects of dust loading on total force were obtained through the comparison of drag coefficients of similar spherical models used on Shot 12 of Operation Teapot and Shot 1 of Operation Redwing. These effects are discussed and the load-increasing effects of dust are qualitatively presented. In addition, it was concluded that the force gage was a useful tool for determining quantitatively the integrated effects of the blast in the field in lieu of extensive static and dynamic pressure, dust density, and particle size and velocity measurements.

A.1.7 Project 1.8. Crater Measurements. Agency: U. S. Army Engineer Research and Development Laboratories. Report Title: Crater Measurements, WT-1307. Project Officer: J. G. Lewis.

The objective of this project was to measure the physical characteristics of craters produced by the detonation of nuclear devices so as to obtain a more thorough understanding of crater-prediction phenomenology.

Crater measurements were made on the five surface or near-surface shots: Lacrosse, Zuni, Seminole, Mohawk, and Tewa. Crater radius, crater depth, and approximate profile were determined by use of aerial photography and lead-line sounding techniques. Aerial mapping photographs were made of the craters after the shots, and these were used to plot ground elevations to give the crater radius. Lead-line soundings were made along the diameter of each crater to determine the depth and average profile.

The data obtained have increased the reliability of crater predictions for saturated soil types and washed craters. Information was obtained on an unwashed crater. There appears to be no justification for the modification of crater-prediction curves in TM 23-200 for surface bursts in the regions of military significance.

A.1.8 Project 1.9a. Direct Water-Wave Measurements. Agency: University of California, Scripps Institution of Oceanography. Report Title: Direct Water-Wave Measurements, WT-1369. Project Officer: L. W. Kidd.

This project had as its objectives the gathering and analyzing of water-wave data from the Bikini and Eniwetok lagoons. The data was required (1) to improve the ability to predict wave effects from operational use of nuclear weapons, and (2) to determine safety criteria for future test operations.

The water-wave time-height history was to be determined at various ranges from ground zero. Where significant, the terminal effects were to be measured as the waves inundated the reefs and islands of the

atoll. The data was to be summarized, integrated with data from Operation Castle (higher yields, identical physical topography), and compared to present theories and concepts of impulsively generated waves.

During Operation Redwing, as in previous test series, principal observations were made by means of bottom-pressure-versus-time recorders of several types adapted to different locations, and by means of technical photography.

Data from this operation, when correlated with all previous pertinent data, has permitted considerable progress in this investigation and in the understanding of all of the various facets of wave systems, but particularly has this been so about the dimensions and the relative importance of the parameters of generation, the separability of observed wave systems, the reflections, and the inundation of shorelines. A scaling law for wave height versus range has been derived, which considers the water depth at the point of generation as well as yield. Possibly, the most significant result at this stage of the continuing investigation has been the demonstration of the limited applicability, for purposes of wave predictions, of wave data collected to date, and from this, recommendations are made for a more conclusive program for further research.

A.1.9 Project 1.9b. Indirect Water Waves from Large-Yield Bursts. Agency: University of California, Scripps Institution of Oceanography. Report Title: Indirect Water Waves from Large-Yield Bursts, WT-1308. Project Officer: W. G. Van Dorn.

The project objective was the determination of the capability of predicting in advance of future tests the nature and characteristics of the long-period waves known to be produced by such tests at ranges well outside the zone of significant blast damage.

Long-period surface water waves produced by megaton-range shots at Bikini Atoll during Operations Castle and Redwing were recorded at Ailinginae, Eniwetok, Wake, Guam, and Johnston Islands. Analysis of the results indicate that the waves originated close to Bikini, and propagated outwards as a train of solitary waves of slowly decreasing amplitude and period, as measured at a single station. In each case, the train was slightly dispersive for roughly the first 200 nautical miles, with wave height decaying inversely with range. It remained essentially unchanged in form thereafter, with height diminishing as the inverse square root of the range. The character of the dispersion and the subsequent behavior of the trains are not predicted by current theory. As measured at any station, the observed wave height varied directly with the shot yield, instead of the square root, as expected from theory. This relation can be explained by shadowing effect of the atoll.

A.1.10 Project 1.10. Measurements of Blast Over Vegetated and Cleared Areas. Agency: Sandia Corporation. Report Title: Blast over Vegetated and Cleared Areas, WT-1309. Project Officer: C. D. Broyles.

The objective of this project was to determine the difference in the blast effects over a vegetated and over a sandy surface in the precursor region and, if possible, to correlate this difference with a difference in preshock sound speed.

Measurements were made to determine the difference in blast effects over a surface covered with low shrubs and grass and over a cleared sandy surface in the precursor region, and an attempt was made to correlate this difference with measurements of preshock sound speed over the surface. Overpressure was measured with ground-baffle gages and with pitot-static gages at 3-foot elevation. Dynamic pressures were measured at the 3-foot elevation with the pitot-static gages. Measurements were made at the same ground ranges for vegetated surface as for the sandy surface. The vegetation reduced the severity of the precursor, showing later arrival times and smaller dynamic pressures than over the cleared area. The overpressures over the vegetation were the same at the ground and 3-foot levels. No measurements of sound speed after zero time were obtained, so a correlation is not possible.

A.2 PROGRAM 2: NUCLEAR RADIATION STUDIES

A.2.1 Project 2.1. Gamma Exposure Versus Distance. Agency: U. S. Army Signal Engineering Laboratories. Report Title: Gamma Exposure versus Distance, WT-1310. Project Officer: Peter Brown.

The objective of this project was to determine gamma exposures versus distance from the point of detonation of various high-yield devices.

The following types of dosimeters were used as gamma-radiation detectors: photographic, quartz-fiber, chemical, and phosphate-glass. Correction factors were applied to compensate for the nonlinear spectral response of the dosimeters, when necessary, and for station shielding. All detectors were calibrated with Co⁶⁰ sources. Photographic dosimeter readings were accepted as the most reliable on a statistical basis and were used as bases for most of the curves plotted. Photographic dosimeter film-badge service and Co⁶⁰ calibration facilities were provided to other projects as requested.

Initial-gamma radiation was measured at a series of stations located at about 1 to 4 miles from ground zero. Mechanisms were installed at some of these stations to shield the detectors from residual radiation. An analysis of the data indicates that the initial-gamma exposure at 3 miles from Cherokee, Zuni, and Navajo was about 1 r. Consequently, initial-gamma radiation was of little military significance to exposed personnel as compared to thermal and blast damage resulting from high-yield devices.

The curves in this report vary from those published in TM 23-200. The field data falls below predictions at longer ranges and is greater than predicted at shorter ranges. This difference between predicted and field data increases with increasing yield.

For fallout residual-gamma radiation measurements, instrument stations were located on almost every island of Bikini Atoll at distances where neutron-induced activity was entirely negligible. The amount of residual-radiation exposure was a function of the fission yield. Residual-gamma radiation data points are mapped in this report for Shots Zuni, Flathead, Navajo, and Tewa.

A.2.2 Project 2.2. Gamma Rate versus Time. Agency: U. S. Army Signal Research and Development Laboratory. Report Title: Gamma Exposure Rate versus Time, WT-1311. Project Officer: Peter Brown.

The primary objective of this project was the measurement of initial- and residual-gamma exposure rates as a function of time at various distances from high-yield thermonuclear detonations. Secondary objectives were to measure the residual-gamma exposure rate at the lip of the crater produced by a high-yield land-surface burst and to field test a prototype thermal detector to be used in a radiological-defense warning system.

The residual-gamma radiation was detected by an unsaturated-ion chamber, whose output determined the frequency of pulses that were recorded on electro-sensitive paper. Most of the initial-gamma-radiation stations consisted of scintillation detectors whose output determined the frequency of pulses that were recorded on magnetic tape. Some initial-gamma instruments were similar to those used during Operation Castle. The exposure rate near the crater was measured with a detector-telemeter unit dropped from a helicopter.

Residual-gamma exposure rate versus time was obtained after Shots Zuni, Flathead, Navajo, and Tewa. The observed average-decay exponents for these events were 1.1 for Zuni and Tewa, 1.2 for Flathead, and 1.3 for Navajo. In some cases, the effect of rainfall in leaching the activity decreased the exposure rate by a factor of two.

Records from Shot Flathead at 7,730 feet and from Shot Navajo at 13,870 feet indicated that at these locations about two-thirds of the total initial-gamma exposure was delivered after the arrival of the shock front.

The crater-lip measurements indicated that the method was a feasible one; however, no usable data was obtained.

The thermal-radiation detector responded satisfactorily to a 5-Mt detonation at a distance of 20 miles.

A.2.3 Project 2.4. Decontamination and Protection. Agency: U. S. Army Chemical Warfare Laboratories. Report Title: Decontamination and Protection, WT-1312. Project Officer: Joseph C. Maloney.

The objectives of this project were to investigate the contaminability characteristics of construction materials exposed at various angles and orientations to contamination resulting from high-yield nuclear detonations and to investigate the effectiveness of various decontamination techniques, in order to obtain data on the radiological recovery of military installations.

Panels of various construction materials were mounted on board the YAG-39 and YAG-40, which were operated through regions of fallout after Shots Cherokee, Zuni, Flathead, Navajo, and Tewa. With the exception of Shot Tewa, the fallout contamination deposited on the YAGs from all these events was insignificant with respect to fulfilling the objectives of this project. The contaminated Shot Tewa panels were, unfortunately, exposed to heavy rainfall prior to receipt for study. Apparently, the rains effectively

decontaminated the panels. The most heavily contaminated surface, an asphalt and gravel built-up roofing panel, read approximately 500 mr/hr when received from Shot Zuni at H+60 hours. Other panels were generally much less contaminated. Some gave readings barely above island background.

The limited data available indicated that small-particulate contamination, similar to Operation Jangle fallout, resulted from the land shots; and liquid contamination, similar to fallout from Shots Romeo and Union of Operation Castle, was produced from the deep-water barge shot. The particulate-type contaminant from Shot Zuni contaminated horizontal surfaces much more heavily than vertical surfaces. This is similar to observations at Operation Jangle. Conversely, the liquid contamination from Shot Flathead contaminated vertical surfaces much more heavily than horizontal surfaces, as was previously noted and reported during Operation Castle.

Contamination levels were generally reduced by factors of two-to-four by detergent scrubbing of the most heavily contaminated panels. Depth of penetration studies in painted wood revealed that the contamination was contained in the paint layers (120 to 300 microns thick). However, in all unpainted wood samples, the contaminant, after wetting, penetrated to depths of 1,000 to 2,000 microns, or more.

A.2.4 Project 2.51. Neutron-Flux Measurements. Agency: U. S. Army Chemical Warfare Laboratories. Report: Neutron-Flux Measurements, WT-1313. Project Officer: Charles W. Luke, Captain, USA.

The objectives of this project were to measure the neutron flux and spectrum from the detonation of selected nuclear devices during Operation Redwing. Primary emphasis was placed on measurements during Shot Cherokee, a thermonuclear, high-yield, air burst, and on [redacted] Yuma and Kickapoo. Measurements were also made on Shots Blackfoot and Erie, [redacted] During the operation, permission was granted to make neutron measurements on Shot Osage, a low-yield prototype stockpile warhead unit in a bomb case. Neutron-dose measurements made by chemical and semiconductor dosimeters were compared with the dose calculated by the single-collision theory from the neutron flux and spectral data. The effect of the presence of different proportions of borax and sulfur on the shielding efficiency of concrete against neutrons was studied during Shot Blackfoot.

Neutron fluxes as a function of distance from ground zero were measured with the following detectors: gold, plutonium, neptunium, uranium, sulfur, and zirconium.

No data were obtained during Shot Cherokee because of the difference between the actual and intended ground zero.

The variation of the neutron flux about the devices fired for Shots Yuma and Kickapoo was energy dependent. The ratios of the neutron flux along a line at 65 degrees to the projection on the ground of the long axis of the device, to that along a line at 0-degrees to this projection for Shot Yuma, were 1.34, 1.91, 1.94, and 1.18 for the plutonium, uranium, sulfur, and gold detectors, respectively. The same ratios between the 85-degree and 0-degree lines for Shot Kickapoo were 1.62, 1.70, 1.62, and 1.22.

Within the range of the measurements made and the accuracy of the threshold detector system there was no variation of the neutron-energy spectrum with increasing distance from the point of detonation.

Any data obtained from an extrapolation of a plot of the neutron flux times slant distance squared versus slant distance to ranges of less than 300 yards may be in error. Theoretical calculations supported by experimental evidence indicate that the relationship is nonlinear in this range.

The neutron dose results obtained by using the USAF chemical dosimeters were not consistent with those obtained by the threshold detector technique, ranging from a factor of 1.26 high for Shot Erie to an average factor of 3.54 low for Shot Blackfoot.

The AEC germanium-dosimeter results were lower by factors of 3.46 to 5.38 than those obtained by the threshold-detector technique.

The AEC chemical-dosimeter system may not be used to measure neutron dose in the range of 25,000 to 856,000 rep, due to saturation of the neutron-sensitive dosimeter and difficulties inherent in obtaining accurate readings.

There is little or no increase in the attenuation of fast-neutrons by adding borax or sulfur to concrete. The attenuation of the thermal-neutron flux is increased by adding borax.

The neutron dose was reduced by a factor of approximately four by a concrete box three feet on a side and 6 inches thick fabricated from a mixture containing 1.6 percent borax by weight. The gamma-ray dose, however, was increased by an average factor of 2.75 by similar concrete boxes containing varying amounts of borax and sulfur.

The measured neutron dose per unit yield was higher for all shots than was predicted by TM 23-200. However, only the Yuma, Blackfoot, Kickapoo, and Osage data falls beyond the factor of reliability stated in the manual.

A.2.5 Project 2.52. Neutron-Induced Soil Radioactivity. Agency: Sandia Corporation. Report Title: Neutron-Induced Soil Radioactivity, WT-1314. Project Officer: Maynard Cowan, Jr.

Soil samples were exposed to neutron radiation from Shot Cherokee to help establish the importance of neutron-induced residual gamma radiation from a large-yield thermonuclear air burst. After exposure and recovery, the samples had no detectable activity because the slant range to the nearest sample was nearly 3.5 miles, due to an error in bomb drop. After this failure, an experiment was designed in the field for Shot Yuma in order that induced-activity data could be obtained for a soil other than Nevada Test Site (NTS) soil. Samples of sodium, manganese, and coral sand from Site Sally were exposed above and below the surface at a slant range of 120 yards. At this same station, gamma dose rates were measured and neutron detectors were exposed by Project 2.51.

The full-field gamma radiation measured was due to a combination of fission-product and neutron-induced activities, the only important induced activity being due to $\text{Na}^{23}(n, \gamma) \text{Na}^{24}$. At 1.1, 3.4, and 10.9 hours after zero time, neutron-induced gamma radiation accounted for 1.2, 1.1, and 0.8 r/hr of the measured 6.0, 2.2, and 1.2 r/hr. These values were found to be within 50 percent of neutron-induced dose rates predicted by the method described in M. Cowan's "Neutron-Induced Gamma Radiation from Nuclear Air Bursts", Sandia Corporation, Albuquerque, New Mexico.

A.2.6 Project 2.61. Rocket Determination of Activity Distribution Within the Stabilized Cloud. Agency: U. S. Naval Radiological Defense Laboratory. Report Title: Rocket Determination of Activity Distribution within the Stabilized Cloud, WT-1315. Project Officer: Richard R. Soule.

Forty especially developed atmospheric-sounding projectiles (ASP) were fired through the clouds resulting from Shots Cherokee, Zuni, Navajo, and Tewa to proof test a system for measuring gamma intensities within the clouds and to explore the spatial distribution of gamma activity within the stem and cloud resulting from the detonation of a nuclear device having a yield in the megaton range. Radiation intensity information was successfully telemetered out of the radioactive clouds by the ASP rockets and recorded on magnetic tape. Radiation intensities as high as 3×10^4 r/hr were encountered within the cloud; intensities at the one measured point in the stem were negligible compared to the peak activity within the cloud. Contamination of rocket surfaces by radioactivity from the cloud did not appear to be of consequence. Total activities in the clouds computed from rocket data agreed in order of magnitude with activities derived from theoretical considerations.

A.2.7 Project 2.62. Fallout Studies by Oceanographic Analysis. Agency: Scripps Institution of Oceanography. Report Title: Fallout Studies by Oceanographic Methods, WT-1316 (Project 2.62a). Background Radioactivity and Oceanographic Conditions, WT-1349 (Project 2.62b). Project Officer: Feenan D. Jennings.

Project 2.62a. The first of five areas of study was the oceanography of the water within a 300-mile radius of Bikini Atoll prior to and during the operation. The objectives were to measure oceanographic parameters affecting the fallout pattern and to determine the radioactive background within the ocean. The results of this study have been presented as a separate report, WT-1349.

The second study involved the determination of fallout by the use of oceanographic methods. In addition to the collection of samples for this and other projects, it was the objective of this survey to measure the intensity and extent of fallout, to convert this to equivalent land values, and to relate the in situ fallout distribution to the oceanographic parameters.

The results of the oceanographic fallout surveys show that: (1) Shot Cherokee (an air burst) produced no measurable fallout. (2) Shot Flathead (a water burst) produced fallout that mixed downward into the ocean water at a rate of 3.5 m/hr and attained an average penetration depth amounting to 75 percent of the thermocline depth. (3) Shot Navajo (a water burst) produced fallout with a mixing rate of 2.3 m/hr and attained an average penetration depth of 75 percent of thermocline depth, and although Navajo had a total yield of [redacted] it produced an area of less than 150 mi² of hazardous dose rates. (4) Shot Tewa (a combination water- and-land burst) exhibited a mixing rate similar to Flathead (3.8 m/hr) and an average penetration depth similar to Flathead and Navajo (75 percent of thermocline depth); this 5-Mt, device produced hazardous dose rates over an area exceeding 2,000 mi². (5) Shot Zuni (a land burst) fallout mixed downward at 11 m/hr and reached an average penetration depth of 107 percent of thermocline depth. (6) Dose rate in fallout resulting from nuclear detonations is directly proportional to the fraction of fission yield. (7) The cube-root scaling laws are valid for fallout dose rates from nuclear detonations over the range from [redacted] to 5.0 Mt.

The third study concerned oceanographic and fallout measurements in the lagoon circulation for various wind conditions and, from this, the prediction of the movement of radioactive water from a knowledge of the winds. The results of the lagoon oceanographic studies have been presented in WT-1349. The

measurements show that the movement of radioactivity with the lagoon water corresponds to the observed current movements. These same measurements have been used in WT-1349 to develop a method of predicting the distribution of radioactivity within the lagoon from a knowledge of current directions and velocities.

The fourth interrelated field of work involved the installation and maintenance of anchored instrument stations in the deep ocean water. The results of this effort have such military and scientific implications that the complete procedure for installing these stations is included as an appendix to WT-1316.

The last study was a radiochemical examination of fallout in the marine biosphere. The results show the distribution of fallout material in the water, the air above the water, the sediments, and marine life. These studies were carried out in the lagoon as well as in the open ocean. Marine organisms selectively absorb such nonfission products as Mn^{54} , Co^{58} , Co^{60} , and Zn^{65} . Oceanic contamination was detected from the Eniwetok Proving Ground to a latitude of 11 degrees south after the completion of the test series.

Project 2.62b. The primary task of this project was to measure and evaluate fallout over the ocean and to convert these measurements to a land-equivalent fallout pattern. In preparation for this and auxiliary tasks, studies were made in three related fields. The results of these studies are presented in this report.

The first chapter presents the results of the study of radioactivity associated with the oceanic environment in the Eniwetok Proving Ground (EPG) prior to the test series in 1956. This background study was necessary to properly evaluate the radioactivity resulting from Operation Redwing.

Past studies of fission products that enter sea water have shown that some of the chemical species are soluble, some insoluble. These previous studies also indicated that marine organisms could assimilate concentrations of radioisotopes a hundredfold over that found in the water in which they lived. It was also shown that the isotopes that were concentrated varied among the different types of organisms.

During the months of April and early May 1956 this background study was undertaken. Water samples and marine life were collected from various depths in the ocean and lagoons. Sediments and bottom-dwelling organisms were collected for analysis of radioactive content. In addition, miscellaneous samples of the flora and fauna from various atolls were analyzed for comparison with marine organisms. Air-borne particulate matter was obtained from various parts of the proving grounds.

Gamma counting using a gamma differential pulse-height analyzer and simple chemical group separations or ion exchange separations were used to determine individual radioisotopes and mixtures of fission products.

Results obtained indicated that widespread radioactive contamination, nonuniform in amount and isotopic content, existed in the proving grounds during April 1956. A separation of the fission products had taken place with concentrations of specific isotopes in specific phases. Hundred to thousandfold concentrations of radiocobalt and radiozinc were observed in clams and fishes. Radioactive contamination of the sea water was low, while the zooplankton showed a hundredfold increase of radioactivity over that of the water.

The most prominent radionuclides detected in living organisms were Zn^{65} , Co^{57} , and Co^{60} , none of which are fission products. The greatest total mass of radioactivity was found to be the Ce^{144} and Ru^{106} distributed over the ocean and lagoon floors.

The second study was concerned with the oceanography of the ocean waters in the proving grounds. Part of this study was accomplished in conjunction with the pre-operation radioactivity measurement.

The current studies confirmed the general circulation obtained during Operation Crossroads and by Japanese cruises. In addition, more explicit information was obtained. Meandering and eddying dominated the flow in the latitude of Bikini; the main flow westward was located at the north side of the EPG. A large scale counterclockwise eddy existed down to depths of at least 500 meters. In April, this eddy was just east of Bikini, in July it was found due north of the atoll. In April the current at the surface attained 0.6 to 0.7 knot speed and averaged 0.3 to 0.4 knot; thence at 500 meters it decreased to a maximum of 0.3 knot and averaged 0.15 knot. In July, the current speeds were about half those found in April and current directions in some locations had reversed. In general, the current system around Bikini was extremely variable and showed fluctuations both in speed and direction over periods as short as a week, and possibly shorter.

The thickness of the wind-stirred layer above the thermocline showed the same short-term fluctuations as the currents. Geographically, the depth to the top of the thermocline ranged from 40 meters to 170 meters, but at any given location, this depth could vary as much as 50 to 100 meters over a 2-week period.

Underwater sound-propagation conditions above the thermocline appeared homogeneous during the entire operation. Sound propagation in the deep water was bottom-limited where depths were less than 1,000 fathoms. The axis of the deep sound channel was between 800 and 1,200 meters (1.3 to 1.5 times as deep as off the west coast of the United States).

The third study involved oceanographic measurements inside Bikini Lagoon. This work was accomplished in the month prior to, and during the first 2 months of Operation Redwing. The physical hydrog-

raphy was similar to that obtained at Operation Crossroads. Surface waters moved downwind, and deep waters flowed in the opposite direction to complete a cellular circulation. At the upwind end of the lagoon, the deep waters were diverted both north and south into two secondary horizontal cells. During southerly and southeasterly winds, most of the inflow occurred through Enyu Channel. During moderate-to-strong trades, water flowed into the lagoon over the windward reefs and also through Enyu Channel; it flowed out over the reefs and through the deep channels on the leeward end of the lagoon.

Speed of the surface current was found to be about 1.6 percent of the wind speed, instead of 3 percent as had been found previously. The deep flow was found to be more variable in direction and of considerably less speed than during previous operations. Following a material decrease in the trades, the surface current stopped within 1 hour and lagoon seiching occurred. When the wind speed again increased, the surface current responded with a time lag of about 5 hours.

It is calculated that, when the east-northeast trades prevail, water in the lagoon is renewed about every 40 days. At times of light southerly or southeasterly winds, an estimated 60 to 100 days are required. No conditions were observed during the operation in which rapid flushing of the lagoon occurred, as apparently took place during Operation Crossroads.

From radioactivity measurements made in the lagoon following one of the detonations, calculations were made to determine the vertical coefficient of eddy diffusivity. Using the values obtained for this constant, an example is presented for determining current velocities from radioactivity measurements. In addition, a method is presented for predicting radiation levels (in various parts of the lagoon) from the early determination of intensity and area of radioactivity.

A.2.8 Project 2.63. Characterization of Fallout. Agency: U.S. Naval Radiological Defense Laboratory. Report Title: Characterization of Fallout, WT-1317. Project Officer: Terry Triffet.

The general objective of this project was to obtain data sufficient to characterize the fallout, interpret the aerial and oceanographic survey results, and check fallout-model theory for Shots Cherokee, Zuni, Flathead, Navajo, and Tewa during Operation Redwing. Detailed measurements of fallout buildup were planned. Measurements of the radiation characteristics and physical, chemical, and radiochemical properties of individual solid and slurry particles and total cloud and fallout samples were also planned, along with determinations of the surface densities of activity and environmental components in the fallout at each major station.

Standardized instruments and instrument arrays were used at a variety of stations which included 3 ships, 2 barges, 3 rafts, 13 to 17 deep-anchored skiffs, and 4 islands at Bikini Atoll. Total and incremental fallout collectors and gamma time-intensity recorders were featured in the field instrumentation. Special laboratory facilities for early-time studies were established aboard one ship. A number of buried trays with related survey markers were located in a cleared area at one of the island stations. Instrument failures were few, and a large amount of data was obtained.

This report summarizes the times and rates of arrival, times of peak and cessation, mass-arrival rates, particle-size variation with time, ocean-penetration rates, solid- and slurry-particle characteristics, activity and fraction of device deposited per unit area, surface densities of chemical components, radio-nuclide compositions with corrections for fractionation and induced activities, and photon and air-ionization decay rates. A number of pertinent correlations are also presented: predicted and observed fallout patterns are compared, sampling bias is analyzed, gross-product decay is discussed in relation to the $t^{-1.2}$ rule, fraction-of-device calculations based on chemical and radiochemical analyses are given, the relationship of film-dosimeter dose to gamma time-intensity integral is considered, a comparison is made between effects computed from radiochemistry and gamma spectrometry, air-sampling measurements are interpreted, and the fallout effects are studied in relation to variations in the ratio of fission yield to total yield.

Some of the more important general conclusions are summarized below:

The airburst of Shot Cherokee produced no fallout of military significance.

Fallout-pattern locations and times of arrival were adequately predicted by model theory.

Activity-arrival-rate curves for water-surface and land-surface shots were similar, and were well correlated in time with local-field ionization rates.

Particle-size distributions from land-surface shots varied continuously with time at each station, with the concentration and average size appearing to peak near time of peak-radiation rate; the diameters of barge-shot fallout droplets, on the other hand, remained remarkably constant in diameter at the ship stations.

Gross physical and chemical characteristics of the solid fallout particles proved much the same as those for Shot Mike during Operation Ivy and Shot Bravo during Operation Castle. New information was obtained, however, relating the radiochemical and physical characteristics of individual particles. Activity was found to vary roughly as the square of the diameter for irregular particles, and as some power greater than the cube of the diameter for spheroidal particles.

Fallout from barge shots consisted of slurry droplets, which were composed of water, sea salts, and radioactive solid particles. The latter were spherical, generally less than 1 micron in diameter, and consisted mainly of oxides of calcium and iron. At the ship locations, the solid particles contained most of the activity associated with the slurry droplets; closein, however, most of the activity was in soluble form.

Bulk rate of penetration of fallout in the ocean was, under several restrictions, similar to both solid and slurry particles. Estimates are given of the amount of activity which may have been lost below the thermocline for the fast-settling fraction of solid-particle fallout.

Fractionation of radionuclides from Shot Zuni was severe while that from Shot Tewa was moderate; Shots Flathead and Navajo were nearly unfractionated. Tables are provided, incorporating fractionation corrections where necessary, which allow the ready calculation of infinite-field ionization rates, and the contribution of individual induced activities to the total ionization rate.

Best estimates are given of the amount of activity deposited per unit area at all sampling stations. Estimates of accuracy are included for the major stations.

A.2.9 Project 2.64. Fallout Location and Delineation by Aerial Surveys. Agency: Health and Safety Laboratory, New York Operations Office, U.S. Atomic Energy Commission. Report Title: Fallout Location and Delineation by Aerial Surveys, WT-1318. Project Officer: Robert T. Graveson.

The objectives were to: (1) survey the gamma radiation from fallout-contaminated ocean areas by means of aerial detectors and (2) from the aerial detectors make air-absorption measurements so that the data might be related to the dose rates at 3 feet above the sea.

Radiation detectors were mounted in P2V-5 aircraft that surveyed the ocean areas of expected fallout after Shots Cherokee, Zuni, Flathead, Navajo, Mohawk, and Tewa. A control center coordinated all air and surface radiation-survey activities to insure complete coverage of the fallout area. The contamination densities in the delineated areas were related to the percentage of the total yield that produced fission products. Gamma-isodose plots were prepared from data obtained during Shots Zuni, Flathead, Navajo, and Tewa. No fallout could be located following Shot Cherokee and only on atoll islands after Shot Mohawk.

Zuni, a land-surface shot, contaminated 13,400 naut mi² of ocean with 48 percent of its fission-product yield.

Navajo, a water-surface shot, contaminated 10,500 naut mi² with 50 percent of the fission-product yield. After Flathead, another water-surface shot, the outer boundary could not be determined because of contamination of project aircraft on D+1 day by airborne radioactive material that resulted in a high background. However, extrapolated values indicate 29 percent of its fission-product yield was present as fallout in the local area. The fallout from the water-surface shots was concentrated primarily in the more remote areas, and a relatively small amount fell close to ground zero.

Tewa, a reef shot, contaminated 43,500 naut mi² of ocean with 28 percent of the fission-product yield. Helicopters and P2V-5 aircraft were used to gather data for air-absorption measurements.

The aerial-survey technique may be used directly for radiological surveys over land. Over the sea, the depth of mixing of the fallout in the water volume must be determined before the survey results may be converted to equivalent land-fallout contours and contamination-density distributions. Data on depth of mixing was obtained from samples of sea water collected by the U.S. Naval Radiological Defense Laboratory and the Scripps Institution of Oceanography. Repeated aerial surveys provided information on the stability of the contaminated volume.

A.2.10 Project 2.65. Land Fallout Studies. Agency: Chemical Warfare Laboratories, Army Chemical Center. Report Title: Land Fallout Studies, WT-1319. Project Officer: Manfred Morgenthau.

The objectives of this project were to obtain fallout samples and perform radiochemical and radiophysical measurements on the samples, prepare dose-rate contours in the immediate area of the atoll, and evaluate the role of base surge in the transport of radioactive material.

Time-incremental and gross fallout samples were collected on islands of Bikini Atoll, on a barge in Bikini Lagoon, and on three ships in the downwind fallout area after Shot Cherokee, an air burst; Shots Zuni and Tewa, land-surface shots; and Shots Navajo and Flathead, water-surface shots. Gross fallout samples were collected on islands of Eniwetok Atoll after Shot Lacrosse, a land-surface shot. Ground contamination was measured after Shots Lacrosse, Zuni, Flathead, Mohawk, Navajo, and Tewa by lowering a probe from a helicopter to a height of 3 feet above ground. Factors for converting dose-rate readings from various altitudes to 3 feet were obtained over Site Charlie after Shots Zuni and Flathead. Photoelectric base-surge detectors were installed at a few close-in stations for Shots Zuni, Flathead, Navajo, and Tewa. No evidence of fallout from Shot Cherokee was found on Bikini Atoll.

Early decay of gamma dose rate agreed well between field and laboratory. The early gamma decay exponent averaged -1.0 for all shots except Shot Lacrosse, for which it was about -1.35. The beta decay

curves of liquid fallout from land-surface shots differed markedly from those of solid fallout.

Most of the fallout radioactivity from land-surface shots was associated with particles between 149 and 420 microns, and the activity per unit weight increased with distance from ground zero.

Significant Shot Zuni fallout arrived on the islands of the atoll between 16 and 40 minutes, reached a maximum between 20 and 90 minutes, and ceased between 2 and 3.5 hours. Shot Flathead fallout was collected at all island stations during the first 30 minutes; the maximum occurred between 1½ and 2 hours; fallout stopped at H+10 hours, started again at H+15½, and continued until H+18 hours. Significant Shot Navajo fallout reached Site Charlie between 30 and 35 minutes, was at a maximum between 45 and 50 minutes, and ceased between 1.5 and 2 hours. Significant Shot Tewa fallout arrived on the islands of the atoll between 30 and 90 minutes, reached a maximum between 1 and 2½ hours, and ceased between 2.5 and 5 hours.

Most of the fallout activity from Shot Flathead was associated with a slurry, or mud, which contained CaCO₃ particles, Fe₂O₃ particles, and NaCl crystals. The Shot Navajo fallout consisted of solid particles, a dried mist, and liquid. The Shots Lacrosse, Zuni, and Tewa fallout consisted chiefly of particles derived from coral. The predominant types were irregular white opaque, irregular translucent, and yellow or white spheres in that order of frequency. Although the spherical particles accounted for no more than 15 percent of the total number, they contributed, at D+10 days, 60 to 80 percent of the fallout activity during Shot Zuni and 25 percent during Shot Tewa. Most of the particles were radioactive throughout their volumes. The frequency of particles active throughout decreased with increasing particle size, while the frequency of those active only on the surface increased. Radiochemical composition differed between cloud and ground samples and varied with particle type, distance from ground zero, and physical state. The particle studies and radiochemical data provided a basis for a proposed mechanism of particle formation.

Methods are presented for calculating field dose rates from laboratory measurements.

The photon energy of the fallout from both land-surface and water-surface thermonuclear shots increased from 0.22 Mev at 100 hours to 0.33 Mev at 300 hours because of the decrease in the contribution of Np²³⁹. The gamma spectrum of the total fallout, from 100 to 300 hours, did not vary with position or with the type of burst except for the influence of activities produced by neutron capture.

Ce¹⁴⁴ appeared to be more representative of the fission product complex than Mo⁹⁹. The Sr⁹⁰/Ba¹⁴⁰ ratio was not so constant as anticipated, but was much more reproducible than either Sr⁹⁰/Mo⁹⁹ or Sr⁹⁰/total beta activity.

The aerial-survey technique proved a practical way of measuring surface contamination in high-radiation fields. H+1 hour dose rates of 10,000 to 13,000 r/hr, the highest ever observed, were measured near the Shot Mohawk crater.

No radioactive base-surge was observed on Sites Charlie and Fox after Shot Flathead.

A.2.11 Project 2.66. Early Cloud Penetrations. Agency: Air Force Special Weapons Center. Report Title: Early Cloud Penetrations, WT-1320 (Project 2.66a); Contact Radiation Hazard Associated with Aircraft Contamination by Early Cloud Penetrations, WT-1368 (Project 2.66b). Project Officer: Ernest A. Pinson, Colonel, USAF.

Project 2.66a. The objective of this project was to measure the radiation dose and dose rate one would experience in flying through the cloud resulting from a megaton-range weapon and some factors affecting personnel safety in the event of an operational situation requiring flights through such clouds.

Specific information was sought on the radiation dose rates inside the cloud, the total dose received in flying through such a cloud, the total dose received on the return flight after flying through the cloud, the internal radiation dose due to inhalation of fission products during such flights, and the conditions of flight inside the cloud.

Twenty-seven penetrations of six radiation clouds from multimegaton-range detonations were made at times ranging from 20 to 78 minutes after detonation and at altitudes ranging from 20,000 to 50,000 feet. Sixteen of these penetrations were earlier than 45 minutes and seven were earlier than 30 minutes.

Maximum radiation dose rates as high as 800 r/hr were encountered, and several flights yielded total radiation doses to the crew of 15 r.

It was found that the average radiation dose rate in the mushroom of the cloud from a 100-percent-fission-yield detonation would be:

$$\bar{D} = 1.0 \times 10^5 t^{-1.7}$$

Where: \bar{D} = average dose rate, r/hr
t = time after detonation, minutes

This relationship holds for times from 3 to 80 minutes after detonation.

The average dose rate in the stem of the cloud from water-surface bursts was found to be less than the dose rate in the mushroom by a factor of from five to ten. The radiation dose rate in the cloud is independent of yield, but is proportional to the ratio of fission yield to total yield.

In a high tropopause area, a flight through a cloud from a 100-percent-fission-yield multimegaton-range weapon in a high-performance aircraft may be made at 45,000 feet at a time of 20 minutes after detonation. The average mission dose of this flight would be 25 r. At 30,000 feet, a penetration of the stem of the cloud may be made as early as 10 minutes after detonation with a radiation dose of the same magnitude.

The dosage received on the return to base flight because of contamination on the aircraft (B-57B) was found to be about 15 percent of the total mission dose for flights lasting about 50 minutes after the cloud penetration.

An investigation of the internal radiation hazard encountered by the flight crews was conducted. The internal hazard was found to be insignificant compared to the external hazard.

Project 2.66b. The objectives of this project were to determine whether any correlation exists between the contact radiation hazard on aircraft that have recently flown through nuclear clouds and the dose rate measured on the surface by an AN/PDR-39 (T1B) survey meter; study the distribution, intensity, and decay of the contamination that causes the contact hazard; and evaluate the amount of protection offered by each of a number of different types of gloves.

The contact hazard which personnel experience when working on radioactively contaminated aircraft was investigated. Measurements of the contact hazard are approximated by surveying the aircraft with a gamma survey instrument (T1B) and applying a correction factor to the readings obtained; 110 times the T1B reading (r/hr) will give the approximate contact dose (rep/hr) to the skin in areas of direct impingement of the contaminant, i. e., leading edge of the wing, nose, etc., whereas 40 times the T1B reading is applicable to the sliding surfaces, i. e., sides of the fuselage.

The protection to an individual from the contact hazard realized by wearing gloves was also investigated. All gloves tested reduced the radiation intensity to the hands by at least 50 percent in addition to preventing the contaminant from coming in direct contact with the skin. Wearing of gloves in radiation fields of 0.1 r/hr or more is recommended.

The project recommended that Air Force publications be revised to indicate the lack of necessity for the decontamination of radioactively contaminated aircraft by Air Force operational organizations.

A.2.12 Project 2.71. Ship-Shielding Studies. Agency: U. S. Naval Radiological Defense Laboratory. Report Title: Ship-Shielding Studies, WT-1321. Project Officer: Heinz R. Rinnert.

The objectives of this project were to determine, for the types of nuclear detonations encountered during Operation Redwing, (1) the relative gamma radiation fields resulting from radioactive contaminants on a ship's weather surfaces, in the surrounding air envelope, and in the surrounding water envelope as a function of time and (2) characteristics of the interaction of gamma radiation with steel as a function of thickness and time after detonation.

Shielded recording gamma-radiation detectors of known geometry were located on two YAG's to permit discrimination between the radiation fields resulting from water-borne and air-borne activities only. Unshielded detectors supplied data on the overall radiation fields on the weather decks. Recording radiation detectors inclosed in steel cylinders of various thicknesses supplied combined absorption and multiple scattering data as a function of time after detonation.

The water contributions to the total radiation aboard an unwashed ship were crudely estimated to be less than: (1) 11 percent in the lower hold; (2) 3.5 percent in the upper hold; and (3) 1 percent on the deck. The values on a washed ship could be as much as six times higher than those on the unwashed ship, and would therefore be of significance in the shielded areas.

The highest estimates of air contribution to the total radiation on deck of a washed ship were: (1) between 32 and 95 percent of the dose rate during the period of maximum fallout; and (2) between 17 and 53 percent of dose accumulated within 24 hours after start of fallout. The comparable estimates for an unwashed ship were lower because of the greater influence of contaminated surfaces, but were still of significance during the period of maximum fallout.

Values of combined absorption and scattering coefficients were found to vary with time after a given shot, and to vary from shot to shot. Results for Shot Navajo indicated an especially different gamma energy spectrum during the first thirty hours after detonation. Differences in spectra are borne out by measurements performed by Project 2.63.

It was concluded and recommended that all calculations of radiation attenuation afforded by ships structures should include consideration of: (1) the changing relationship among the significant contributions of the several radiation sources and (2) the significant variation of the gamma radiation absorption and scattering characteristics of steel with respect to shot type and time after detonation. These variables should be investigated for as many shot conditions as may be practicable, especially for underwater detonations where significantly different results may be expected in the relationships among radiation sources.

A.2.13 Project 2.72. Evaluation of Standard Navy Dosimeters DT-60/PD and IM-107/PD in Residual Radiation Fields Aboard Ships. Agency: Bureau of Ships, U. S. Navy. Report Title: Evaluation of Standard Navy Dosimeters DT-60/PD and IM-107/PD in Residual Radiation Fields Aboard Ships, WT-1350. Project Officer: Samuel C. Rainey.

The objective of this project was to determine the effectiveness of regular production IM-107/PD and DT-60/PD dosimeters in reading the proper depth dose for personnel in residual radiation fields aboard ships. Through the use of a large number of dosimeters, an attempt was made to evaluate the extent to which any single detector worn by shipboard personnel could form the basis of a tactical or administrative decision.

Standard Navy dosimeters DT-60/PD (phosphor glass) and IM-107/PD (quartz fiber) were mounted on the surface of masonite man-sized phantoms and exposed to radiation fields caused by deposited fallout on the YAG-39 and YAG-40 in order to evaluate their response in terms of the 3-to-5-cm-depth dose. This dose is considered a more satisfactory indicator for the evaluation of acute effects to personnel in nuclear warfare than is the air dose. Depth-dose configurations in these phantoms were determined by means of phosphate-glass needles. The radiation doses indicated by the surface detectors were compared with those at a depth of 3 cm. Differences and scatter in the readings of the two types of standard dosimeters, and differences between the surface readings and the depth readings, indicate that the DT-60/PD and IM-107/PD dosimeters are not satisfactory in their present form for proper measurement and interpretation of the radiation dose received by shipboard personnel above decks in a fallout field.

A.2.14 Project 2.8. Shipboard Countermeasures Methods Studies. Agency: U. S. Naval Radiological Defense Laboratory. Report Title: Shipboard Radiological-Countermeasure Methods, WT-1322. Project Officer: Raymond H. Heiskell.

The objective of this project was to evaluate in the field several laboratory methods of shipboard protection and decontamination that had been under development since Operation Castle and to obtain information to aid in the improvement of countermeasures.

Various test surfaces and specimens were exposed on YAG-39 and YAG-40 to fallout from Shots Zuni, Flathead and Tewa. Contaminability-decontaminability (C-D) studies were conducted when the ships returned to Eniwetok Lagoon.

Three days after Zuni the average reading in the nonwashdown area of the YAG-40 was approximately 350 mr/hr and in the washdown area approximately 90 mr/hr. When the decontamination studies were initiated, the average levels after Flathead were lower than those after Zuni by a factor of 10. The average nonwashdown reading was 35 mr/hr and the washdown reading, 10 mr/hr.

The removal of the removable radiological protective coating (RRPC) after Zuni in the nonwashdown area removed all but 0.5 to 8.0 percent of the contaminant, while firehosing alone left a residual of 6 to 28 percent. Firehosing plus removal of the RRPC removed all but 0.2 to 3.0 percent of the activity. In the washdown area, the RRPC removal left 6 to 9 percent residual contamination as compared to 16 to 40 percent after decontamination of an uncoated area, with a hot-liquid jet cleaning unit. After Flathead, the removal of the RRPC from a nonwashdown area left a residual of only 3 percent as compared to 18 percent residual after firehosing and hand scrubbing. Removal of the coating in the washdown area showed only 20 percent reduction of the original contaminant, but the initial level was actually too low to give reliable instrument readings.

Mechanical scrubbing of surfaces exposed at either Zuni or Flathead was slightly inferior to manual brushing, but operators felt no fatigue and stated that long scrubbing times could easily have been endured.

Wire ropes and manila lines 1 inch or more in diameter will create a long-term radiation source. Protective coatings on canvas and canvas substitutes show promise in reducing the hazard from this material. Firehose exposed to fallout when coiled will create a more severe long-term radiation hazard than when stored uncoiled.

Surface roughness of wood decking was a major factor in determining the initial contamination level. Penetration of the fallout contamination into the wood beyond the rough surface layer was negligible, but decontamination to a residual of 2 percent would have required removal of approximately 2 mm of the surface layer because of the roughness. The payed joints between the wooden planks presented no additional

problem, as long as the joints were free of fissures and pockets.

Soap plus water and ammoniacal petroleum-based waterless cleaner were equally effective in removing the fission product contamination from the hands.

Beta measurements provided the best assessment of surface decontamination effectiveness, and 3-foot gamma measurements provided the best data in determining the overall ship decontamination effectiveness.

The basic C-D studies showed that it was more difficult to remove the Zuni contaminant than that of Flathead, confirming the results of other studies that showed this difficulty was mainly due to the difference in mass involved. These studies also showed that EDTA and Orvus solution were far superior decontamination agents than C-7907 or water alone. Allowing the activity to remain on the surface for two weeks made it more difficult to remove than if decontamination was performed one day after the surface was contaminated.

Radiological warfare may require new standards of cleanliness for naval ships. Wood decking should be maintained as smooth as possible with no raw wood exposed. All payed joints should be free of fissures and pockets. Nothing, including wire ropes, manila lines, and firehoses not required during attack, should be stored on the main deck. After contamination, any materials that cannot be destroyed should be stored uncolled to minimize the radiation field, or stored in an unfrequented location.

A.2.15 Project 2.9. Standard Recovery Procedure for Tactical Decontamination of Ships. Agency: Bureau of Ships, U.S. Navy. Report Title: Standard Recovery Procedure for Tactical Decontamination of Ships, WT-1323. Project Officer: Frank S. Vine.

The objectives of this project were (1) to proof test a proposed standard recovery procedure for the tactical decontamination of Navy ships and (2) to perform, as required, an operational decontamination of each of three test ships to enable them to make their next scheduled participation.

Three washdown-equipped test ships, the YAG-39, the YAG-40, and the LST-611, served as fallout-collection stations and test platforms for other Program 2 projects. These ships were successively contaminated by radioactive fallout from Shots Zuni, Flathead, Navajo, and Tewa.

Because of insufficient contamination aboard the ships on their arrival at Eniwetok Lagoon following their several missions, the primary objective was not fulfilled. Therefore, the function of Project 2.9 was generally restricted to operational decontamination between shots. The proof-testing of the standard recovery procedure, which consisted of firehosing, hand-scrubbing, and firehosing again, which was planned for execution aboard the YAG-39, was therefore not attempted until after Shot Tewa. A shipboard gamma-radiation dose of 2 to 5 r/hr, considered to represent a minimum tactical situation, was not obtained. The measured average dose rate aboard the YAG-39 in the nonwashdown area at the start of decontamination after Shot Tewa was about 230 mr/hr.

In this test, the standard recovery procedure proved to be practicable for the conditions encountered; however, in order to determine the absolute satisfactoriness of this procedure for the tactical situation, a further evaluation will be required.

A second procedure, hot-liquid-jet cleaning, was also investigated under like conditions and was found to be equally as effective as the standard recovery procedure at approximately twice the rate of surface coverage; however, insufficient evidence was obtained for a conclusion that the greater operating rate (and presumable reduced dosage of personnel involved) would justify the expenditure of large sums for the special equipment required.

A.2.16 Project 2.10. Verification of Washdown Effectiveness as a Shipboard Radiological Countermeasure. Agency: Bureau of Ships, U.S. Navy and U.S. Naval Radiological Defense Laboratory. Report Title: Verification of Shipboard Washdown Countermeasure, WT-1324. Project Officer: W.J. Armstrong.

The objective of this project was to verify the effectiveness of a washdown system as a radiological countermeasure for ships. The evaluations were made possible by the requirement for washdown-equipped ships to be stationed within the region of tactically significant fallout in order to support several projects in the fallout characterization program of Operation Redwing.

To fulfill the instrumentation requirements of Program 2, the Bureau of Ships test ships, YAG-39 and YAG-40, were employed. Washdown effectiveness was measured by a comparison of gamma-radiation field measurements taken in the unwashed control area forward and the washed after portion of each ship.

The test ships participated in five shots and at least one of them was sufficiently contaminated in four of these to make washdown evaluation feasible. Maximum levels of gamma radiation encountered ranged from 266 mr/hr at 11 hours after Shot Flathead to 21.2 r/hr at 4.6 hours after Shot Tewa. The four events provided two general types of contaminant, a solid particulate material from Shots Zuni and Tewa and a salt-water slurry from Shots Flathead and Navajo. The latter contaminant was similar to that encountered from Shots 4 and 5 during Operation Castle.

Total accumulated gamma dose at the time of cessation of fallout was reduced 95 to 97 percent in the case of the slurry material, and 76 to 86 percent for the dry fallout. Total dose rates were reduced at the end of washdown 85 to 98 and 85 to 95 percent for the slurry and dry fallout types respectively. Removal of the dry material deposited on the ships varied from 74 to 96 percent at the time washdown was secured.

The results from Operation Castle concerning washdown effectiveness against relatively small amounts of salt-water slurry-type fallout are confirmed, and recommendations for further testing are made.

A.3 PROGRAM 3: EFFECTS ON STRUCTURES

Project 3.1. Effect of Positive Phase of Blast. Agency: Structures Division, Research Directorate, Air Force Special Weapons Center, Kirtland Air Force Base, and University of Illinois. Report Title: Effect of Length of Positive Phase of Blast on Drag-Type and Semidrag-Type Industrial Buildings, WT-1325. Project Officer: R. E. Grubaugh, Captain, USAF.

The primary objective of this project was to obtain information regarding the effect of the duration of the positive phase of blast on the response of drag and semidrag structures. The project was in two parts. The first part involved participation during Operation Teapot, wherein the response of typical single-story industrial buildings to blast from a nuclear detonation of approximately 1 Mt was studied. The second part, of which WT-1325 is the final report, involved the testing of identical industrial structures during Operation Redwing, wherein a detonation of approximately 1 Mt was used.

A total of six steel-frame buildings were tested during Operation Redwing. The buildings were approximately 30 feet in overall height, 40 feet in span, and consisted of two 20-foot bays for the drag structures and four such bays for the semidrag structures. The drag structures had light asbestos-sheet siding and roofing, which were expected to fail before much load could be transferred by them to the frame. The semidrag structures also had light asbestos-sheet roofing, but the walls were constructed of reinforced concrete. A window opening, comprising about 30 percent of the full wall area, was furnished in the form of a single band running the full length of the building.

The structure of each type nearest ground zero was located so that if the yield of the weapon was near the lower limit of its predicted range, it would probably undergo considerable inelastic deformation. Conversely, those structures farthest from ground zero were located so that if the yield of the nuclear device was near the upper limit of its predicted range, they would be substantially deformed, but would not collapse. The third building of each type was located at an intermediate point between these two extremes.

Instrumentation was provided to obtain records of the transient structural deflections, strains, and accelerations, as well as of overpressure and dynamic pressure versus time at the sites of the various test structures.

Since the structures studied during Redwing were identical to those tested during Teapot, the natural periods of vibration and the resistance functions as determined during Teapot were assumed to be correct. Consequently, these measurements were not repeated during Redwing.

Because of the large drop error of Shot Cherokee, the actual ground zero was about 20,000 feet from intended ground zero for the Redwing test. As a result of this error, all six test structures were subjected to pressures higher than were expected and, in addition, neither the structures nor the pressure gages were oriented normal to the direction of blast propagation. The peak overpressure intensities obtained from the self-recording gages of Project 1.1 at the sites of each structure were 8.5, 7.5, and 6.1 psi for the drag structures and 7.5, 6.1, and 5.0 psi for the semidrag structures. The angle of orientation, referred to normal incidence, varied from 58 degrees for the drag structure nearest ground zero to 33 degrees for the semidrag structure most distant from ground zero.

Due to this set of circumstances, all of the structures suffered complete collapse. Consequently, the desired gradation of damage was not obtained and the intended comparison with the Teapot results was seriously impaired.

To make possible such a comparison, the effects of orientation on the loading of the test structures were studied in model tests conducted in a shock tube. The results, used in conjunction with the overpressure data obtained from Project 1.1, made possible the estimation of the loads that acted on the structures to produce collapse. The results obtained by Project 3.7, Operation Teapot, were extrapolated to produce reliable estimates of the loads which would have produced collapse of the Teapot structures. The estimated collapse loadings for the two operations were then compared to obtain a quantitative idea of the effect of positive-phase duration of blast on the response of the two types of structures. On this basis, it was found that to produce collapse of the drag structures, the peak overpressure from a 1 Mt detonation need be no greater than approximately 60 percent of the overpressure that would be required from a 1 kt detonation. Similarly, to produce collapse of the semidrag structures, the overpressure from a 1 Mt detonation need be no greater than about 80 percent of that required from a 1 kt detonation. These percentages are admittedly approximate, but it is believed that they represent reasonably well the minimum probable effectiveness of increased positive-phase duration of blast waves.

Despite the difficulties encountered, the effect of long positive-phase duration was clearly demonstrated in at least one instance. During Teapot, a drag structure experienced a maximum deflection of only 22 inches under a peak overpressure of 6.5 psi, whereas a comparable structure during Redwing oriented 42 degrees off the direction of shock propagation collapsed under an overpressure of only 6.1 psi. Since the lack of normal incidence of blast in Redwing reduced the effective load produced on the structure in its weak direction, the demonstration is even more conclusive than a direct comparison of the two pressure levels indicates.

A.4 PROGRAM 4: BIOMEDICAL EFFECTS

Project 4.1. Chorioretinal Burns. Agency: School of Aviation Medicine, Randolph Air Force Base, Texas. Report Title: Chorioretinal Burns, WT—1326. Project Officer: Richard S. Fixott, Colonel, USAF (MC).

The primary objective of this project was to determine the requirements for protection of the eyes against chorioretinal burns from nuclear detonations of various yields. Corollary technical objectives were to: (1) determine whether blink reflexes will prevent chorioretinal burns; (2) ascertain which portions of the time-intensity pulse can produce thermal injury to the retina and choroid of the eye; (3) determine the time required for blink reflex (BRT) in rabbits and monkeys exposed to the extreme light intensity of the nuclear detonation; (4) explore the feasibility of ocular protection by means of fixed-density optical filters or combinations of filters; and (5) test, under field conditions, protective shutter devices that are in the developmental state and are designed to close much more rapidly than the BRT.

This project was a sequel to the study of chorioretinal burns during Operation Upshot-Knothole in 1953, in which nuclear devices in the range of 20 kt produced burns in the eyes of rabbits at distances of 2 to 42.5 statute miles from ground zero. Additionally, four cases of accidental burns were produced at distances of 2 to 10 miles.

The project was designed to furnish supplemental information on the requirements for protection against retinal burns utilizing both rabbits and monkeys as experimental animals. Chorioretinal burns were produced by various segments of the thermal pulse. This was accomplished by two series of time-fractionating shutters. The first group, the early-closing shutters, were open at time zero and closed at increasing intervals of time. The second series, the delayed-opening shutters, were closed at time zero and subsequently opened for preselected time increments during the flash. The feasibility of protection by fixed-density optical filters was explored. Two types of developmental protective electronic shutters were field tested.

Results at yields of { } demonstrated that the blink reflex does not protect against chorioretinal burns. Average BRT for rabbits was essentially the same on both shots: 362 and 382 msec at respectively. In contrast, the average BRT for monkeys at 160 msec for nearly doubled to 293 msec for. The shot caused retinal lesions at 8.1 statute miles. The device of intermediate yield, produced burns at 7.6 miles but not as far as 14.4 miles. Additional information is needed in order to determine the limiting parameters for retinal burning over the entire range of weapon yield.

In the case of the device, no burns were produced by the first pulse alone, which terminated at 13.1 msec. Retinal burns were not sustained until the interval of 0 to 67.5 msec was reached, after which the incidence was about 65 percent. The failure to produce injury by exposures of less than the initial 67.5 msec of the detonation discounts the contribution of the first pulse to burn production under the experimental conditions.

Four of thirteen exposures during the first pulse of the device produced retinal burns, not including one case of shutter failure. Both explosions produced a number of burns during the second pulse. Of the rabbits protected only by their natural blink reflex, about 80 percent received burns at 8.1 miles from the device and at 7.5 miles from the device. In the comparable group of monkeys, 75 and 100 percent received chorioretinal burns from the smaller and larger devices, respectively. In both rabbits and monkeys, the device at 7.5 miles produced lesions approaching one human optical disk diameter—about four times greater in diameter than those caused by exposure to the smaller device at about the same distance (8.1 miles). Evidence obtained on early closing shutters indicated that a dosage of about 20 to 30 mg cal/cm² at the cornea will produce burns during the initial 70 to 100 msec of the nuclear explosion.

Burns were not obtained from weapons of multimegaton yield at distances of 10.6 and 21.6 miles. Actually, the total thermal yield received at these distances was on the order of 1,800 mg cal/cm² and 1,000 mg cal/cm², respectively, which was ample for retinal burning. Although not conclusive, it appears that the low irradiance during the first 300 msec of the blast failed to deliver energy sufficient for burning before blinking occurred, but possibly was enough to cause blinking that could provide protection during the remainder of the blast. Animals exposed at 10.7 miles from the detonation did not receive burns. A contributing factor undoubtedly was attenuation by severe rain squalls at the time of detonation.

The optical filters tested at near-threshold distances prevented retinal burns. At intermediate distances, filters reduced the incidence and severity of the lesions. The results obtained on protective shutters were inconclusive with respect to protection against retinal burns; however, information was obtained invaluable to the future development of this equipment.

Loss of animals from sun stroke or heat prostration during the afternoon of D - 1 threatened to be a problem, particularly where repeated shot postponement occurred after the animals were placed in the exposure racks. There was also some indication that light reflected to the unexposed eye may have caused blinking before certain of the shutters opened. Recommendations include provision for a trailer type of exposure facility, light-tight and airconditioned.

A.5 PROGRAM 5: EFFECTS ON AIRCRAFT STRUCTURES

A.5.1 Project 5.1. Thermal and Blast Load Effects on a B-47E Aircraft in Flight. Agency: Wright Air Development Center, Air Research and Development Command, USAF, Wright-Patterson Air Force Base, Ohio. Report Title: Thermal and Blast Load Effects on a B-47E Aircraft in Flight, WT-1327. Project Officer: Lt R. C. Laumann.

Project 5.1 was established to measure overpressure, gust, and thermal effects on a B-47E aircraft in flight and to provide additional research information on the effects of nuclear explosions on the aircraft. Results of this project will be used to correct the B-47E Weapons Delivery Handbook. Previous tests were conducted on a B-47E in Operations Ivy and Castle. Data obtained on these operations were primarily measurements of thermal effects. For Operation Redwing, a B-47E aircraft was instrumented for measurement of overpressures, irradiance, radiant exposure, and of bending, shear, and torsion in the wing and stabilizer. Further instrumentation was made to measure thermal strain and the effect of high thermal inputs upon thin skins and supporting structures. Instrumentation was also installed to obtain bending, shear, and torsion responses of the fuselage when subjected to combined side and vertical loading.

The general positioning criteria for the aircraft were wing bending up to 95 percent of design limit and/or a temperature rise of 600 to +700° F in the thin-skinned elevator and aileron. In order to attain high temperature rises on participations in which the aircraft was gust critical, it was necessary to paint the thin-skin surfaces with high absorptivity paint. Temperatures of 430 to 547° F received during Shots Zuni and Dakota caused only minor permanent buckling in the aileron and elevator and resulted in no control problems or noticeable increase in drag. During Shot Dakota, the aircraft sustained 89 percent of design limit wing bending and an overpressure of 0.80 psi. On other participations, wing loading ranged from 46 to 75 percent of design limit, and no damage resulted.

The data obtained by participation of the B-47E aircraft in Operation Redwing are sufficient for correction of the existing B-47E Weapons Delivery Handbook. The data should also be useful as basic research information to aid in design of future USAF aircraft.

A.5.2. Project 5.2. In-Flight Participation of a B-52. Agency: Wright Air Development Center, Wright-Patterson Air Force Base, Ohio. Report Title: In-Flight Participation of a B-52, WT-1328. Project Officer: F. L. Williams, Capt, USAF.

The primary objective of this project was to obtain measured-energy input and aircraft-response data on an instrumented B-52 aircraft when subjected to the thermal, blast, and gust effects of a nuclear explosion.

To accomplish this objective an analysis was performed to determine the effects of nuclear explosions on the B-52 aircraft. This analysis was used in selecting the spatial location for the B-52, relative to a detonation, that would result in the desired aircraft inputs and responses. In addition, the analysis was used in determining the desired locations for the sensing components of the instrumentation system. The B-52 (AF 52-004) was extensively instrumented for participation in Operation Redwing with the major portion of the instrumentation devoted to measuring aircraft responses.

The actual positioning of the B-52 relative to the detonation was accomplished by use of the aircraft Bombing Navigation System (BNS). The B-52 participated in nine shots, including one shot which the aircraft aborted just prior to time zero because of BNS difficulties. The reliability of the instrumentation system was between 95 and 100 percent throughout the test program.

The aircraft received up to 110 percent of the allowable limit overpressure, 100 percent of the allowable limit moment on the horizontal stabilizer, and 82 percent of the allowable bending moment of the wing. Except on Shot Huron, aircraft damage was confined to thermal damage on secondary items such as seals, paint on thin skin, and rain-erosion coating on the majority of the exposed plastic surfaces.

During Shots Huron and Tewa the special shoring for both the electronic-countermeasures (ECM) radome and bomb-bay doors was removed to verify that damage to these items would occur in the normal-mission configuration of the aircraft. Prior to Shots Huron and Tewa the ECM radome and bomb bay doors were shored to achieve a more thorough investigation at near-limit inputs of weapon effects on primary structure. As predicted, during Shot Huron the ECM radome suffered complete failure and the bomb-bay doors received moderate buckling because of overpressure.

The objective established for Project 5.2 was successfully accomplished during Operation Redwing.

It is recommended that the B-52 not participate in future nuclear tests as a weapons-capability aircraft under the delivery conditions stated in the present B-52 Special Weapons Delivery Handbook.

A.5.3 Project 5.3. In-Flight Participation of a B-66 Aircraft. Agency: Aircraft Laboratory, Wright Air Development Center, Wright-Patterson Air Force Base, Ohio. Report Title: In-Flight Participation

of a B-66 Aircraft, WT-1329. Project Officer: Richard W. Bachman.

The objectives of this project were to determine the response of the B-66B aircraft in flight to the blast, gust, and thermal effects of nuclear explosions, primarily for the purpose of defining the delivery capabilities of the aircraft and secondarily to obtain basic information relative to thermoelastic response of aircraft structures. The tests were conducted at the Eniwetok Proving Ground during Operation Redwing.

Highest temperature recorded was 451° F on the 0.016-inch-thick aluminum elevator skin that had been painted gray to an absorptivity factor of 0.45. This represented a temperature rise of 381° F.

Maximum overpressure received was 1.165 psi, and maximum gust load factor was 3.35 g at the center of gravity of the aircraft, with peak material velocity calculated to be 90.58 ft/sec. Highest percent of limit allowable bending moment was 61.0 recorded at Wing Station $X_w = 407$.

Assumed atmospheric conditions, used in the prediction of inputs, were very close to the actual conditions on all tests.

When correlated with the effects obtained during Operation Redwing, the calculated effects in the B-66B Special Weapons Delivery Handbook are conservative. Based upon these results, it can be concluded that the B-66B has nuclear weapon delivery capabilities equal to or in excess of those stated in the delivery handbook.

A.5.4 Project 5.4. In-Flight Participation of a B-57 Aircraft. Agency: Wright Air Development Center, Wright-Patterson Air Force Base, Ohio. Report Title: In-Flight Participation of a B-57B, WT-1330. Project Officer: H. M. Wells, Jr., 1st Lt, USAF.

This project was established to determine the response of the structure of the B-57 aircraft in flight to thermal, gust, and overpressure effects of large-yield nuclear explosions primarily for the purpose of defining the delivery capabilities of the aircraft and secondarily to obtain basic information relative to the thermoelastic response of the aircraft structure.

In order to obtain the data necessary to accomplish this objective, the aircraft was instrumented to measure the overpressure, gust, and thermal inputs, and the response of various components of the structure to these inputs. The instrumented aircraft was positioned at predetermined points in space in the vicinity of several nuclear detonations. The positions were selected such that design limits would be approached.

A maximum skin temperature of 400° F was the criterion for determination of the amount of thermal radiation which the B-57B could absorb without sustaining permanent buckling of the skin, and 600° F was the criterion for the maximum safe limit. In thermally critical participations, the aircraft was normally positioned for the 400-degree limit for the design yield and for less than 600 degrees for the positioning yield.

With respect to gust, the aircraft was limited by 100 percent of the design limit shear at Wing Station 123. The aircraft experienced loads of from 14 to approximately 61 percent of the design limit load.

During Shot Apache, the aircraft was positioned for both overpressure and a high horizontal gust component. The results substantiated the theoretical alleviating effect of the horizontal gust component. Blast overpressures of 53 percent of the overpressure limit were received.

Sufficient data were obtained for the determination of the delivery capability of the B-57B aircraft: It was found to be better than the capability described in the B-57B Phase I-A Special Weapons Studies.

A.5.5 Project 5.5. Blast and Thermal Effects on the F-84F Aircraft in Flight. Agency: Wright Air Development Center, Wright-Patterson Air Force Base, Ohio. Report Title: In-Flight Participation of F-84F Aircraft, WT-1331. Project Officer: M.H. Lewin, Capt, USAF.

The response of the F-84F aircraft to inputs from nuclear detonations was studied for verification or modification of the weapon-delivery handbook pertaining specifically to the F-84F weapon system. In addition, the study started during Operation Teapot on the dynamic response of an aircraft structure to side blast loads resulting from a nuclear detonation was continued.

Two manned F-84F aircraft were exposed to shots of low, medium, and high yields. One aircraft was instrumented to collect thermal, overpressure, and gust data for verification of the F-84F weapon-delivery capabilities. The second aircraft was instrumented to measure overpressure and gust data to define the dynamic response of fighter structures to asymmetric loadings.

The positioning of the aircraft at a point in space to receive the desired inputs was accomplished with a Raydist System on Bikini shots and by an AN/MSQ-1A ground-control radar system for Eniwetok missions. The capabilities aircraft was positioned in seven shots to obtain a predicted 60 to 80 percent of limit gust load at the critical station and a temperature rise that would cause buckling in the critical skin. The

research aircraft was positioned in ten shots to receive 40 to 80 percent of limit side fuselage bending moment at various angles of incidence to the blast wave.

The maximum loads experienced by the capabilities aircraft occurred during Shot Dakota, when the aircraft received a temperature rise of 698° F, causing buckling on the 0.025-inch 24S-T flap skin, a pressure rise of 1.67 psi, and an incremental vertical bending moment at right-wing Station 34 of 73 percent of limit load. The maximum fuselage side bending moment was 72 percent of limit load, recorded by the research aircraft during Shot Erie. Results obtained from the engine instrumentation indicated that the effects of gust on engine performance were negligible.

Visible damage to the test aircraft consisted of considerable buckling of the gray-painted test areas on the capabilities aircraft caused by the high thermal loading during Shot Dakota, with the flap proving the most-vulnerable aircraft surface. Some damage attributed to overpressure was also observed. In addition, evidence of scattered thermal radiation was obtained on the top of the capabilities aircraft during Shot Mohawk. The thermal curtain effectively protected pilots from personal injury and assumes added importance with the possibility of scattered radiation reaching the cockpit.

The data indicated that the project successfully accomplished its objectives. It is therefore concluded that the F-84F aircraft need not participate in future nuclear tests for determination of the weapon-delivery capabilities of the aircraft.

A.5.6 Project 5.6. Blast and Thermal Effects on the F-101A Aircraft in Flight. Agency: Wright Air Development Center, Wright-Patterson Air Force Base, Ohio. Report Title: In-Flight Participation of an F-101A Aircraft, WT-1332. Project Officer: M. H. Lewin, Captain, USAF.

The primary objective of this project was to determine the responses of an in-flight F-101 aircraft system to the blast, gust, and thermal effects of a nuclear detonation.

In order to accomplish the objective, the test aircraft was instrumented to measure the gust, blast, and thermal inputs and the responses to these inputs on various components of the airframe and engine. The aircraft was then positioned at predetermined points in space in the vicinity of nuclear detonations. The positions selected were not necessarily representative of delivery maneuvers, but were at points in space where conditions approaching limit would theoretically be received.

The aircraft successfully participated in nine events with yields ranging from approximately 1.44 kt to 4.8 Mt. The limiting conditions on the aircraft were either 100 percent of the design limit allowable bending moment on the wing, or a 350° F temperature rise on a honeycomb surface. All of the gust and the larger thermal inputs were symmetrically received on the aircraft in a tail-to aspect. During Shot Mohawk, the aircraft was flown at supersonic speeds, outrunning the measurable gust effects. Also on this shot, the aircraft experienced reflected thermal radiation while in a cloud layer.

The maximum temperature rise experienced on the natural finish critical surface was 305° F on Shot Dakota. This temperature rise was almost duplicated on Shot Mohawk. By painting a wing-honeycomb surface black, the 350° F limit was intentionally exceeded. A temperature rise of approximately 450 to 500° F was received on this surface during Shot Dakota resulting in 100 percent unbonding of the skin from the core.

Maximum gust loading occurred during Shot Inca, when 95 percent wing bending moment was measured. The maximum free-stream overpressure measured during the operation was 1.17 psi on Shot Navajo.

From the participation of the F-101A aircraft in this operation, it can be concluded that its delivery capability exceeds that which is predicted in the report "Special Weapon Explosion Effects and Weapon Delivery Capability of F-101A Airplane (Phase I)," by The McDonnell Aircraft Corporation. It can further be concluded that the data collected is sufficient to verify and/or correct the above report.

A.5.7 Project 5.7. Albedo and Thermal-Flux Measurements from Aircraft. Agency: Air Force Cambridge Research Center, L. G. Hanscom Field, Bedford, Massachusetts. Report Title: Thermal-Flux and Albedo Measurements from Aircraft, WT-1333. Project Officer: R. L. Dresser, Major, USAF.

Calorimetric, photographic, and spectrographic records were obtained by means of calorimeters, radiometers, spectrographs, and cameras placed in each of four aircraft.

Radiant exposure and irradiance were measured for 10 events and spectra for 11 events. Filters were used with many of the instruments, isolating various parts of the visible and near-infrared spectrum. Records were obtained from the calorimeters aimed directly at the fireball, from the instruments directed toward the water underneath the aircraft, and from calorimeters pointing away from the fireball. The purpose of the latter was to measure the back-scattered radiation.

The thermal records reaffirm the reduced transmission of radiant energy in the near infrared because of absorption by water vapor and carbon dioxide.

The equation developed by Chapman and Seavey for predicting the radiant exposure on a horizontal surface and its modification to a surface oriented normal to the fireball was tested against the collected data and was found to satisfactorily predict the radiant exposure. A simple equation, essentially a modification of that by Chapman and Seavey, is also presented and tested against the data. The uniform meteorological conditions accompanying these tests allow the use of the simpler equation.

Comparison between the air drop event, Cherokee, and a barge shot of similar yield, Zuni, indicated no significant differences in the irradiances or radiant exposures measured at the aircraft.

Measurements of the back-scattered radiation, where available, were found to be two or three orders of magnitude lower than the radiant energy received directly from the fireball, with the exception of a single instrument reading on a single event on which the B-52 flying in severe cloud conditions measured 50 percent back-scatter into the cockpit.

The photographic records were taken at 64 frames/second on 16-mm high resolution emulsions, from aircraft at slant ranges on the order of several kilometers from ground zero. The exposures started before time zero and lasted until the thermal pulse was effectively over. The cameras had various fields of view and were aimed at the detonation site. Coverage of the series of detonations varied from only 1 successful film to a total of some 20 series from 4 aircraft. Infrared (0.70 to 0.90 μ), blue (0.35 to 0.45 μ), and linearly polarized (0.40 to 0.70 μ) filter systems were used, the cameras being paired. Appropriate transfer (H and D) curves, relating optical density of the developed film to illumination intensity, were available. The bulk of the information was gained from microdensitometer traces of the negative strip; further information came from size measurements on the film, and from qualitative observation of the developing phenomena.

Such ancillary features as the Wilson cloud, plume, and bright spots appearing near shock-wave breakaway, were found to perturb the thermal output by less than 15 percent. The air shock appears to attenuate the blue light; the shocked volume is visible in the infrared because of scattering from the denser air. No polarization phenomena, other than the expected difference in specular scattering from the undisturbed ocean surface, were resolved.

It was found that an attenuating mantle (absorption shell) surrounds the fireball from after breakaway until the end of the thermal pulse. This shell develops to a thickness of about one-fourth the fireball radius; it is somewhat more strongly attenuating in the blue than the infrared. Data on properties of this absorbing shell, such as dimensions versus time, and effect on limb darkening (decrease in brightness toward the edges of the fireball), are presented.

The spectral histories of all events appear quite similar, regardless of the yield; a large amount of NO_2 is formed quite early and persists throughout the entire event.

Aureole (air-scattered) light is found to be an order of magnitude more intense than the light reflected from the unshocked water surface, for the typical moist atmospheric conditions of the Pacific Proving Ground. This aureole is white and unpolarized. The shock froth albedo is about 12 times the unshocked water albedo. In general, the total red light reflected or scattered into the typical camera fields of view, from aureole, clouds, and water was about equal to the direct flux from the fireball. Most of this was scattered from the shock-frothed water. The blue albedo was lower, presumably because of the air-shock attenuation. Furthermore, the blue fireball showed considerably more limb darkening.

Both air-shock and fireball dimensions were found to obey the predicted scaling laws. There is evidence that the fireball surface temperature is not symmetric with azimuth in some cases as the thermal flux appears higher from certain (large) regions.

Reproductions of several series of photographs containing different views of Shot Dakota are presented, as well as a typical single series for each of the other detonations having photographic coverage; the photographs are discussed.

Suggestions for the further analysis of existing Redwing data, as well as the improvement of future tests, are presented.

A.5.8 Project 5.8. Evaluation of the Model A3D-1 Aircraft for Special Weapons Delivery Capability.
Agency: Bureau of Aeronautics, Department of the Navy. Report Title: Evaluation of the A3D-1 Aircraft for Special Weapons Delivery Capability, WT-1334. Project Officer: P. S. Harward, LCDR, USN.

The primary objective of this project was to determine the response of the structure of the A3D-1 aircraft to the thermal effects of a thermonuclear explosion, primarily for the purpose of establishing critical thermal envelopes for the aircraft when utilized for the delivery of large-yield devices.

The A3D is a twin-engine, swept-wing, carrier-based jet airplane which is intended for use as a high-altitude bomber having relatively long range and high performance.

On the basis of existing structural strength it was determined that actual delivery capability limitations of the A3D as a high-altitude bomber would be caused by thermal response rather than response to gust inputs.

Therefore, participation in Operation Redwing was limited to shots for which thermal response would be the limiting factor.

In Project 5.8, the A3D airplane participated in seven shots: Cherokee [redacted] Zuni (3.5 Mt), Flathead [redacted]; Apache [redacted]; Navajo [redacted] Tewa (5.0 Mt), and Huron [redacted].

Since thermal effects were critical for A3D high-altitude delivery, the emphasis of the instrumentation was on measuring the thermal energy received at the airplane and its effect on the temperature response in the thin skin panels on the lower surface of the airplane.

Additional instrumentation was installed to measure overpressure, effect of shock wave on engine performance, and aircraft response to shock wave gust loadings. Originally the gust instrumentation consisted of accelerometers at the airplane center of gravity, but during the test operation additional accelerometers and some strain gages were added in the wing.

Results of the tests are presented as direct and indirect irradiance and radiant exposure versus time, temperature in thin skin areas versus time, maximum temperature rise at each thermocouple location, peak overpressure, time of shock arrival, and limited data on structural loads and accelerations caused by the shock wave gust. Calculated weapon effects and aircraft response are compared with the measured results to show the adequacy of prediction methods.

Prediction methods presented in this report for the thermal effects gave good agreement with the measured results for thermal fields, temperature time history, and maximum temperature rise. Although agreement was good, results indicate a need for additional information and understanding of the atmospheric attenuation and the heat transfer properties of the air flowing over the airplane surfaces.

Excellent agreement was obtained between the measured and calculated peak overpressure and time of shock arrival.

No undesirable engine response was observed at shock arrival. Observed changes in engine performance were no larger than possible variations caused by accuracy of the measuring and recording equipment.

As previously stated, the emphasis of the instrumentation was on thermal effects. Structural load instrumentation was limited to a few strain gages installed at the EPG during the test program. Despite the questionable accuracy and meagerness of the wing response data, fuselage accelerometer data confirmed the original estimates that gust response would not be critical for the mission being considered. In general, the gust response instrumentation was not complete enough to permit improvements in the structural response prediction methods.

Maximum temperature rise experienced during the tests was 370° F. Therefore, although it is not possible to define an absolute upper limit, it can be stated that the airplane safely withstood this temperature rise without any damage.

With regard to the delivery capability of the A3D airplane, it can be stated that all the test positions, with the exception of Shot Cherokee, were closer to the explosion than if the airplane had dropped the device and executed a horizontal turn escape maneuver.

In view of the good agreement of the weapons effects prediction methods with the experimental values, delivery capability studies based on these methods may be considered valid.

A.5.9 Project 5.9. Weapon Effects on Missile Structures and Materials. Agency: Wright Air Development Center, Wright-Patterson Air Force Base, Ohio. Report Title: Weapon Effects on Missile Structures and Materials, WT-1335. Project Officer: C. J. Cosenza, Lt, USAF.

The objective of this project was to investigate the vulnerability of basic missile structures and materials to fireball and associated phenomena of a nuclear detonation.

Tests consisted of exposing a total of 103 specimens, comprising over 30 different designs, within the fireballs of Shots Erie and Mohawk. On Shot Erie, exposures were made at seven locations ranging from 25 to 300 feet from the burst point; on Shot Mohawk, specimens were exposed at two elevations on a tower 525 feet from ground zero. As much as possible, the specimens were designed so that the effects of each of the several mechanisms causing thermal damage could be evaluated individually.

Eighty-eight of the 103 specimens which were exposed were recovered: 79 out of 94 from Shot Erie and all 9 from Shot Mohawk. The high radiation level after the shots delayed the major recovery effort for approximately 3 months. Results of the material evaluation studies showed that 8-inch-diameter spheres of stainless steel, molybdenum, and titanium sustained approximately equal mass ablation which was 0.08 psi at 100 feet and 0.06 psi at the 200-foot range. Copper sustained 2 to 4 times the mass ablation of the above three metals, and plastic experienced substantially less than any of the metals for the exposure conditions on Shot Erie. The existence of an attenuating vapor layer was substantiated by the data, and a few specimens indicated that the removal of this vapor layer by hydrodynamic means had affected the ablation. The apparent anomaly of approximately equal ablation experienced by the 12-inch-diameter steel spheres at Stations 150, 200, 250, and 300 on Shot Erie could, for the most part, be explained on the basis of

ablation by melting after emergence from the fireball. It was shown that removal of a molten layer by spinning off drops of the material could lead to total ablation and would be important in ICBM destruction if the missile had an appreciable angular velocity.

The electrically instrumented Operation Redwing specimens have shown that it is feasible to record data electrically inside the fireball of a nuclear detonation with a system similar to that used on Redwing. The velocity-distance impact gages which were adequately protected from the effects of overpressure and material ablation operated satisfactorily and yielded apparently reliable velocity versus distance data. It has been shown also that ball-crusher gages may be successfully employed to observe experimentally peak fireball pressures and accelerations, provided the approximate shape of the dynamic input is known.

A.6 PROGRAM 6: ELECTROMAGNETIC EFFECTS

A.6.1 Project 6.1a. Accurate Location of an Electromagnetic Pulse Source. Agency: Air Force Cambridge Research Center, Bedford, Massachusetts. Report Title: Short-Baseline Narol Measurements, WT-1336. Project Officer: Richard A. Houghten, Major, USAF.

The objective of this project was to study the feasibility of using the electromagnetic pulse emanating from a nuclear detonation to determine the ground-zero position and yield with equipment located from 200 to 5,000 miles from the source.

Narol time-to-arrival bomb detectors were established in Hawaii and California to use the electromagnetic pulse from a nuclear detonation to locate the detonation position. Two short-baseline Narol nets are required to determine actual ground-zero fixes, but during Operation Redwing, single nets determined lines of position and demonstrated the feasibility of the system.

The ability to isolate the bomb pulse from noise determines the operational range of a system. The Hawaiian net, located at a distance greater than its estimated operational range, detected and reported each shot before postshot confirmation, and by the end of the operation it was determining and reporting line of position within $\frac{1}{2}$ hour after shot time. More difficulty was experienced at the California net: exact shot time was required to identify the bomb pulse from some of its film record.

Of a total of 17 shots in the test series, the Hawaiian net was alerted for 15 and the California net for 14. The equipment operated and recorded data at all stations for these shots. Except for Shot Seminole, lines of position were successfully determined on each shot from the film of the Hawaiian net and the California net. Seminole was detonated in a tank of water that attenuated the electromagnetic pulse to a point where it was not detectable on the high-gain-film record.

Lines of position determined at the Hawaiian net had an average error of plus or minus 1.4 nautical miles. Lines of position at the California net had an average error of 5.4 nautical miles. Relative device yields measured from the electromagnetic field strength of the received pulse were accurate only to within a factor of three.

A.6.2 Project 6.1b. Accurate Location of an Electromagnetic Pulse Source. Agency: Air Force Cambridge Research Center, Bedford, Massachusetts. Report Title: Field-Strength Measurement for Accurate Location of Electromagnetic Pulse Sources, WT-1351. Project Officer: E. A. Lewis.

The primary objective of this project was to determine the accuracy with which sources of electromagnetic radiations resulting from atomic explosions could be located at ranges of 1,450 to 6,200 nautical miles. Sperry Gyroscope Company was assigned the task of operating and testing two inverse-hyperbolic atomic strike recorder networks based on the use of Cytac, a low-frequency, loran-type, pulsed-signal system operating on 100 kc. One net was located in the Central Pacific, the other in the United States.

The two networks employed the Cytac equipment for a fine-measurement synchronizing signal (tenths of a μ sec), and radio stations WWV and WWVH for coarse synchronizing signals (msec). The equipment used was a further development of that used during Operation Teapot. Data was recorded photographically and sent for analysis to a net control station and information was interchanged between nets. Preliminary data bulletins were issued immediately after each shot.

Seventeen shots were fired. Of these, the Pacific net recorded data on 14 and the United States net recorded data on 11. The average fix error at 2,000 nautical miles was about 5.5 miles with a standard deviation of 4 miles. At 5,800 nautical miles, the average line of position (LOP) error was about 4 miles with a standard deviation of about 15 miles for the three LOP's used. Fix errors for the United States net resulting from the poor geometry of the system averaged 116 and 93 miles. Failure to obtain data because of equipment nonperformance was less than 4 percent.

LOP errors resulted mainly from geographic position determination of the sites with respect to EPG, from the propagation constants used, and from the poor crossing angles (10 degrees). Longer base lines and optimum station configuration would improve the fix accuracy by a figure of seven.

Considerable field-strength data was gathered which will be of value in the design and operation of future systems.

Conclusions reached as a result of Operation Redwing indicate that a fully automatic ASTREC System can be developed for detecting and locating nuclear explosions, to assist in damage assessment, and to determine explosion locations. The system can be adapted to satisfy the requirements of the three major Air Force Commands, Air Defense Command (ADC), Tactical Air Command (TAC), and Strategic Air Command (SAC).

A.6.3 Project 6.3. Effects of Nuclear Detonations on the Ionosphere. Agency: U. S. Army Signal Engineering Laboratories. Report Title: Ionospheric Effects of Nuclear Detonations, WT-1337. Project Officer: Arthur K. Harris.

The major objectives of this experiment were to investigate the area of absorption believed to be due to radioactive particles from large nuclear detonations and to study the effect of orientation of the path from the blast site to the observer relative to the geomagnetic field upon F2-layer effects of such detonations. Other objectives concerned distant effects, boundaries of rising air thought to result from strong shock waves, and accumulation of other ionospheric data.

To accomplish these objectives, ionosphere recorders were located about 240 km to the east of Bikini at Rongerik, about 740 km to the south at Kusale, and aboard an aircraft operated within about 400 km of ground zero.

Strong radio-wave absorption was experienced at the aircraft when underneath the radioactive cloud. Measurements and theoretical studies have been combined to determine the amount of absorption as a function of time, yield, and radio frequency.

F2-layer effects occurred to the south that differed decidedly from those to the east; the former were more pronounced, longer-lasting, and included discrete moving disturbances attributable to compressional and hydromagnetic waves.

The rising F2-layer effect that was first observed following the Ivy Mike shot was not observed during Operation Redwing. A theory was developed that explains why this convectional effect is found only for shots of about 10 Mt and greater.

A.6.4 Project 6.4. Test of Airborne Antennas and Phototubes for Yield Determination. Agency: Air Research and Development Command, Wright-Patterson Air Force Base. Report Title: Airborne Antennas and Phototubes for Determination of Nuclear-Weapon Yield, WT-1352. Project Officers: Alan J. Waters and Roger E. Clapp.

The objectives of this project were to determine: (1) the suitability of flush-mounted airborne antennas for the type compatible with supersonic aircraft for detecting the pertinent features of the low-frequency electromagnetic radiation; (2) the quantitative characteristics of both the thermal and low-frequency electromagnetic radiation in an airborne vehicle as a function of range to the burst; and (3) the effects of ambient conditions upon both parameters.

A nuclear detonation generates three categories of characteristic phenomena which can be measured from a high-speed aircraft: (1) low frequency electromagnetic radiation which can be received by an electric or magnetic antenna; (2) thermal radiation detectable by phototubes; and (3) pictorial characteristics which can be photographed.

Airborne equipment has been designed for determining the location and yield of a nuclear detonation. This equipment for indirect bomb damage assessment (IBDA) determines yield from a measurement of the interval between the time of the burst and the time of the second peak in the thermal radiation intensity curve. Flush-mounted ferrite-core magnetic loop antennas, for use in detecting the electromagnetic signal and thus fixing the time of burst, performed successfully during Operation Redwing. Two kinds of phototubes for detecting the second thermal peak were tested and were found about equally satisfactory. The method selected for yield determination gave results accurate to ± 16 percent for five shots with yields in the range from 1 to 5.0 Mt.

A detailed study of the collected data showed that the electromagnetic signal, consisting of a direct pulse followed by a series of ionosphere-reflected sky waves, could be used in many ways to give information concerning the detonation and the ionosphere. From the time intervals between the ground wave and sky waves it was found possible to compute both the distance between burst and receiver and the height of the reflecting ionosphere layer. From the oscillatory period of the individual sky waves or ground wave the yield could be estimated. The wave form of a sky wave could be used for an estimate of the height of the receiving equipment. The amplitudes in a sequence of sky waves could be used to give the radian frequency, ω_p , characterizing the ionosphere, and to extrapolate to the amplitudes of other sky waves or the ground wave.

For a number of test shots, the thermal radiation intensity data was compared with the expected irradiance to give estimates of atmospheric attenuation due to clouds and haze. Measurements of ambient light intensity and of the variability of ambient light were also made, to aid in the evaluation of the IBDA system.

On the sequence photographs the position of the burst could be determined from: (1) the intersection of bright radial lines; (2) the center of symmetry of the condensation dome (see below); (3) the fireball itself; or (4) the stem of the nuclear cloud. When the fireball was visible, its radius could be used as a measure of yield, provided that the timing of the picture and the range between burst and camera were known. The condensation dome, produced in humid air by the rarefaction phase of the shock wave, appeared in all burst sequences and was found useful in determining a rough value of the range and of the time of the burst relative to the timing of the photographs.

A.6.5 Project 6.5. Measurement of Radio Frequency of Electromagnetic Radiation from Nuclear

Detonations. Agency: U. S. Army Signal Engineering Laboratories, Fort Monmouth, New Jersey. Report Title: Measurement of Radio-Frequency Electromagnetic Radiation from Nuclear Detonations, WT-1353. Project Officer: Charles J. Ong, 1st Lt, USA.

The objective of this project was to obtain, at several distances, oscillographic wave forms of the electromagnetic pulses generated by each of the nuclear detonations during Operation Redwing. These wave forms were to be analyzed to determine if correlation existed between selected pulse characteristics and various bomb parameters (yield, height of burst, device characteristics, etc.). Additional data was desired on the variation of pulse shape and field strength with distance. Information obtained from this study was to supply design information for a system to detect detonations, locate ground zero, and measure yield and possibly height of burst at remote distances.

During Operation Redwing, radio-frequency electromagnetic pulses generated by nuclear detonations at Eniwetok and Bikini were detected and recorded both at Eniwetok and Kwajalein. Oscillographic wave forms recorded at various speeds showed details of the initial portion of the signal as well as the complete signal and an ionospheric reflection.]

Wave forms were analyzed to determine peak field strength, times to peak negative and positive deflections, and times to zero crossings. Fourier integral analyses were performed to obtain the frequency spectrum of each wave form. Analysis revealed that correlations existed between yield and each of the wave-form duration characteristics and also between yield and the frequency corresponding to the spectrum peak amplitude in the VLF region. Changes in wave forms observed at different distances were attributed to effects of propagation. Correlations of field strength with yield and with distance were found to exist for kiloton-yield devices. However, no such correlations could be found for megaton-yield devices. Field strengths were lower than observed for devices of comparable yield in Operation Teapot.

The single wave form recorded for the 4,000-foot altitude shot exhibited a variation in wave-form characteristics which distinguished it from all ground-based shots of comparable yield. The recorded wave forms known to result from sferics did not exhibit the characteristics observed for detonation-generated wave forms. Participation in future tests is needed to obtain a comprehensive catalog of signal and noise wave-form characteristics.

Approximate distances to the source were obtained from a single station by utilizing sky-wave delay. Tests indicated that time of signal arrival could be measured with 0.1- μ sec resolution and that signals from a [] device could be detected at 420 miles.

Wave forms should provide valuable information for the development of systems to detect and locate the source of nuclear explosions. Work should continue on design of a location system for use at 500 miles, with automatic features and noise-filtering characteristics. The system should use wave-form data as basic information.

A.6.6 Project 6.6. Attenuation of Super High Frequency and Ultra High Frequency by Ionization Resulting from Nuclear Explosions. Agency: U. S. Naval Research Laboratory, Washington, D. C. Report Title: Attenuation of Telemetry Frequencies by Nuclear Detonations, WT-1346. Project Officer: P. A. Caldwell.

Preliminary design considerations for a telemetry link for use during weapon-effects tests indicated that ionization in the neighborhood of a transmitter placed near a nuclear explosion might cut off the transmission at early times. This experiment was designed to determine whether an instantaneous telemetry link was possible, since storage of broad band information is difficult.

Project 6.6 was established to measure electromagnetic attenuation at early times with 1- μ sec resolution. Since attenuation is a function of the electron density and the electron collision frequency, a measurement of attenuation versus time would enable one to calculate electron density versus time.

Available super-high frequency (SHF) ($\approx 10,000$ Mc) and ultra-high frequency (UHF) ($\approx 2,000$ Mc) receivers and 30-mw klystron-tube transmitters and a 2C39 1-watt UHF oscillator were used with high-gain antennas. A radial transmission path was chosen. The locations of the transmitters were chosen so that the calculated peak attenuations would be within the dynamic range of the receiving equipment. Single-trace oscilloscope pictures were made of the attenuation with 1- μ sec resolution for 50 μ sec and with less resolution to 500 μ sec.

The data from Shots Osage and Blackfoot indicated that the signal level dropped approximately 6 db at zero time and took approximately 10 μ sec to recover completely. The measured attenuation was shown to agree with the calculated attenuation from these shots. Electromagnetic and blast effects made interpretation of the Shot Inca data difficult.

A.7 PROGRAM 8: THERMAL RADIATION AND EFFECTS

A.7.1 Project 8.1a. Basic Thermal Radiation Measurements from Ground Stations. Agency: U. S. Naval Radiological Defense Laboratory. Report Title: Basic Thermal Radiation Measurements from Ground Stations, WT-1338. Project Officer: W. B. Plum.

The objectives of this project were to determine the characteristics of the thermal radiation emitted by three of the nuclear devices detonated at the Eniwetok Proving Ground (EPG) during Operation Redwing. The three devices were a

Results of thermal-radiation measurements, including thermal energy as a function of time, broad spectral band, field of view, photographic data, and irradiance versus time, are reported for Shots Lacrosse, Cherokee, and Zuni.

These data were analyzed to obtain fireball radii versus time, color and power temperatures versus time, and estimated thermal yields. The results are presented together with a brief description of the methods of interpretation used by the authors.

The data from Shots Lacrosse and Zuni (39.5-kt and 3.38-Mt surface bursts, respectively) indicate the possibility of a correlation between thermal output and weapon environment. The thermal yields for these two bursts were about as anticipated.

The results from Cherokee could not be accurately analyzed due to the unknown effects of cloud cover. It is estimated that the thermal yield of Cherokee was greater than 30 percent of the total yield and that the peak temperature was in excess of 6,000 K.

Scaling considerations are discussed briefly pending the analysis of data from previous field tests.

A.7.2 Project 8.1b. Measurement of Irradiance at High Time Resolution. Agency: U. S. Naval Radiological Defense Laboratory. Report Title: Measurement of Irradiance at High Time Resolution, WT-1347. Project Officer: W. B. Plum.

The principal objective of this project was to attempt to determine the distribution of thermal radiant power as a function of time during the detonation of a nuclear device.

Irradiance versus time was recorded for two multimegaton detonations. Data on the Cherokee shot was not obtained due to the large drop error. Satisfactory performance was obtained from the instrumentation on the Zuni shot.

Evidence is presented to show that considerable care must be exercised in the interpretation of the data. The Pacific atmosphere makes it essentially impossible to extrapolate from irradiance measurements at a distant point back to the device itself. Evidence is presented to show that considerable care must be exercised in the interpretation of the data.

A.7.3 Project 8.1c. Spectral Distribution of Irradiance with High Time Resolution. Agency: U. S. Naval Radiological Defense Laboratory. Report Title: Spectral Distribution of Irradiance with High Time Resolution, WT-1348. Project Officer: W. B. Plum.

The principal objective of this project was to measure the spectral distribution of the irradiance from a >1-Mt air burst with as high a time resolution as practical in the interval between 2,500 and 25,000 Å. The secondary objective was to measure the spectral distribution of a multimegaton surface burst in the same manner, so that a comparison could be made between these two types of explosions.

A multichannel recording spectrometer with high time resolution in the spectral range of 2,500 Å to 25,000 Å was used to measure the spectral distribution of the irradiance as a function of time received at two locations for Shot Cherokee and at one location for Shot Zuni. Due to a large drop error, the point of detonation occurred outside of the field of view of both instruments on Cherokee.

The spectral distribution of the irradiance received at the time of the second maximum for Shot Zuni showed that a large portion of the energy was in the infrared region of the spectrum. The distributions at other times are not reported, since the irradiance levels were much lower than expected because of considerable cloud obscuration of the fireball.

A.7.4 Project 8.2. Thermal Effects on Cellulosic Materials. Agency: U. S. Department of Agriculture Forest Service, Division of Fire Research. Report Title: Thermal Effects on Cellulosic Materials, WT-1339. Project Officer: W. L. Fons.

This project had as its primary objectives the determination of (1) the minimum thermal-ignition energies for fine kindling fuels as a check on laboratory data obtained by the U. S. Forest Service (USFS) and the U. S. Naval Radiological Defense Laboratory (NRDL) and (2) the depth of char in wood as a check on equations

developed from laboratory data obtained by NRDL with a carbon arc.

Test specimens of alpha-cellulose paper of various thicknesses, densities, and carbon contents; six common kindling fuels (cotton denim, rayon cloth, newspaper, pine needles, dry grass, and corrugated fiberboard); and three species of wood (maple, willow, and balsa) were exposed to the radiation from Shot Cherokee at Sites Dog and George. The specimens were exposed to thermal radiation directly and, also, behind attenuating screens of different transmissions. For different moisture contents, part of the specimens were in containers vented to the atmosphere and part in moisture-proof containers containing a desiccant. Because the bomb burst was not directly over planned target zero, the direct radiation from the entire fireball entered the cells at an appreciable angle, irradiating only a small portion of each specimen at Site George and missing the specimens entirely at Site Dog. For this reason, the depths of char of the wood specimens were without significance.

Data were obtained that permitted an estimate of the critical ignition energy for newspaper, pine needles, and ten of the black papers. Analysis of the black-paper data indicates that the minimum thermal energy causing ignition was increased by moisture content, density, and thickness raised to about the 0.7 power, also that moisture content and density had more effect on the critical ignition energy of the thick papers than of the thin papers.

The primacord technique of triggering a mechanism just before shot time was entirely successful and should prove useful in a wide variety of applications in future test operations.

A.7.5 Project 8.3. Evaluation of Self-Recording Thermal Radiation Instruments. Agency: Army Chemical Center. Report Title: Evaluation of Self-Recording Thermal Radiation Instruments, WT-1340. Project Officer: J. J. Mahoney.

Three types of self-recording thermal indicators—two types of Chemical Corps self-recording calorimeters and the pulse recorder made by Walter Kidde Nuclear Laboratories, Garden City, New York—were to be tested for response to maximum (40-cal/cm²), optimum (20-cal/cm²), and minimum (3-cal/cm²) values of radiant exposure from a nuclear detonation. The Chemical Corps thermistor calorimeter, used successfully during Operation Teapot, provided a relative standard for comparison of exposure measurements.

The tests of the Type 1 and Type 2 Chemical Corps self-recording calorimeters on Shot Cherokee resulted in the conclusion that the Type 1 instruments were unsatisfactory and that the Type 2 instruments successfully integrated radiant exposures of long duration. Instrumentation with the self-recording calorimeters and the Kidde pulse recorder for a short-duration pulse, planned for Shot Blackfoot, was not feasible because of the station contamination resulting from a prior shot; therefore, instrument functioning for short-duration pulses was not determined, and the Kidde pulse recorder, which was designed only for short-duration pulses, has not received a valid test.

The actual burst point for Shot Cherokee deviated considerably from the planned burst point, resulting in a significant angle of incidence of the thermal energy on the instruments.

The data presented in this report represent the thermal radiant energy actually recorded by the thermal-radiation detection instruments at the various stations. Since the objective of the project was to test and evaluate the instruments, no attempt has been made to correct the data received for such factors as angle of incidence and atmospheric transmission in order to extrapolate to the radiating properties of the fireball.

The data obtained with these instruments was compared with that obtained by the NRDL at essentially the same locations. This comparison of the results as measured by the thermistor instrument, Type 2 self-recording calorimeter, and NRDL disk calorimeters shows good agreement (within ± 12 percent) of the mean values.

Since these new instruments, as presently designed, are inaccurate for radiant exposures of less than 3 (cal/cm²)/sec, the results at Station How, of about 84,000-foot distance, are only of qualitative interest.

A.7.6 Project 8.4. Thermal Response of Aircraft Structural Panels of the Bonded Sandwich Type. Agencies: Bureau of Aeronautics and Cook Research Laboratories. Report Title: Thermal Effects on Strength of Aircraft Structural Sandwich-Type Panels, WT-1341. Project Officer: A. Julian, LCDR, USN.

This project was conducted to determine the effects of thermal radiation on sandwich-type aircraft structural panels. Test panels of varied construction materials and facing thickness were subjected to transient heat pulses in unloaded and prestressed conditions to determine if any change in structural integrity could be noted.

Initial specimens were instrumented for measurement of temperature-time history at the core-to-facing bond and exposed to thermal radiation during Operation Redwing. Forty unloaded panels and two FJ-4 elevators were exposed at Station 840.01 on Island George during Shot Cherokee. Small groups of similar specimens were mounted on the Project 5.8 aircraft and exposed during the test series.

Recorded peak temperature rises at the ground station were in the range from 100 to 350° F, which was less than 50 percent of the expected and desired range. These low temperatures are attributed to obscuration

of the test array by smoking of the gray-painted samples at relatively low temperatures, and a much-higher rate of heat conductivity to the core and rear facing than was originally expected. Obvious physical separation of the facing-to-core was noted only in samples of 5-ply (approximately 0.016-inch) and 7-ply (approximately 0.025-inch) phenolic face on balsa core, as indicated by marked convexity of the separated areas.

Results of comparative post-exposure mechanical tests on field-exposed, aluminum-facing samples showed no noteworthy change in strength characteristics as a result of the radiant exposure. However, tests conducted on similar specimens pulse-heated in a restrained and prestressed condition showed that failure will occur at temperatures well within the range of that developed in the field-exposed specimens. Results show that 0.020-inch aluminum facing on balsa-core specimens will fail at temperature rises of approximately 200° F when subjected to relatively low stresses during the heating cycle. Additional data from this load test program will be published under BuAer Contract No. A(S) 56-367C, and BuAer Project TED NAM AD 4002.

Analysis of the recorded field-temperature response and subsequent laboratory pulse-heating tests led to the necessity for a complete study of the heat-transfer characteristics of sandwich construction. As a result of this study, a mathematical formulation has been derived. When these formulas were programed for digital computer use, accurate results were obtained. This program can be used with confidence to predict thermal response to heat pulses from nuclear weapons or laboratory heat sources, and could also be used in establishing material criteria for sandwich structures having superior thermal tolerance.

A.7.7 Project 8.5. Airborne Spectral Analysis of Thermal Radiation with High Time Resolution. Agency: Bureau of Aeronautics. Report Title: Airborne High-Resolution Spectral Analysis, WT-1342. Project Officer: Ralph Zirkind.

The objectives of this project were to: (1) compare the measurements of the spectral irradiance recorded at an airborne station with that recorded by a ground station for an air burst of a device in the megaton region and a surface burst of a device in the same yield range; (2) measure the spectral characteristics of the thermal radiation as a function of time from a fireball unperturbed by the reflected shock during the early portion of the thermal pulse; (3) accumulate narrow-band spectral data with a high time resolution heretofore unavailable over a large range of yields; (4) determine the time variation of the irradiance color temperature; (5) correlate results of high-resolution spectroscopy with broad-band calorimetry; (6) check existing thermal scaling laws and modify and extend them wherever possible and necessary; and (7) compare the thermal data from surface detonations with that from air bursts.

The project report contains irradiance data in the region of 0.25μ to 2.8μ as a function of time for four of six detonations in which this project participated during Operation Redwing. The data were obtained by mounting in an aircraft a Hilger medium-quartz spectrometer with thirteen photo-sensitive receivers near the focal plane and recording the output on an Ampex 814 magnetic-tape recorder, which has a time resolution of $50\mu\text{sec}$. In addition, a two-channel transmissometer, 0.3μ to 0.6μ , and 0.6μ to 1.05μ , in conjunction with a calibrated light source, provided data on atmospheric transmittance.

The six detonations covered the approximate range of $\frac{1}{2}$ to 4 Mt. Included were three surface shots, one tower shot, one air burst, and one detonation tamped with water. In two shots, a multimegaton air burst and a multimegaton surface burst, the airborne station was located above a surface station for comparison purposes. Due to a bombing error, neither station obtained useful data for the air burst. For the tower shot, the aircraft was located directly above ground zero at an altitude of 22,000 feet and measured the irradiance of an unperturbed fireball. The remaining participation covered surface bursts with yields of approximately $\frac{1}{2}$ Mt. the purpose was to accumulate additional spectral data. In the case of the tamped water shot, the aircraft aborted prior to time zero; therefore, no data was obtained.

Sufficient data was obtained to satisfy the objectives of this project. The significant results include: (1) the irradiance history as a function of wave length; (2) spectral dependence of the basic time parameters of the thermal radiation; (3) agreement between airborne and surface measurements of $t_{1\text{min}}$ and $t_{2\text{max}}$ when atmospheric effects are taken into consideration; and (4) agreement between airborne and ground-station observations of the estimated irradiance color temperatures.

The transmittance results are difficult to interpret and therefore, only estimates of the atmospheric transmission were made. The only positive result is that the transmittance in the 0.3μ to 0.6μ region is about half of values in the region of 0.6μ to 1.05μ .

A.8 PROGRAM 9: GENERAL SUPPORT

A.8.1 Project 9.1a. Cloud Photography. Agencies: Edgerton, Germeshausen, and Grier, Inc. and the 6007th Reconnaissance Group. Report Title: Cloud Photography, ITR-1343. Project Officer: Lt Colonel J.G. James, USAF.

This project was organized to document nuclear cloud phenomena during Operation Redwing by means of aerial photography. It supplemented Project 15.1 (Los Alamos Scientific Laboratory) and Project 23.2 (University of California Radiation Laboratory) studies of early rise conducted with the use of ground-based cameras.

Three RB-50 aircraft were flown at altitudes of 20,000 to 30,000 feet and at distances of 40 to 120 miles from ground zero. Aerial cameras were installed on A-28 stabilized mounts, as during Operation Castle. Photographs were taken from three directions. Timing data were photographed automatically and position data were supplied by the aircraft navigators.

Twenty-seven missions were scheduled, but two planes did not fly because of mechanical difficulties. Adverse weather conditions in the proximity of the aircraft were responsible for the lack of data from Shot Mohawk. Only one of six films was readable, and the one provided only sparse information. Similar but less extensive loss of data occurred from Shots Cherokee, Flathead, Dakota, and Apache. The early detonation time of Shot Tewa, with resultant minimizing of sky light, apparently caused the loss of all exposures on the first photographic run after the initial bomb light faded.

Nevertheless, the total data obtained were more accurate and covered longer periods than those from any previous operation. Measurements of cloud height and diameter up to 17 minutes were made by Edgerton, Germeshausen and Grier, Inc. (EG&G) on most shots. For Mohawk and Tewa a shorter interval was covered.

Corrections were applied for the altitude of the plane, the earth's curvature, atmospheric refraction, and where necessary, for slight camera platform tilt. The data agree quite well from one plane to another, and the results are considered to possess a high degree of reliability. However, a significant correction to adjust the height to top measurements for the inability to measure the true top of the cloud has not been made. The information necessary for this correction, the shape of the cloud top, is not known; assuming a flattened shape would be too speculative. This correction, at maximum, is subtractive in the order of several thousands of feet.

In general, drift measurements, essential to other measurements after 20 minutes, are unsatisfactory, and the data after that time are therefore less reliable.

The data indicate that Redwing late cloud photography was superior to that of previous operations, with significant advancement noted in the total time interval covered and considerable improvement made in the keeping of navigational logs. It is considered that definitive data have now been obtained concerning the growth and dispersal of atomic clouds during the first 15 to 20 minutes for the entire yield range of current test devices.

A.8.2 Project 9.1b. Documentary Photography. Agencies: Edgerton, Germeshausen, and Grier, Inc., Los Alamos Scientific Laboratory, and Lookout Mountain Laboratory. Project Officer: Lt Colonel J.G. James, USAF.

The objectives of this project were to plan, program, and supervise technical and documentary photographic services for all DOD projects participating in the weapon-effect phase of the operation.

Technical photography in support of all projects, such as high-speed, time-lapse, and function-of-time photography was performed by Edgerton, Germeshausen, and Grier, Inc. under contract.

Technical documentary photography in support of projects for illustrating preliminary and final reports was conducted by Task Group 7.1, Task Unit 8. All project requirements were coordinated through Program 9.

A documentary motion-picture film to document the technical and scientific aspects of weapon-effect tests was made by Lookout Mountain Laboratory under the supervision of Task Unit 3.

The 6007th Reconnaissance Group, Far East Air Forces, provided controlled mosaics for Shots Lacrosse, Zuni, Seminole, and Mohawk in support of Project 1.8, Crater Survey.

Requirements were generated in the field for aerial photography of Eniwetok and Bikini Atolls. These were low-altitude uncontrolled mosaics and proved to be of value to planning operations. As a result of these surveys, other outlying atolls were photographed for current and future planning purposes.

REFERENCES

1. "Fallout Symposium"; AFSWP-895; January 1955; Armed Forces Special Weapons Project (now DASA), Washington 25, D. C.; Secret Restricted Data.
2. J. Malik; "Summary of Information on Gamma Radiation from Atomic Weapons"; LA-1620, January 1954; Los Alamos Scientific Laboratory, Los Alamos, New Mexico; Secret Restricted Data.
3. B. L. Tucker; "Fraction of Redwing Radioactivity in Local Fallout"; AFSWP-1053 (RM-1932), 9 July 1957; The RAND Corporation, Santa Monica, California; Secret Restricted Data.
4. "Capabilities of Atomic Weapons"; TM 23-200, November 1957; Armed Forces Special Weapons Project, Washington 25, D. C.; Confidential.
5. E. A. Shuert; "A Fallout Forecasting Technique with Results Obtained at the Eniwetok Proving Ground"; USNRDL TR-139, 3 April 1957; U. S. Navy Radiological Defense Laboratory, San Francisco, California; Unclassified.
6. R. M. Chapman, and M. H. Seavy; "Preliminary Report on the Attenuation of Thermal Radiation from Atomic or Thermonuclear Weapons"; AFCRC-TN-5A-25, November 1954; Air Force Cambridge Research Center, Bedford, Massachusetts; Secret Restricted Data.
7. "Analysis of Atomic Weapons Effects Programs"; AFSWP-807, July 1954; Armed Forces Special Weapons Project, Washington 25, D. C.; Secret Restricted Data.
8. H. C. Kranzer and J. B. Keller; "Water Waves Produced by Explosions"; AFSWP-713, September 1955; New York University, Institute of Mathematical Sciences, New York, N. Y.; Unclassified.
9. "The Generation of Long Period Waves by Nuclear Explosions"; AFSWP-1106; Secret Formerly Restricted Data.
10. F. H. Shelton; "The Precursor—Its Formation, Prediction, and Effects"; SC-2850 (TR), 27 July 1953; Sandia Corporation, Sandia Base, New Mexico; Secret.